

# How good is good enough in DP calculations? a case study into uncertainties involved in the DP capability prediction process

S.J.B. van 't Klooster





# How good is good enough in DP calculations?

# a case study into uncertainties involved in the DP capability prediction process

by

S.J.B. van 't Klooster

in partial fulfillment of the requirements for the degree of

## **Master of Science**

### in Offshore and Dredging Engineering

at the Delft University of Technology,  
to be presented publicly on

Wednesday June 27th, 2018 at 2:00 PM.

Student number: 4020197  
Project duration: October 4, 2017 – June 27, 2018

Thesis committee: Prof. dr. ir. A. P. van 't Veer Delft University of Technology  
Dr. ir. A. Vrijdag Delft University of Technology  
Dr. ir. I. Akkerman Delft University of Technology  
Ir. M. Cleijsen Damen Shipyards

An electronic version of this thesis is available at <http://repository.tudelft.nl/>.



# Abstract

Currently there are three methods of calculating the Dynamic Positioning capability of a vessel namely: static calculations, real-time time domain simulations and fast-time time domain simulations, although the outcome of the last two should be identical. In each of these methods a set of input variables is required to perform the calculations. These inputs are not always exactly known and are therefore sometimes estimated or taken from databases. It is not always clear how big the uncertainty in these estimated inputs is, and on top of that: how big the effect on the predicted DP capability is. To be able to quantify how certain a DP capability calculation is and which input data contribute most to the output uncertainty, in this thesis the input uncertainties for both static and fast-time dynamic calculations are investigated. Each method is subdivided in three different design stages which are: conceptual design, preliminary design and as built design. For the static calculations all three design stages are evaluated but for the fast-time dynamic simulations only the as built stage is considered.

The static calculation part of the analysis consists of determining the input uncertainties, the input sensitivities to the output and finally calculating the output uncertainty. The method used for this calculation assumes that either the relation between input and output is linear or can be linearised at the point of interest. The input uncertainties are calculated using historical data of the Bibby Wavemaster 1 which is the vessel used as case study throughout this thesis and is specifically designed for the purpose of servicing offshore wind farms. It is observed that the input uncertainties of the main dimensions of the vessel are clearly reducing when moving through the design stages. Furthermore it is concluded that the environmental coefficients of wind, waves and current are the most uncertain, even in the conceptual design stage where input parameters of the main dimensions of the vessel vary the most. When considering the sensitivity in the three design stages no big changes were observed, meaning that in all design stages the main dimensions of the vessel are most sensitive to the output. Finally the uncertainty in the output was evaluated where it was observed that for the as built stage still a standard deviation of 4% uncertainty of the output is present, resulting in a calculated 99.7% confidence interval of either 12% too high or too low.

In the dynamic calculation part only the as built stage is considered. Again the uncertain parameters are defined but due to the PID controller in the dynamic model some new input parameters are now present. The gains of this PID controller are assumed to be uncertain and are therefore taken into account during the dynamic uncertainty analysis. Due to a limitation in the aNySIM licence bought by Damen it is impossible to change the wave coefficients which causes their uncertainty not to be taken into account. Since the dynamic simulations are considered to have strong non linearities and possibly even discontinuities due to thruster saturation, the calculation method used for the static part is not applicable anymore. Therefore it is decided to use Monte Carlo simulations to quantify the uncertainty in dynamic DP calculations. Due to the large computational time required to perform large amounts of Monte Carlo simulations with aNySIM, a machine learning method is used to capture the dynamic behaviour of the vessel. A small number of simulations performed by aNySIM is required to train the model which are selected using the Sobol design of experiments technique. This technique optimises the choice of the simulation points to make sure the complete space of possible inputs is covered. By using the machine learning model to obtain an output of a dynamic simulation only a fraction of a second is required instead of 17 minutes when using aNySIM. By running the Monte Carlo simulation on the created machine learning model it was observed that the 97.7% confidence interval for offset can either be calculated up to 8.7% too low or too high whereas the prediction for heading up to 23.1% too low or too high when compared to the base case. It is concluded that using DP for the purpose of people transferring by means of a "Walk To Work" bridge, uncertainties should be taken into account to reduce both safety and contractual requirements risks.



# Acknowledgements

Although the concluding part of writing a thesis, to obtain the MSc degree Offshore and Dredging Engineering at Delft University of Technology, is seen as a individual accomplishment, I could not have done it without the help of some very talented, caring and enthusiastic people around me.

First of all I would like to thank the entire research and development department at Damen Shipyards Gorinchem, where all doors are always open to ask questions on the most divergent topics. A special thanks goes to Marcel Cleijsen, my daily supervisor at Damen, who gave me the complete freedom to compose my graduation assignment and also provided me with very constructive feedback. I would also like to thank Nico van den Heuvel for sharing his programming knowledge and explaining me the backbone of DPlab.

Another thanks goes to Sanne Dekker and Carola Servaas who did their utmost best to find me a graduation spot within the Damen organisation and gave me the opportunity to organise and attend various Damen events and activities, which resulted in meeting a lot of new people throughout the whole company.

Furthermore I would like to thank Arthur Vrijdag who, from the beginning, believed in the concept of determining and quantifying uncertainties in the DP calculation process. He proved to be a tremendous help during the multiple sparring sessions we had and I admire his dedication and involvement throughout the entire duration of my graduation thesis.

Finally I would like to thank my family of which my parents in particular. They showed nothing but support throughout the entire duration of my study, even when the choices I made did not seem the most logic. They gave me the complete freedom to develop myself in all different aspects imaginable of which I still experiencing the benefits today. I can not describe how privileged I feel to receive this amount of unconditional support.



# Nomenclature

## Abbreviations

API	American Petroleum Institute
CAPEX	Capital Expenditures
CFD	Computational Fluid Dynamics
COG	Center Of Gravity
D-gain	Derivative gain
DARPS	Differential Absolute and Relative Positioning System
DGPS	Differential Global Positioning System
DNV	Det Norske Veritas
DOE	Design Of Experiments
DOF	Degrees Of Freedom
DP	Dynamic Positioning
DSA	Differential Sensitivity Analysis
DT	Dynamic Tracking
ERN	Environmental Regularity Number
FEM	Finite Element Method
FMF	Force Multiplication Factor
FPSO	Floating Production Storage and Offloading
GPS	Global Positioning System
GUI	Graphical User Interface
HF	High Frequency
HPR	Hydroacoustic Positioning Reference
I-gain	Integral gain
IMCA	International Marine Contractors Association
IMO	International Maritime Organisation
LF	Low Frequency
LOOCV	Leave One Out Cross Validation
M	Mean
MAE	Mean Average Error
MAESTD	Mean Average Error Standard Deviation

MARIN	Maritime Research Institute Netherlands
MCS	Monte Carlo Simulation
NPD	Norwegian Petroleum Directorate
NRSA	Nominal Range Sensitivity Analysis
P-gain	Proportional gain
PCA	Pearson Correlation Analysis
PID	Proportional Integral Derivative
QTF	Quadratic Transfer Function
RAO	Response Amplitude Operator
ROV	Remotely Operated Vehicle
RSM	Response Surface Methods
SCA	Spearman's Correlation Analysis
SI	Sensitivity Index
WDF	Wave Drift Forces
WWC	Wind, Wave and Current

### Symbols

$\alpha$	Empirically derived coefficient	[ $-$ ]
$\alpha$	Phase	[ $rad$ ]
$\epsilon$	Phase	[ $rad$ ]
$\eta$	Wave elevation	[ $m$ ]
$\gamma$	Peak-enhancement factor	[ $-$ ]
$\nabla$	Displacement	[ $m^3$ ]
$\omega$	Angular frequency	[ $rad/s$ ]
$\rho$	Density	[ $kg/m^3$ ]
$\sigma$	Peak-width parameter	[ $-$ ]
$\zeta$	Wave height	[ $m$ ]
$a$	Wave amplitude	[ $m$ ]
$B$	Breadth	[ $m$ ]
$b$	Damping coefficient	[ $kg/s$ ]
$c$	Spring stiffness coefficient	[ $N/m$ ]
$C_{F_X}$	Dimensionless force coefficient	[ $-$ ]
$E$	Wave spectral density	[ $m^2/Hz$ ]
$f$	Frequency	[ $Hz$ ]
$F_X$	Force in longitudinal direction	[ $N$ ]

$F_Y$	Force in lateral direction	[N]
$g$	Gravitational acceleration	[m/s <sup>2</sup> ]
$h$	Height	[m]
$H_s$	Significant wave height	[m]
$L$	Length	[m]
$M_z$	Moment of force around vertical axis	[Nm]
$\rho_a$	Air density	[kg/m <sup>3</sup> ]
$\rho_w$	Water density	[kg/m <sup>3</sup> ]
$T$	Draught	[m]
$t$	Time	[s]
$T_{mean}$	Mean wave period	[s]
$V$	Velocity	[m/s]
$z_0$	Surface roughness length	[m]
$A$	Projected area	[m <sup>2</sup> ]

### Subscripts

$c$	Current
$J$	JONSWAP
$L$	Lateral
$s$	Submerged
$T$	Transverse
$w$	Wind
$PM$	Pierson-Moskowitz
$ref$	Reference
$wl$	Waterline



# Contents

<b>Abstract</b>	<b>iii</b>
<b>Acknowledgements</b>	<b>v</b>
<b>Nomenclature</b>	<b>vii</b>
<b>1 Introduction</b>	<b>1</b>
1.1 Background . . . . .	1
1.2 DP capability methods. . . . .	2
1.2.1 Static capability methods . . . . .	2
1.2.2 Dynamic capability methods . . . . .	3
1.3 Problem definition . . . . .	4
1.3.1 Research question . . . . .	5
1.3.2 Objectives . . . . .	5
<b>2 Literature</b>	<b>7</b>
2.1 Dynamic positioning . . . . .	7
2.1.1 Dynamic positioning and dynamic tracking . . . . .	7
2.1.2 DP applications, strengths and weaknesses . . . . .	7
2.1.3 DP system blocks . . . . .	8
2.1.4 Power system . . . . .	8
2.1.5 Thruster system . . . . .	9
2.1.6 Position reference system . . . . .	10
2.1.7 Control system . . . . .	11
2.1.8 DP classification . . . . .	11
2.2 Environmental forces . . . . .	12
2.2.1 Wind . . . . .	12
2.2.2 Waves . . . . .	14
2.2.3 Current . . . . .	16
2.3 Hydrodynamics . . . . .	17
2.3.1 1st order wave forces . . . . .	17
2.3.2 2nd order wave forces . . . . .	17
2.4 Time domain model . . . . .	19
2.5 Frequency domain model . . . . .	20
2.6 Static DP capability calculation . . . . .	20
2.6.1 Wave drift multiplier . . . . .	20
2.6.2 Force multiplication factor . . . . .	21
2.7 Time domain DP capability simulation . . . . .	21
2.7.1 The dynamic margin . . . . .	21
2.7.2 DP capability for different operational activities . . . . .	22
2.8 Comparison different DP capability methods . . . . .	25
2.8.1 Hyun-Joe Kim . . . . .	25
2.8.2 Liping Sun . . . . .	26
2.9 DP calculation tools . . . . .	27
2.9.1 DPlab . . . . .	27
2.9.2 aNySIM . . . . .	27

2.10 DP design process . . . . .	28
2.10.1 Excel sheet . . . . .	28
2.10.2 DPLab . . . . .	29
2.10.3 aNySIM . . . . .	29
2.10.4 DOLPHIN real-time simulator . . . . .	29
2.10.5 Model tests . . . . .	29
2.11 Types of uncertainty . . . . .	29
2.11.1 Theory uncertainty . . . . .	29
2.11.2 Model uncertainty . . . . .	30
2.11.3 Parameter and variable uncertainty . . . . .	30
2.11.4 Measurement uncertainty . . . . .	31
2.12 Uncertainty calculation methods . . . . .	31
2.12.1 Linear uncertainty calculation . . . . .	31
2.12.2 Combined uncertainty calculation . . . . .	32
2.12.3 Non linear uncertainty calculation . . . . .	33
2.13 Sensitivity . . . . .	33
2.13.1 Differential sensitivity analysis . . . . .	33
2.13.2 Nominal range sensitivity analysis . . . . .	34
2.13.3 Pearson Correlation Analysis . . . . .	34
2.13.4 Spearman's correlation analysis . . . . .	34
<b>3 Methodology . . . . .</b>	<b>35</b>
3.1 General plan of approach . . . . .	35
3.2 Static DP analysis . . . . .	36
3.2.1 Sensitivity analysis parameter variation . . . . .	36
3.2.2 Input uncertainty . . . . .	37
3.3 Dynamic DP analysis . . . . .	37
3.3.1 Model description . . . . .	38
3.3.2 Simulation time . . . . .	38
3.3.3 aNySIM outputs . . . . .	39
3.3.4 Input uncertainty . . . . .	39
3.3.5 Response surface methods . . . . .	40
3.3.6 Machine learning . . . . .	40
3.3.7 Design of experiments . . . . .	42
3.3.8 Goodness of fit . . . . .	43
3.3.9 Sensitivity analysis . . . . .	45
3.3.10 Parameter variations . . . . .	46
3.3.11 Time step . . . . .	46
<b>4 Results . . . . .</b>	<b>49</b>
4.1 DPLab capability sensitivity . . . . .	49
4.1.1 Conceptual design stage . . . . .	49
4.1.2 Preliminary design stage . . . . .	53
4.1.3 As built design stage . . . . .	56
4.2 DPLab capability input uncertainty . . . . .	59
4.2.1 Conceptual design stage . . . . .	59
4.2.2 Preliminary design stage . . . . .	61
4.2.3 As built design stage . . . . .	64
4.3 DPLab capability output uncertainty . . . . .	67
4.3.1 Conceptual design stage . . . . .	67
4.3.2 Preliminary design stage . . . . .	70
4.3.3 As built design stage . . . . .	73
4.3.4 Total capability output uncertainty . . . . .	75
4.4 DPLab capability confidence interval . . . . .	76
4.4.1 Conceptual design stage . . . . .	77
4.4.2 Preliminary design stage . . . . .	78
4.4.3 As built design stage . . . . .	79

4.5 aNySIM goodness of model fit . . . . .	81
4.5.1 R squared and LOOCV R squared . . . . .	81
4.5.2 Mean absolute error and LOOCV mean absolute error . . . . .	83
4.5.3 Mean absolute error standard deviation and LOOCV mean absolute error standard deviation . . . . .	83
4.5.4 Residual . . . . .	83
4.6 aNySIM offset analysis . . . . .	85
4.6.1 Maximum offset analysis . . . . .	85
4.6.2 Offset interval analysis . . . . .	89
4.7 aNySIM heading analysis . . . . .	92
4.7.1 Maximum heading . . . . .	92
4.7.2 Heading interval . . . . .	97
<b>5 Conclusions and recommendations</b>	<b>101</b>
5.1 Conclusions . . . . .	101
5.1.1 Static . . . . .	101
5.1.2 Dynamic . . . . .	102
5.2 Recommendations . . . . .	103
5.2.1 Static . . . . .	103
5.2.2 Dynamic . . . . .	104
<b>List of Figures</b>	<b>105</b>
<b>List of Tables</b>	<b>109</b>
<b>A Project overview</b>	<b>111</b>
<b>B Data types</b>	<b>113</b>
B.1 Nominal . . . . .	113
B.2 Dichotomous . . . . .	113
B.3 Ordinal . . . . .	113
B.4 Interval . . . . .	113
B.5 Ratio . . . . .	113
B.6 Monotonic relationship . . . . .	114
<b>C Dimensional analysis</b>	<b>115</b>
<b>D DPlab</b>	<b>123</b>
D.1 Sensitivity . . . . .	125
D.2 Input uncertainty . . . . .	126
D.2.1 Main particulars . . . . .	126
D.2.2 Wind coefficients . . . . .	127
D.2.3 Current coefficients . . . . .	128
D.2.4 Water density . . . . .	128
D.2.5 Air density . . . . .	129
D.3 Wind wave relation . . . . .	129
<b>E aNySIM</b>	<b>131</b>
E.1 Parameter variation . . . . .	133
E.2 PID gains . . . . .	133
E.3 Environmental angle converter . . . . .	135
E.4 aNySIM info sheet . . . . .	135
<b>F Model validation</b>	<b>139</b>
F.1 Residuals . . . . .	139
F.2 (LOOCV) R squared, MAE and standard deviation . . . . .	152
<b>Bibliography</b>	<b>159</b>



# 1

## Introduction

*This chapter starts with some background information on why Dynamic Positioning (DP) is a relevant topic today as well in the future. Thereafter a brief introduction is given on the different Dynamic Positioning capability methods, a more detailed elaboration on Dynamic Positioning is given in section 2.1. Finally the research questions and objectives are described*

### 1.1. Background

Nowadays a tremendous amount of offshore activities can be found all across the globe. One of the biggest offshore markets is oil and gas for which numerous platforms were built offshore to extract raw materials from earth that provided us with energy for decades. However, people become more aware of the fact that these sources don't last forever and an alternative is required to provide a planet for future generations. The growing global awareness together with the fact that the oil price is down quite a bit [1] results in a rapidly increasing offshore wind industry [2]. All those platforms and windmills need to be installed, maintained and eventually decommissioned.

In the early days the installation of platforms, windmills and the drilling of wells was done by vessels that were moored or anchored to the sea bottom or by using jack-up platforms. Jack-up platforms are barges that are towed or can sail to the location of interest where they extend their legs until they stand solid on the sea bottom. As technology evolved people were looking into ways to keep vessels in place by just using their thrusters which is known as Dynamic Positioning vessels. These vessels measure or estimate environmental forces and act up on them to stay in their desired position. DP vessels are now being used for multiple purposes including but not limited to: installation, maintaining and decommissioning platforms and windmills.

One can imagine that these vessels are a big investment for a company and therefore a detailed specification of the DP capability is desired so that an assessment can be made whether a ship is capable of performing certain operations. In general three motions of the vessel are compensated by the DP system namely: surge, sway and yaw as illustrated by the orange arrows in figure 1.1. These motions are induced due to the environmental forces that act on the vessel, illustrated by the red arrows, which are wind, waves and current. To maintain position the thrusters generate a force, illustrated by the green arrows, which counteracts the environmental forces. When determining these capabilities different methods can be used and are briefly discussed in section 1.2.

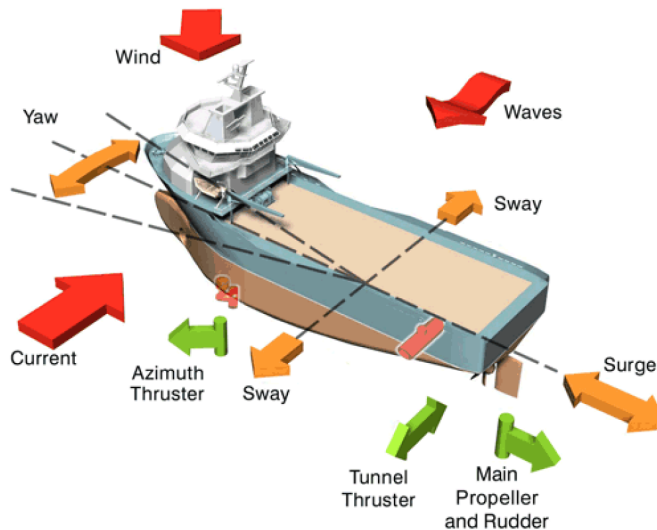


Figure 1.1: Dynamic Positioning - Vessel Motions, Environmental Forces and Thruster Forces [3]

## 1.2. DP capability methods

When designing DP vessels, several methods and tools can be used throughout the designing process of the vessel [4] as is depicted in table: 1.1. Roughly two different methods can be distinguished which are: static and dynamic capability methods, both of them are shortly evaluated below.

Design Stage	Tools	Accuracy / Error
Concept Design	Database / empirical functions / Static Calculations	±30%
Basic Design	Static / Dynamic Calculations	±20%
Detailed Design	Dynamic Calculations / Model tests	±15%
"As-Built"	DP-system / Operator	0%
Design parameters	Importance	Accuracy needed
DP class	High	100%
Environmental data	Medium / High	90%
Force characteristics	High	70-85%
DP Control system	Medium	50%
Measuring system	Medium / High	80%
Thrusters	Medium	80-95%

Table 1.1: Various design stages DP system with accuracy [4]

### 1.2.1. Static capability methods

The most basic method to assess the capability of a DP vessel is by means of a static calculation and therefore neglecting the dynamic influences that are present. A simple condition must be met which states that the resultant of the thrust generated by the thrusters must equal the resultant of the external mean forces acting on the vessel. The results of these static DP calculations are visualised in so called DP capability plots of which an example is shown in figure 1.2. The DP capability plot shows for a given amount of thrust up to what environmental conditions, expressed in wind speed, a vessel can still maintain its position. This is done for different angles of attack from which the environmental loads can approach the vessel, but is at least calculated once every 15° according to the International Marine Contractors Association (IMCA) guidelines [5]. Important to state is that most of these calculations are performed with the assumption that all the environmental forces are collinear, meaning that wind current and waves are assumed to have the same direction.

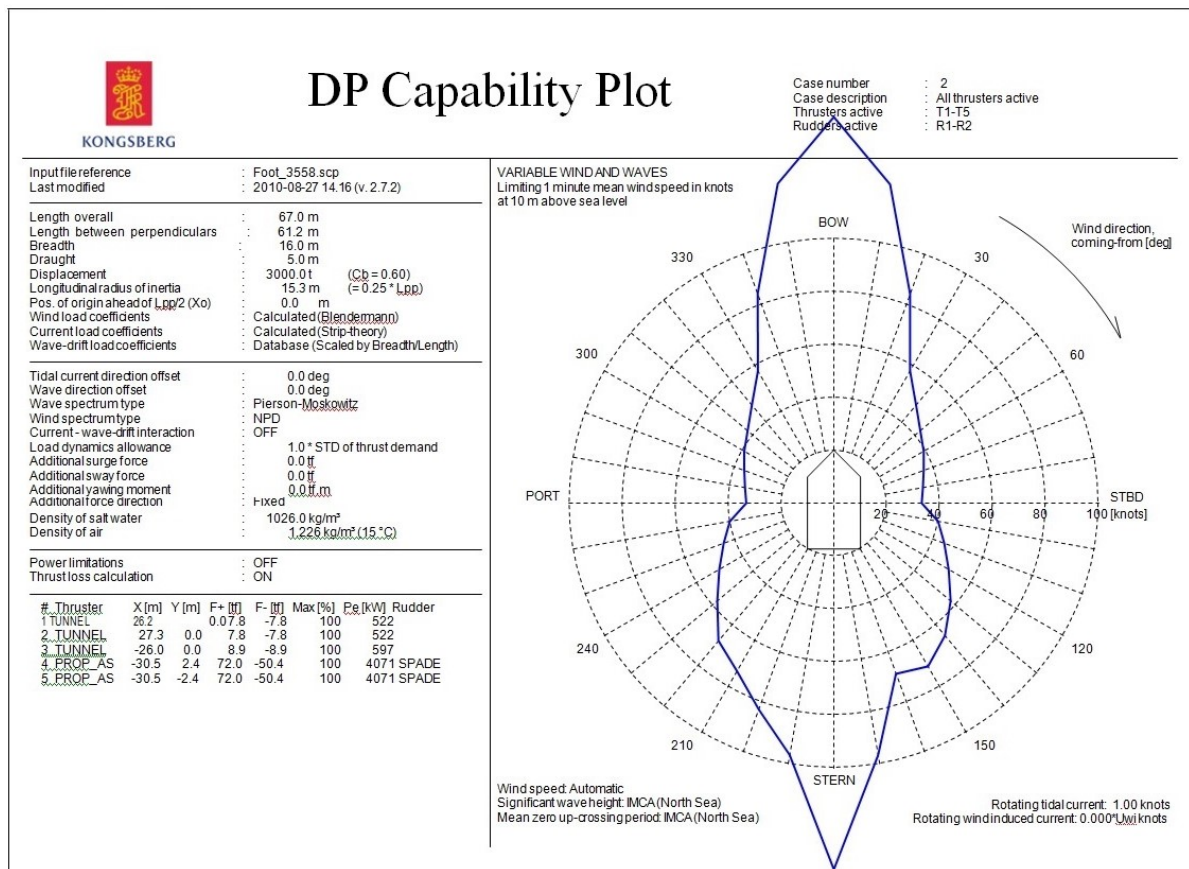


Figure 1.2: Kongsberg DP capability plot [6]

### Quasi static capability method

Despite the fact that the above calculation method is performed in a static manner, time varying environmental forces can be accounted for in static DP capability calculations by means of several methods. The method mostly used throughout the maritime and offshore industry is the use of a Dynamic Margin. This Dynamic Margin is taken on the thrusters of the vessel and states that the maximum thruster usage, in the static DP calculations, must not exceed 80% to account for the time varying environmental forces [7].

Another method to account for time varying environmental forces in static capability calculations is by means of a DP factor. The DP factor is a multiplier on the mean environmental loads and roughly varies between 1 and 2 [8] [9]. However this factor depends very strong on the experience of the company, the environmental conditions and the type of vessel.

### 1.2.2. Dynamic capability methods

A more extensive way of determining the capability of a DP vessel is by means of dynamic methods. Here a distinction is made between mathematical calculation methods, such as time domain and real time simulations, and model testing which is also a dynamic method but strictly speaking no calculations are performed.

#### Time domain simulations

Several software packages are commercially available to perform time domain simulations. One of the big differences compared to static calculation methods is that it is possible to determine the position of the vessel at any point in time and in 6 Degrees Of Freedom (DOF). The dynamic calculations include first and second order wave forces whereas for the static calculation method only the mean second order wave drift forces are considered. Another difference is that with time domain simulations the DP control system is included in the calculations. It is known that the settings of the control systems can

influence the capability of the vessel [10] so including it in the calculations will result in a more realistic capability prediction.

### Real time simulations

Another way of dynamically determining the capability of a vessel is by means of a real time simulator. A real time simulator visualises the vessels motions real time in 3D and offers the possibility to connect other systems to the hydrodynamic model of the vessel. This results in the possibility to connect an actual DP control system to the model and determine the vessels capability. Another system that can be included in the simulation is the usage of a "walk to work" bridge of which the Ampelman is one of the best known examples. This bridge makes it possible for crew to be safely transported from a ship to a platform, windmill or another vessel.

At Damen Shipyards a DOLPHIN real time simulator was bought at Maritime Research Institute Netherlands (MARIN) that contains the hydrodynamic model of the ASV9020 Walk to Work vessel, also known as the Bibby Wavemaster 1. Connected to the simulator is the Kongsberg DP control system as used on the actual vessel. In addition a model of the "walk to work" bridge is connected to the simulator, the UPTIME Gangway large, which is also installed on vessel. Combining both the Kongsberg DP system and the UPTIME Gangway bridge in one model it is possible to determine the capability of the vessel and the bridge combined.

### Model tests

In the final stages of designing a DP vessel, model tests can be performed to determine its capability. The aim of model testing is to be as close to reality as possible. One of the places where these model tests can be performed is at MARIN. When performing the model tests, MARIN uses their in house designed Proportional Integral Derivative (PID) controller but also offers the possibility include a DP control system from another brand to determine the vessels capability. This way the DP control system installed on board of the actual vessel can already be implemented and tested beforehand.

## 1.3. Problem definition

Damen Shipyards just finished building its first dedicated offshore wind farm servicing vessel, the ASV9020 Walk to Work vessel, also known as the Bibby Wave Master 1. This is the first ship that was sold under the terms that it should be able to transfer people from the vessel to the windmills for a certain minimum sea state resulting in a specific operational window. Similar contractual requirements are expected in the future. The possibility to transfer people is a combination of station keeping capability of the ship itself and the capabilities of the gangway. The disturbances that act on the ship are wind, waves and current and are stochastic by nature. Given this stochastic nature the question arises how, and in what way, the transferring capability of a specific ship can be quantified or even guaranteed up to a certain weather condition.

Current industry standard to predict station keeping capability is to make static DP capability plots [5]. However, with the upcoming wind turbine installation and servicing industry, customers do not only ask for class specifications anymore but also make demands about the operability of the vessels DP system. As stated before, this is called the DP station keeping. A possibility to say something about DP station keeping is to make dynamic simulations, taking into account both the static and dynamic characteristics of the ship and environment. The amount of required ship information drastically increases. This approach can be carried out in fast-time or in real-time, although this should not matter for the end result. Another approach could be to carry out model scale tests, also in that case there are many relevant system parameters that should be taken into account.

After analysing the DP design process at Damen it became clear that a lot of input parameters in the static DP capability calculation are uncertain. Furthermore the sensitivity of the output to the (uncertain) parameters is not always clear. This means that there could potentially be a significant uncertainty in the output of the DP calculations. It could be that the only reason that this has not led to contractual problems is that the DP capability is not easily verified on full scale. The thought about uncertainty can be extended to the dynamic DP predictions. In the case that operations are carried

out close to fixed structures the relevance of knowing and understanding the limitations of the system becomes even greater.

To determine these uncertainties an uncertainty analysis should be performed. It is important to realise that there are 2 different inputs namely: given inputs and adjustable inputs. An example of a given input is for instance the wind speed, this will not change in case the design of the vessel changes. However when looking at an adjustable input, like for instance the length of the vessel, this can change when the vessels design is adjusted. Important to note is that an input which given does not necessarily has zero uncertainty. For a schematic overview see figure: 1.3.

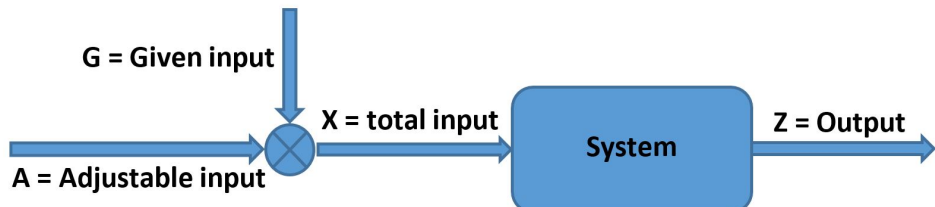


Figure 1.3: Input-output flowchart

To define the given and adjustable inputs in a better and more structured way three different vessel design stages are considered as summarised in table 1.2

Table 1.2: Design stages

Design	Explanation
Conceptual	Design stage with very big geometrical changes, typically a complete new product
Preliminary	Small changes in geometrical dimensions and to on board systems will still occur
As built	Complete geometrical dimensions and on board systems of the vessel are known

### 1.3.1. Research question

Combining the information presented above a logical research question and sub questions that are answered during this thesis are formulated as follow:

- How should parametric and data uncertainties be managed in the DP calculation process
  - Which parametric and data inputs are considered to have uncertainties?
  - What are the magnitudes of the uncertainties of the parametric and data inputs?
  - What are the sensitivities of the parametric and data inputs to the model outputs?
  - Which parametric or data inputs have the most significant contribution to the uncertainty of the Dynamic Positioning station keeping output?

### 1.3.2. Objectives

During this thesis research a distinction is made between static and dynamic DP calculations since it is expected that the uncertainty will differ for both methods and it is important to asses which method is most suitable for specific calculation purposes. The distinction is also visible in the objectives set for this thesis research:

- Acquire knowledge about the effect of the input uncertainties on static DP calculation output
- Acquire knowledge about the sensitivities in static DP calculation methods
- Acquire knowledge about the effect of the input uncertainties on dynamic DP calculation output
- Acquire knowledge about the sensitivities in dynamic DP calculation methods



# 2

## Literature

*This chapter starts with explaining the basic components present in a DP system and elaborating on the applications of DP vessels. Also the environmental forces acting on a vessel and how these forces should be calculated is evaluated after which a more in depth analysis is performed concerning the wave forces. The difference between time domain and frequency domain analysis is elaborated on and evaluation of some former research on DP calculations is presented. Calculation tools to perform DP analysis are discussed and the DP design process Wavemaster 1 is reviewed. Finally different types of uncertainty and sensitivity are described.*

### 2.1. Dynamic positioning

#### 2.1.1. Dynamic positioning and dynamic tracking

Dynamic Positioning is a term widely used in the offshore and maritime industry but is sometimes used for two different phenomena. The first is Dynamic Positioning (DP) and the second is Dynamic Tracking (DT). Although it may seem that both have the same meaning a small but significant difference makes them different from each other. The definitions used throughout this report are [4]:

- **Dynamic Positioning** is a method to automatically maintain a vessel on its predefined position and/or heading by use of its thrusters and/or rudders.
- **Dynamic Tracking** is a method to automatically maintains a vessel's predefined track and/or heading by using its thrusters and/or rudders.

A vessel that has Dynamic Tracking capability can also perform Dynamic Positioning operations but the conversely is not necessarily true.

#### 2.1.2. DP applications, strengths and weaknesses

There are several reasons why one could choose to use a DP system. Deep water is one of them since it could be too expensive or maybe even impossible to use an anchor-leg mooring system. When conducting short-term moorings it could also be less expensive and way more flexible than a conventional anchor-leg mooring system. Another scenario is when the vessel operates in situations where it should be able to sail away quickly in case of an emergency or extreme weather. DP systems are used more and more often for a variety of applications which include but are not limited to [4]:

- |  |   |
|--|---|
| <ul style="list-style-type: none"><li>• Drill rigs</li><li>• Diving / Remotely Operated Vehicle (ROV)</li><li>• Pipe laying</li><li>• Rock dumping</li></ul> | <ul style="list-style-type: none"><li>• Dredging</li><li>• (Tandem) Offloading</li><li>• Floating storage and production</li><li>• Military</li></ul> |
|--|---|

- Yachts
- Heavy lift operations
- Decommissioning operations
- People transferring

As the operation where DP is used differs also the required offset differs in each case. Where a decommissioning operation requires maybe a maximum of  $0.5m$  deviation, a deep water drilling vessel may be able to deviate up to 2% of the water depth which means sometimes a deviation up to a hundred meter is still acceptable. The usage of a DP system, as every system, has its strengths and weaknesses and are summarised below [4]:

#### Strengths:

- Applicable in shallow and deep water
- Cost & performance independent of water depth
- Quick mooring and disconnecting
- No tugs required for operation
- Rapid response to weather and operational changes
- No seabed or subsea infrastructure impairment

#### Weaknesses:

- High Capital Expenditures (CAPEX)
- (High) Fuel consumption
- Risk of losing position due to equipment failure
- Thruster can be hazardous for divers and a ROV
- Higher maintenance
- Not always usable in high sea states

#### 2.1.3. DP system blocks

Although almost every DP system is different, as different suppliers have different design philosophies and each system is tuned and optimised to its application, still a general layout of components is always found in every DP system which are essential to make the system work as a whole. These components can be subdivided in four blocks namely:

- Power System
- Thruster System
- Control System
- Position Reference System

The complete DP system, when activated, is a continuous loop that is constantly exchanging information between the four different blocks to keep the vessel in its required position. The relation between the separate components and blocks is visualised in figure 2.1. Here the wind feed forward option is also shown which is used in the more modern DP systems. This feed forward measures the wind speed and therefore makes it possible to predict the vessel's movement due to, for instance, wind gusts. Therefore the DP system can already start reacting to these forces resulting in a smaller offset of the vessel.

#### 2.1.4. Power system

The power system delivers the required power to keep position or track. To better understand the interaction between the components it is important to have a basic knowledge about the components that are part of it. According to [12], [13] and [14] the following components are part of the power system:

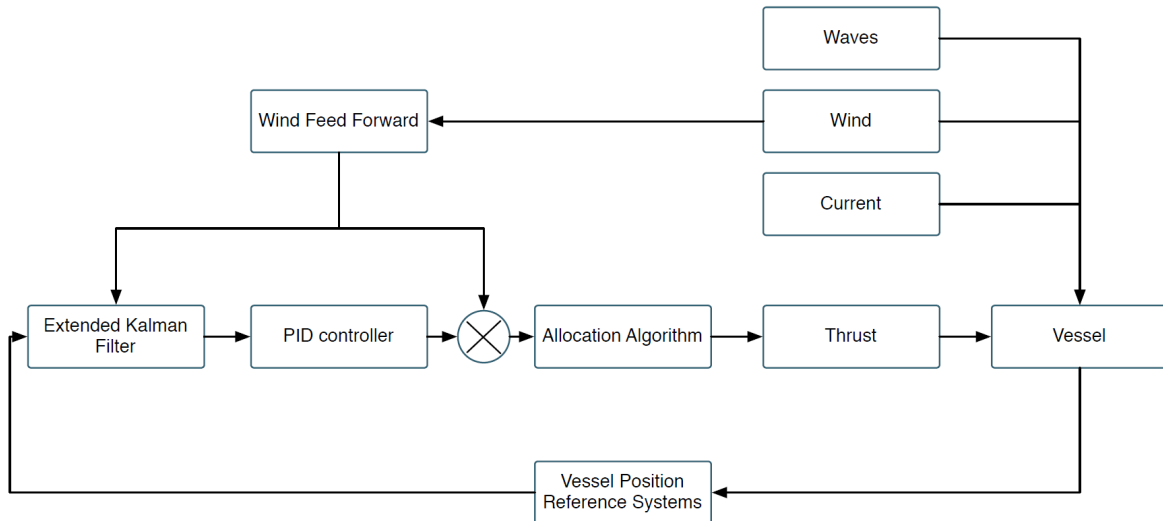


Figure 2.1: DP system block diagram [11]

- Prime movers with auxiliary systems and piping
- Generators
- Switchboards
- Distribution system (cabling and cable routing)
- Uninterruptible power supplies and batteries
- Power management system

### 2.1.5. Thruster system

A wide variety of propulsion systems was invented over the years in the maritime and offshore industry. In this thesis however only the propulsion present on the DAMEN ASV 9020 Walk to Work, also known as the Bibby Wavemaster 1, is evaluated. According to [14] the following components are part of the thruster system:

- Thruster with prime movers, auxiliary systems and piping
- Main propellers and rudders (if under control of DP system)
- Thruster control electronics
- Manual thruster controls
- Associated cabling and cable routing

The thrusters present on the Bibby Wavemaster 1 are at the aft of the ship: 2 azimuth thrusters and at the bow of the ship: 1 retractable azimuth thruster and 2 tunnel thrusters. These 3 different thrusters are briefly discussed below.

#### Azimuth thruster

The azimuth thruster is a thruster that can rotate 360° without having to rotate back at any point. The rotation is performed in the XY plane and gives the vessel the opportunity to apply thrust with maximum efficiency in the direction that is required. Instead of changing the direction of the propeller the azimuth thruster can rotate 180° to apply backward thrust. Although modern azimuth thrusters can rotate relatively fast still some delay is present due to the rotation. In figure 2.2 an illustration is given of two azimuth thrusters.

#### Retractable azimuth thruster

A retractable azimuth thruster is basically the same as a normal azimuth thruster, the difference is however that the retractable thruster is only used for DP operations. When a DP operation is started this thruster is lowered from the ship into the water and afterwards is retracted again in order to minimise the drag on the vessel during transit. This is not only helpful for DP operations but also convenient for servicing since the thruster can be accessed from within the ship and no dry-docking is necessary.

### Tunnel thruster

The tunnel thruster, also known as bow thruster, generates thrust transversely to the vessel. The main difference with the azimuth thruster is that the tunnel thruster is fixed (transversely) in the vessels hull. These thrusters are mostly found in the bow of the vessel but sometimes also in the stern. Since these thrusters are placed far away from the Center Of Gravity (COG) they can induce big moment of forces so that heading and sway can be compensated for very effectively. An example of a tunnel thruster is given in figure 2.3.



Figure 2.2: Azimuth Thrusters [15]



Figure 2.3: Tunnel Thrusters [16]

### 2.1.6. Position reference system

According to [17] the position reference system includes: all hardware, software and sensors that supply information necessary to give position references. It should also be designed such that it is in line with the redundancy requirements of the DP classification which are discussed in section 2.1.8. Several reference systems are briefly explained in this section.

#### Satellite positioning systems

The Global Positioning System (GPS) is the most well known satellite positioning system in the world. Originally it was developed for the U.S. Department of Defence but nowadays it is widely implemented in all day equipment like navigation systems and mobile phones. The accuracy one can achieve on a mobile phone is typically around 4.9m [18].

The Differential Global Positioning System (DGPS) is a GPS enhanced with fixed ground based reference stations. These ground based stations know their exact position and by continuously comparing the position of the satellite and GPS receiver they can correct for the error present at that time. This boosts the accuracy of the GPS system to a couple of centimetres [18].

#### Hydroacoustic positioning reference

This system makes use of sound waves passing through the water. A transducer is placed on the ships hull and several transponders are placed on the seabed. The transducer sends an acoustic sound which is picked up by the transponders and is then reflected back to the transducer. Unfortunately these signals can be disrupted by ambient noise. The system is used in water depths between shallow and medium depth water and has great accuracy. However the accuracy decreases with increasing water depth.

Three different Hydroacoustic Positioning Reference systems (HPR) can be distinguished which are: long baseline, short baseline and ultra short baseline. These systems differ in the amount of transducers and transponders required and how they are configured. Different HPR systems can also be combined to improve robustness, redundancy and accuracy [4].

#### Relative position reference

Several methods are used for Relative Position Reference, one of those is to use some kind of a laser beam or microwaves to measure the relative distance from the source to the target position. The time that it takes for the signal to travel from the source to the target can be deducted and therefore the distance can be calculated.

A second method is the use of a Differential, Absolute and Relative Positioning System (DARPS). This system is often used in tandem offloading operations and combines a (D)GPS (absolute) with an relative system on both vessels. By doing so maximum accuracy and reliability is assured during the offloading operation.

#### Inertial position reference

When using an inertial position reference system the position is determined relative to a starting point. In general gyroscopes and accelerometers are used for generating this data. The downside of these measurements is that they develop a measurement error which becomes larger due to disturbances over time. Therefore inertial systems are not used as autonomous systems but are often combined with other reference systems. By doing so the inertial system can continuously be re-calibrated so that the accuracy of the combined system becomes very high.

### 2.1.7. Control system

The DP control system can be seen as the brain of the DP system. It is the most intelligent part where all the data is continuously gathered, evaluated and acted upon. The two main parts of the control system are briefly discussed below.

#### PID-controller

The Proportional, Integral, Derivative (PID) controller is a general control loop feedback mechanism which is commonly used in industrial control systems. In the case of the DP system the PID controller tries to minimise the difference between the required and actual position of the vessel, also referred to as the offset. The PID controller has 3 gains that can be set to optimise the response of the controller to wit:

- **Proportional (P-gain)**, this gain influences the instantaneous offset of the vessel
- **Integral (I-gain)**, this gain influences the permanent, or steady-state error, offset of the vessel
- **Derivative (D-gain)**, this gain influences the rate of change in offset of the vessel

One could also state that the Proportional gain acts on the present offset, the Integral gain acts on the past offset and the Derivative gain acts on the future offset.

#### Kalman filter

The Kalman filter was designed to minimise the disadvantages of the standard PID-controller, which suffered from relatively slow integration action and has a substantial amount of phase lag. The concept of the Kalman filter is based on the predictor corrector estimator model [19]. The main objective for the Kalman filter is to estimate the state of the vessel.

The Kalman filter will predict the state of the vessel by using the vessel's model and will correct this prediction using the measurements from the position reference systems. This is done by assigning weights to the measurements and the vessel's model data to evaluate which of the two should be taken into account more than the other. How much weight is given is determined by the Kalman gain, the lower the Kalman gain the more weight is given to the model. The Kalman filter is an optimal filter as it calculates the best possible estimate, or minimum variance, for the state of the system. [19]

### 2.1.8. DP classification

There are numerous classification bureaus worldwide which have specified guidelines for DP-systems, a short overview of the most commonly known and used classifications is given in the following section.

#### DP redundancy classification

Every classification bureau has its own DP redundancy classes, however all of them are based on the International Maritime Organisation (IMO) equipment class guidelines [13] which are:

- **Class-0** Manual position control and automatic heading control under specified maximum environmental conditions (actually means that no DP-system is present).

- **Class-1** Automatic and manual position and heading control under specified maximum environmental conditions.
- **Class-2** Automatic and manual position and heading control under specified maximum environmental conditions, during and following any single fault excluding loss of a compartment. (Two independent computer systems).
- **Class-3** Automatic and manual position and heading control under specified maximum environmental conditions, during and following any single fault including loss of a compartment due to fire or flood. (At least two independent computer systems with a separate back-up system separated by A60 class division).

An overview of the different classification bureaus and their redundancy classifications of DP-systems can be found in figure 2.4.

DP class notation												
IMO equipment class	ABS	BV	CCS	DNV		GL	IRS	KR	LR	NK	RINA	RS
	American Bureau of Shipping (USA)	Bureau Veritas (France)	China Classification Society (China)	Det Norske Veritas (Norway)		Germanischer Lloyd (Germany)	Indian Register of Shipping (India)	Korean Register of Shipping (Korea)	Lloyds Register (UK)	Nippon Kaiji Kyokai (Japan)	Registro Italiano Navale (Italy)	Russian Maritime Register of Shipping (Russia)
	DPS-0	DYNAPOS SAM		DYNAPOS AUTS	DPS 0				DP (CM)		DYNAPOS SAM	
Class 1	DPS-I	DYNAPOS AMIAT	DP-I	DYNAPOS AUT	DPS I	DP I	DP(I)	DPS (I)	DP (AM)	Class A DP	DYNAPOS AMIAT	DYNPOS-I
Class 2	DPS-2	DYNAPOS AM/AT R	DP-2	DYNAPOS AUTR	DPS 2	DP 2	DP(2)	DPS (2)	DP (AA)	Class B DP	DYNAPOS AM/AT R	DYNPOS-2
Class 3	DPS-3	DYNAPOS AM/AT RS	DP-3	DYNAPOS AUTRO	DPS 3	DP 3	DP(3)	DPS (3)	DP (AAA)	Class C DP	DYNAPOS AM/AT RS	DYNPOS-3

Figure 2.4: DP classes overview [20]

### DP position keeping classification

Det Norske Veritas (DNV) has an additional classification next to the redundancy classes which is called the Environmental Regularity Number (ERN). The ERN is built up as follows: ERN(a,b,c,d) where a,b,c,d are integer numbers between 0 and 99 reflecting probable regularity for keeping position in a defined area [21] where:

- **a:** The first number shall represent optimal use of all thrusters (Transverse thrust generated by the combined use of main propellers and rudders shall not be taken into consideration.)
- **b:** The second number shall represent minimum effect of single-thruster failure
- **c:** The third number shall represent the maximum effect single-thruster failure
- **d:** The fourth number shall represent the effect of the worst case single failure(s)

## 2.2. Environmental forces

In this section the environmental forces acting on a vessel at sea are discussed which are wind, waves and current.

### 2.2.1. Wind

Like all environmental phenomena, wind forces are highly dependent on time and location and therefore are of stochastic nature [22]. The fluctuations of wind forces can be quite significant due to large velocity and directional changes. In practice the wind velocity is often given in terms of an average over a certain time. Generally used time-spans range from 1 to 60 minutes but sometimes even longer time averages are used.

Local wind is often expressed as an average velocity with an average direction at a standard height of 10m above ground or still water level. To determine the wind velocity at other elevations numerous relations can be used, both theoretical and empirical. Two commonly used relations are: the power

law wind profile as defined in equation 2.1 and the logarithmic wind profile as defined in equation 2.2. It is stated by [23] that the logarithmic wind profile is most suitable between 10 – 20m height and the power law wind profile is most suitable for heights above 100m, in between they both work fairly well. It is furthermore suggested to use the the logarithmic wind profile for wind speeds up to 60m height and the power law wind profile for wind speeds from 60m height.

$$V_w(h) = V_w(h_{ref}) \cdot \left( \frac{h}{h_{ref}} \right)^\alpha \quad (2.1)$$

$$V_w(h) = V_w(h_{ref}) \cdot \frac{\ln\left(\frac{h}{z_0}\right)}{\ln\left(\frac{h_{ref}}{z_0}\right)} \quad (2.2)$$

Where:

- $V_w(h)$  = Wind speed at the desired height [ $\frac{m}{s}$ ]
- $V_w(h_{ref})$  = Wind speed at the reference height of 10m [ $\frac{m}{s}$ ]
- $h$  = Desired height [m]
- $h_{ref}$  = Reference height of 10m [m]
- $z_0$  = Surface roughness length  $\approx 0.0002$  at sea [m]
- $\alpha$  = Empirically derived coefficient  $\approx 0.11$  over open water (sea) [-]

There are also models that take the varying part of the wind better into account than the two earlier named wind profiles. Those models are: the Davenport spectrum, the Harris spectrum, the Norwegian Petroleum Directorate (NPD) spectrum and the American Petroleum Institute (API) spectrum. They give spectra related to frequency to be able to account for the changing amplitude and direction of the wind [24].

If the variation of the wind forces are considered to be much smaller than the other variations of environmental forces, the wind force can sometimes be considered as constant. This can be the case when the variations of the second order wave drift forces are much bigger than the variations of the wind forces, see figure 2.7. When a constant wind speed is assumed the forces due to wind can be calculated as follow:

$$F_{Xw}(\alpha_w) = \frac{1}{2} \cdot \rho \cdot V_w^2 \cdot C_{F_{X,w}}(\alpha_w) \cdot A_T \quad (2.3)$$

$$F_{Yw}(\alpha_w) = \frac{1}{2} \cdot \rho \cdot V_w^2 \cdot C_{F_{Y,w}}(\alpha_w) \cdot A_L \quad (2.4)$$

$$M_{Zw}(\alpha_w) = \frac{1}{2} \cdot \rho \cdot V_w^2 \cdot C_{M_{Z,w}}(\alpha_w) \cdot A_L \cdot L \quad (2.5)$$

Where:

- $F_{Xw}$  = Force in longitudinal direction (function of wind direction) [N]
- $F_{Yw}$  = Force in transverse (lateral) direction (function of wind direction) [N]
- $M_{Zw}$  = Moment of force around vertical axis at COG (function of wind direction) [Nm]
- $\rho$  = Density of air [ $\frac{kg}{m^3}$ ]
- $V_w$  = Wind velocity [ $\frac{m}{s}$ ]
- $C_{F_{X,w}}, C_{F_{Y,w}}, C_{M_{Z,w}}$  = Dimensionless wind force coefficients (function of wind direction) [-]
- $A_T$  = Transverse projected wind area [ $m^2$ ]
- $A_L$  = Lateral projected wind area [ $m^2$ ]
- $(\alpha_w)$  = Wind direction [-], from astern is zero
- $L$  = Length between the perpendiculars of the ship [m]

### 2.2.2. Waves

One of the most extensively modelled environmental contributions are waves. Waves can be quite significant considering the forces exercised on a vessel and are induced by several events [22].

- Waves generated by a ship or another floating structure. These waves can be induced by a constant forward speed or by carrying out an oscillatory motion.
- Waves generated by interaction between wind and the sea surface.
- Waves generated by astronomical forces such as tides.
- Waves generated by earthquakes or submarine landslides such as tsunamis.

The waves considered throughout this research are: waves generated by interaction between wind and the sea surface, also referred to as wind generated waves. These wind generated waves can be divided into two categories namely: sea and swell which are described below.

#### Sea waves

A sea wave is a wave train that is driven by a local wind field. These waves are short-crested and these crests have 2 – 3 times the length of the wave length. Sea waves are also very irregular which means that high waves can be followed unpredictably by low waves and the other way around. The wave crests are relatively sharp and sometimes small waves can be observed on top of a crest. The wave crests seem to propagate in different directions with a significant deviation, typically tens of degrees, from the mean.

#### Swell waves

Swell waves are waves that have propagated out of the area where they were initially induced by local wind. Therefore they don't depend on wind anymore and can propagate hundreds of kilometres further if they travel through areas where the wind is relatively calm. Swell waves are more regular than sea waves and their crests are also more rounded compared to sea waves. The length of the crest is around 6 – 7 times the wavelength and the wave height is more predictable. When high swell waves are observed around 5 – 6 waves of equal height can occur. However when swell waves are fairly low, propagation of equal height waves can be observed for up to more than a minute.

#### Wave elevation

The modelling of waves is done by means of the superposition principle where many simple regular harmonic waves are summarised as shown in figure: 2.5. Each of these waves has its own length, amplitude, period or frequency and direction of propagation. By doing so a very complex and irregular sea state can be composed with simple theory of regular waves. The representation of the surface elevation of a unidirectional random sea-state, or irregular sea, can be done by means of the relation defined in equation 2.6. The underscores indicate that these variables are now random variables [25].

$$\underline{\eta}(t) = \sum_{i=1}^N \underline{a}_i \cos(2\pi f_i t + \underline{\alpha}_i) \quad (2.6)$$

Where:

- $\underline{\eta}(t)$  = Wave elevation as function of time [m]
- $\underline{a}_i$  = Amplitude of the wave [m]
- $f_i$  = Frequency of the wave [Hz]
- $\underline{\alpha}_i$  = Phase of the wave [rad]
- $t$  = Time at which the wave elevation is evaluated [s]
- $N$  = a large number of frequencies [-]

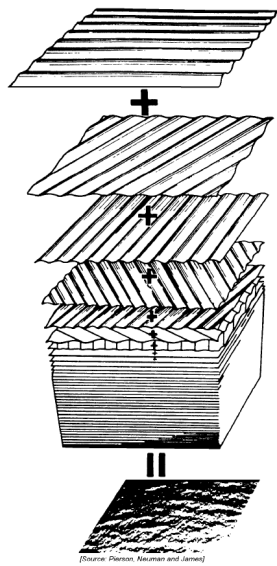


Figure 2.5: Superposition of Waves [22]

Alternatively equation 2.6 may also be written in the form of a Fourier series as illustrated in equation 2.7. Again the underscores indicate that these variables are random variables [26].

$$\underline{\eta}(t) = \sum_{n=1}^N \underline{a}_n \cos(\omega_n t) + \underline{b}_n \sin(\omega_n t) \quad (2.7)$$

Where:

- $\underline{\eta}(t)$  = Wave elevation as function of time [m]
- $\underline{a}_n$  = Fourier coefficient [m]
- $\underline{b}_n$  = Fourier coefficient [m]
- $\omega_n = \frac{2\pi n}{T}$  [rad/s]
- $T$  = Time interval over which the surface elevation is represented [s]
- $t$  = Time at which the wave elevation is evaluated [s]
- $N$  = a large number of frequencies [-]

### Wave spectra

The Joint North Sea Wave Project (JONSWAP) spectra defines the distribution of energy according to the frequency of the ocean. It is actually composed by the Pierson-Moskowitz spectrum and is supplemented with a peak enhancement function and is one of the most widely used spectra [25].

$$E_J(f) = E_{PM}(f) \cdot \gamma^{\exp\left[-\frac{1}{2}\left(\frac{f/f_p^{-1}}{\sigma}\right)^2\right]} \quad (2.8)$$

$$E_{PM}(f) = \alpha g^2 (2\pi)^{-4} f^{-5} \exp\left[-\frac{5}{4} \cdot \left(\frac{f}{f_p}\right)^{-4}\right] \quad (2.9)$$

with:

- $E_J(f)$  = JONSWAP spectrum energy as function of frequency [ $m^2/Hz$ ]

- $E_{PM}(f)$  = Pierson Moskowitz spectrum energy as function of frequency [ $m^2/Hz$ ]
- $\gamma$  = Peak-enhancement factor [-]
- $f_p$  = Frequency scale parameter [-]
- $\sigma$  = Peak-width parameter [-]
- $\alpha$  = Energy scale parameter [-]
- $g$  = Gravitational acceleration [ $m/s^2$ ]
- $f$  = Frequency [Hz]

### 2.2.3. Current

According to [22] there are several independent phenomena that are responsible for the presence of current which are:

- The ocean circulation system resulting in steady current
- The cyclical change in lunar and solar gravity causing tidal currents
- The presence of wind that results in a current
- Difference in seawater density's caused by differences in temperature results in currents

The governing current loads on the vessel are expected to come from surface currents, however a current velocity distribution as a function of depth can occur in shallow water. During this thesis it is assumed that the current velocity is constant and does not change with water depth, which is essentially a deep water assumption, the mean current loads can be calculated as follows:

$$F_{Xc}(\alpha_c) = \frac{1}{2} \cdot \rho \cdot V_c^2 \cdot C_{F_{X,c}}(\alpha_c) \cdot A_{TS} \quad (2.10)$$

$$F_{Yc}(\alpha_c) = \frac{1}{2} \cdot \rho \cdot V_c^2 \cdot C_{F_{Y,c}}(\alpha_c) \cdot A_{LS} \quad (2.11)$$

$$M_{Zc}(\alpha_c) = \frac{1}{2} \cdot \rho \cdot V_c^2 \cdot C_{M_{Z,c}}(\alpha_c) \cdot A_{LS} \cdot L \quad (2.12)$$

Where:

- $F_{Xc}$  = Force in longitudinal direction as function of current direction [N]
- $F_{Yc}$  = Force in transverse direction as function of current direction [N]
- $M_{Zc}$  = Moment of force around vertical axis at COG as function of current direction [Nm]
- $\rho$  = Density of water [ $\frac{kg}{m^3}$ ]
- $V_c$  = Current velocity [ $\frac{m}{s}$ ]
- $C_{F_{X,c}}, C_{F_{Y,c}}, C_{M_{Z,c}}$  = Dimensionless current force coefficients as function of current direction [-]
- $A_{TS} \approx B \cdot T$  = Submerged transverse projected area [ $m^2$ ]
- $A_{LS} \approx L \cdot T$  = Submerged lateral projected area [ $m^2$ ]
- $B$  = Beam of the ship [m]
- $L$  = Length between the perpendiculars of the ship [m]
- $T$  = Draught of the ship [m]

## 2.3. Hydrodynamics

As stated before vessels at sea are subjected to several forces which results into the motion of the vessel. In this section the forces due to waves are further elaborated on as the understanding of the ship movements due to these forces are of great importance while a ship is in DP mode. The sources [22], [27], [28] are used throughout the section. In general wave forces can be subdivided into the following two types:

- First order wave forces
- Second order wave forces
  - Difference of frequencies: Low Frequency Wave Drift Forces (LF WDF)
  - Mean Wave Drift Forces (M WDF)
  - Sum of frequencies: High Frequency Wave Drift Forces (HF WDF)

Where the second order wave force has three different contributions which are: mean wave drift, difference frequencies and sum frequencies. The HF WDF do not contribute significantly to the vessels motion and therefore also not on the DP station keeping of a vessel. Before the second order wave drift forces are treated, the first order wave forces are considered since they do have a big influence on the actual position of the vessel.

### 2.3.1. 1st order wave forces

First order motions have a zero mean and are not reacted upon by the vessels DP control system. This is due to the fact that these motions are of such a high frequency that either the thrusters are not fast enough to respond to these motions and if they would try it would cause too much wear and tear of the thrusters. The first order forces will however result in a significant motion which can be described by so called force Response Amplitude Operator (RAO).

$$F^{(1)}(t) = \sum_{i=1}^N RAO_i \cdot a_i \sin(\omega_i t + (\epsilon_i + \epsilon_{RAO_i})) \quad (2.13)$$

### 2.3.2. 2nd order wave forces

The total expression for the second order wave forces is:

$$\begin{aligned} \vec{F}^{(2)} = & -\frac{1}{2} \rho g \oint_{wl} \left( \zeta_r^{(1)} \right)^2 \cdot \vec{n} \cdot dl \\ & + \frac{1}{2} \rho \iint_{S_0} \left( \vec{\nabla} \Phi^{(1)} \right)^2 \cdot \vec{n} \cdot dS \\ & + \rho \iint_{S_0} \vec{X}^{(1)} \cdot \vec{\nabla} \frac{\partial \Phi^{(1)}}{\partial t} \cdot \vec{n} \cdot dS \\ & + m \cdot R^{(1)} \cdot \vec{X}_G^{(1)} \\ & + \rho \iint_{S_0} \vec{\nabla} \frac{\partial \Phi^{(2)}}{\partial t} \cdot \vec{n} \cdot dS \end{aligned} \quad (2.14)$$

Where the following contributions can be distinguished:

I: Relative wave height contribution:

$$-\frac{1}{2} \rho g \oint_{wl} \left( \zeta_r^{(1)} \right)^2 \cdot \vec{n} \cdot dl \quad (2.15)$$

II: Pressure drop due to velocity squared (Dynamic (Bernoulli) pressure integral):

$$+\frac{1}{2} \rho \iint_{S_0} \left( \vec{\nabla} \Phi^{(1)} \right)^2 \cdot \vec{n} \cdot dS \quad (2.16)$$

III: Pressure due to product of gradient of first order pressure and first order motion (moving body in oscillating pressure field):

$$+ \rho \iint_{S_0} \vec{X}^{(1)} \cdot \vec{\nabla} \frac{\partial \Phi^{(1)}}{\partial t} \cdot \vec{n} \cdot dS \quad (2.17)$$

IV: Contribution due to product of pitch motion and heave inertia force (Rotation of inertia forces):

$$+ m \cdot R^{(1)} \cdot \vec{\dot{X}}_G^{(1)} \quad (2.18)$$

V: Contribution due to the second order potential, which is zero in regular waves and in deep water (pressure integral of second order wave potential (set-down)):

$$+ \rho \iint_{S_0} \vec{\nabla} \frac{\partial \Phi^{(2)}}{\partial t} \cdot \vec{n} \cdot \quad (2.19)$$

### Quadratic transfer function

The surface elevation due to first order incoming undisturbed waves of an irregular sea state can be described as a summation of harmonic components as follows:

$$\zeta^{(1)}(t) = \sum_{i=1}^N \zeta_i^{(1)} \cdot \cos(\omega_i t + \tilde{\epsilon}_i) \quad (2.20)$$

The first order relative wave height at a point  $l$  on the waterline of the body can be written as:

$$\zeta^{(1)}(t, l) = \sum_{i=1}^N \zeta_i^{(1)} \cdot \zeta_{r_i}^{(1)'}(l) \cdot \cos(\omega_i t + \tilde{\epsilon}_i + \epsilon_{r_i}(l)) \quad (2.21)$$

When equation 2.21 is now substituted in equation 2.15 using two different waves the following is obtained:

$$\begin{aligned} F^{(2)}(t) &= \sum_{i=1}^N \sum_{j=1}^N \zeta_i^{(1)} \zeta_j^{(1)} P_{ij} \cdot \cos\{(\omega_i - \omega_j)t + (\tilde{\epsilon}_i - \tilde{\epsilon}_j)\} \\ &\quad + \sum_{i=1}^N \sum_{j=1}^N \zeta_i^{(1)} \zeta_j^{(1)} Q_{ij} \cdot \sin\{(\omega_i - \omega_j)t + (\tilde{\epsilon}_i - \tilde{\epsilon}_j)\} \end{aligned} \quad (2.22)$$

Equation 2.22 is called the Quadratic Transfer Function (QTF), where  $P$  is real valued and  $Q$  is the imaginary part of the QTF. The  $P$  matrix represents the contribution of the wave drift force which is in phase with the wave group while the  $Q$  matrix is the contribution to the wave drift force which is out of phase with the wave group. When the most elementary sea state is considered which consists of two regular waves with amplitude, frequency and a random phase of  $\zeta_1, \omega_1, \epsilon_1$  and  $\zeta_2, \omega_2, \epsilon_2$  with  $\omega_1 > \omega_2$  the surface elevation can be evaluated by:

$$\zeta(t) = \zeta_1 \cdot \cos(\omega_1 t + \epsilon_1) + \zeta_2 \cdot \cos(\omega_2 t + \epsilon_2) \quad (2.23)$$

The second order wave drift force in this case can be calculated with the following QTF:

$$\begin{aligned} F^{(2)}(t) &= \zeta_1^2 \cdot P_{11} + \zeta_2^2 \cdot P_{22} \\ &\quad + \zeta_1 \zeta_2 (P_{12} + P_{21}) \cdot \cos\{(\omega_1 - \omega_2)t + (\epsilon_1 - \epsilon_2)\} \\ &\quad + \zeta_1 \zeta_2 (Q_{12} + Q_{21}) \cdot \sin\{(\omega_1 - \omega_2)t + (\epsilon_1 - \epsilon_2)\} \end{aligned} \quad (2.24)$$

### Phasor representation of the QTF

Another way of evaluating the QTF is by means of phasor calculations [29]. When taking the amplitude of the wave equal to one, it is possible to represent the relative wave height of two waves as follow:

$$\left(\zeta_r^{(1)}(t, l)\right)^2 = \left(\overline{\zeta_{r1}} \cdot e^{-i\omega_1 t} + \overline{\zeta_{r2}} \cdot e^{-i\omega_2 t}\right)^2 \quad (2.25)$$

Expanding equation 2.25 gives:

$$\left(\zeta_r^{(1)}(t, l)\right)^2 = \overline{\zeta_{r1}}^2 \cdot (e^{-i\omega_1 t})^2 + 2 \cdot \overline{\zeta_{r1}} \overline{\zeta_{r2}} \cdot e^{-i\omega_1 t} e^{-i\omega_2 t} + \overline{\zeta_{r2}}^2 \cdot (e^{-i\omega_2 t})^2 \quad (2.26)$$

Using the mathematical rule for phasor multiplication:

$$A \cdot B = \frac{1}{2} (A \cdot B + A \cdot \overline{B}) \quad (2.27)$$

With  $\overline{B}$  is the complex conjugate of  $B$ , when using this expression the following is obtained:

$$\begin{aligned} \left(\zeta_r^{(1)}(t, l)\right)^2 &= \frac{1}{2} \overline{\zeta_{r1}}^2 + \frac{1}{2} \overline{\zeta_{r1}}^2 \cdot e^{-i \cdot 2\omega_1 t} \\ &\quad + \overline{\zeta_{r1}} \overline{\zeta_{r2}} \cdot e^{-i(\omega_1 + \omega_2)t} + \overline{\zeta_{r1}} \widetilde{\zeta_{r2}} \cdot e^{-i(\omega_1 - \omega_2)t} \\ &\quad + \frac{1}{2} \overline{\zeta_{r2}}^2 + \frac{1}{2} \overline{\zeta_{r2}}^2 \cdot e^{-i \cdot 2\omega_2 t} \end{aligned} \quad (2.28)$$

With  $\widetilde{\zeta_{r2}}$  being the complex conjugate of  $\overline{\zeta_{r2}}$ . When equation 2.28 is now substituted in equation 2.15 the QTF in phasor representation can be obtained.

## 2.4. Time domain model

In this section the basic equations required to model a vessel in the time domain are discussed. Through this section the following sources are used: [30], [22] and [31]. To model a motion of a body in the time domain the analogy of an mass damper spring system can be used. The most simplistic form of such a system is described as follows:

$$F(t) = m\ddot{x} + b\dot{x} + cx \quad (2.29)$$

where:

- $m$  = the mass of the system [ $\text{kg}$ ]
- $b$  = the damping of the system  $\left[\frac{\text{kg}}{\text{s}}\right]$
- $c$  = the spring stiffness of the system  $\left[\frac{\text{N}}{\text{m}}\right]$

When evaluating vessels in the time domain there are two extra components to account for which are: frequency dependent added mass and frequency dependent damping. When taking these components into account the Equation Of Motion (EOM) for the vessel will look as follows:

$$F(\omega, t) = (m + a(\omega))\ddot{x} + b(\omega)\dot{x} + cx \quad (2.30)$$

Added mass is the additional force necessary to accelerate the fluid particles surrounding the vessel when comparing the oscillation in air. The potential damping is the damping due to generation of waves by oscillation of the vessel, these oscillations withdraw energy from the motions of the vessel. Since equation 2.30 is frequency dependent it is not suitable for time domain simulations. Cummings [30] describes a way to make this EOM frequency independent making it suitable for time domain simulation. The EOM for all six modes of the vessel can be written as follows:

$$\sum_{j=1}^6 (M_{kj} + A_{kj}) \cdot \ddot{x}(t) + \int_0^\infty B(\tau) \cdot \dot{x}(t - \tau) \cdot d\tau + C \cdot x(t) = F(t) \quad (2.31)$$

with:

$$B(\tau) = \frac{2}{\pi} \cdot \int_0^{\infty} b(\omega) \cdot \cos(\omega\tau) \cdot d\omega \quad (2.32)$$

$$A = a(\omega) + \frac{1}{\omega} \cdot \int_0^{\infty} B(\tau) \cdot \sin(\omega\tau) \cdot d\tau \quad (2.33)$$

Where  $a(\omega)$  is valid for any value of  $\omega$ , and thus also for  $\omega = \infty$ . Meaning that  $A = a(\omega) = a(\infty)$ . It can now be seen that both  $A$  and  $B(\tau)$  are frequency independent and therefore the EOM equation 2.31 is frequency independent.

## 2.5. Frequency domain model

The reason why DP simulations should be done in the time domain instead of the frequency domain is because frequency domain analysis is considered to be unreliable since the DP control systems behaviour is highly non linear. This non linear behaviour is mainly due to the limitations of the thrusters, also referred to as thruster saturation. It is possible that when the thrusters already deliver 100% thrust the DP algorithm requires even more thrust to counteract the environmental forces. An analytical transfer function that includes saturation has not yet been found [9]. Figure 2.6 shows a comparison of a second order motion spectrum, calculated using a frequency domain transfer function, and two time domain simulations. One of the numerical time domain simulations includes thruster saturation and the other one excludes thruster saturation. From this graph it can be concluded that a wide range of frequencies are not represented well by the theoretical frequency domain calculation method.

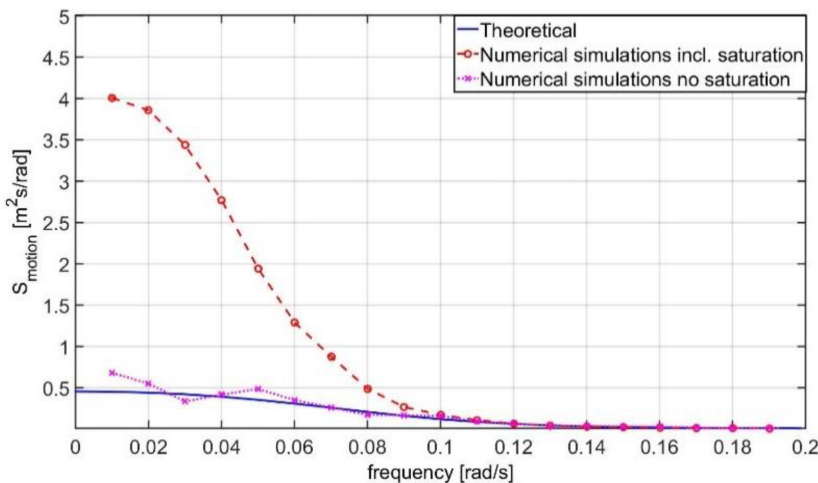


Figure 2.6: Second order motion spectrum comparison [9]

## 2.6. Static DP capability calculation

In this section some former research on static and quasi static DP calculation methods are discussed.

### 2.6.1. Wave drift multiplier

The research of Riaan van 't Veer [8] made a first step in accounting for the dynamic effects in static calculation methods by means of different factors for different dynamic contributions. In this research it was suggested that every environmental force should have its own DP factor and the magnitude of this factor was investigated for the 2nd order wave drift forces. This because the time varying component of the 2nd order wave drift forces relative to the mean was shown to be the biggest compared to wind and current, see figure 2.7. It was shown that this so called "wave drift multiplier" is sea-state dependent and for the investigated deep water drilling vessel, particular headings and sea state had a magnitude of 2. It was also concluded that the heading of the vessel can be maintained very well even in large sea states, therefor drift-off will occur before heading capability is lost. The wave drift multiplier was derived by means of time domain simulations.

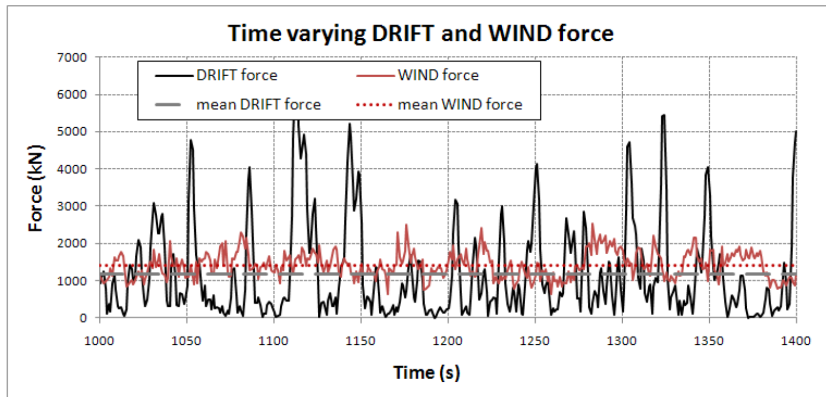


Figure 2.7: Time variable second order wave drift and wind forces [8]

### 2.6.2. Force multiplication factor

A followup research was performed by Wouter Antheunisse [9] where the possibility to include an offset requirement in static calculation methods was investigated. This was done by means of introducing a Force Multiplication Factor (FMF) for the second order wave drift forces. These FMF's were determined using time domain simulations and it was shown that these FMF's are dependent on vessel type, heading, sea state and maximum allowable offset. Also a relation was found between the impulse peak extreme, which is the maximum integral of the wave drift force and time-trace graph above the mean wave drift force, and the FMF's. This research was only executed for a deep sea drilling ship and therefore relatively large offsets between 20 – 100m. The sensitivity of the FMF's to the main dimensions of the vessel was not investigated making it difficult to conclude if these FMF's can also be used for other types of vessels.

## 2.7. Time domain DP capability simulation

In this section some former research on time domain calculations are discussed where also some quasi static comparisons are performed to increase the accuracy of static calculations.

### 2.7.1. The dynamic margin

Extensive research was done by Joost van der Weiden [32] to understand which dynamic effects are taken into account by the dynamic margin and how these effects influence the magnitude of the dynamic margin. Calculations were done using AnySim and the parameters that were varied between: -10%, -5%, +5%, +10% are:

- Mean wind speed
- Significant wave height
- Mean wave peak period
- Mean current velocity
- PID gains of the DP controller
- The mechanical response time

The biggest influence found was the change of the mean current velocity, by increasing the mean current velocity with 10% the DP capability reduced the most when evaluating the critical Wind, Wave and Current (WWC) direction. Another analysis was executed were the effect on the dynamic margin by switching parameters on and off was investigated. The following phenomena were switched on and off:

- Wind feed-forward
- Thruster-thruster interaction
- Thruster-hull interaction
- Thruster-current interaction
- Wind speed spectrum (NPD, Harris and Davenport)
- Wind speed directions spectrum (Gaussian)

It was found that by switching the thruster-current interaction on the biggest influence was obtained, the dynamic margin decreased with 6% for the most critical Wave, Wind and Current direction. It was also observed that superposition of single contributions that were tested in the research of van der Weiden do not give a correct dynamic margin. Therefore the superposition principle does not hold for all of the single contributions of the tested dynamic parameters.

Another parameter investigated proved to have a major influence on the dynamic margin. This parameter is the offset in surge and sway direction as is depicted in figure 2.8, the offset for yaw was not investigated. In this research it was stated that the influence on the dynamic margin by the offset requirement was relatively constant for all WWC-directions unlike the behaviour of the other tested parameters. It was also shown that with different offset criteria the influence on the dynamic margin by the mechanical response time also differed. The influence of other parameters when changing the offset requirement was not investigated.

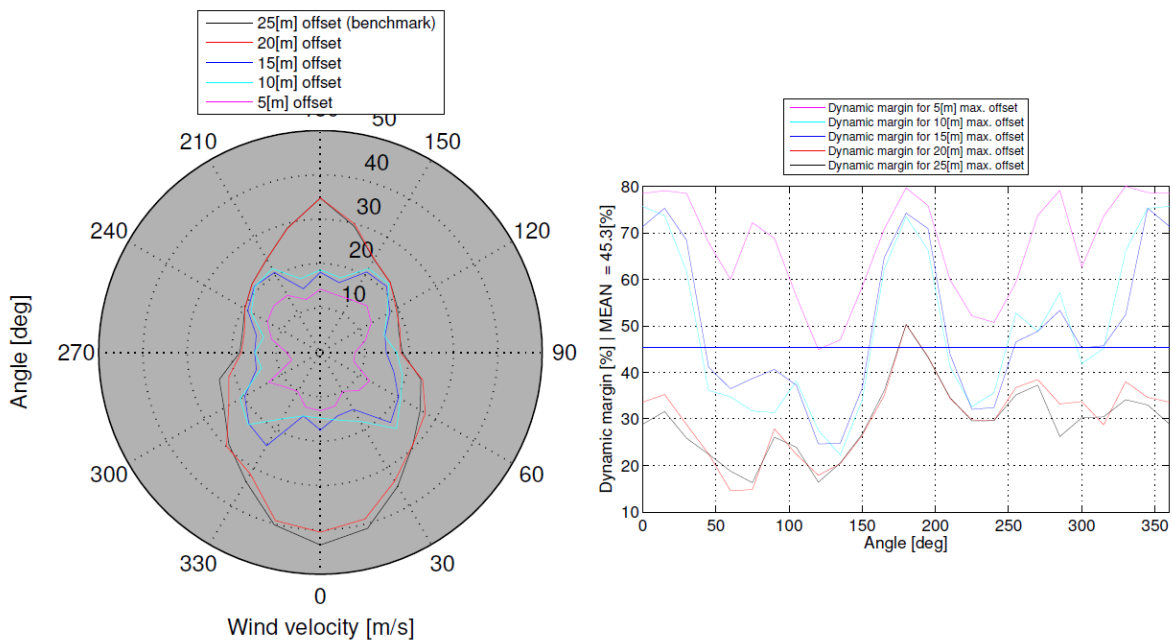


Figure 2.8: Dynamic margin for different offsets [32]

### 2.7.2. DP capability for different operational activities

The research of Cedric Brun et al [33] was focused on DP capability in different operational activities where different influences are present, the three influences that were investigated are:

- Hulls vicinity influence
- Shallow water influence
- Pipe-laying loads influence

#### Hull vicinity influence

Here an Floating Production Storage and Offloading (FPSO) vessel next to a DP assisted floatel is considered as illustrated in figure 2.9. The DP assisted floatel is connected to the FPSO through a gangway to transfer people from and to the FPSO. During this research the FPSO was assumed to have very low heading with respect to wind and current, this means that the shielding effect is not considered. Hydrodynamic calculations have been carried out to asses the interaction between the two hulls due to the proximity. It was shown that the interaction changes the low-frequency loads which have to be compensated by the DP system. The comparison of wave drift loads between the DP assisted floatel alone (single body), the DP assisted floatel side by side with the FPSO (multi-body) and the specifications from the DP manufacturer is illustrated in figure 2.10 for head and beam seas.

Needless to say is that the difference in wave drift loads results in a different DP capability of the vessel, which is shown in figure 2.11

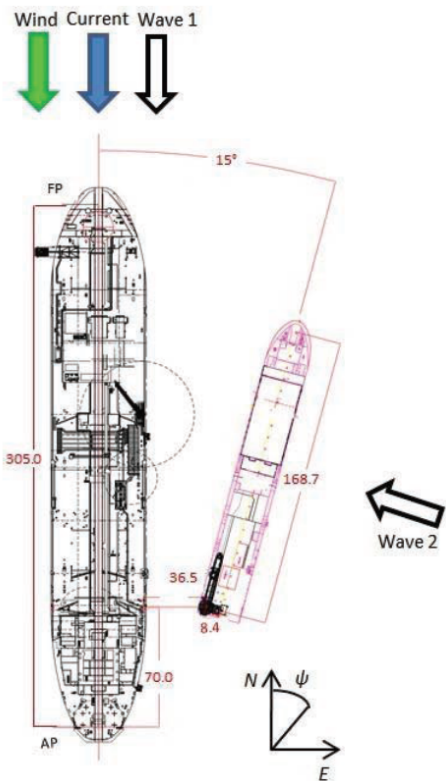


Figure 2.9: Hull vicinity influence layout [33]

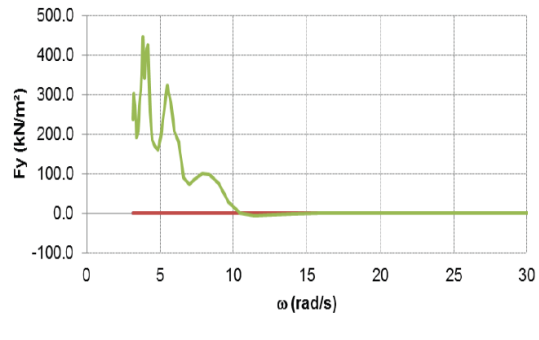


Fig. 9. Transverse drift loads for head sea

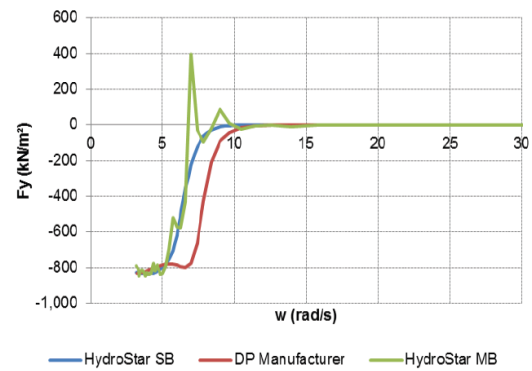


Figure 2.10: Hull vicinity drift loads influence for head and beam seas [33]

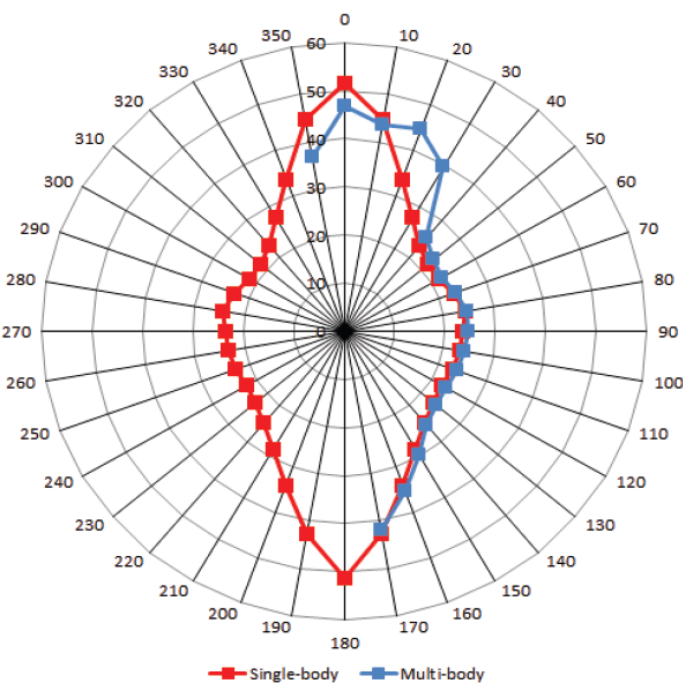


Figure 2.11: DP capability hull vicinity influence [33]

### Shallow water influence

The second operation that was considered is when the same DP assisted floatel is operating in shallow water on its own, this because shallow water affects the low-frequency loads. In figure 2.12 a comparison of the loads specified by the DP manufacturer, loads including the water-depth influence (w/ WD) and the loads excluding the water-depth influence (w/o WD) have been made. It can be seen that these loads differ and therefore the DP capability of the vessel will also be different as seen in figure 2.13.

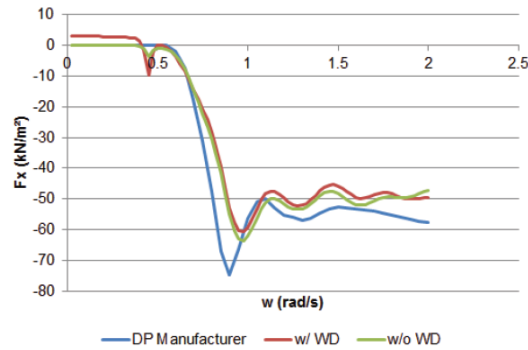


Fig. 12. Longitudinal drift loads for a 60° wave heading

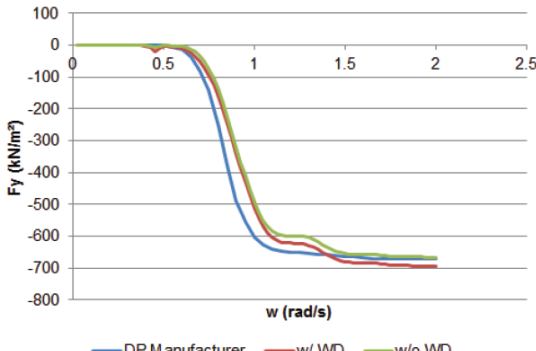


Fig. 13. Transverse drift loads for a 60° wave heading

Figure 2.12: Shallow water influence on drift loads [33]

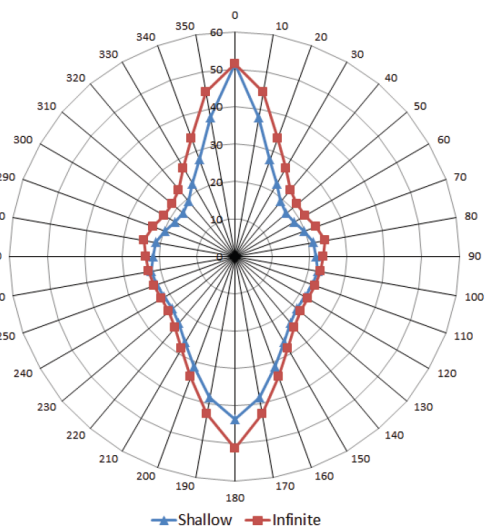


Figure 2.13: Shallow water influence on DP capability [33]

### Pipe-laying loads influence

The third operation that was considered is pipe-laying using a DP assisted vessel. Here the effect of the pipe hanging down at the aft of the ship on the DP capability of the vessel was investigated. The load of the pipe is considered to be a constant restoring force, acting astern in surge direction. The influence of this restoring force is illustrated in figure 2.14. It can be seen that the vessel has a lower capability during pipe-laying operation from environmental loading coming from head direction. However the DP capability is improved for astern environmental loads.

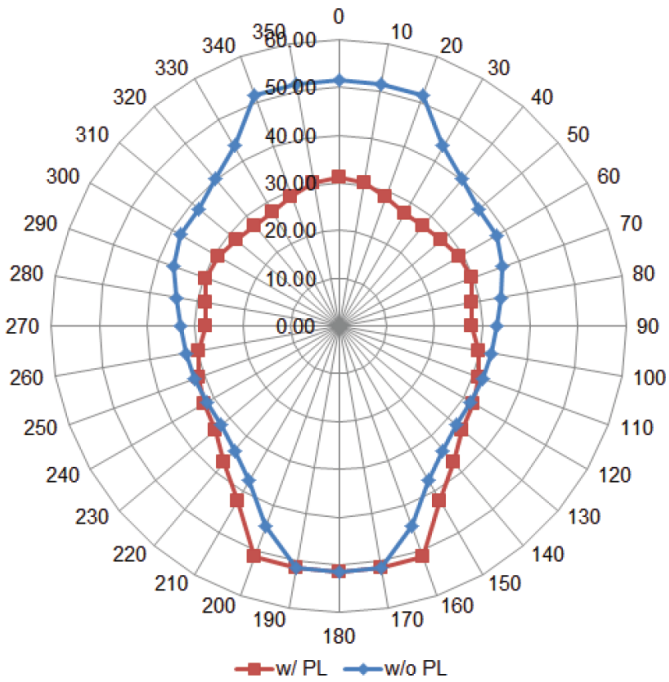


Figure 2.14: DP capability pipe-laying influence [33]

## 2.8. Comparison different DP capability methods

When performing DP calculations multiple methods can be used as stated before. In this section literature that compares static and dynamic calculation methods are discussed and are also compared with model tests.

### 2.8.1. Hyun-Joe Kim

Hyun-Joe Kim et al. did a comparison study between static calculations, time domain simulations and model testing. This research was done for a shuttle tanker in full load and ballasted condition and the DOF that was observed was only the heading (yaw angle) of the vessel [34]. For the static calculations two scenario's were distinguished, one with a maximum of 80% thruster usage and one with 100% thruster usage to illustrate the dynamic margin widely used throughout the industry. From the results depicted in figure 2.15 it can be seen that the model tests were shown to be the most conservative. The resulting heading window is the window where the vessel can still maintain heading. If the heading angle becomes larger or smaller than the given limits the vessel will not be able to return to the required heading.

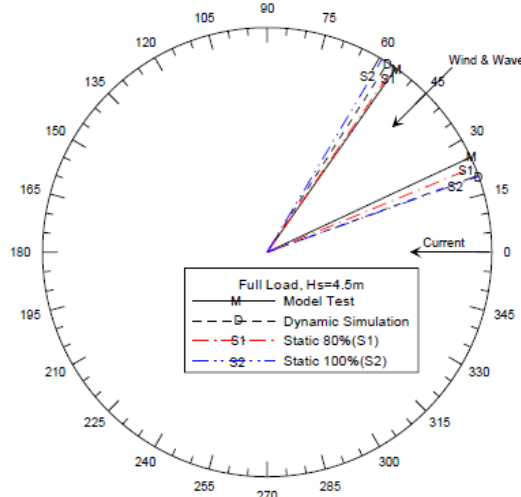


Fig. 8 Heading Window Results in Full Load Condition (Env.1)

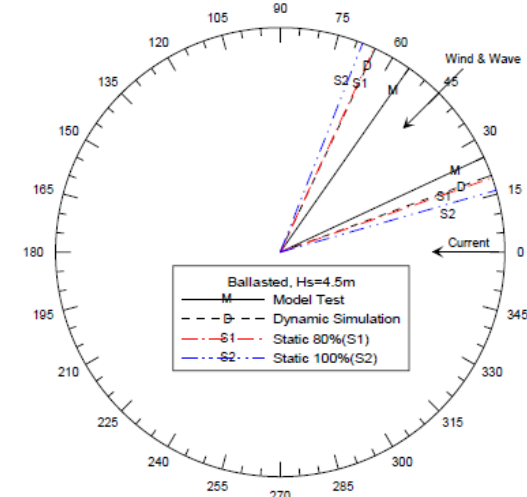


Fig. 10 Heading Window Results in Ballasted Condition (Env. 1)

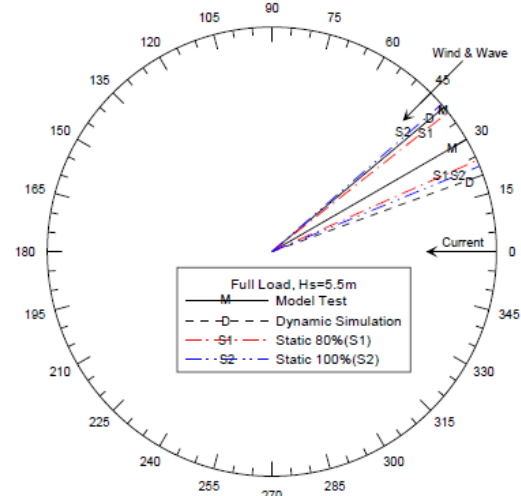


Fig. 9 Heading Window Results in Full Load Condition (Env.2)

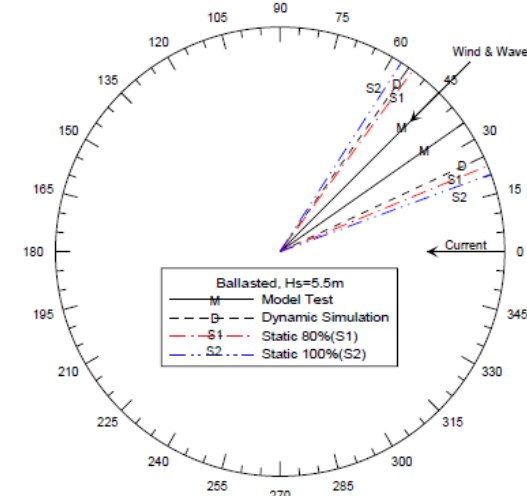


Fig. 11 Heading Window Results in Ballasted Condition (Env. 2)

Table 5. Heading Window Results in Full Load Condition

Analysis Methods	Heading Window (deg.)			
	Environment 1		Environment 2	
	Min.	Max.	Min.	Max.
Model Test	25.0	55.0	30.0	40.0
Dynamic Analysis	20.0	57.5	20.0	40.0
Static 80%	22.33	55.57	24.0	38.36
Static 100%	19.73	59.25	22.39	41.0

Table 6. Heading Window Results in Ballasted Condition

Analysis Methods	Heading Window (deg.)			
	Environment 1		Environment 2	
	Min.	Max.	Min.	Max.
Model Test	25.0	55.0	35	45
Dynamic Analysis	20.0	65.0	25	55
Static 80%	19.36	65.29	22.45	53.76
Static 100%	16.0	68.49	20.15	57.32

Figure 2.15: Heading window comparison results [34]

### 2.8.2. Liping Sun

Liping Sun et al. performed a similar research as Hyun-Joe Kim where static and dynamic calculation methods were compared for a deep water pipe-lay crane vessel [35]. The focus of this research was however on the total thrust utilisation. It was shown that the thruster utilisation in time domain simulation is higher than when performing a static calculation as is illustrated in figure 2.16.

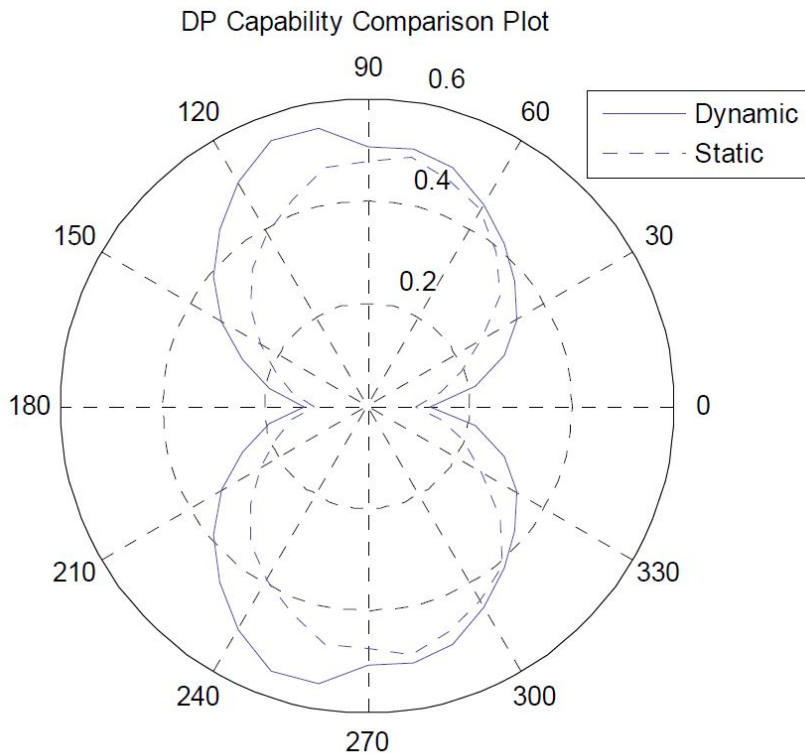


Figure 2.16: Thruster utilisation comparison [35]

## 2.9. DP calculation tools

In this section the tools used for calculating DP capabilities are discussed. Although there are multiple commercially available packages to perform DP calculation only two are briefly discussed in this section.

### 2.9.1. DPlab

Damen Shipyards developed their own DP capability calculation tool called DPlab. At first this tool was programmed in excel but from the beginning of 2014 the tool was improved and programmed in MATLAB where a Graphical User Interface (GUI) was included to simplify the visualisation of the results. The tool is capable of producing DP-capability plots for a particular vessel and environmental condition. The WWC forces are calculated using a static calculation method after which the required thrust for the vessel to remain position is calculated. The required thrust is distributed over the thrusters using a mathematical solver to minimise the total required thrust. The input parameters required when performing a calculation in DPlab are listed in appendix D.

#### Coordinate system definition

The coordinate system used in DPlab is illustrated in figure 2.17. In DPlab wind, waves and current directions are specified as "**coming from**". When an environmental angle of 180 degrees is elaborated on it is meant that the environmental forces are coming from 180 degrees.

### 2.9.2. aNySIM

aNySIM is a time domain simulation program developed by MARIN for the analysis of multibody dynamics in offshore operations. The fast-time simulations are able to capture the response of the bodies due to the mechanic and hydromechanic forces that are calculated by the program. aNySIM is suitable for the analysis of terminal availability, operability of lifting operations, dynamic positioning performance, mooring fatigue and other applications. More info on the program aNySIM can be found in appendix E.4.

### Coordinate systems

The Coordinate System used in aNySIM is the ENU-system sign convention(East-North-Up) and is shown in figure 2.18. The Wind, Wave and Current directions in aNySIM are specified as “**going to**”. It is immediately clear that this differs from DPlab which is not very convenient when using both methods in the same report. The conventions used in this thesis for the aNySIM results are as follows. The coordinate system of aNySIM will remain unchanged making it immediately visible if the results are generated by DPlab or aNySIM. The Wind, Wave and Current directions are shown as “**coming from**” just as with DPlab. A table is constructed to convert angles from the different axis systems and conventions which can be seen in table E.5.

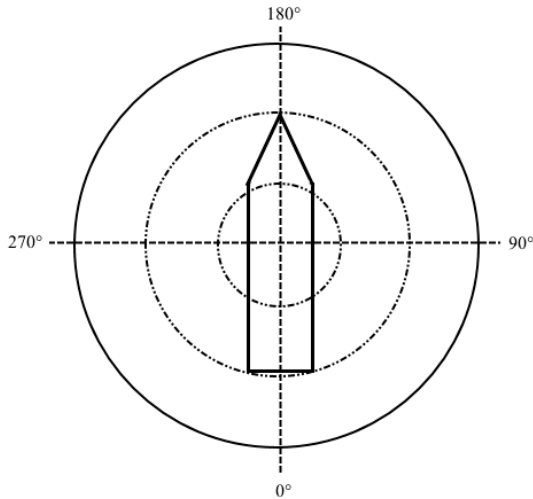


Figure 2.17: Coordinate System DPlab

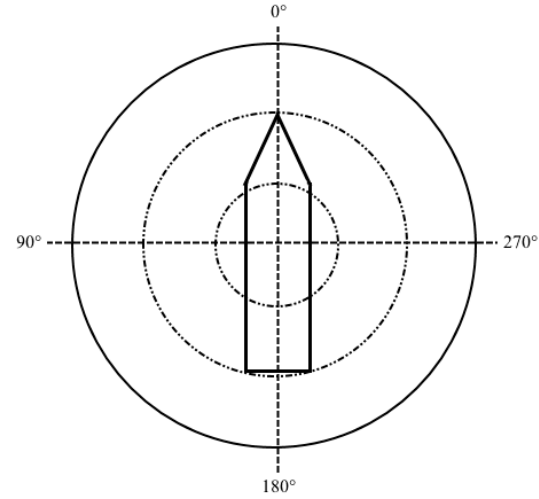


Figure 2.18: Coordinate System aNySIM

## 2.10. DP design process

In this section the design cycle of the Bibby Wavemaster 1 is briefly elaborated on. Since this vessel was under development for multiple years the tools used for DP calculation changed over time. In figure 2.19 a schematic thruster layout of the Bibby Wavemaster 1 is shown.

### 2.10.1. Excel sheet

The first DP capability calculation done for the Bibby Wavemaster 1 was performed using an excel sheet. In this sheet the hydrodynamic database of the PSV3300, once provided by MARIN for another project, is made dimensionless so it can be used for the Bibby. Using this dimensionless database and the JONSWAP wave-spectrum, with specified  $T_{mean}$ ,  $H_s$  and  $\gamma$ , the mean wave drift forces for each heading are calculated. The current forces acting on the vessel are calculated using the current coefficients of the PSV3300 and by using the formulas as explained in section 2.2.3. The wind forces acting on the vessel are calculated with dimensionless coefficients taken from brix figure I.13. The next step is to define the thrusters, it should be stated where they are positioned and how much thrust they can generate. After this a static equilibrium can be calculated to determine if the thrusters can withstand the environmental loads.



○ Azimuth / Retractable Thruster

◇ Bow Thruster

Figure 2.19: Schematic thruster layout Bibby Wavemaster 1

### 2.10.2. DPLab

The excel sheet DP capability tool was expanded and turned into a MATLAB executable tool. Here still the hydrodynamic database of the PSV3300 was used to calculate the mean wave drift forces as well as the current coefficients of the PSV3300. For the most recent DP capability calculation the wind coefficients are still taken from brix but a different relations were used throughout the process of which the latest is figure I.6. In DPLab a solver is implemented that calculates the minimum total thrust required to obtain a static equilibrium, by doing so the most optimal thruster utilisation is obtained.

### 2.10.3. aNySIM

Since not only the capability of the vessel is required but also the station keeping during people transfer operations aNySIM simulations were performed during October 2014 and again in January of 2015. The main purpose of these calculations is to check whether the vessel can stay within a certain offset and heading. These output parameters cannot be obtained by means of a static calculation.

### 2.10.4. DOLPHIN real-time simulator

The operational profile of the Bibby Wavemaster is a combination of the station keeping of the vessel and the walk to work bridge. Since the walk to work bridge cannot be included in the aNySIM simulations another simulation tool was used for specifically this purpose. In the DOLPHIN simulator the model of the vessel and the bridge are combined together with the DP control system of Kongsberg as installed on the vessel. This enables Damen to test the complete system on-board of the vessel already in the office.

### 2.10.5. Model tests

After performing multiple simulation with aNySIM and the DOLPHIN real time simulator also model tests were done to check the transit time between two windmills in DP mode. This is done to avoid the half hour filling of the Kalman filter when servicing multiple windmills in a row. During the model tests the Kongsberg DP system as installed on board of the actual vessel was used to obtain results as reliable as possible.

## 2.11. Types of uncertainty

Uncertainty is often referred to as the absence of exact knowledge however, it can also be stated that it is a situation of inadequate information, Refsgaard [36], Funtowicz and Ravetz [37]. Another thing to realise is that uncertainty can also prevail in situations where there is already a lot of information available. That said increasing the amount of new information can decrease but also increase the level of uncertainty. This can be explained by the fact that new information may reveal the presence of uncertainties which were previously understated or unknown, Walker et al [38]. This shows that more information may reveal the understanding of the system is less than thought or the system is more complex than it was thought of beforehand.

When considering mathematical models, several uncertainty-sources can be distinguished which all contribute to the uncertainty of the model output. Schulten and Stapersma [39] composed a list of possible uncertainty sources that should be kept in mind:

- Theory uncertainty
- Model uncertainty
  - Model structure
  - Model detail
  - Extrapolation
  - Model resolution
- Parametric/data uncertainty
  - Input variable uncertainty
  - Model parameter uncertainty
  - Physical parameter uncertainty
- Measurement uncertainty

### 2.11.1. Theory uncertainty

With theory uncertainty the physical principles of the mathematical model are meant. Well known physical principles are for instance Newton's law, the ideal gas law and the conservation of mass, energy

and momentum. When modelling on meso scale these principles can be considered to be certain. However, when modelling more on a micro scale such as quantum mechanics, theory uncertainties can play a role of significance. One of the things often used in engineering are empirical laws. Whether these are uncertain depends on the application and allowed range of the specific law but also the used parameters. These are however already considered in the parameter uncertainty.

### 2.11.2. Model uncertainty

Models are by definition a simplified representation of the reality, this therefore results in an additional source of uncertainty. The causes of model uncertainty can be divided into four categories:

#### 1. Model structure

With the model structure is meant the assumptions and physical principles that were used when creating the model. When other models are also available uncertainty can arise when these other models give different results. When combined with data the model assumptions can be assessed and compared which might result to the discarding the worst performing model.

#### 2. Model detail

As stated before models are by definition a simplified representation of the reality. This is mostly done to decrease the amount of simulation time. The uncertainty can be found when comparing a simplified model with a less simplified model which describe the same process. An example is calculating the resistance of a ship which can be done by only the drag coefficient of the ship or by also taking into account viscous and wake effects.

#### 3. Extrapolation

When a model is designed such that it performs well for a certain operational window it does not necessarily mean that it performs with the same uncertainty when the model is used outside these boundaries. When it is looked at for instance static DP capability calculation methods, the amount of thrust used is always calculated in limiting environmental conditions. It could be that the same assumptions in the model are no longer true when looking at non limiting environmental conditions.

#### 4. Model resolution

The model resolution usually dictates the trade-off between accuracy and computation time. The higher the resolution, the lower the uncertainty will be. An example for instance a Finite Element Method (FEM) analysis of a vessel hull, the chosen grid determines the uncertainty in the output of for example stresses and deformation.

The estimation of model uncertainty is not really easy to achieve. The model detail, resolution and extrapolation uncertainty can be somehow easily estimated when the model outputs are compared for more detail, higher resolution and a wider operating range. However, determining the model structure uncertainty might prove to be very difficult. To obtain a satisfying result all the physical en technical assumptions of the model should be recognised, thereafter all possible alternative assumptions should be implemented and compared. This proves to be virtually impossible and therefore the model structure is normally accepted or rejected in the validation phase.

### 2.11.3. Parameter and variable uncertainty

For parameter and variable uncertainty three different categories are distinguished which are: Input variable uncertainty, physical parameter uncertainty and model parameter uncertainty.

#### 1. Input variable uncertainty

Consider the fictional model shown in figure 2.20. Both sub-models share the input variables  $x_s$  with associated uncertainties. The models also have a number of inputs that are unique to a certain sub-model namely  $x_A$  and  $x_B$ , which also have their own uncertainty. The last variables that need to be considered are the output variables from one sub-model that serve as input to another sub-model namely  $y_A$  and  $y_B$ . What can be seen from this is that if only  $x_A$  has a uncertainty, this uncertainty can travel through the model by means of  $y_A$  and therefore both outputs  $r_A$  and  $r_B$  will be uncertain.

## 2. Physical parameter uncertainty

These parameters are associated with for instance physical dimensions, material properties etc. Most of the time they can be measured and remain constant during a simulation.

## 3. Model parameter uncertainty

Model parameters are a result of the assumed physical model. The main difference between model parameters and physical parameters is that physical parameters always exist since they are associated with physical objects and therefore always exist. However model parameters only exist because of the model, also they cannot be directly measured but one has to deduce them using measurements.

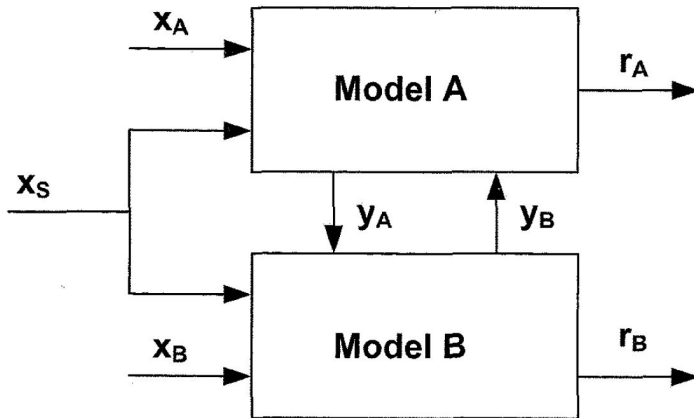


Figure 2.20: Relation between two sub-models [39]

### 2.11.4. Measurement uncertainty

To be able to validate the designed model and its outputs, extensive measurements need to be done which introduces another source of uncertainty. When enough measurements are performed and available the uncertainty can be determined using statistical methods. If no data or measurements are available the opinion and experience of experts can be used to determine a certain input. This could however lead to an error which is bigger when performing a measurement.

## 2.12. Uncertainty calculation methods

In this thesis only input parameter uncertainty is considered, therefore two methods able to calculate those are treated below. The main difference between the two is that one method is relatively quick and only needs a few calculations but is limited to linear models or models that can be linearised on the specific point up for consideration. The other one is more comprehensive and can deal with non linear models. However for this method a lot more calculations are required.

### 2.12.1. Linear uncertainty calculation

The input uncertainty is based on two different parameters namely: the mean and the standard deviation. The normalised input uncertainty is defined as:

$$\sigma_x^* = \frac{\sigma_x}{\mu_x} \quad (2.34)$$

With:

- $\sigma_x^*$  = normalised input uncertainty
- $\sigma_x$  = input standard deviation
- $\mu_x$  = mean input value

Now the normalised output uncertainty can be defined as:

$$(\sigma_z^*)^2 = \sum_i \left( \frac{\partial z^*}{\partial x_i} \right)^2 \cdot (\sigma_{x_i}^*)^2 \quad (2.35)$$

Where:

$$\frac{\partial z^*}{\partial x} = \frac{\partial z}{\partial x} \cdot \frac{x_0}{z_0} \quad (2.36)$$

With:

- $\sigma_z^*$  = normalised output uncertainty
- $\frac{\partial z^*}{\partial x}$  = normalised sensitivity
- $x_0$  = nominal input value
- $z_0$  = nominal output value

Equation 2.36 is referred to as the normalised output sensitivity, it states how much the output of interest changes when a certain input is changed. When using the normalised form a more intuitive interpretation can be made since then it can be seen how much percent the output changes if the input changes with a certain percentage.

### 2.12.2. Combined uncertainty calculation

Sometimes it is required that a uncertainty is calculated for a parameter that consist out of more than one variable, each with their own mean and standard deviation. This means that the calculation of the mean and standard deviations requires some extra attention. The calculation of these combined means and standard deviations is explained below.

#### Combined mean calculation

Let's consider the dimensionless parameter  $\frac{L}{B}$  which consist out of 2 variables namely  $L$  and  $B$ , which have mean values of:  $\mu_L$  and  $\mu_B$ . In general when multiplying, adding or dividing these variables the same can be done for their means [40]. Here the mean of  $\frac{L}{B}$  denoted with  $\mu_{\frac{L}{B}}$  is calculated as follow

$$\mu_{\frac{L}{B}} = \frac{\mu_L}{\mu_B}.$$

#### Combined standard deviation calculation

Again let's consider the the dimensionless parameter  $\frac{L}{B}$  which consist out of 2 variables namely  $L$  and  $B$ , which have standard deviations of:  $\sigma_L$  and  $\sigma_B$ . Since the standard deviation of the dimensionless parameter  $\frac{L}{B}$ , denoted by  $\sigma_{\frac{L}{B}}$ , cannot be calculated in the same way as the mean a variable called the relative uncertainty is defined as [40]:

$$\sigma_x^* = \frac{\sigma_x}{\mu_x} \quad (2.37)$$

with  $\mu_x$  the mean of parameter of interest. When multiplying or dividing relative uncertainty the following equation can be used [40].

$$f = x \cdot y \quad \text{or} \quad f = \frac{x}{y} \quad \sigma_f^* = \sqrt{\sigma_x^{*2} + \sigma_y^{*2}} \quad (2.38)$$

It is now possible to calculate  $\sigma_{\frac{L}{B}}$  by rewriting equation 2.37 and substitute  $\frac{L}{B}$ . In the same way the standard deviation of  $\frac{B}{T}$  and  $C_B$  can be calculated.

$$\sigma_{\frac{L}{B}} = \sigma_{\frac{L}{B}}^* \cdot \mu_{\frac{L}{B}} \quad (2.39)$$

### 2.12.3. Non linear uncertainty calculation

For non linear uncertainty calculation more comprehensive methods are required like for instance sampling. One of the most well known sampling methods is the Monte Carlo Simulation (MCS). With MCS the inputs of a model are not quantified as a single value but instead a probability distribution is used. Every input that has an uncertainty can have its own probability density distribution. For each calculation a sample is drawn from all the different input variable distributions and these values are used to calculate the model with. This is repeated multiple times depending upon the number of uncertainties, but also the ranges that are specified for them. A MCS could involve thousands or sometimes even tens of thousands of recalculations before it is complete but when finished it has produced a distribution of possible outcomes.

## 2.13. Sensitivity

Mathematical models are mostly designed to approximate various complex phenomena of which examples are: engineering, economic, physical, social and environmental. The development of these models is divided in several steps where one of these steps should always be determining the parameters which are most influential on the output of the model. This analysis is called a sensitivity analysis and is a way to validate the model but can also serve as a guide for future research. A sensitivity analysis can be conducted for several reasons [41] including:

- Identify which parameters require additional research to increase the knowledge base and thereby reducing the output uncertainty.
- Identify which parameters are insignificant and as a result might even be removed from the model
- Identify which inputs have the biggest contribution to the output variability
- Identify which inputs are mostly correlated with the output
- Identify what the resulting model consequences are when changing a given input parameter

Conducting a sensitivity analysis can be done in many different ways however, various analysing methods may produce different results if little care is taken when choosing a suited method for a specific situation [42]. A selection of different practical sensitivity methods are briefly explained, where practical means the calculational ease and usefulness of the results is taken into account.

### 2.13.1. Differential sensitivity analysis

Differential Sensitivity Analysis (DSA), also known as the direct method, is elaborated on first since this method proves to be the backbone of most other sensitivity analysis techniques. This method can be used to solve simple partial derivatives but also spatial and temporal analysis can be performed. Sensitivity in its most general form is basically the ratio of the change in output to the change in input while all other parameters remain constant [41]. This is always done with respect to a base case where all model parameters are set to their mean. DSA is most applicable for calculating small input deviations around this base case, often plus or minus one percent. The definition of the DSA is as follow:

$$\frac{\partial z^*}{\partial x} = \frac{\partial z}{\partial x} \cdot \frac{x_0}{z_0} \quad (2.40)$$

#### Advantages

DSA is relatively easy to apply and is especially useful when a high degree of certainty is desired around the base case scenario.

#### Disadvantages

DSA does not take into account the whole possible range of input values. Therefore no relations regarding global sensitivity can be constructed. When DSA is performed on non linear models the fault margin increases making it less reliable.

### 2.13.2. Nominal range sensitivity analysis

The Nominal Range Sensitivity Analysis (NRSA) is used for local sensitivity analysis [43] and can also be referred to as the sensitivity index (SI) [41]. Two choices are available for determining the effect of varying the model inputs namely: varying inputs over their entire range or using plausible values only. This method is used to determine the effect of changing one input parameter at a time only and can be repeated for any number of input parameters. The NRSA results are most valid when using a linear model and when applied with this condition it is possible to rank the input parameters to the order of relative importance. The definition of the NRSA is as follow:

$$Sensitivity_{NRSA} = \frac{Output_{max\ input} - Output_{min\ input}}{Output_{nominal\ input}} \quad (2.41)$$

#### Advantages

NRSA is a relatively simple method that is easily applied. It works well when the model is linear and if a good idea of a plausible range for each input is known beforehand.

#### Disadvantages

NRSA does not address the whole space of potential input values since interactions between inputs are difficult to capture using this method. Combined effects due to simultaneous changes in multiple input parameters are not shown by the NRSA if the model is non linear. Therefore rank ordering for other than linear models using the NRSA will be unreliable.

### 2.13.3. Pearson Correlation Analysis

The Pearson product-moment Correlation Analysis (PCA) is part of the correlation analysis methods. A correlation analysis is able to measure the strength of a relationship between an input and its output. The PCA specifically can be used to determine the strength of a linear relationship between an input and the output [44]. The correlation coefficient can range from -1 to 1 where a correlation coefficient of 0 states that there is a lack of correlation. The types of data that can be used in the PCA are: interval or ratio scale [45]. For more information about data types see Appendix B.

#### Advantages

Relatively easy to compute and widely available in commercial software packages.

#### Disadvantages

The PCA is only useful for linear models. Furthermore a correlation does not necessarily implies causation. Direct interaction between the inputs can not be dealt with.

### 2.13.4. Spearman's correlation analysis

The Spearman's rank-order Correlation Analysis (SCA) is closely related to the Pearson Correlation Analysis. Both these methods determine correlation meaning they measure the strength of a relationship between an input and its output [44]. The SCA measures the strength of a monotonic relationship between two variables, this enables the SCA to also account for non linear monotonic relations between input and output. More information on monotonic relations is found in Appendix B. The data types that can be used for SCA are: ordinal, interval or ratio.

#### Advantages

Relatively easy to compute and widely available in commercial software packages. SCA can deal with non linear relationships as long as the input-output relation is monotonic.

#### Disadvantages

A correlation does not necessarily implies causation. Direct interaction between the inputs can not be dealt with.

# 3

## Methodology

*This chapter starts with the general plan of approach used to execute the research. A division is made in a static and a dynamic part including the different design stages the vessel can be in. Next the dimensional analysis performed during the static part to calculate the output uncertainty is discussed. For the dynamic part of the analysis first the model used is briefly discussed after which a small introduction to machine learning is made. The method used to create a model for the purpose of determining the output uncertainty is discussed and the justification methods used to determine why this model is accurate enough to determine uncertainty*

### 3.1. General plan of approach

To be able to perform this research several steps are to be taken by the author, first of all basic knowledge of DP systems was gained mainly by acquiring literature. DP applications were described and the main components present in a DP vessel were investigated. The environmental forces acting on the vessel during DP were elaborated on and the distinction between first and second order waves forces was touched up on. Former research on DP was studied to set the boundaries of this research and determine where value could still be added.

The difference between sensitivity and uncertainty was extensively explained and different methods to asses sensitivity and uncertainty were discussed. After selecting the preferred methods know how of the static simulation program DPlab and the dynamic simulation program aNySIM was gained. Test cases were developed and analysed to fully understand the operation of the different programs. An overview of inputs and outputs was constructed for both simulation programs to generate insight in the data that could be obtained.

Multiple scripts were written including but not limited to: a script for running batch simulations in DPlab which is normally operated using a GUI. Scripts to determine sensitivity, make tornado plots and generate windrose plots for several purposes. Also an input file generator for aNySIM was programmed and a script to run multiple aNySIM simulations in parallel, something that was not built in the software functionality itself. Furthermore scripts to extract the required output from the aNySIM time series were programmed and a script to determine the required time step for the simulations.

As stated before, two different simulation methods are distinguished which are: static and dynamic. For both these simulation methods the sensitivity, input and output uncertainty are the points of interest. When evaluating static and dynamic simulations the considered outputs will differ and are described in appendix D and E. The input uncertainty is acquired by gathering historical data on the Bibby Wavemaster 1 that was used throughout its design period. When designing a vessel, three different design stages are defined and listed in table 3.1, the input uncertainty will adjust accordingly.

Table 3.1: Design stages

Design	Explanation
Conceptual	Design stage with very big geometrical changes, typically a complete new product
Preliminary	Small changes in geometrical dimensions and on board systems will still occur
As built	Complete geometrical dimensions and on board systems of the vessel are known

The aim is to determine the output uncertainty of both simulation methods so it can be assessed whether incorporating these uncertainties should be done in the future. This analysis will serve as a guide that shows which input data needs to be more certain, during a specific design stage and for a specific heading, to reduce the uncertainty in the output of DP calculations. Using this it will also quickly enable naval architects to improve Dynamic Position performance for the heading that is most desirable.

## 3.2. Static DP analysis

For the static part of the uncertainty analysis the method from chapter 2.12.1 is used. The benefit of this method is that it is relatively easy and fast to apply and gives an indication of which parameter has the most influence on the output uncertainty of the vessel. For this method the input uncertainty of the data needs to be determined and the sensitivity of the model should be calculated after which the output uncertainty can finally be assessed. The output of interest in the static DP analysis is the capability of the vessel expressed in  $\frac{m}{s}$  of wind speed. The corresponding wave height can be found in table: D.7 and the current velocity is always kept constant at 0.75  $\frac{m}{s}$ .

### 3.2.1. Sensitivity analysis parameter variation

The sensitivity method required for the chosen uncertainty method is the Differential Sensitivity Analysis (DSA) as described in chapter 2.13.1. When performing the sensitivity calculations one can not just vary every parameter one by one. It is important to see that only the independent variables should be varied to obtain a practical realistic sensitivity analysis.

To derive the independent variables the Buckingham Pi theorem is used. The complete derivation of the independent dimensionless groups can be found in appendix C from which it can be seen that the sensitivity of the following parameters should be considered:

$$\begin{aligned}
 \Pi_1 &= \frac{L_{wl}}{B} = \lambda \\
 \Pi_2 &= \frac{B}{T} = \beta \\
 \Pi_3 &= \frac{\nabla}{L_{wl}BT} = \frac{m}{\rho_w \cdot L_{wl}BT} = C_b \\
 \Pi_4 &= \frac{Af_w}{TB} \\
 \Pi_5 &= \frac{Al_w}{TL} \\
 \Pi_6 &= \frac{\rho_w}{\rho_a} \\
 \Pi_7 &= \frac{Azi\ Pos_x}{L_{wl}} \\
 \Pi_8 &= \frac{Azi\ Pos_y}{B} \\
 \Pi_9 &= \frac{Retr\ Pos_x}{L_{wl}} \\
 \Pi_{10} &= \frac{Retr\ Pos_y}{B} \\
 \Pi_{11} &= \frac{Bow\ Pos_x}{L_{wl}} \\
 \Pi_{12} &= \frac{Bow\ Pos_y}{B} \\
 \Pi_{13} &= \frac{Azi_T}{m \cdot g} \\
 \Pi_{14} &= \frac{Retr_T}{m \cdot g} \\
 \Pi_{15} &= \frac{Bow_T}{m \cdot g} \\
 \Pi_{16} &= C_x \text{ (wind)} \\
 \Pi_{17} &= C_y \text{ (wind)} \\
 \Pi_{18} &= C_n \text{ (wind)} \\
 \Pi_{19} &= C_x \text{ (current)} \\
 \Pi_{20} &= C_y \text{ (current)} \\
 \Pi_{21} &= C_n \text{ (current)} \\
 \Pi_{22} &= C_x \text{ (waves)} \\
 \Pi_{23} &= C_y \text{ (waves)} \\
 \Pi_{24} &= C_n \text{ (waves)}
 \end{aligned}$$

These parameters are varied one at a time while keeping all the other parameters constant. The variations made for the environmental coefficients are done for all angles at the same time but separately for  $C_x$ ,  $C_y$  and  $C_n$ . For the specific case of the wave coefficients the variation is done for all angles and all frequencies at the same time but again separately for  $C_x$ ,  $C_y$  and  $C_n$ .

### 3.2.2. Input uncertainty

The uncertainty in the input variables can be quantified and determined in multiple ways. If data is available this can be used extracted the input uncertainty from. When no data is available experts can be consulted to estimate the uncertainty for a certain parameter, and when both data and experts are not available an educated guess could also be made based on logic reasoning. When quantifying the input uncertainty mostly a Gaussian (normal) distribution is assumed since a lot of phenomena can be described with this probability distribution. The Gaussian distribution can be defined by a mean value  $\mu$  and a standard deviation  $\sigma$ . With these definitions a confidence interval can be defined such as 95% or 99.7% which are often used.

Historic data on the Bibby Wavemaster 1 Walk to Work vessel was collected. The data was extracted out of 44 memo's on different dates that were used for calculating power-speed relations, execute Computational Fluid Dynamics (CFD) analysis or determine DP capability. After the data was categorised to match one of the design stages, as stated in table 3.1, the minimum and maximal values of each parameter were taken where after the average of this minimum and maximum was taken as the mean value for each design stage.

Furthermore the maximum deviation from the mean was taken to be three times the standard deviation for all parameters except for the environmental coefficients. With this a normal distribution can be defined which can be used for uncertainty calculation purposes. The main reason for this approach is to avoid unrealistic extreme values and means for the main dimensions of the vessel that would not occur in reality. For the environmental coefficients the maximum deviation from the mean was taken to be two times the standard deviation instead of three times because it is uncertain that the whole range of possibilities is already covered with the coefficients used for calculation. Therefore the chance of values laying outside the maximum deviation is still present.

For thrust it is assumed that even in case only one value is used for calculation in the historic data, still a uncertainty is present due to the specific thrust which is not always exactly as the supplier states. This results in a uncertainty in the thrust that a thruster will generate during its DP operation. A complete overview of the design stages with their corresponding means and standard deviations can be found in appendix D.

From section 3.2.1 it can be seen that the dimensionless independent parameters all consist out of more than one variable, each with their own mean and standard deviation. The calculation of these combined means and standard deviations is explained in section 2.12.2.

## 3.3. Dynamic DP analysis

For the dynamic part of the uncertainty analysis the method used for the static part will not be applicable anymore since non linear effects due to for instance the introduction of the PID controller are to be expected. This will result in using more advanced methods for calculating the output uncertainty and the corresponding sensitivity for each input variable. One of the obvious methods to use is sampling of which the Monte Carlo Simulation is a very well known example as explained in section 2.12.3. The downside of the Monte Carlo Simulation method is that the amount of simulations required to perform a statistical sensible simulation is relatively high, therefore the number of simulations is reduced by using a response surface method which is explained in section 3.3.5. Using this method a fixed number of simulations is done in the time domain after which a function can be fitted through the data. With this function the Monte Carlo simulations can be done in a very fast manner.

### 3.3.1. Model description

The model parameters used to perform the dynamic simulations are shown in table E.1 for the as built design stage. The environmental coefficients are shown in tables D.3 and D.4. A JONSWAP spectrum is taken for the waves and a NPD spectrum is taken for wind, the current is assumed to be constant meaning that no spectrum is present. The simulation is performed in non limiting conditions of which the environmental details are listed in table 3.2.

Table 3.2: Environmental Variables

Variable	Magnitude or Type	Unit
Wave Spectrum	JONSWAP	[–]
Wave height	2.6	[m]
Peak Period	7.8	[s]
Wind Spectrum	NPD	[–]
Wind Speed	10.01	[m/s]
Current Speed	0.5	[m/s]

### 3.3.2. Simulation time

For the purpose of time planning it is necessary to estimate the time required for dynamic simulations since in general time domain simulations are quite expensive in terms of time and data storage. During this research the dynamic simulations performed with aNySIM are done on a twelve core desktop computer at Damen Shipyards Gorinchem. Of these twelve cores ten are used for time domain simulations while the other two are kept for other operating processes. After each simulation a .res file is generated by aNySIM which is essentially a text file with the complete time trace of the vessel and its outputs. Since the data is being processed with MATLAB afterwards this file is immediately converted to a .mat file to reduce both the loading time when analysing the data and the storage required for the data.

#### Statistical significance

To guarantee that enough waves have passed during one simulation to statistically say something sensible about the behaviour of the vessel a minimum duration of the simulation should be determined. In [25] it is explained that in order to obtain a 99% confidence interval, of all wave heights present in a wave train for a chosen significant wave height, around a 1000 wave encounters should be simulated which comes down to approximately three hours of simulation. This three hours of simulation is seen as an industry standard and can also be found throughout other literature [9] [32]. To make sure no start up phenomena of the controller are seen in the dynamic analysis an extra half hour is simulated resulting in a total simulation time of three and a half hours. When the simulation is finished the first half hour is discarded to prevent the start up phenomena of the controller to be analysed.

#### Total simulation time

A comparison between using the response surface method (RSM), created by a machine learning model, and a full time domain Monte Carlo Simulations (MCS) is made in table 3.3. Here the minimum amount of simulations required to create the response map is determined using the theory in section 3.3.7 and proved to be 136 when fitting a 2<sup>nd</sup> order polynomial with different inputs. Another case is evaluated where 600 points are used to create the response map which is a bit more than the bare minimum and is therefore expected to give more accurate results. For the Monte Carlo Simulations the amount of data points required for calculation is set at 10,000 per angle which is commonly used for other MCS purposes. Looking at the comparison it becomes clear immediately that a full Monte Carlo Simulation using only time domain simulations is not viable since the time required to simulate is almost half a year.

Table 3.3: Comparison of simulation time between Response Surface Method and Monte Carlo Simulation

	RSM	RSM	MCS	Unit
Amount of variables	15	15	15	[–]
Amount of environmental angles	13	13	13	[–]
Time per simulation	17	17	17	[min]
Data file size when .res	60	60	60	[MB]
Data file size when .mat	23	23	23	[MB]
Amount of simulations per angle	136	600	10000	[–]
Total number of simulations	1768	7800	130000	[–]
Total amount of data when .res file	106	468	7800	[GB]
Total amount of data when .mat file	41	179	2990	[GB]
<b>Total simulation time with 10 cores</b>	<b>2.09</b>	<b>9.21</b>	<b>153.72</b>	[days]

### 3.3.3. aNySIM outputs

The complete list of outputs produced by aNySIM during the time domain simulations can be consulted in appendix E. From these obtained outputs several self defined outputs can be derived which are evaluated and listed below. The most interesting outputs are the position and heading station keeping and the maximum obtained position and heading since with these outputs an operational profile can be constructed.

- Position
  - Position station keeping, 95% of the time within a certain offset
  - Maximum obtained position
  - Amount of offset breakouts
  - Average duration out of position
  - Maximum duration out of position
- Heading
  - Heading station keeping, 95% of the time within a certain offset
  - Maximum obtained heading
  - Amount of heading breakouts
  - Average duration out of heading
  - Maximum duration out of heading

In static calculations only the forces due to the mean second order wave forces can be taken into account, therefore during the dynamic calculations also only second order wave forces are considered. This results in the cancellation of the first order forces and therefore also no first order movements of the vessel are calculated. This is merely done since a well set DP controller will only react to the second order forces. The reaction of the DP controller to the input parameters is the output of interest. In aNySIM however not only the mean second order wave forces are taken into account but also the low varying second order wave forces which occur due to the difference frequencies.

### 3.3.4. Input uncertainty

The input uncertainty used for the dynamic analysis will not differ from the static part. Meaning that still the three different design stages are present as listed in table 3.1. However the input data variables will differ and for some input variables no data might be present. If this is the case the uncertainty of this data is generated by assuming a certain value based on logic reasoning. A complete overview is given in table/appendix E.1

### 3.3.5. Response surface methods

Response Surface Methods (RSM) are used to approximate both experimental and numerical phenomena which results in reducing the computational effort required compared to a situation when no RSM method is used. In figure 3.1 an example of a response surface map of 2 input variables and 1 output variable is shown. Here the simulations are plotted as spheres and are called expensive since they take relatively a lot of time to calculate. When a reasonable number of simulations is performed a response plane can be fitted through the points which can be used to calculate all the input parameters that were not simulated. Since these response maps are often low order polynomial functions the computational effort drastically reduces and is therefore considered a cheap way of calculating. The knowledge of RSM can also be extended to more than 2 input variables but then strictly speaking the expression surface does not apply anymore since the response is found in a N dimensional space.

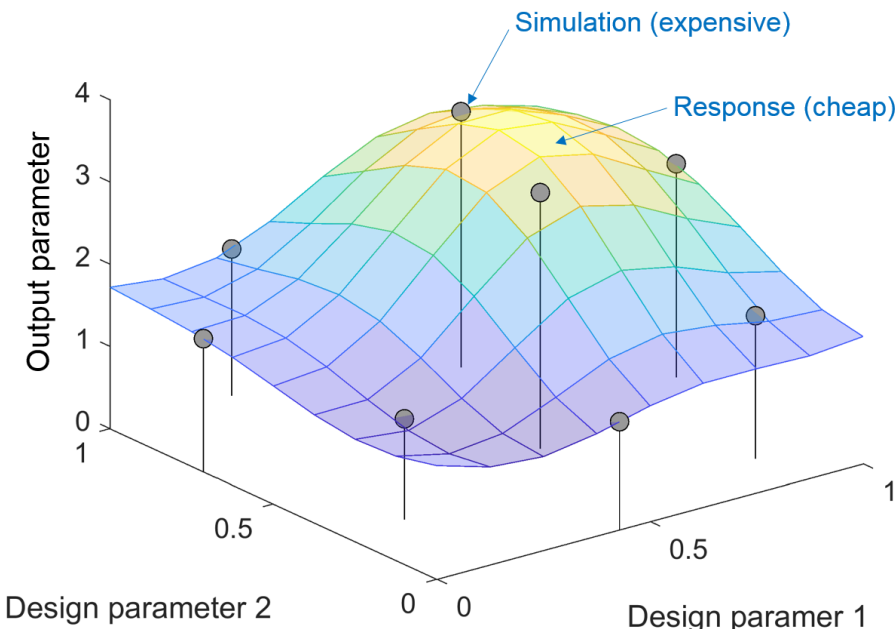


Figure 3.1: Response Surface Map

### 3.3.6. Machine learning

For creating the response surface the simulations executed are analysed with a machine learning algorithm. In general there are four different machine learning styles [46] as shown in figure 3.2 which are briefly discussed below.

#### Supervised learning

Let's consider a set of data containing multiple input variables  $X$  and an output variable  $Y$ . It is now possible to use an algorithm to construct the mapping function from the input  $X$  to the output  $Y$ . This is called supervised learning because the algorithm is learning from a training data set. It is possible to look at this training data set as a teacher who supervises the learning process, the algorithm iteratively tries to make predictions and is corrected by the teacher who knows the correct answers. When the algorithm performance reached an acceptable level of performance the learning will stop. Supervised learning can be subdivided into continuous and classification problems. Continuous problems have a continuous scale like speed, length or weight. Classification problems are problems where the output variable is a category like "success" and "no success" or "healthy" and "unhealthy" or "red" and "green".

#### Unsupervised learning

With unsupervised learning there is only input data  $X$  and no corresponding output variables  $Y$ , the main purpose for unsupervised learning is to access the underlying structure of the data to learn more about it and find hidden patterns. The reason why this is called unsupervised learning is because there

are no correct answers and no teacher that corrects the algorithm. It is all up to the algorithm itself to find and present the interesting structures and patterns in the data. Unsupervised learning can be subdivided into clustering and association problems. Clustering is used when it is desired to discover groupings in the data, an example of this is when customers are grouped by purchasing behaviour. Association is used when rules that describe large parts of the data should be discovered. An example of this could be: people that buy a bike, also buy a lock for it.

### Semi-Supervised learning

Semi-Supervised Learning is a combination of supervised and unsupervised learning meaning that a large amount of input data  $X$  is available and for only a small fraction of the data also the output  $Y$  is known or labelled. An example of this could be for instance a photo archive where only some of the images are labelled, (e.g. car, bike, motorbike) but still the majority of the images are unlabelled. Real world problems often fall into this area since it is relatively easy to acquire unlabelled data but very expensive or time consuming to label it. It is possible now to use unsupervised learning techniques to discover and find hidden patterns in the input variables. Supervised learning techniques could however also be used to make estimates about the unlabelled data which on its turn can be used as training data to make the algorithm even more robust.

### Reinforcement learning

Reinforcement learning is a way of learning what to do and how to act in specific situations. The aim of reinforcement learning is to maximise a specific target which is called the reward. The learning algorithm is not told which action to take but must discover itself which action will yield the maximum reward. Reinforcement learning is very commonly used in real life, lets consider a dog that should learn to stand still before crossing the street. In this case it is impossible to tell the dog what to do, instead a reward is given if the dog decides to take the right action. For this the dog can observe the environment and will see that his owner stops before crossing the street, the dog has however the possibility to make its own decision. If he chooses to walk along the owner can pull the leash which is considered a negative reward. If the dog decides to stand still, just like the owner, the dog is given a cookie which is considered to be a positive reward. Over time the dog will teach itself to stand still before crossing the street since this maximises the amount of cookies it will get from his owner.

Supervised	Unsupervised	Semi-Supervised	Reinforcement
<ul style="list-style-type: none"> <li>Data has <b>known labels</b> or output</li> </ul>	<ul style="list-style-type: none"> <li>Labels or output unknown</li> <li>Focus on <b>finding patterns and gaining insight</b> from the data</li> </ul>	<ul style="list-style-type: none"> <li>Labels or output known for <b>a subset of data</b></li> <li>A blend of supervised and unsupervised learning</li> </ul>	<ul style="list-style-type: none"> <li>Focus on <b>making decisions</b> based on previous experience</li> <li>Policy-making with feedback</li> </ul>
<ul style="list-style-type: none"> <li>Insurance underwriting</li> <li>Fraud detection</li> </ul>	<ul style="list-style-type: none"> <li>Customer clustering</li> <li>Association rule mining</li> </ul>	<ul style="list-style-type: none"> <li>Medical predictions (where tests and expert diagnoses are expensive, and only part of the population receives them)</li> </ul>	<ul style="list-style-type: none"> <li>Game AI</li> <li>Complex decision problems</li> <li>Reward systems</li> </ul>

Figure 3.2: Machine Learning Styles [47]

From the above it is clear that in this research the supervised learning method should be used because the data is generated to specification and therefore both input and output are known. Furthermore the goal of this research is to predict an output given inputs that are not present in the data set. Since the output of the data is continuous the specific type of supervised learning that should be used is the continuous method as explained earlier. When using machine learning it is never exactly clear beforehand which method will give the most satisfying results, mostly trial and error is used to

obtain the best method for each problem. A number of often used algorithms in supervised continuous learning methods are [48]:

- Linear Regression
- Polynomial Regression
- Random Forest Decision Tree
- Neural Network
- Gradient Boosting Regression Tree

In chapter 4 it is seen that the behaviour of the inputs can be most likely very well modelled using a second order polynomial. Therefore the polynomial regression method is used first to see if desirable results can be obtained.

### 3.3.7. Design of experiments

Before fitting a polynomial first data needs to be generated. For the generation of this data a set of input parameters is required. This is also known as a Design Of Experiments (DOE). When performing a DOE the objective function, or output, is called "the response variable" and the set of experiments to be performed, or input, is called "the sample space". The question arises how does one define a sample space that gives a good response variable while minimising the computational time. Multiple DOE techniques to acquire this are available of which three are explained below.

The minimum amount of experiments required to make a reliable fit through the data points is calculated using the binomial coefficient  $\binom{N}{k}$ . The binomial coefficient calculates the amount of terms that are required to describe a polynomial when the amount of inputs and the order of the polynomial are known [49]. The resulting relation used for the calculation of the amount of simulations is shown in equation 3.1.

$$\binom{N + D}{D} \quad (3.1)$$

where:

- $N$  = the amount of input variables
- $D$  = the degree of the fitted polynomial

#### Random DOE

One of the best space filling techniques, in terms of capturing the complete behaviour of the output to the input, is random sampling. In this particular technique the designed sample space is filled by uniformly distributed randomly created samples. Because of the purely random nature of this method it proves not to be particularly efficient. This because the randomness of the method could result in the clustering of samples near to each other which is obviously not desirable in the aim of uniformly filling the design space. The random method space filling is illustrated for 2 variables in figure 3.3. Here the clustering of points is clearly visible. Although for the purpose of illustration two variables are used the usage can be extended to  $N$  number of variables.

#### Full factorial DOE

The full factorial space filling technique is one of the most common and probably the most intuitive strategy of DOE. For the purpose of illustrating a DOE with a sample space containing 2 variables is used but the usage can be extended to  $N$  number of variables. When performing a full factorial DOE the sample space is designed such that all the input variables are evenly distributed over the sample space and with constant distances between the different points. This is illustrated in figure 3.4. Although this method provides a good sample space for the purpose of fitting a response variable it requires quite some simulations and a potential loss of capturing information could occur due to the non randomness selection of the input points.

### Sobol DOE

The Sobol DOE is a pseudo-random space filling technique. Pseudo-random number generators create series of numbers which are able to pass the randomness tests [50]. The main difference with a normal random technique is that with Sobol some optimisation is performed. Lets consider the two dimensional sample space in figure 3.5, here the sample space is divided in sixteen blocks by the grid lines. Now the Sobol DOE is used to randomly draw a value within each box while trying to maximise the minimum distance between the different points. The result is a relatively uniformly filled design space which uses less data points than full factorial and gives comparable performance [50]. Although for purpose of illustration two variables are used the usage can be extended to N number of variables.

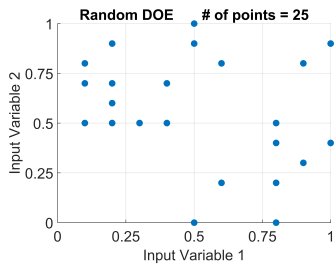


Figure 3.3: Random DOE

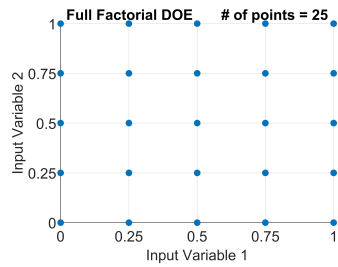


Figure 3.4: Full Factorial DOE

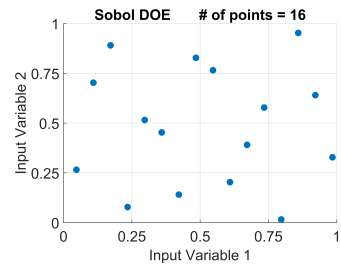


Figure 3.5: Sobol DOE

### 3.3.8. Goodness of fit

After the simulations are executed with aNySIM and a model is fitted with the machine learning algorithm it is important to assess whether the created model describes the aNySIM calculations accurate enough so that it can be used for the purpose of uncertainty calculations. One can imagine that if the error made by using the model is close to or bigger than the uncertainty of a calculation by aNySIM it cannot be used for the purpose of uncertainty calculations. To evaluate this several parameters are considered which are:

- R squared
- Residual
- Mean Absolute Error (MAE)
- Standard Deviation of the Mean Absolute Error (MAESTD)
- Leave One Out Cross Validation
  - R squared (LOOCV R squared)
  - Mean Absolute Error (LOOCV MAE)
  - Standard Deviation of the Mean Absolute Error (LOOCV MAESTD)

#### R squared

The R squared is a goodness of fit measure for regression models meaning that it can be applied to models that are used for the purpose of prediction. In general, when the observed values and the model predicted values are unbiased and small one could state that the model fits the data well. The R squared is sometimes also explained as: how close the data is to the fitted regression line or as: the variance explained by the model divided by the total variance. The magnitude of R squared is normally between 0 – 1 or when stated as percentages between 0 – 100% where 0% means that the model does not explain any of the variation and 100% means the model explains all the variation. If the R squared is found to be negative it means that the model does not fit the trend of the data and is a worse fit than a horizontal straight line. In practice it is very unlikely to find a regression model with an R squared of 100% since it would mean that all the observations fall exactly on the regression line. A visual representation of a relatively low and high R squared is found in figures: 3.6 and 3.7. The mathematical representation of R squared is found in equation 3.2.

$$R^2 = 1 - \frac{SS_{res}}{SS_{tot}} \quad (3.2)$$

$$SS_{res} = \sum_{i=1}^n (y_i - \hat{y}_i)^2 \quad (3.3)$$

$$SS_{tot} = \sum_{i=1}^n (y_i - \bar{y})^2 \quad (3.4)$$

with

- $R^2$  = R squared
- $SS_{res}$  = The sum of squares of the residuals
- $SS_{tot}$  = The total sum of squares
- $n$  = amount of observations
- $y$  = observation
- $\hat{y}$  = prediction
- $\bar{y}$  = mean of the observed data

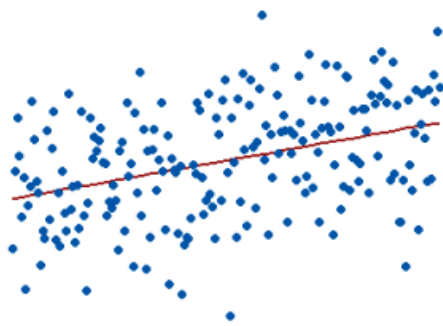


Figure 3.6: Low R Squared [51]

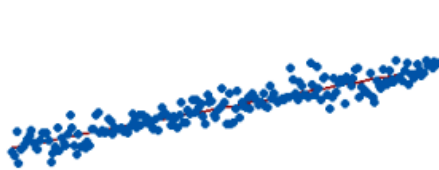


Figure 3.7: High R Squared [51]

### Residual

The R squared is unable to determine whether the model estimations and predictions are biased, this is where the residuals should be used for. The distance between the data point used for fitting the model and the regression line is called the residual. These residuals can be used to determine if a model is under or over predicted systematically meaning that the model is biased and therefore indicates a bad fit. In figure 3.8 an example is shown of a regression made on the relationship between a semiconductor electron mobility and the natural log of the density for real experimental data [52]. The R squared in this specific example is calculated to be 98.5% which is considered to be really good. This is also visible as the regression line seems to be a good representation of the data points. However when looking at the residuals plot in figure 3.9 it is clearly visible that the model systematically under and over predicts the values rather than showing randomness. Therefore this model indicates a bad fit and shows the importance of considering the residuals.

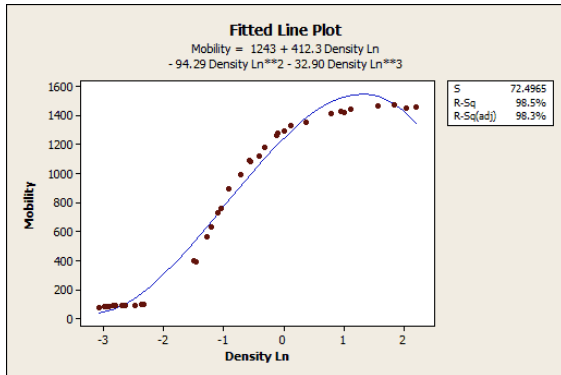


Figure 3.8: Regression with R squared = 98.5% [52]

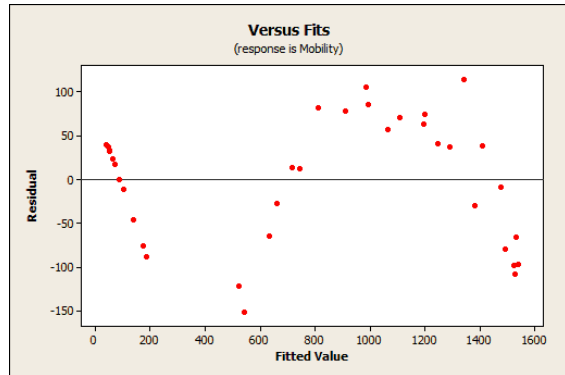


Figure 3.9: Biased Residuals [52]

### Mean absolute error

The Mean Absolute Error (MAE) is one of the most common ways to measure accuracy for continuous variables [53]. The MAE measures the average magnitude of the differences between the prediction and the actual observation where all individual differences have equal weight and without considering their direction. In short the MAE expresses the average model prediction error in units of the variable of interest. In this thesis however the MAE is normalised meaning that it represents a percentage of error. The mathematical representation of the MAE is shown in equation 3.5.

$$MAE = \frac{1}{n} \sum_{i=1}^n |y_i - \hat{y}_i| \quad (3.5)$$

with:

- $n$  = amount of observations
- $y$  = observation
- $\hat{y}$  = prediction

### Standard deviation of the mean average error

After checking if the MAE is small enough the Standard Deviation of the MAE should be considered. Needless to say is that it's important since the MAE can be fairly small but when the standard deviation is large still the chance of big errors in the prediction can be relatively high.

### Leave one out cross validation

When a predictive accuracy of a model is required and independent validation data is absent re-sampling the original data to create a different independent test set is very commonly done and is called cross validation [54]. Leave One Out Cross Validation (LOOCV) is a particular case of the k-fold Cross Validation with  $k = 1$  meaning that every observation is chosen once to be the test set and the rest of the observations are used as training set. Using this, a model can be fitted  $n$  times on the training set and afterwards be validated every time on a single test point. After this is performed the results can be averaged and all the parameters listed above can be evaluated once again. This way it is checked how the model will generalise to an independent unknown data set. The LOOCV is especially helpful when the data set is relatively small and when regression analysis is performed. For other methods it can become very computational expensive.

### 3.3.9. Sensitivity analysis

The differential sensitivity analysis as used in the static DP analysis will not perform optimally when used in the dynamic DP analysis since it does not work very well for non linear cases. Therefore the SCA method as explained in chapter 2.13.4 is used if the outputs are observed to be monotonic.

### 3.3.10. Parameter variations

The variation of parameters in the dynamic DP analysis is slightly different compared to the static DP analysis. First of all only the design stage "as built" is considered since in the conceptual design stage dynamic DP simulations are normally not done since a lot of required information for simulation is not available yet. A full list of varied parameters and their boundary values can be found in table E.1.

#### Wave coefficients

It should be noted that the wave coefficients can not be varied since the licence of aNySIM that was bought by Damen does not allow so. Therefore the influence and the uncertainty from the wave coefficients is unfortunately not taken into account. The wave coefficients are however derived especially for the Walk to Work vessel and therefore it is assumed that the uncertainty is relatively small especially when looking at the wind and current coefficients which are still taken from brix tables and databases respectively.

#### PID gains

When looking at the PID controller gains it is seen that all integrator terms are set to 0. This means that the vessel does not correct for the steady state error meaning that it will never be exactly in its set point position. This is done to simplify the settings of the PID controller so that the focus can be on the actual behaviour of the vessel. This simplification can simply be corrected since it is assumed that the behaviour of the vessel stays the same but concentrates around another point than its set point position. Therefore the mean of the x, y positions and the heading is subtracted so that the behaviour is again around the set point. The assumption that the behaviour of the vessel is not largely effected is justified by the fact that when the vessel is already moving on average around the set point the integrator term only has a very small contribution. It was also shown by van der Weiden [32] that the integrator term has virtually no influence on the behaviour of the vessel other than reducing the steady state error. A more detailed explanation on how the initial PID gains are calculated and how they affect the behaviour of the vessel can be found in appendix E.2.

### 3.3.11. Time step

Before simulations can be done it is of utmost importance to choose the right settings regarding the solver used in aNySIM. One of the most important setting for dynamic simulation is the time step taken for each calculation. If the time step is relatively large, less computational time and storage space is required, when the time step is chosen too big it is possible that some data will be lost and certain phenomena can not be captured anymore.

To check whether all relevant information is included in the simulation, ten different simulations were done using time steps between 1 and 0.1 seconds with a step size of 0.1 second. Additionally three more simulations were done with time steps of 0.05, 0.025 and 0.01 seconds. The output data as listed in chapter 3.3 is compared and an example of this can be seen in figure 3.10 for offset and in figure 3.11 for heading, both examples are for an environmental of 90 degrees. On the left y axis in these figures the magnitudes of the output values are listed, the right axis states the percentage of change when the time step is reduced to the next step. For example when looking at figure 3.10 to the maximum offset at time step 0.2 seconds, the change of the maximum offset is approximately 1.7% when the time step is reduced to the next step, which in this case is 0.1 seconds.

What stands out is that for none of the parameters real convergence takes place. When looking at the graphs it can be seen that for each time step decrease the output parameters will still change. For an elaboration on this MARIN was consulted but were not able to give a satisfying answer yet. However for the purpose of this research it will not have an influence on the results since not the absolute values of the outputs are most important but the uncertainty is. When Damen is thinking of using aNySIM for commercial purposes it would be advisable to discuss again with MARIN why this behaviour occurs. This because if a certain output does not fulfil the specification that was set simply decreasing the time step could be used to meet the requirements. In this thesis a time step of 0.25s was chosen in consultation with MARIN.

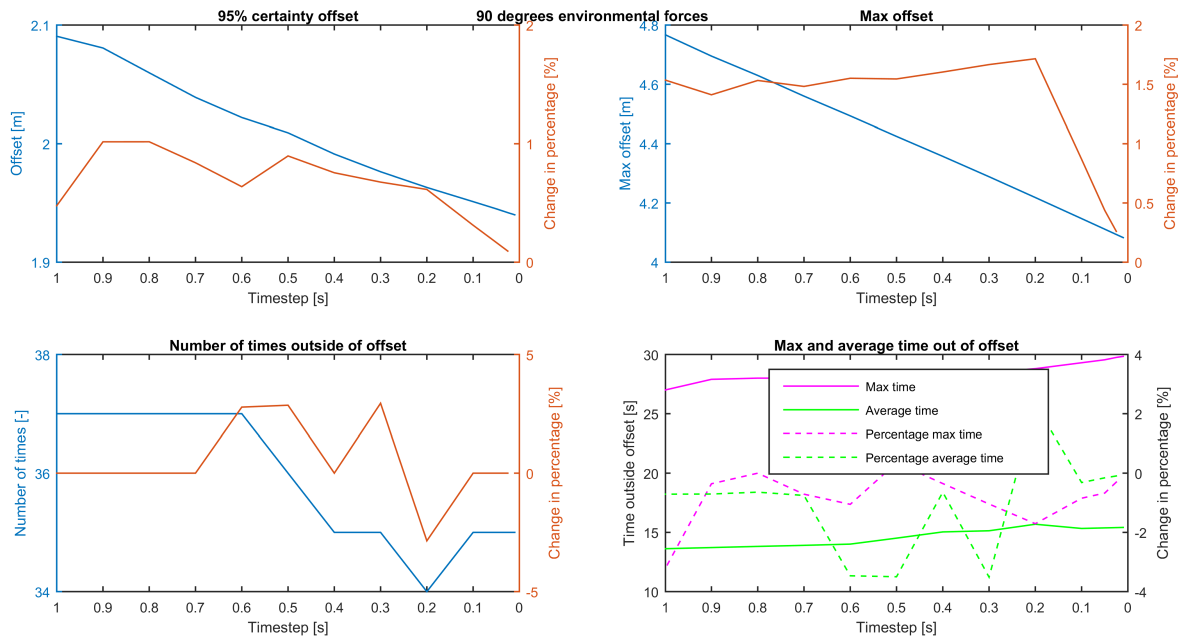


Figure 3.10: Time step offset 90 degrees

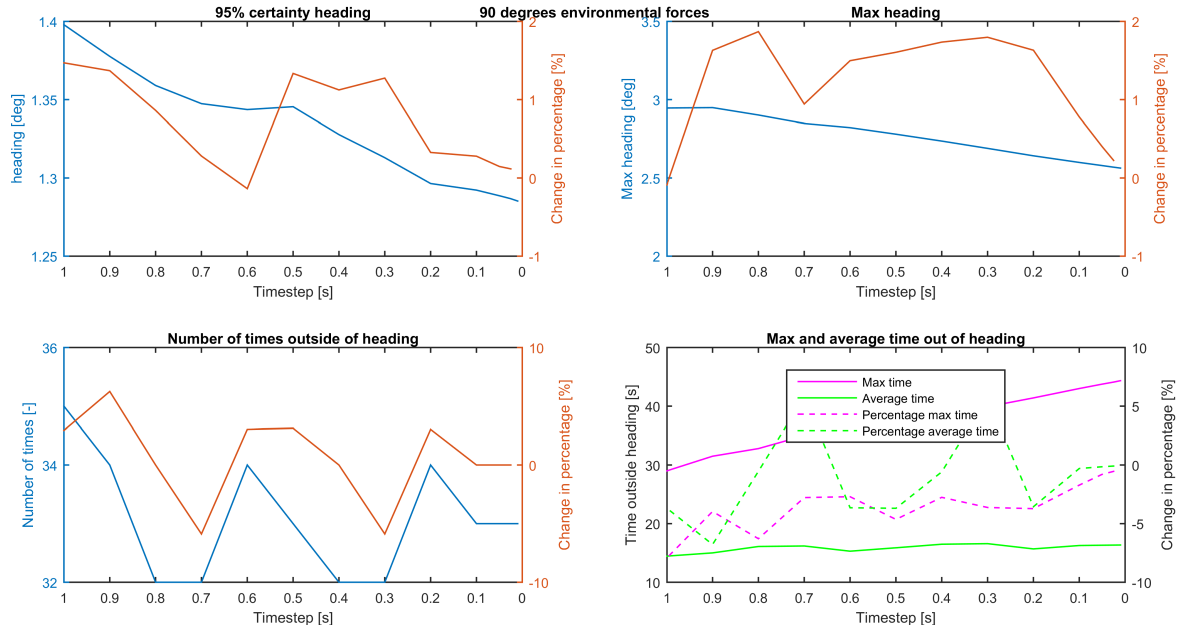


Figure 3.11: Time step heading 90 degrees



# 4

## Results

In this chapter the results obtained by performing the analysis and calculations as described in chapter 3 are discussed. The static analysis is elaborated on first where the sensitivity, the input uncertainty and finally the output uncertainty are discussed. Using these results the capability confidence intervals of each design stage are determined. For the dynamic analysis it is first checked if the model created by the machine learning algorithm is accurate enough for the purpose of uncertainty calculation. After the check is performed the uncertainty for offset and heading are discussed.

### 4.1. DPlab capability sensitivity

For the ease of understanding the sensitivity is plotted in a polar plot, by doing this the directional dependence of the input parameters on the output can be clearly seen at a glance. The sensitivity plotted is the normalised sensitivity as seen in equation 2.36, meaning that if the input changes with 1% the plot shows the percentage of change of the output. In the polar plots the absolute value of the normalised sensitivity is shown, meaning that all the values are positive which is done to make the plots more clear. The resulting consequence is that it can not be seen immediately if a certain parameter increases or decreases the output up for consideration. If the above would be desirable tornado plots can provide this information, however the directional dependency is less obviously visible in this specific representation.

The output capability is expressed in  $\frac{m}{s}$  wind speed, it states until what environmental condition the vessel is still able to maintain position. The environment consists out of wind, waves and current. During all calculations wind, waves and current are simulated collinear, meaning that they all act from the same direction. The wind wave relation used is found in table: D.7 and the used current speed is taken constant with magnitude:  $0.75 \frac{m}{s}$ . DPlab starts with the first entry of the wind wave relation table, adds the current and calculates if the vessel can maintain position. If so, it increases the magnitude of wind and waves. During this calculation wind speed and wave height are not restricted making it a case where limiting conditions are present, therefore saturation of at least one thruster will occur.

The main dimensions used for each design stage are listed in table D.2. Furthermore the influence of each parameter on the forces in x, y and the moment in z direction are summarised in table D.1.

#### 4.1.1. Conceptual design stage

From figures 4.1 and 4.2 it can be clearly seen that the basic dimensions of the vessel are the most sensitive parameters when a static DP calculation is performed. These parameters are  $L/B$ ,  $C_b$ , *Lateral Wind Area / TL* and  $B/T$  and have an influence for almost all environmental angles. Two other parameters that have a relatively high sensitivity are *azimuth thrust / mg* and the parameter *bow thruster thrust / mg* which was to be expected since these are directly counteracting the environmental forces. The difference between the azimuth and bow thruster sensitivity is not particularly in the magnitude but more in the environmental angles for which they are sensitive. The azimuth thruster

has a high sensitivity for angles between 80-280 degrees and between 170-190 degrees where the bow thruster has a high sensitivity for angles between 110-160 degrees and 200-250 degrees.

Two parameters that perhaps were not expected to be as sensitive are *Wind coefficient Cy* and *Density water / Density air* which also have an influence for almost all angles. Furthermore the sensitivity of *Wind coefficient Cx* is also quite significant but its influence is limited to 170-190 and 350-10 degrees.

In figure 4.2 and 4.3 it can be seen that the *Azimuth X position / L* and the *Tunnel X position / L* also have a moderate sensitivity, mostly for angles between 30-150 and 210-330 degrees. From figure 4.4 and 4.5 it becomes clear that the sensitivity of wave and current coefficients is very low in static DP calculations. It is also important to realise that non of the parameters concerning the retractable thruster has a sensitivity since it is not present in this design stage yet.

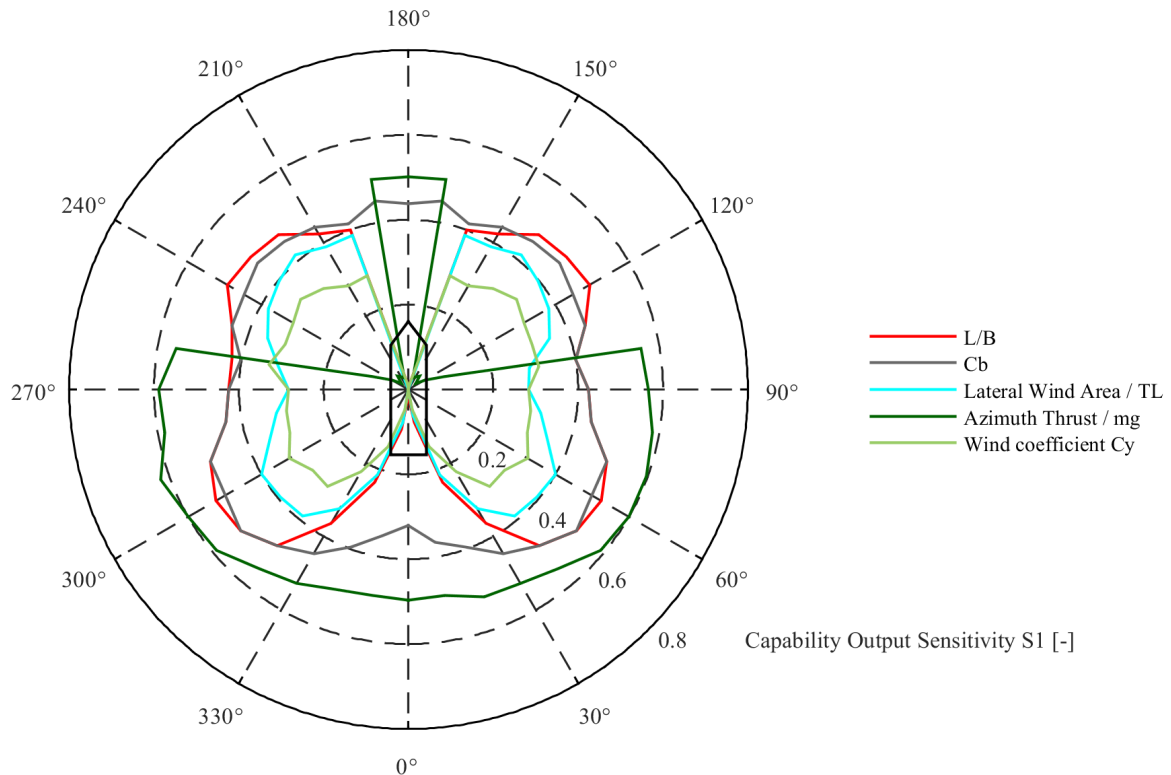


Figure 4.1: Capability Output Sensitivity +1% axis 0.8

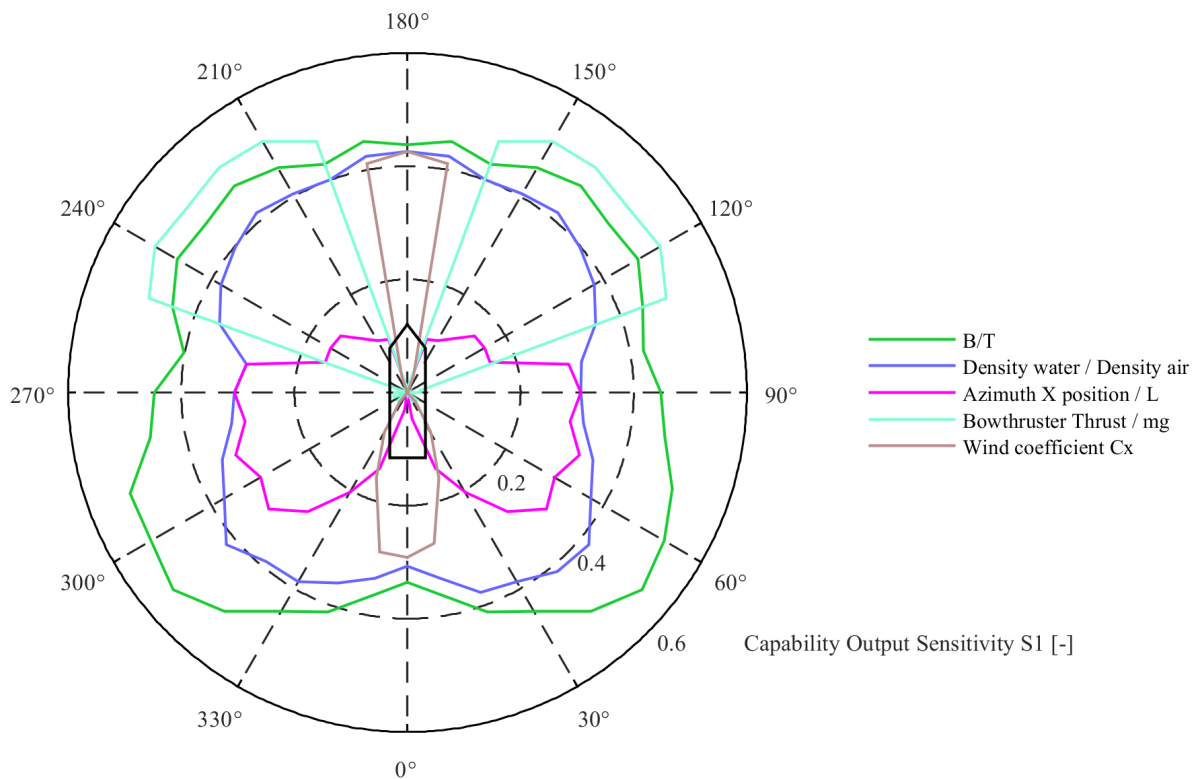


Figure 4.2: Capability Output Sensitivity +1% axis 0.6

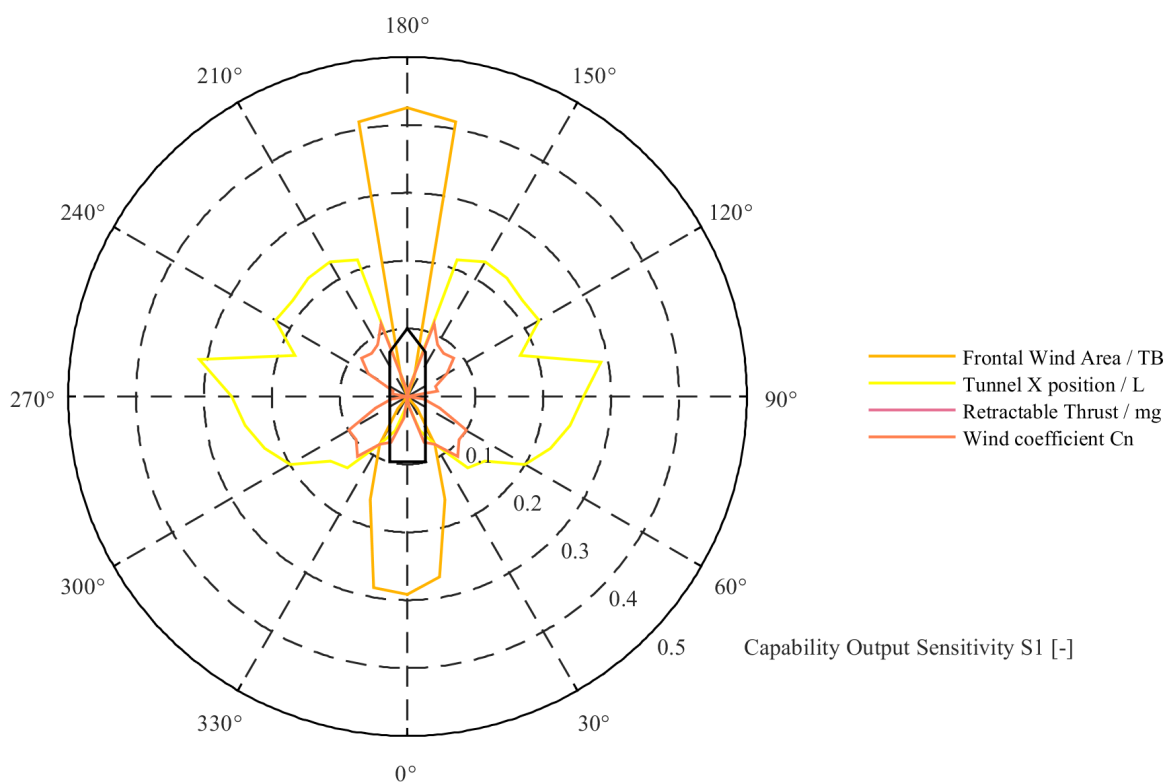


Figure 4.3: Capability Output Sensitivity +1% axis 0.5

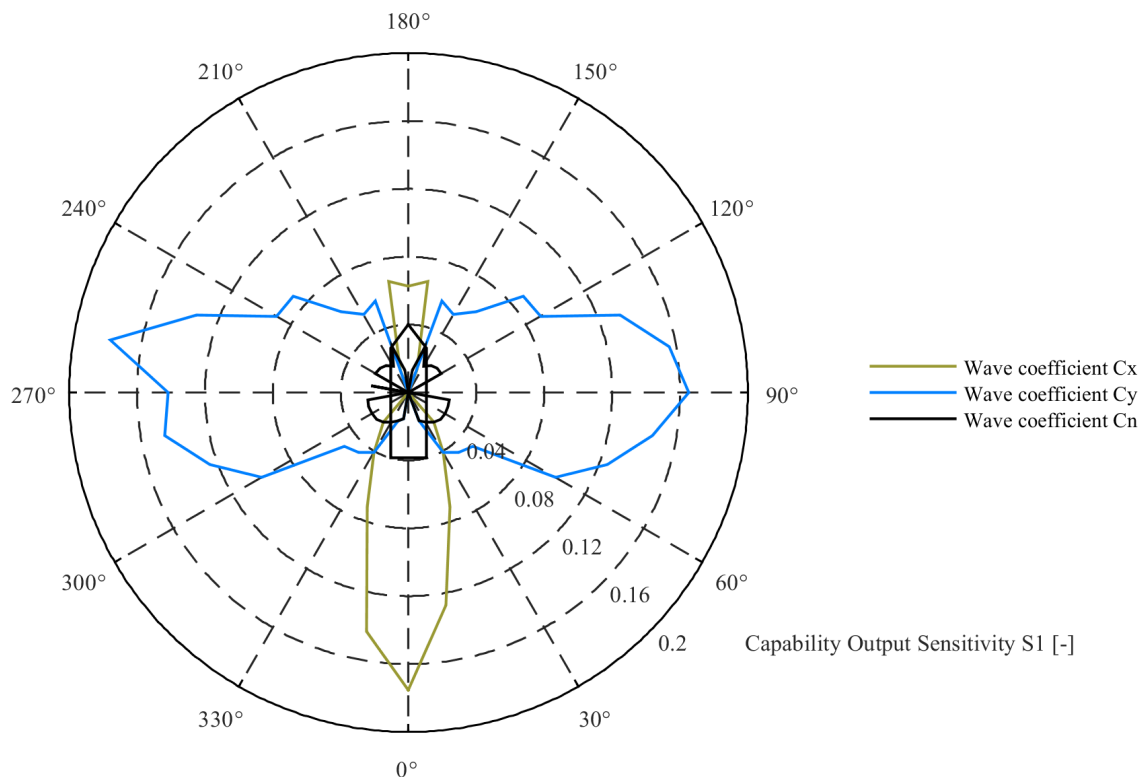


Figure 4.4: Capability Output Sensitivity +1% axis 0.2

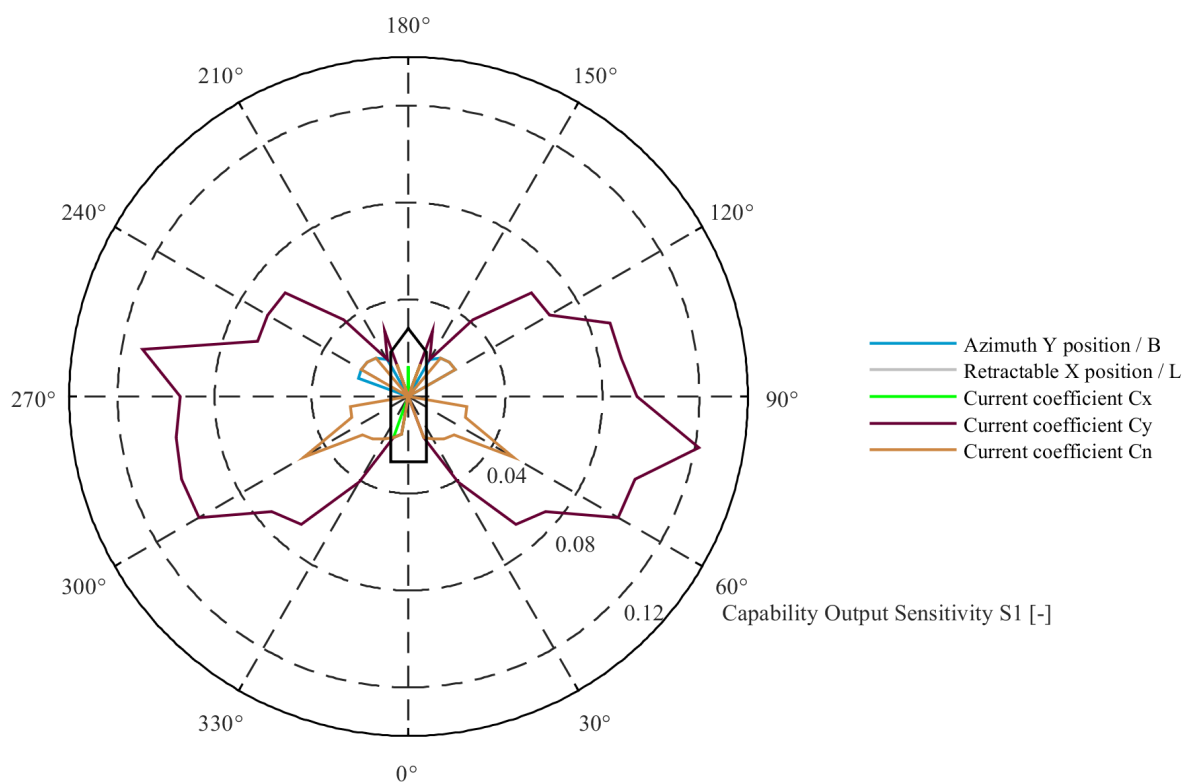


Figure 4.5: Capability Output Sensitivity +1% axis 0.14

#### 4.1.2. Preliminary design stage

Overall one could state that the trends and magnitudes for the sensitivity of the preliminary design stage are comparable with those of the conceptual design stage as described in section 4.1.1. Minor changes are however observed when looking at for instance the *azimuth thrust / mg* in figure 4.6. It is clearly visible that the sensitivity of this parameter is reduced to a smaller range of angles namely 320-40 and 170-190 degrees. However when looking at *bowthruster thrust / mg* in figure 4.7 the behaviour is opposite since here the influence of the sensitivity by this parameter is expanded to 60-170 and 190-300 degrees. This behaviour can be explained by the fact that now also the retractable azimuth thruster is present resulting in a different allocation of the thrusters. This is also visible when looking at figure 4.10 since now the *Azimuth Y Position / B* has a bigger sensitivity compared to the conceptual design stage.

The effect of the retractable thruster is also visible in figures 4.8 and 4.10 when looking at the parameters *Retractable Thrust / mg* and *Retractable X position / L*. These parameters show some sensitivity although their magnitude is relatively small.

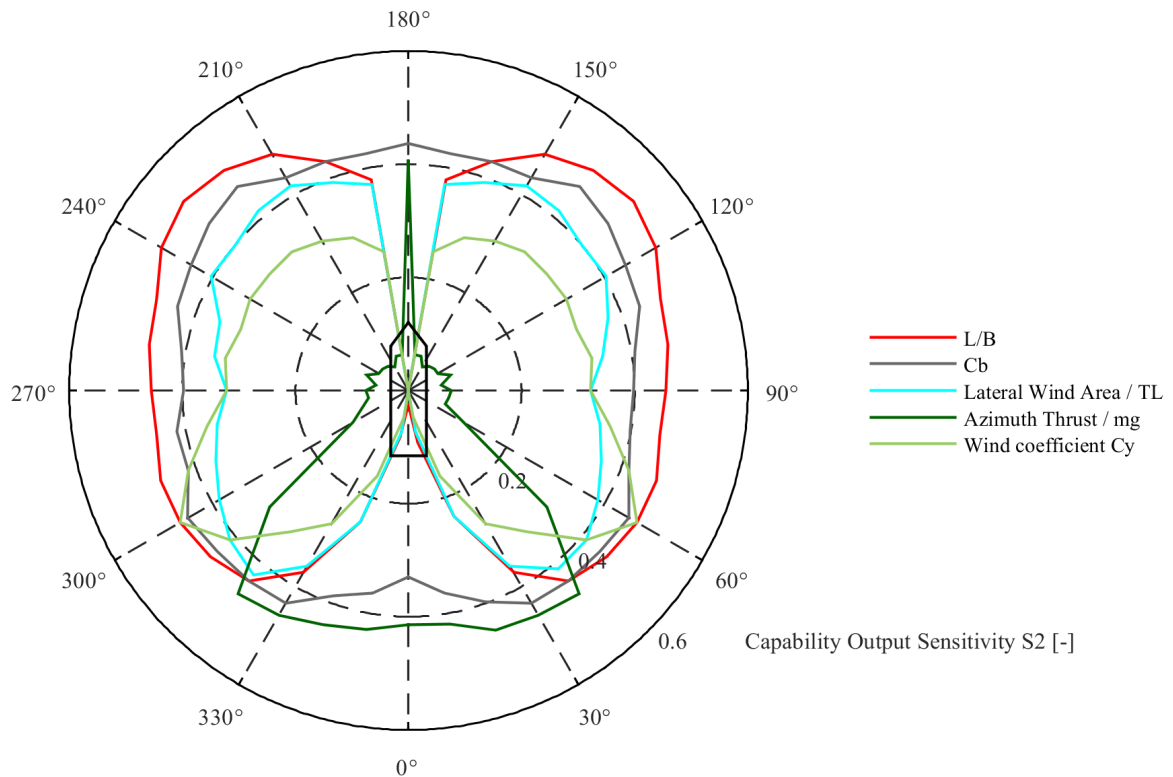
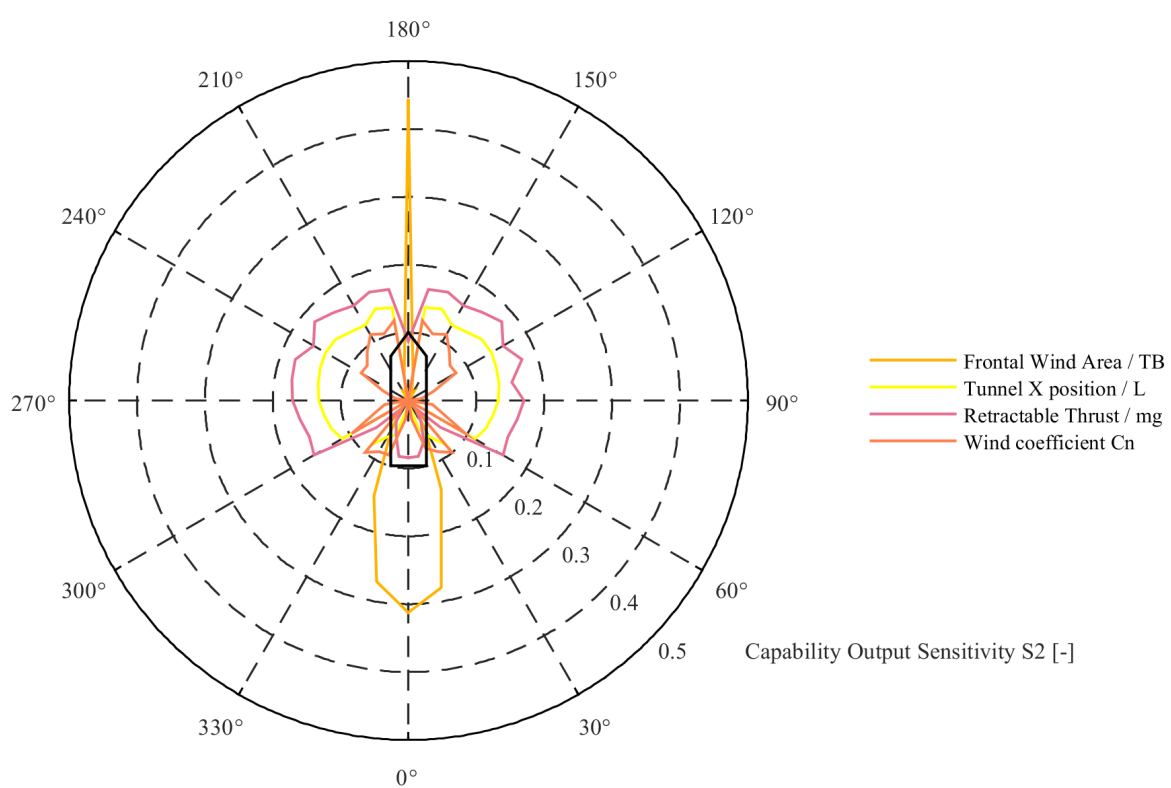
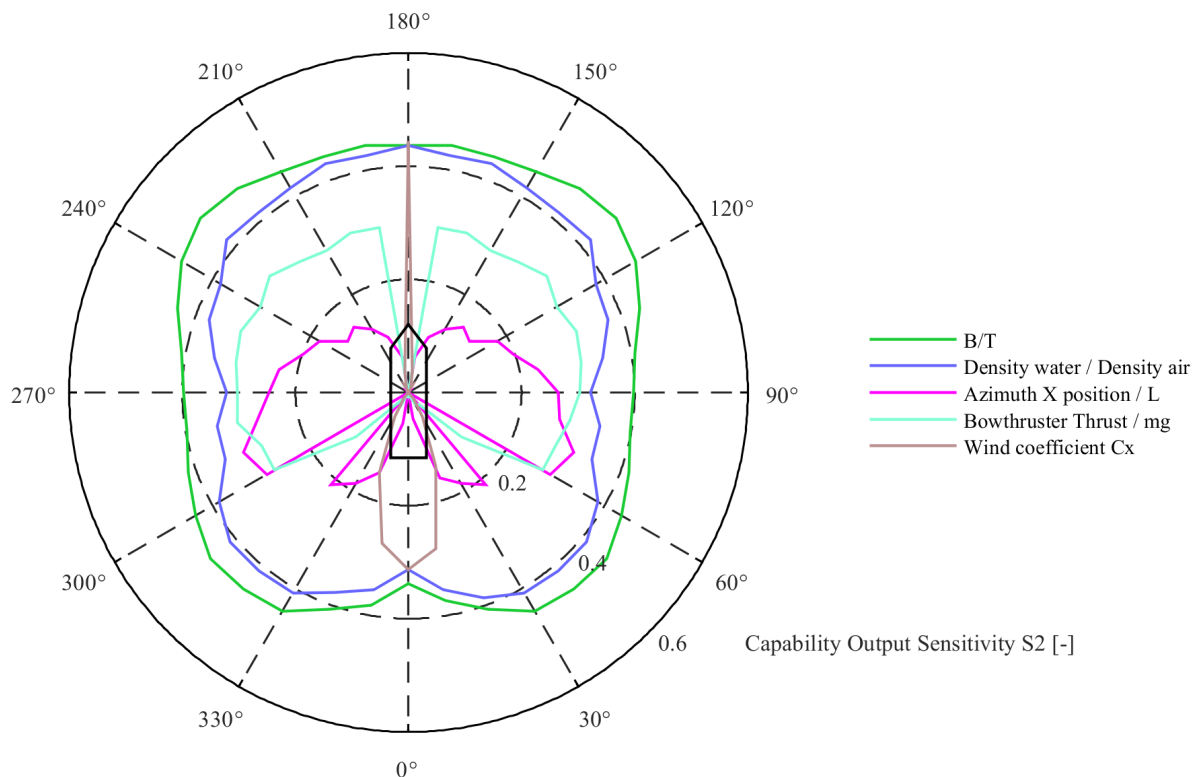
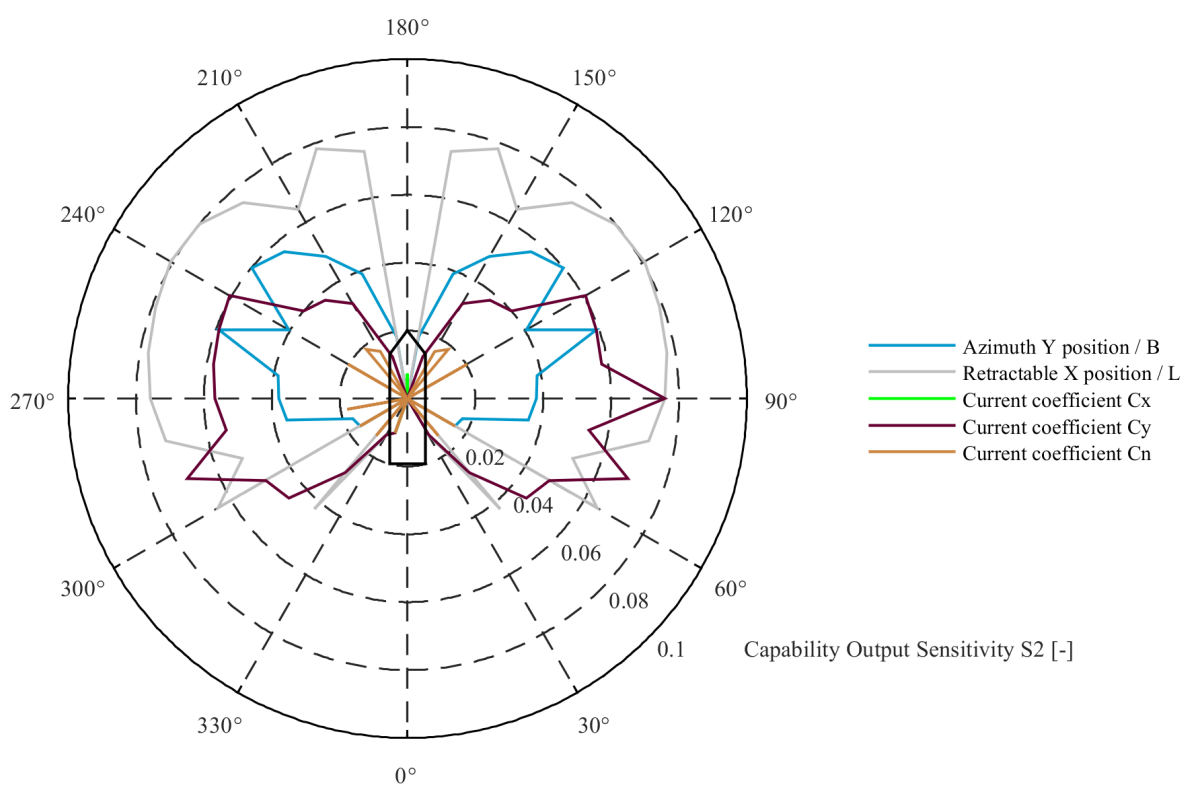
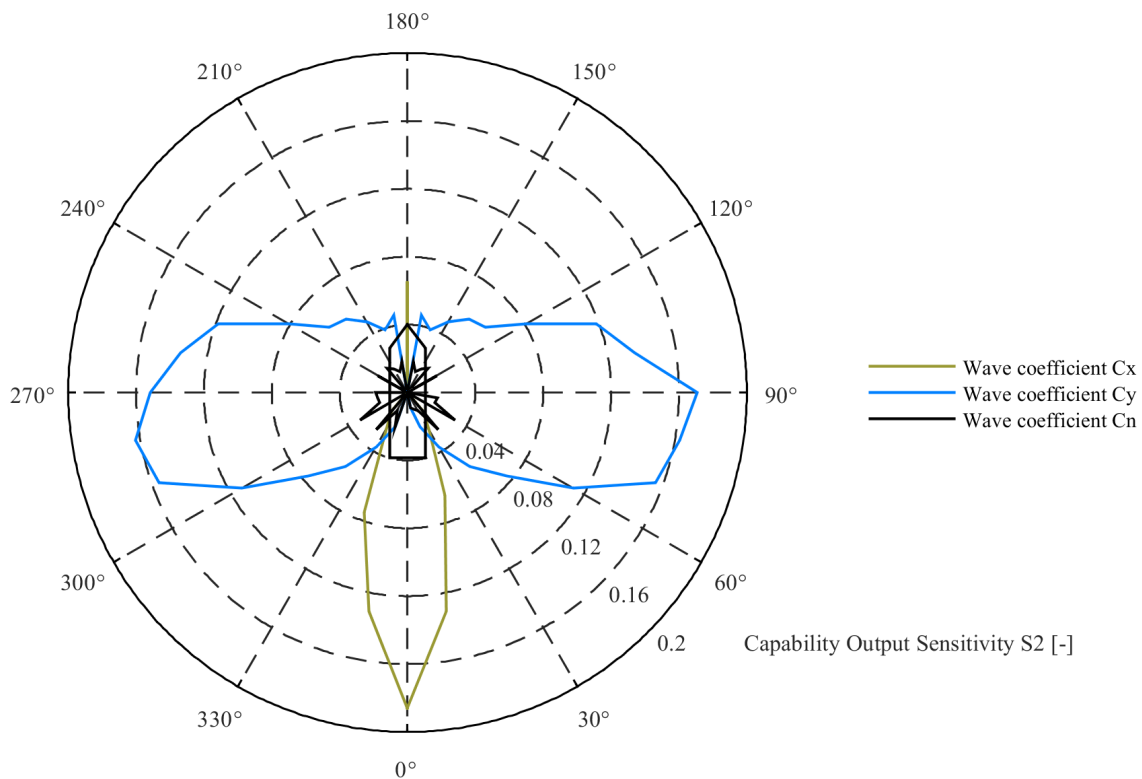


Figure 4.6: Capability Output Sensitivity +1% axis 0.6





#### 4.1.3. As built design stage

The sensitivities in the as built design stage are almost identical to the preliminary design stage which is to be expected since the mean of the input variables only differs slightly as seen in table D.2. The basic dimensions of the vessel are again the most sensitive parameters when a static DP calculation is performed. Current and wave coefficients proved to be relatively non sensitive.

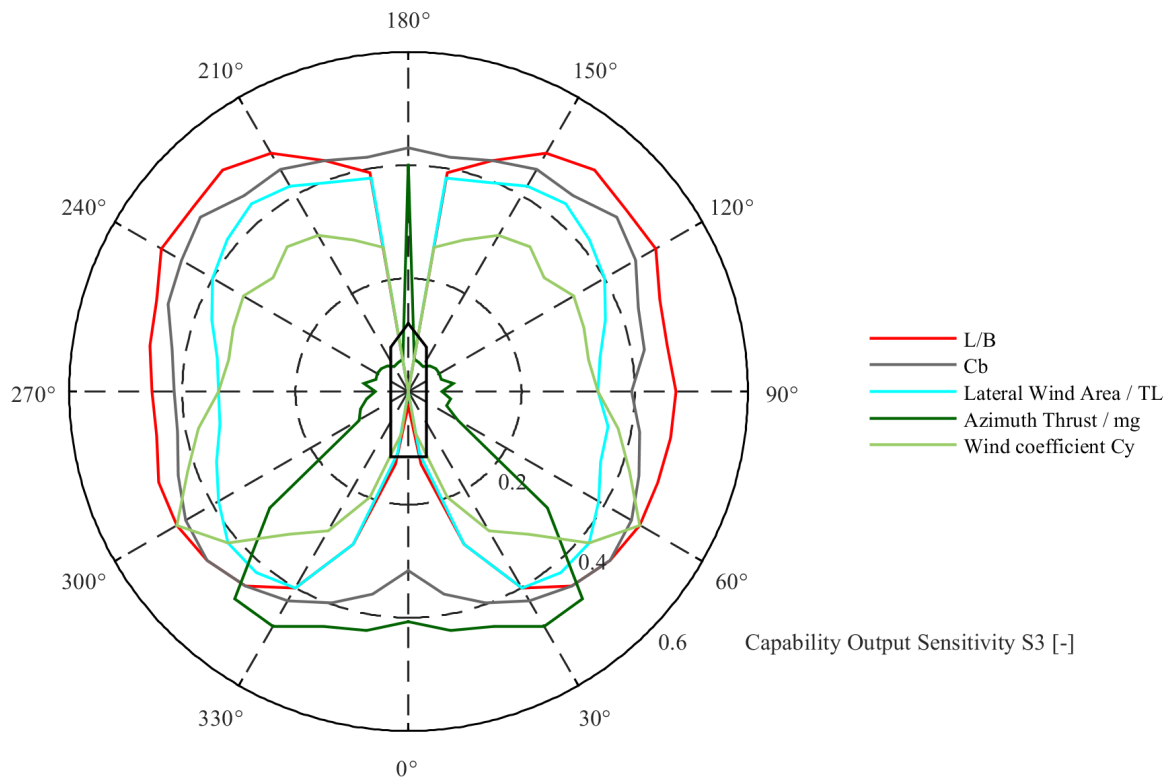


Figure 4.11: Capability Output Sensitivity +1% axis 0.6

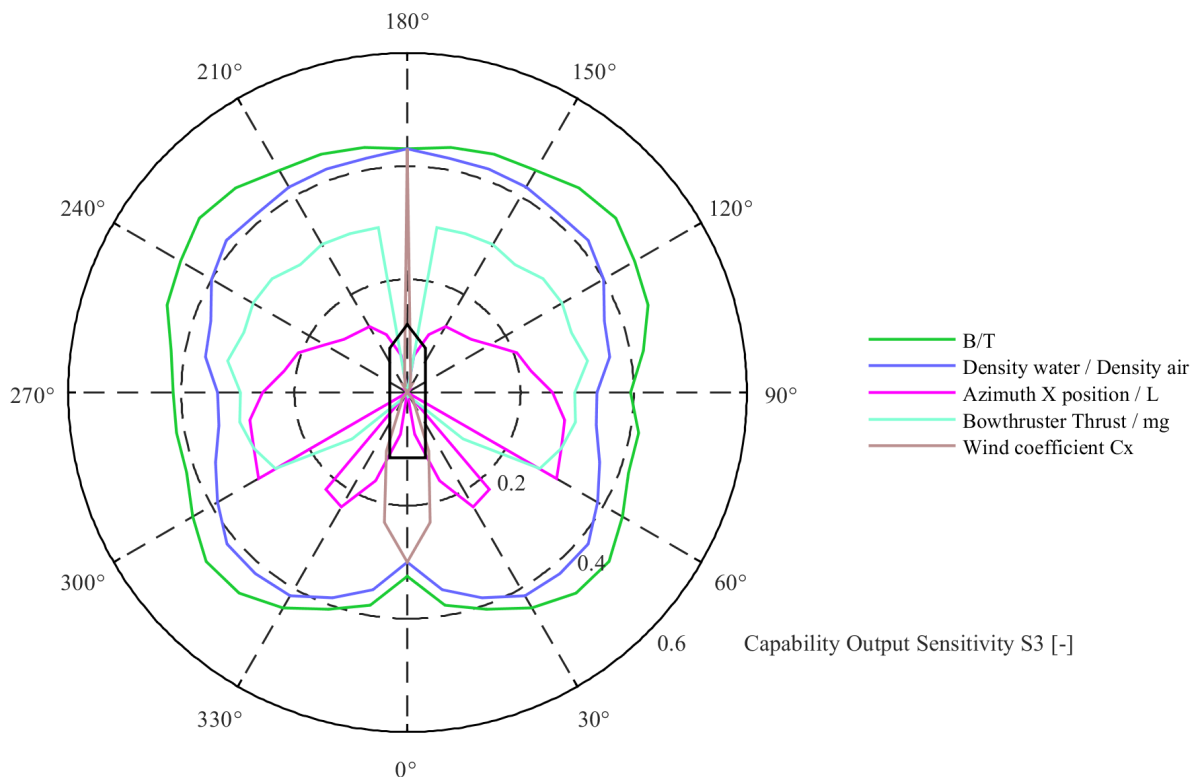


Figure 4.12: Capability Output Sensitivity +1% axis 0.6

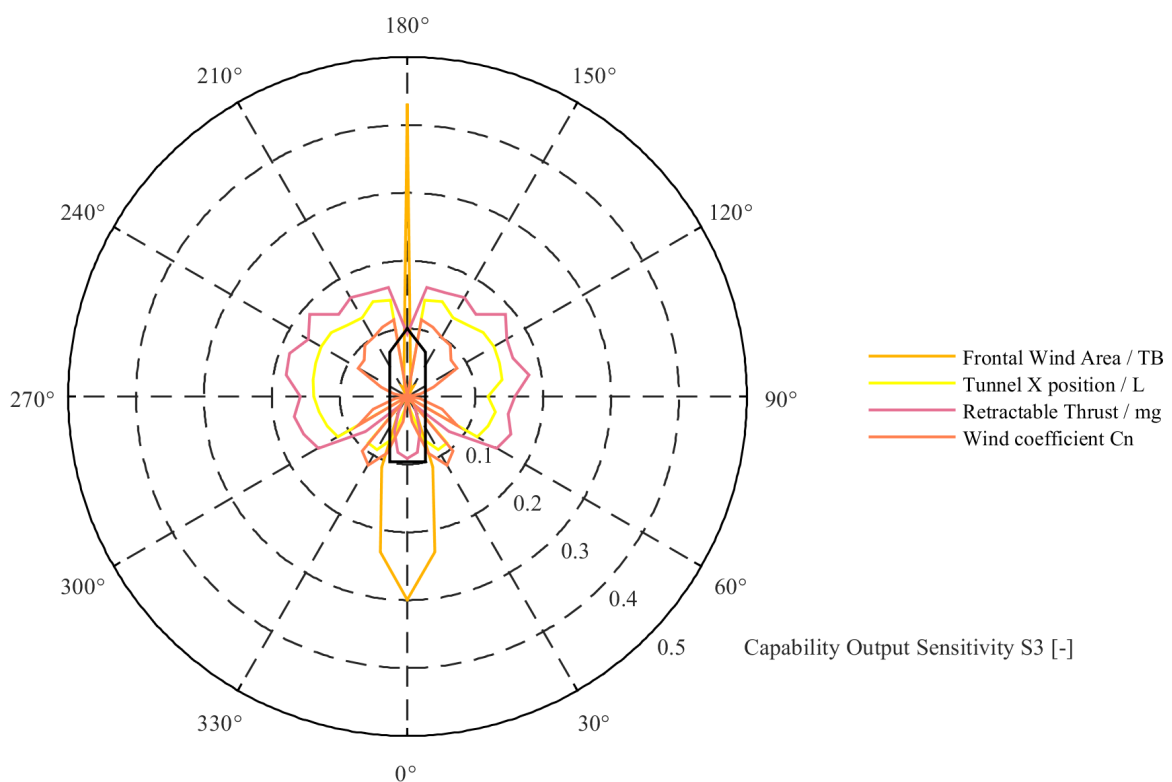


Figure 4.13: Capability Output Sensitivity +1% axis 0.5

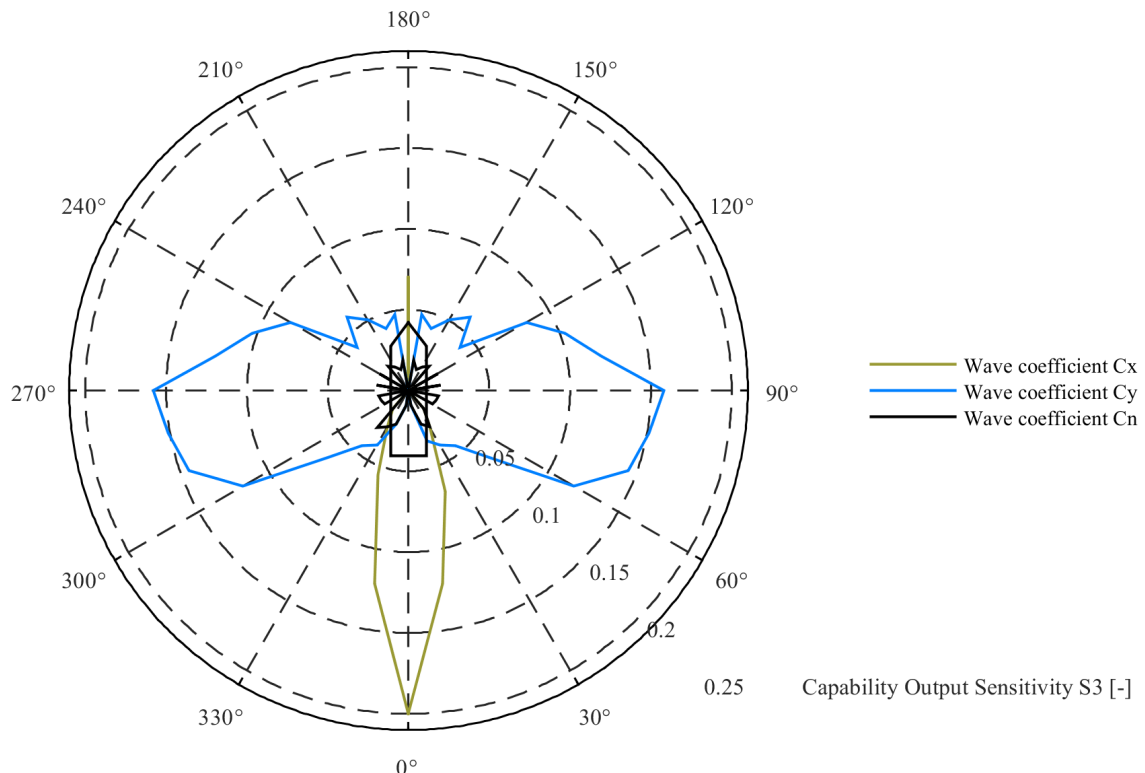


Figure 4.14: Capability Output Sensitivity +1% axis 0.21

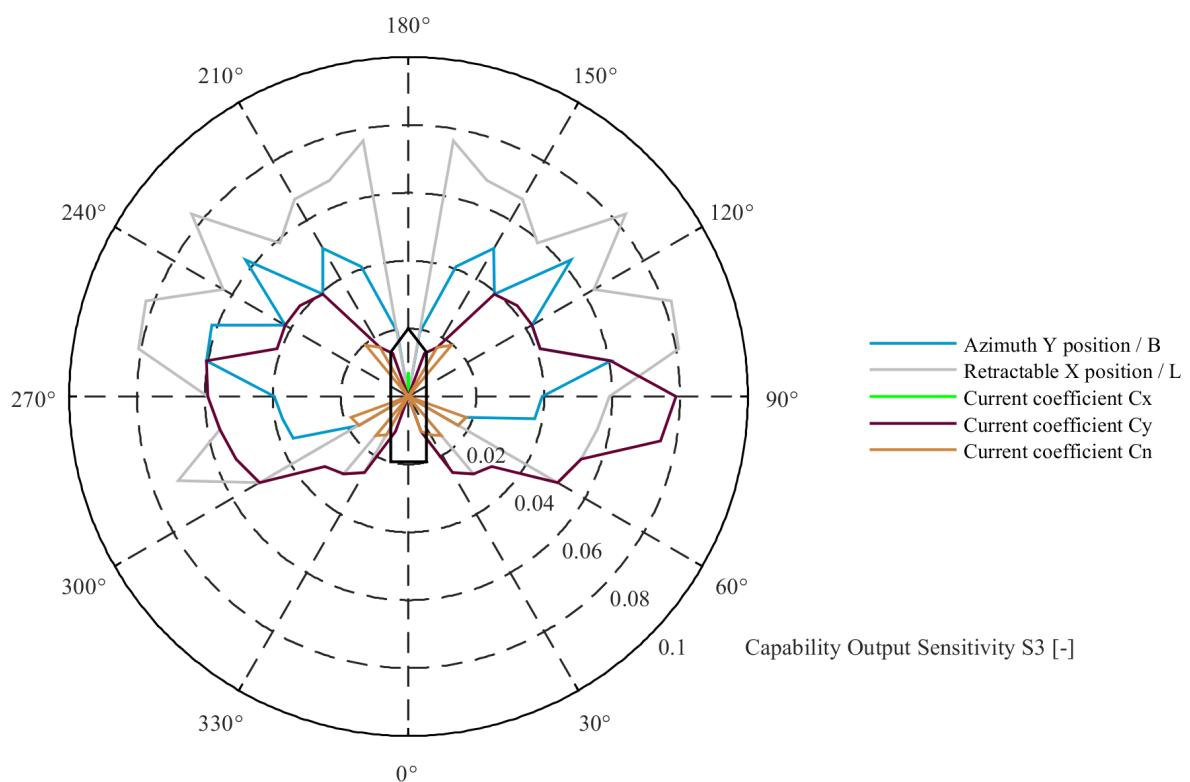


Figure 4.15: Capability Output Sensitivity +1% axis 0.1

## 4.2. DPlab capability input uncertainty

When considering the input uncertainty again the three different design stages are distinguished as described in table 1.2. How the input uncertainty is defined, collected and calculated is described in section 2.12, section 3.2.2 and appendix D.

### 4.2.1. Conceptual design stage

Although of all design stages the conceptual design stage is the one with the biggest basic dimensions input uncertainty, these do not have the biggest magnitude overall. When considering figures 4.16 and 4.17 it can be seen that the *Wind coefficient  $C_x$* , *Current coefficient  $C_x$*  and  $C_y$ , and the *Wave coefficient  $C_x$ ,  $C_y$ , and  $C_n$*  have by far the biggest input uncertainty. What can also be concluded is that these uncertainties are not constant for all angles but differ quite significant. The wave coefficients are an exception to this since their input uncertainty was estimated based on the trends of wind and current coefficients resulting in a relatively smooth uncertainty plot.

In figures 4.18 and 4.19 it is seen that the basic dimensions of the vessel and the placement of the thruster are the next most uncertain parameters. When looking at these figures it is seen that some parameters, like for instance *Wind coefficient  $C_y$*  in figure 4.18, the plotted line is interrupted around 0 and 180 degrees. This does not mean that there is no uncertainty but is explained by the fact that the uncertainty at that point is to big to be plotted on the current scale. For the specific case of the *Wind coefficient  $C_y$*  this is due to the fact that the value of this coefficient is almost zero at these points resulting in a fraction, see equation 2.34, that becomes relatively big. This behaviour also occurs for the parameters *Wind coefficient  $C_x$* , *Wind coefficient  $C_n$* .

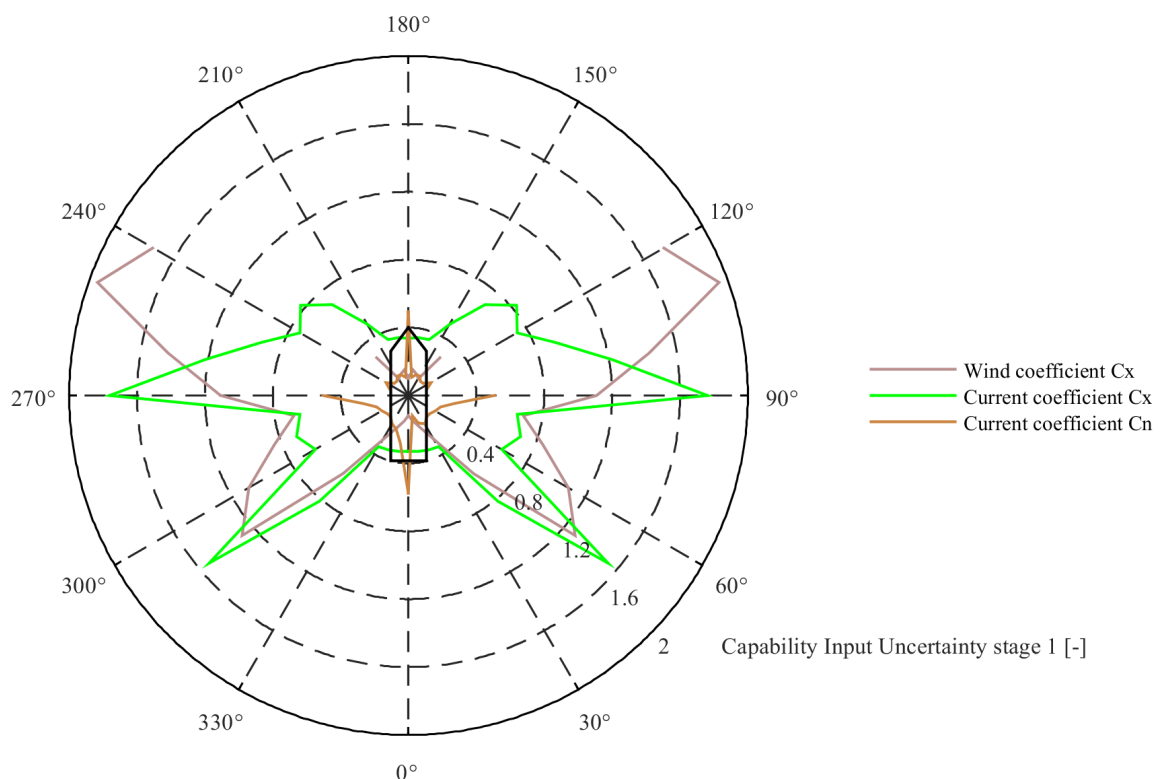
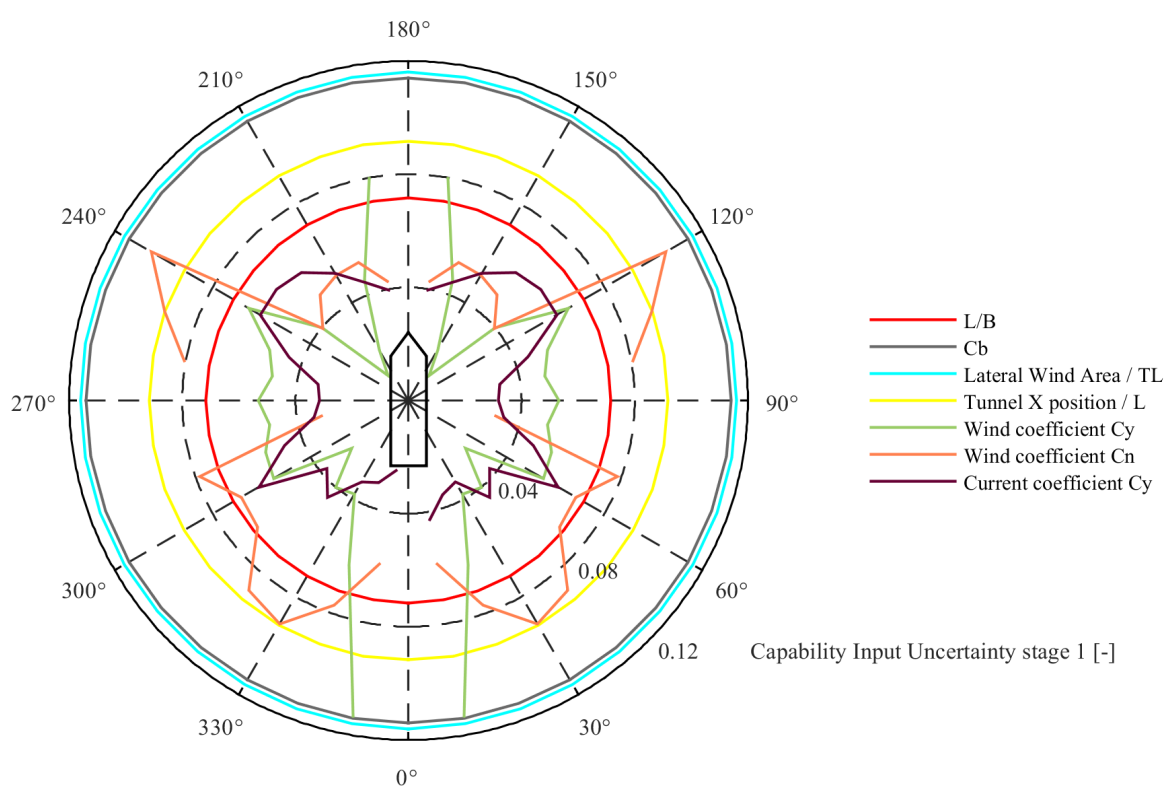
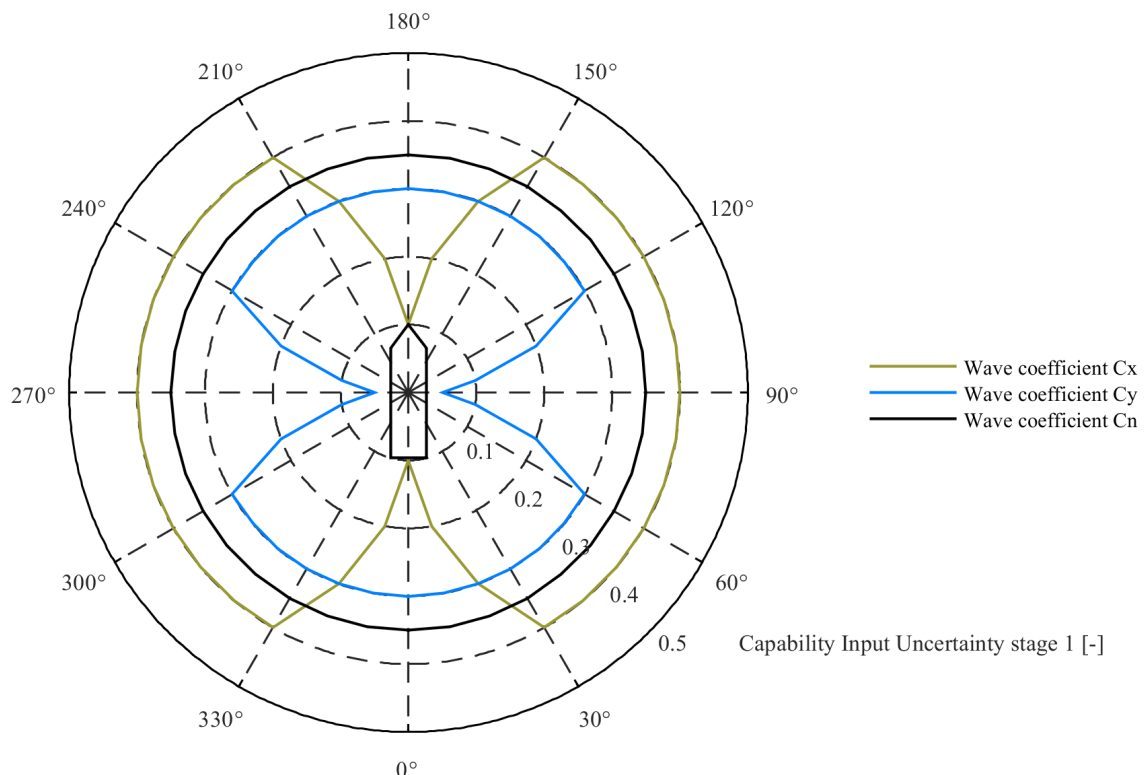


Figure 4.16: Capability input uncertainty axis 2.0



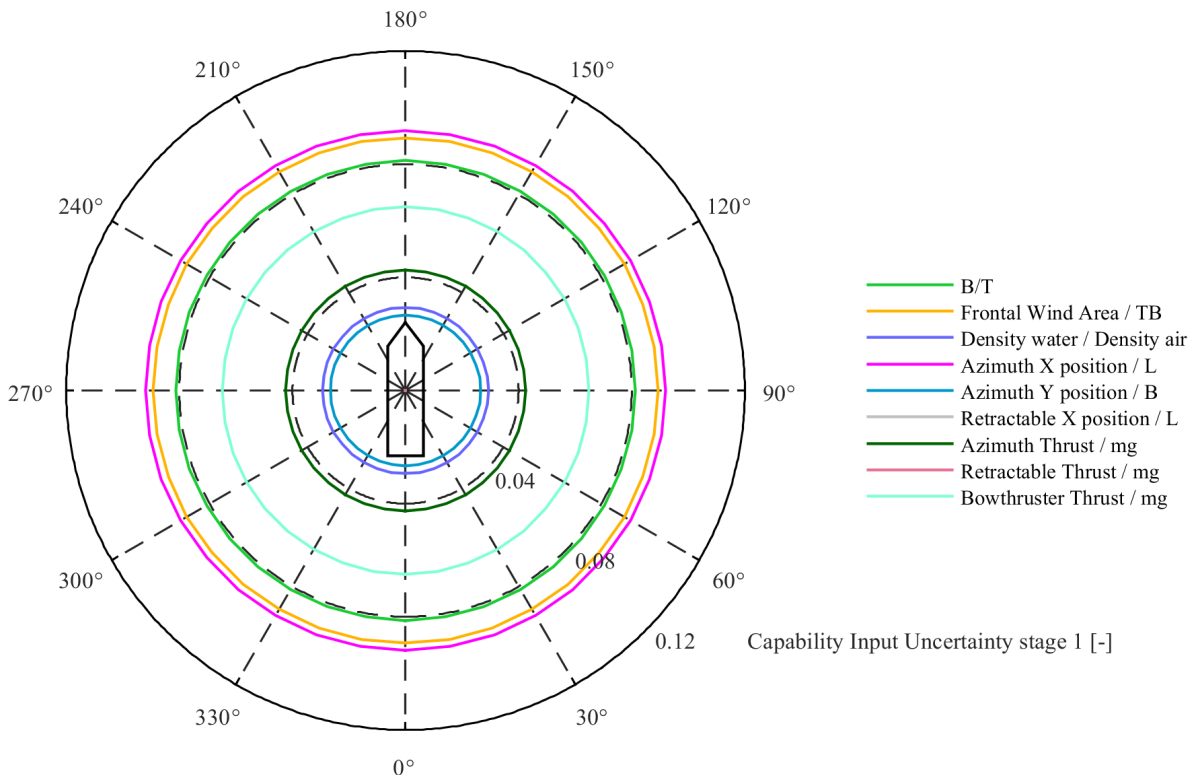


Figure 4.19: Capability input uncertainty axis 0.12

#### 4.2.2. Preliminary design stage

Similar as in the conceptual design stage the same parameters have the biggest input uncertainty which are: *Wind coefficient  $C_x$ , Current coefficient  $C_x$  and  $C_y$ , and Wave coefficient  $C_x$ ,  $C_y$ , and  $C_n$*  which is illustrated in figures 4.20 and 4.21. This can be explained by the fact that there is no clear indication which of the different sets of coefficients should be used for calculation and could therefore in theory be all used for each design stage. This means that the input uncertainty of those coefficients will not change over the different design stages.

What is observed from figures 4.22 and 4.23 is that the uncertainty of the basic dimensions of the vessel are decreased which can be explained by the fact that a much clearer view of the shape of the vessel is obtained. The uncertainty in bow and azimuth thrust is increased most likely due to the fact that in the preliminary design stage more attention is paid to the demands and regulations of the vessel which results in different requirements for the thrusters whereas in the conceptual design stage more the dimensions of the vessel are considered.

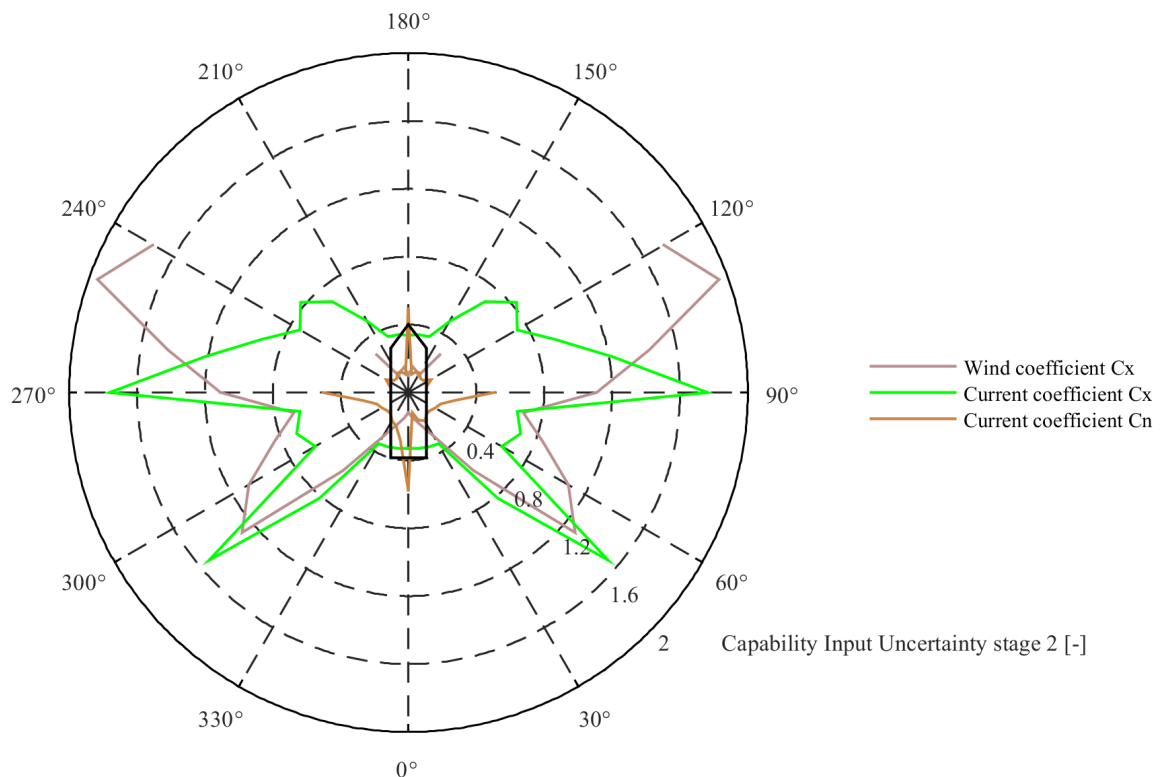


Figure 4.20: Capability input uncertainty axis 2.0

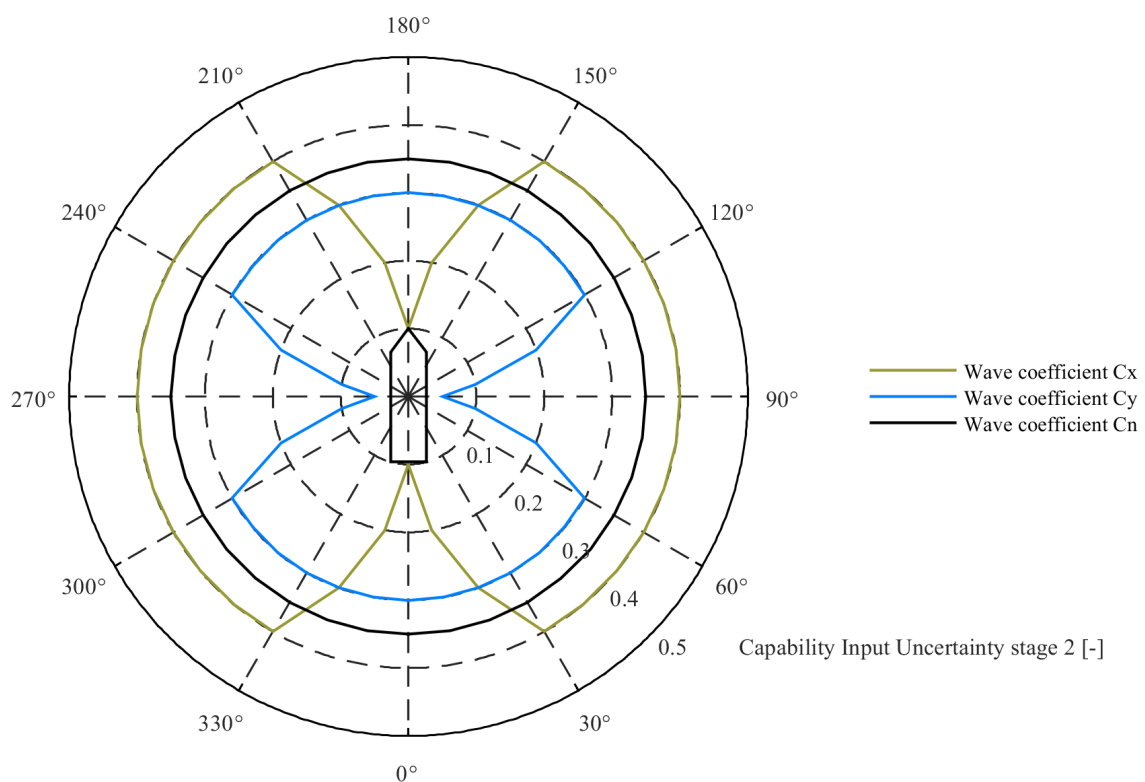


Figure 4.21: Capability input uncertainty axis 0.5

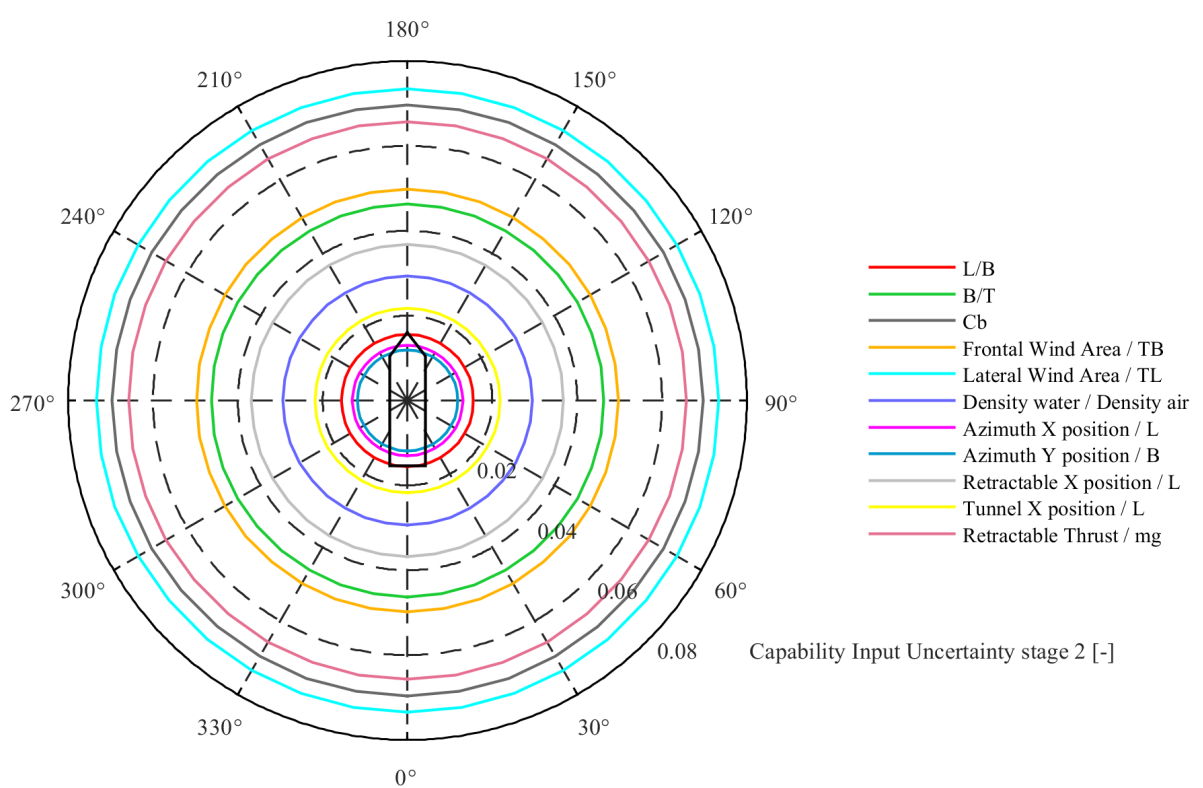
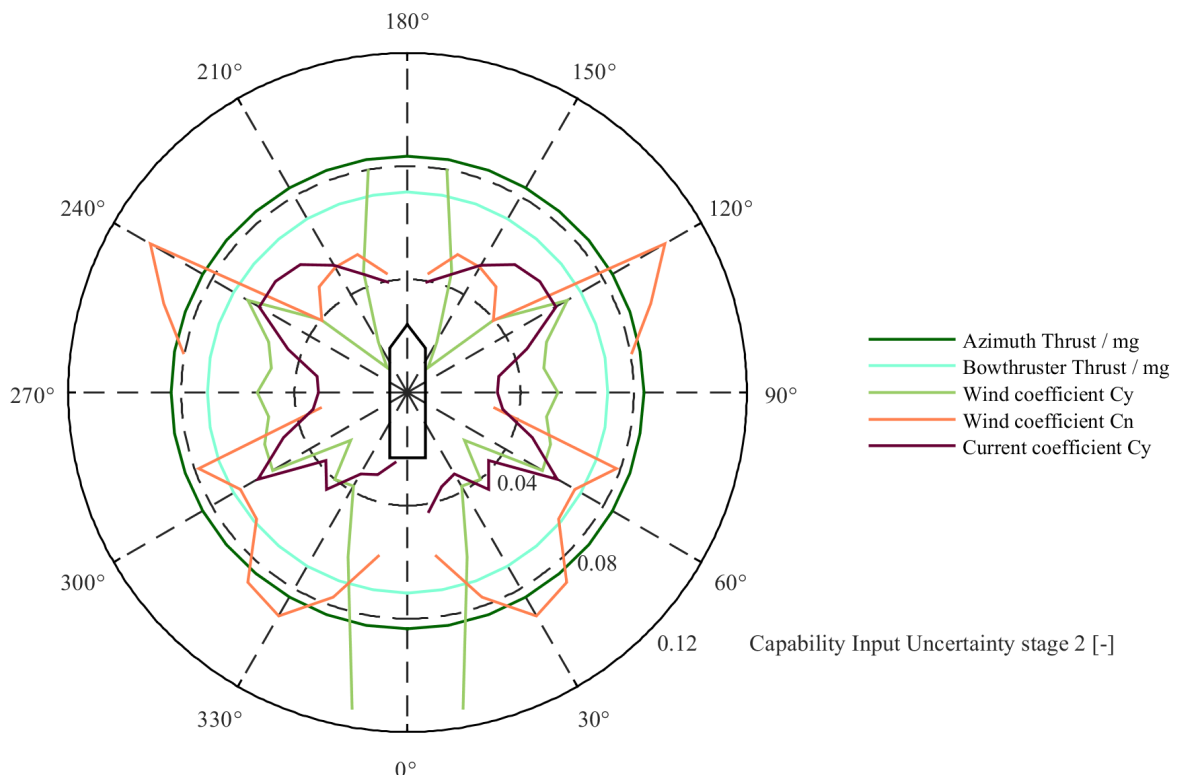


Figure 4.23: Capability input uncertainty axis 0.08

### 4.2.3. As built design stage

In the as built stage no uncertainties are present in the basic dimensions of the vessel anymore which leaves only the environmental coefficients, the thrust and the density of air and water uncertain as can be seen in the figures below. The uncertainty of the thrust is still present here as explained in 3.2.2.

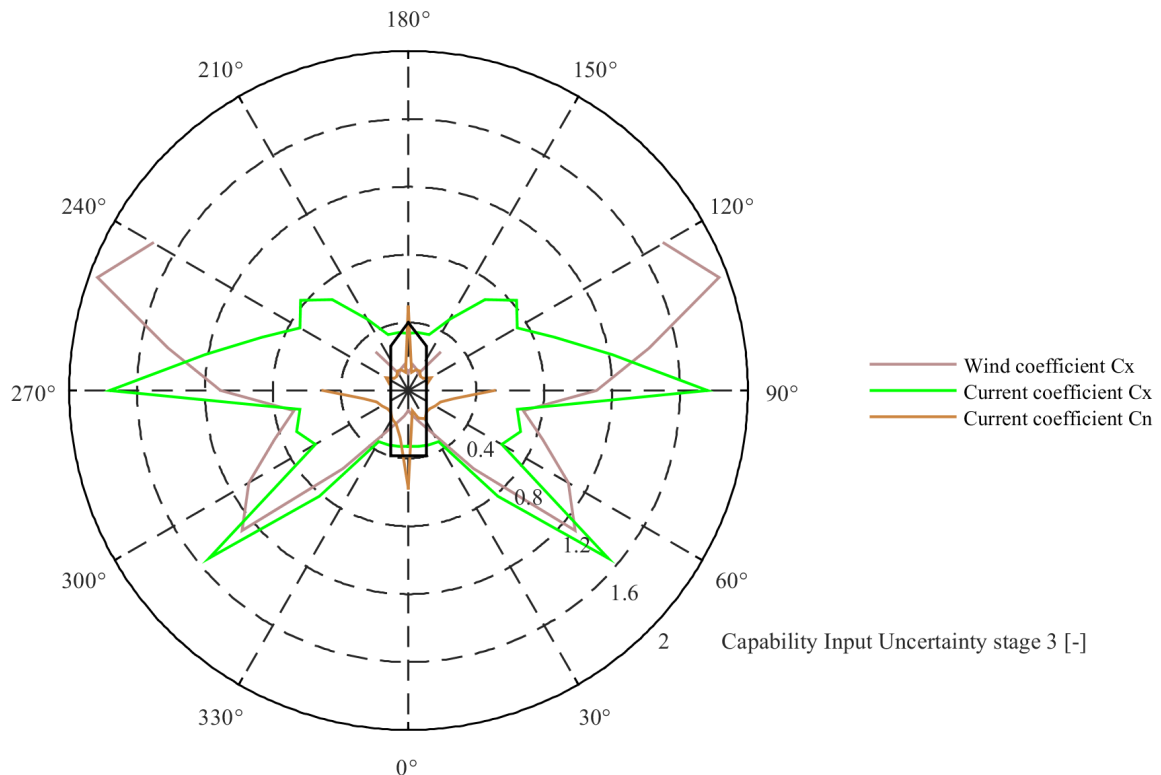


Figure 4.24: Capability input uncertainty axis 2.0

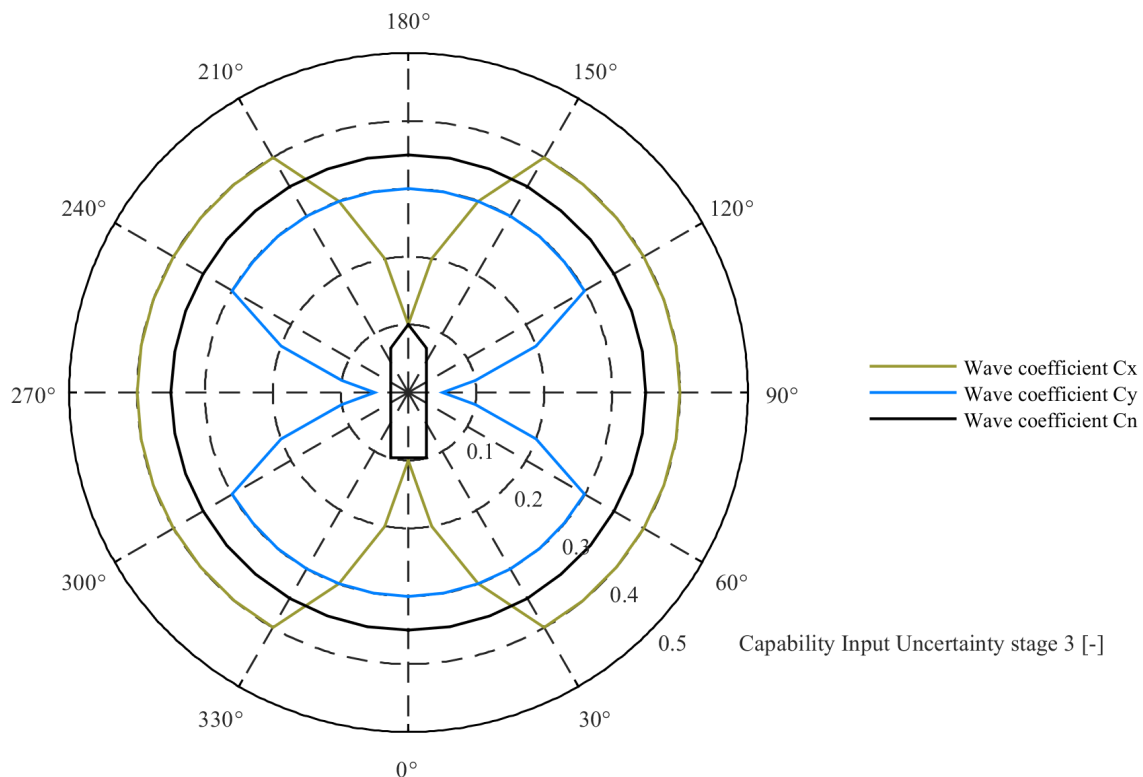


Figure 4.25: Capability input uncertainty axis 0.2

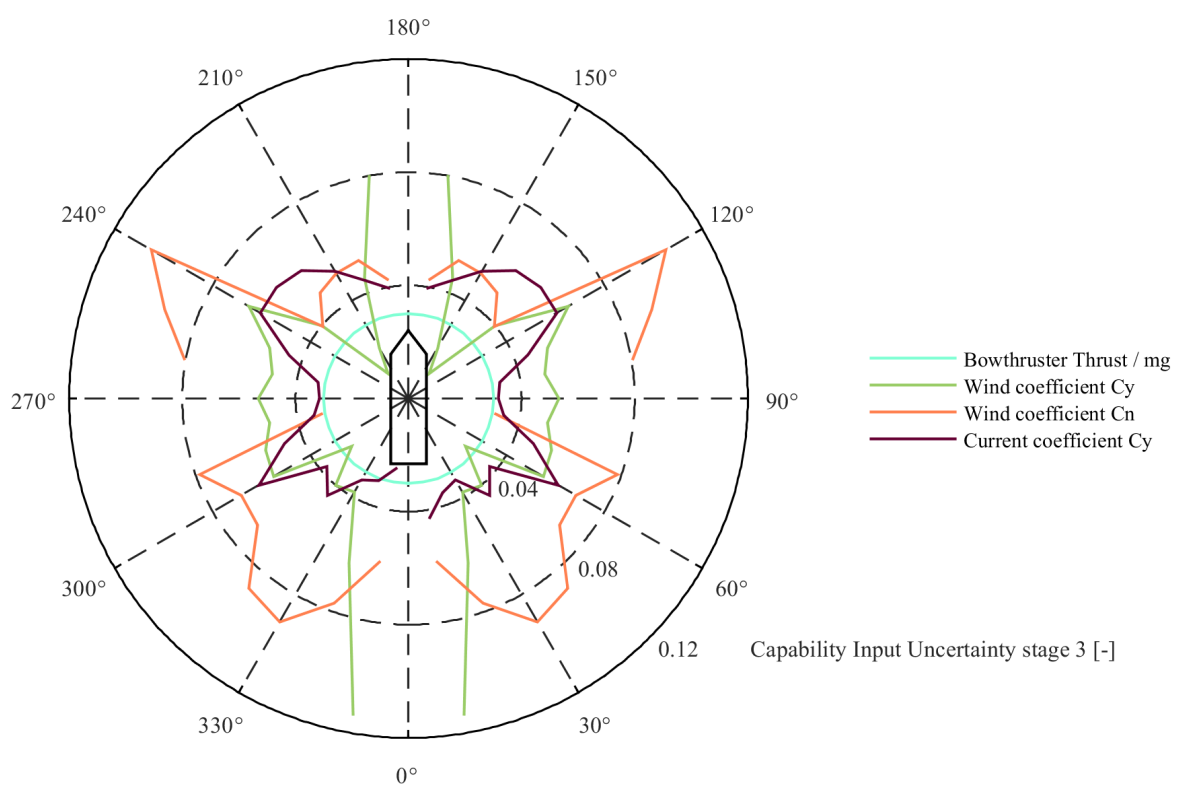


Figure 4.26: Capability input uncertainty axis 0.12

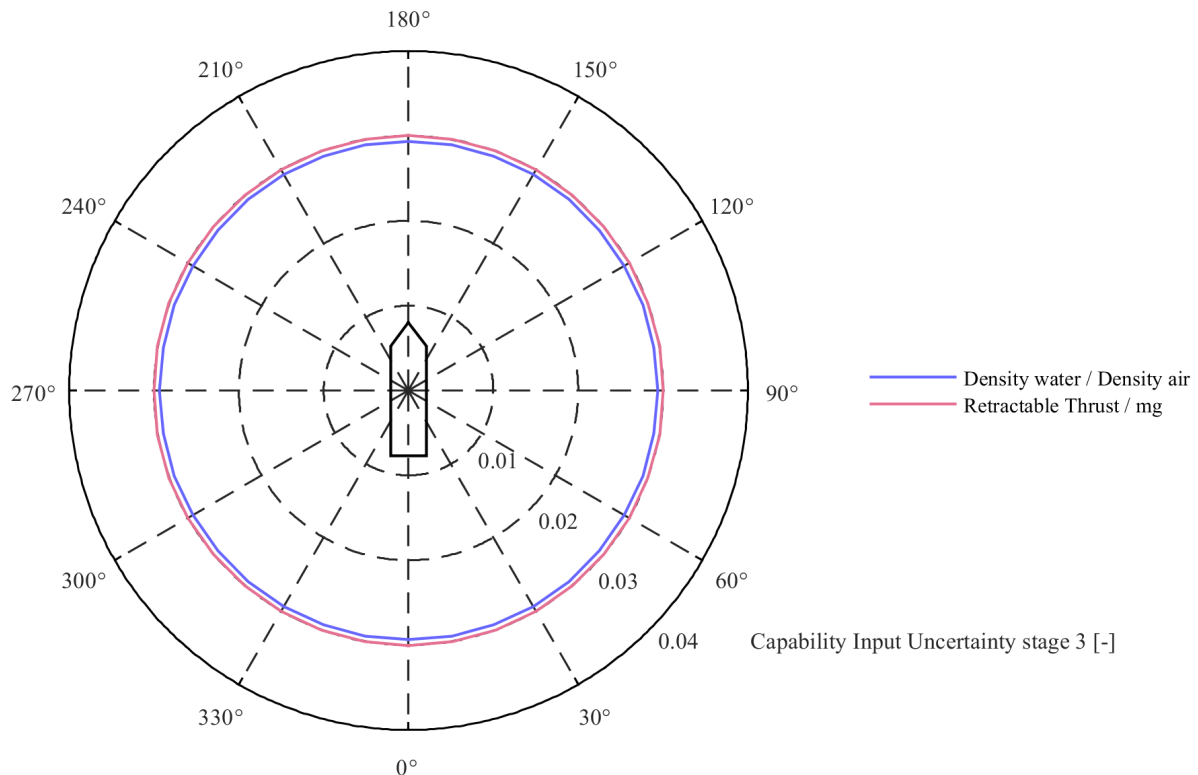


Figure 4.27: Capability input uncertainty axis 0.04

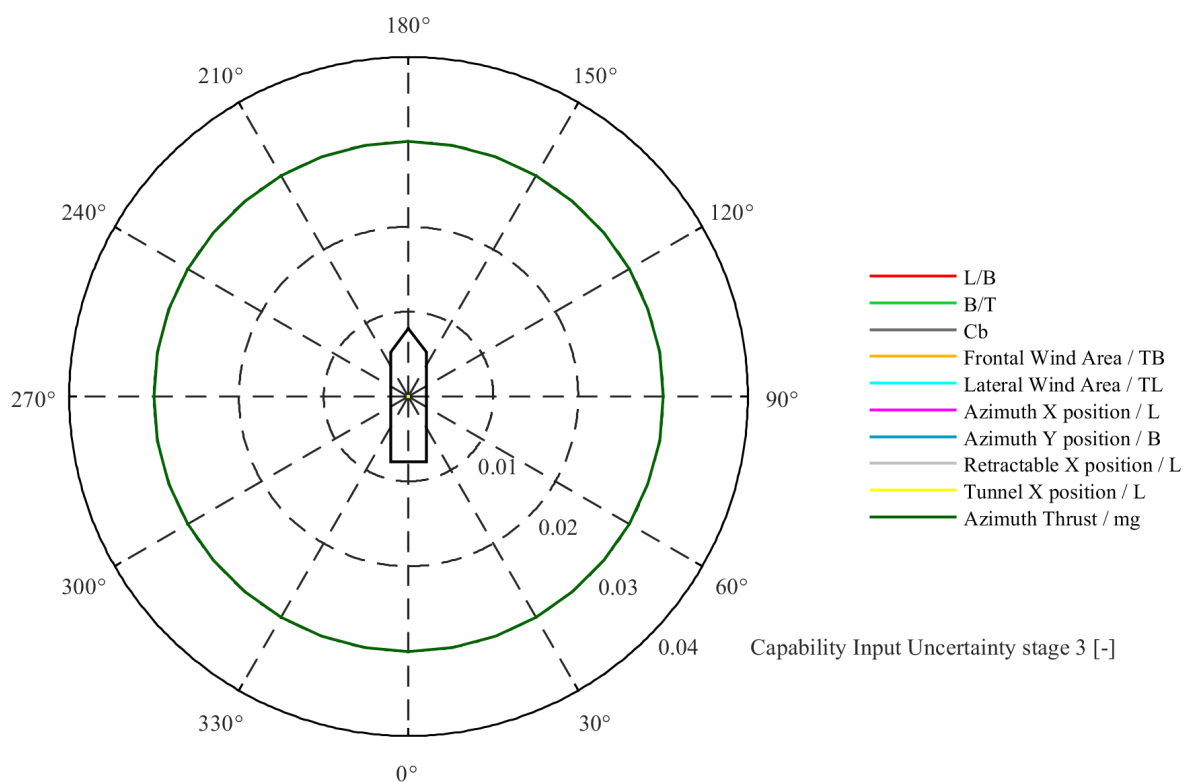


Figure 4.28: Capability input uncertainty axis 0.04

## 4.3. DPlab capability output uncertainty

In this section the capability output uncertainty is evaluated. When looking back at equation: 2.35 it is seen that the capability output uncertainty is taken as the square root of the sum of the individual multiplications of sensitivity and input uncertainty. This gives a good indication of the total output uncertainty but in order to have an idea which parameter contributes most to total output uncertainty, the square root of the individual multiplications of sensitivity and input uncertainty are shown first. The mathematical representation of this is shown in equation 4.1.

$$\text{Separate parameter output uncertainty} = \sqrt{\left(\frac{\partial z^*}{\partial x_i}\right)^2 \cdot (\sigma_{x_i}^*)^2} \quad (4.1)$$

It is important to note that the total output uncertainty is not just the summation of these separate terms since first the summation should be done after which the square root can be taken. This is illustrated in equation 4.2.

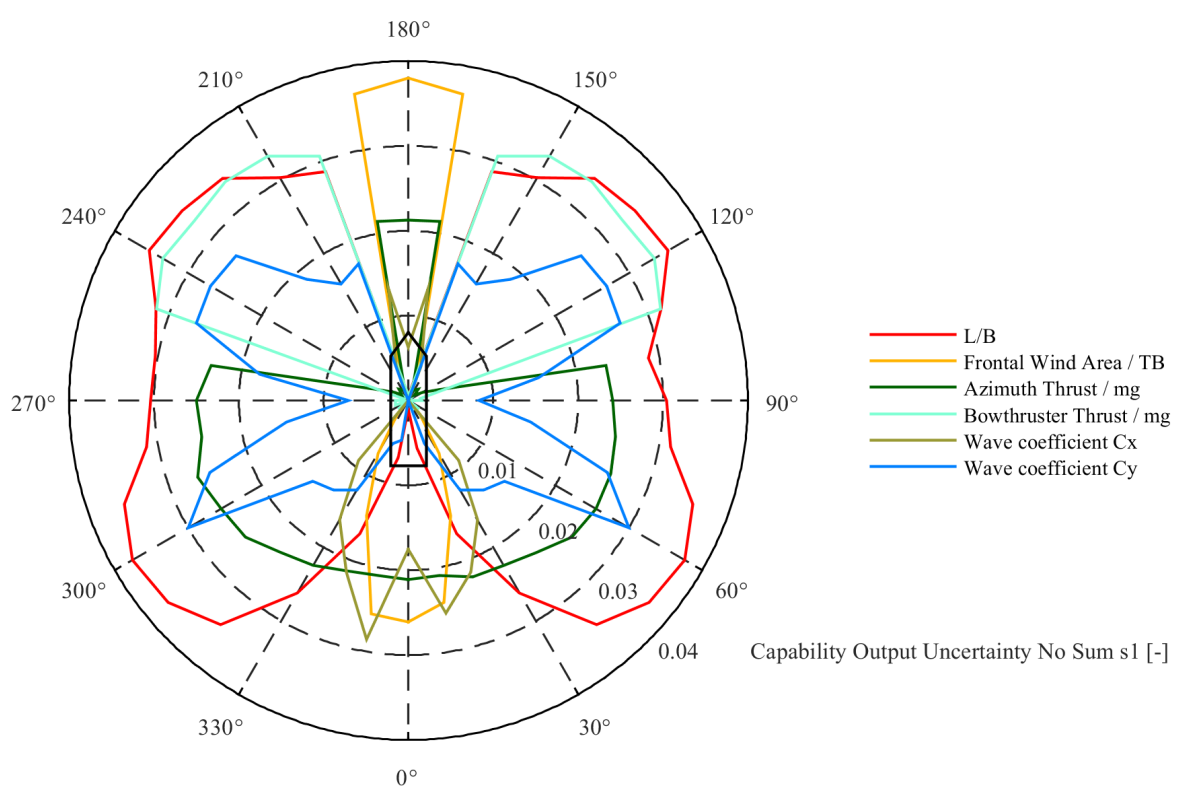
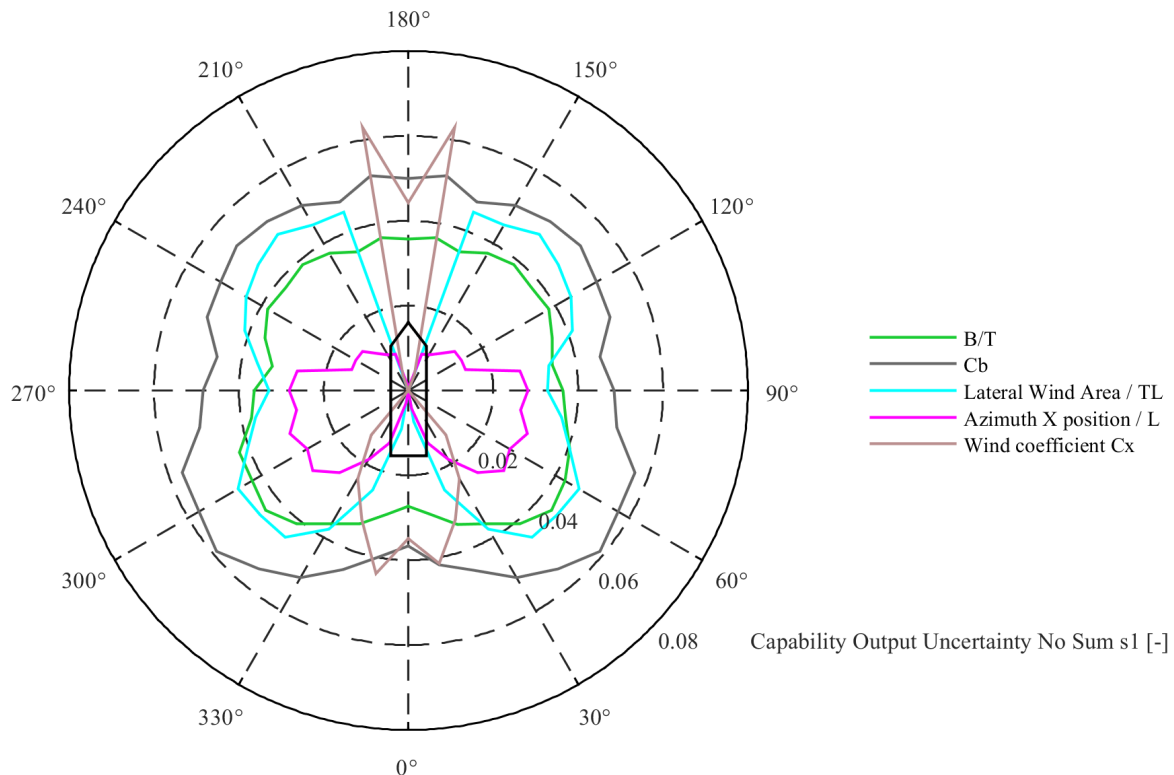
$$\sqrt{\sum_i \left(\frac{\partial z^*}{\partial x_i}\right)^2 \cdot (\sigma_{x_i}^*)^2} \neq \sum_i \sqrt{\left(\frac{\partial z^*}{\partial x_i}\right)^2 \cdot (\sigma_{x_i}^*)^2} \quad (4.2)$$

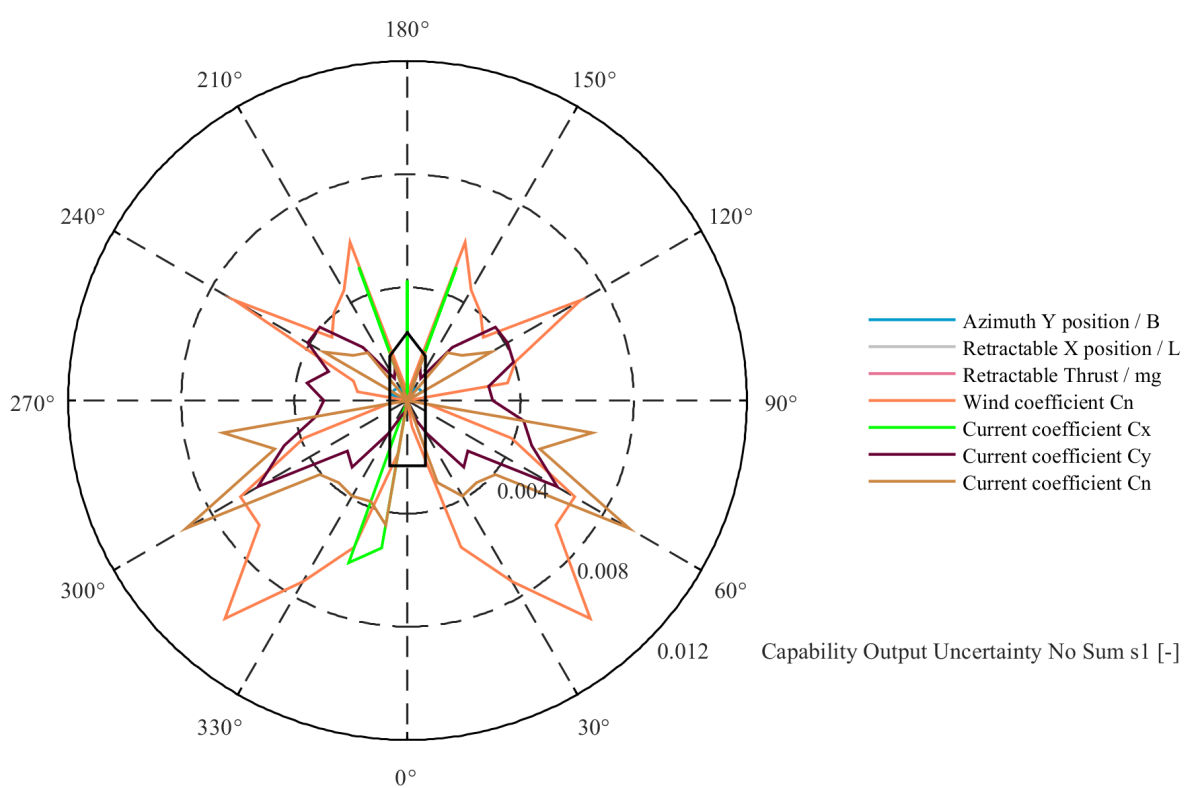
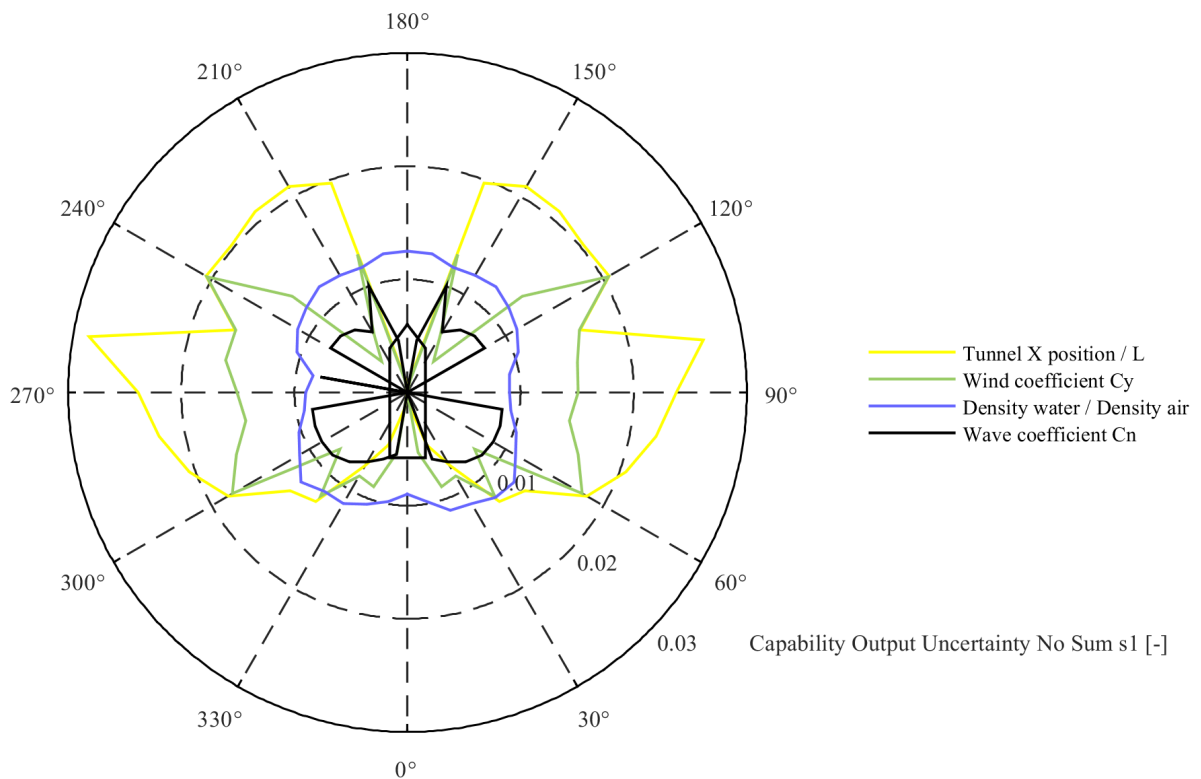
### 4.3.1. Conceptual design stage

The first thing to notice in figure 4.29 is that the variables contributing mostly to the output uncertainty for the conceptual design stage are the basic dimensions of the vessel. The first non basic dimension that contributes significantly to the output uncertainty is the *Wind Coefficient Cx* which only has an influence around the angles 0 and 180 degrees as would be expected. In figure 4.30 the remaining basic dimensions are found together with the *Azimuth Thrust / mg* and *Wave Coefficients Cx and Cy*.

The *Wave Coefficient Cy* decreases for 90 and 270 degrees and this trend is also seen somewhat for *Wind Coefficient Cy* and *Current Coefficient Cy*. This is explained by the fact that the uncertainty of these coefficients is the smallest at these specific angles making the contribution to the output smaller. However when looking to the *Wave Coefficient Cy* a bit closer it is seen that this trend is more extreme compared to wind and current. This is most likely due to the fact that the uncertainty of the wave coefficients is guessed based on trends of the other environmental coefficients. Therefore it could be that for instance the input uncertainty might be estimated a bit on the low side for the angles 90 and 270 degrees which results in a lower output uncertainty.

In figure 4.32 the current coefficients are found and showing almost no significant contribution to the output uncertainty.





### 4.3.2. Preliminary design stage

In the preliminary design stage it is visible that the contribution of the basic dimensions of the vessel on the output uncertainty is decreased when comparing to the conceptual design stage. This is explained by the fact that the sensitivity of the basic dimensions do not significantly change throughout the design stages but the input uncertainty reduces resulting in a lower contribution on the output uncertainty. The contribution to the output uncertainty of the environmental coefficients stays almost the same compared to the conceptual design stage since the sensitivity of these coefficients does not change significantly throughout the design stages and the input uncertainty stays constant.

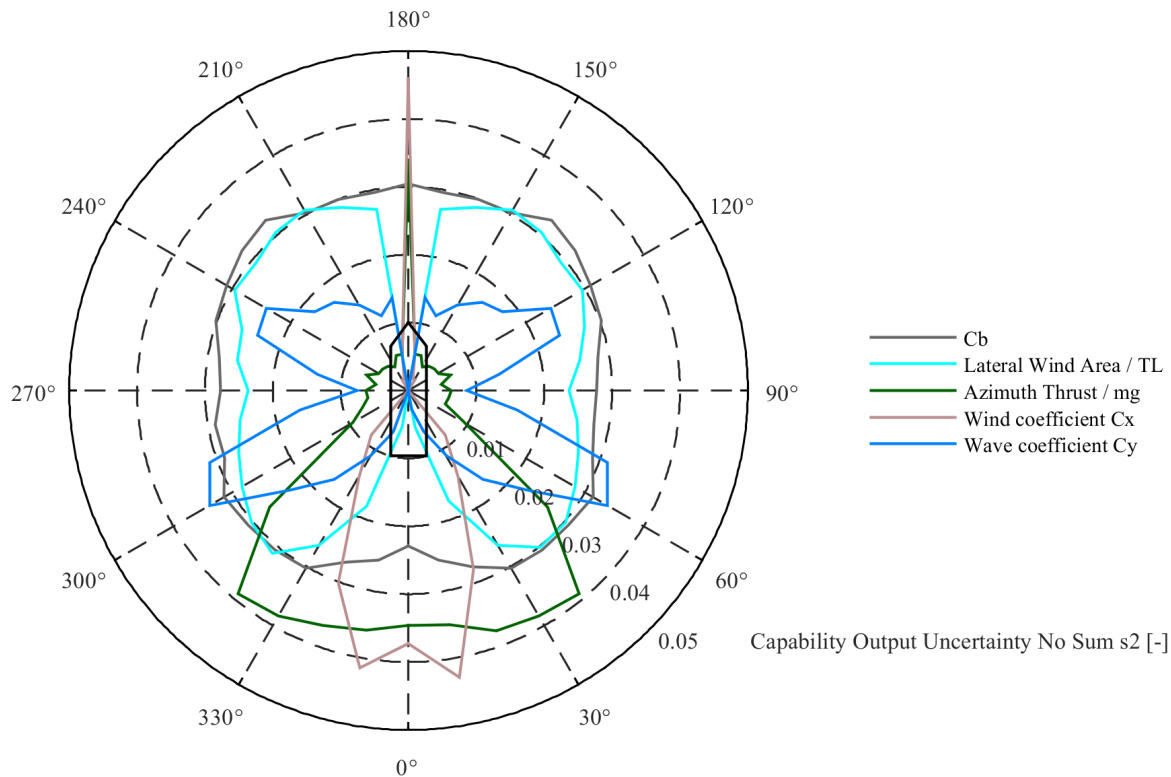
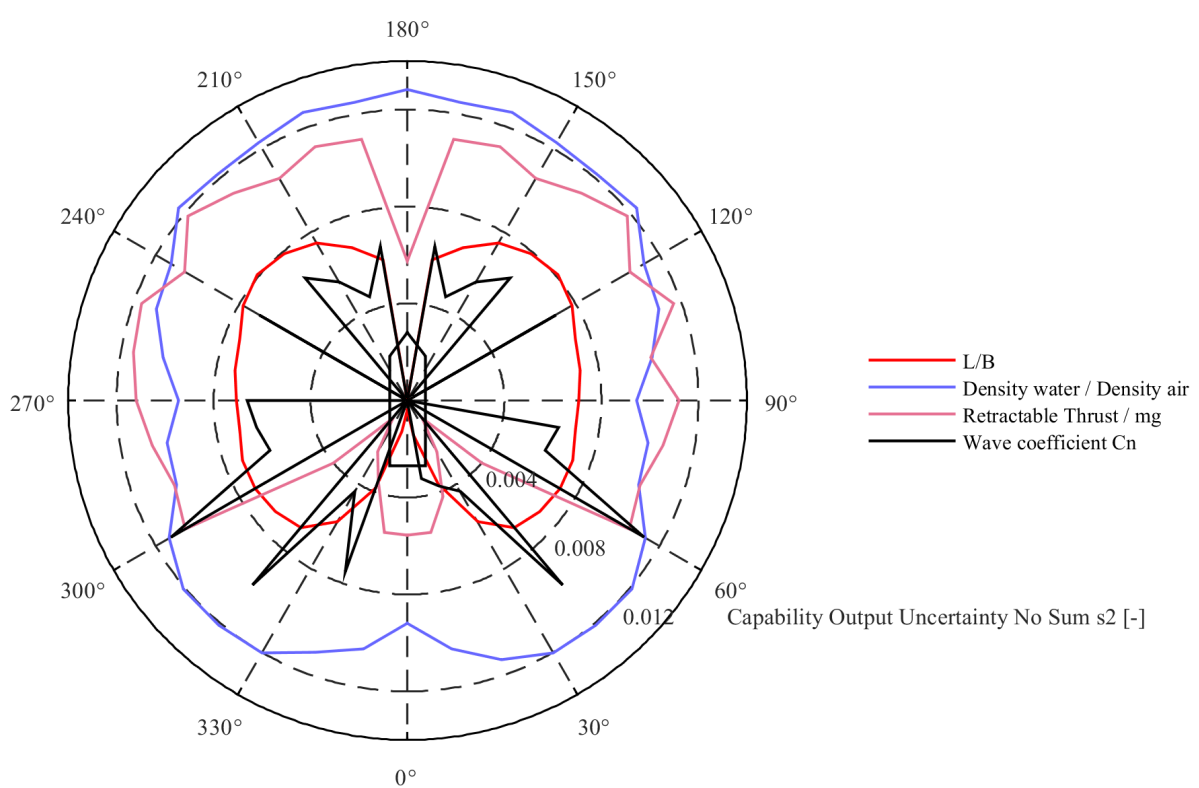
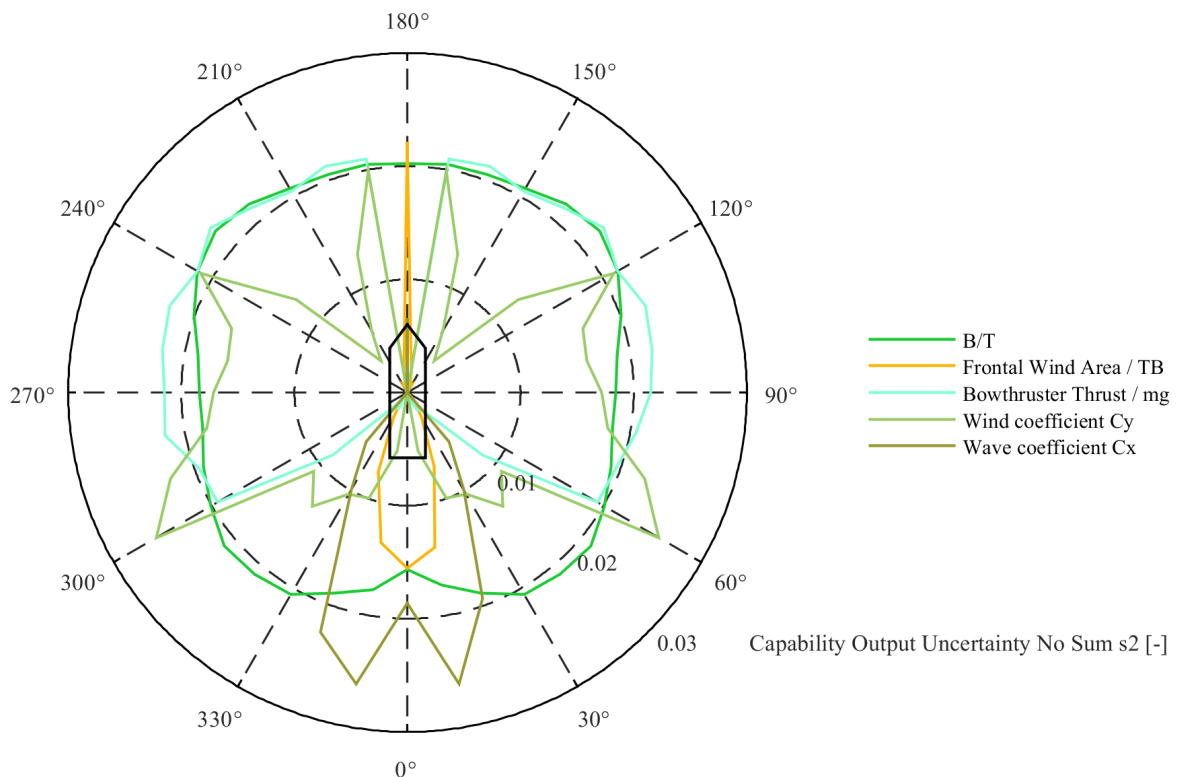


Figure 4.33: Capability output uncertainty axis 0.05



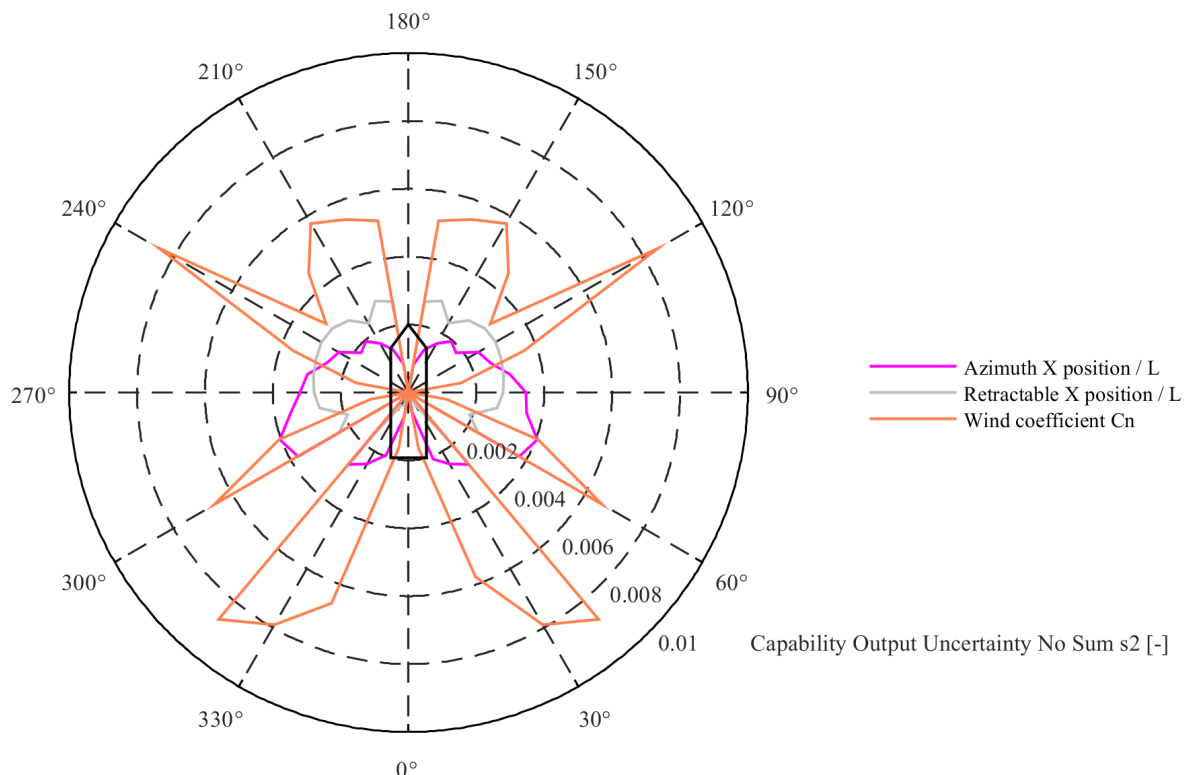


Figure 4.36: Capability output uncertainty axis 0.01

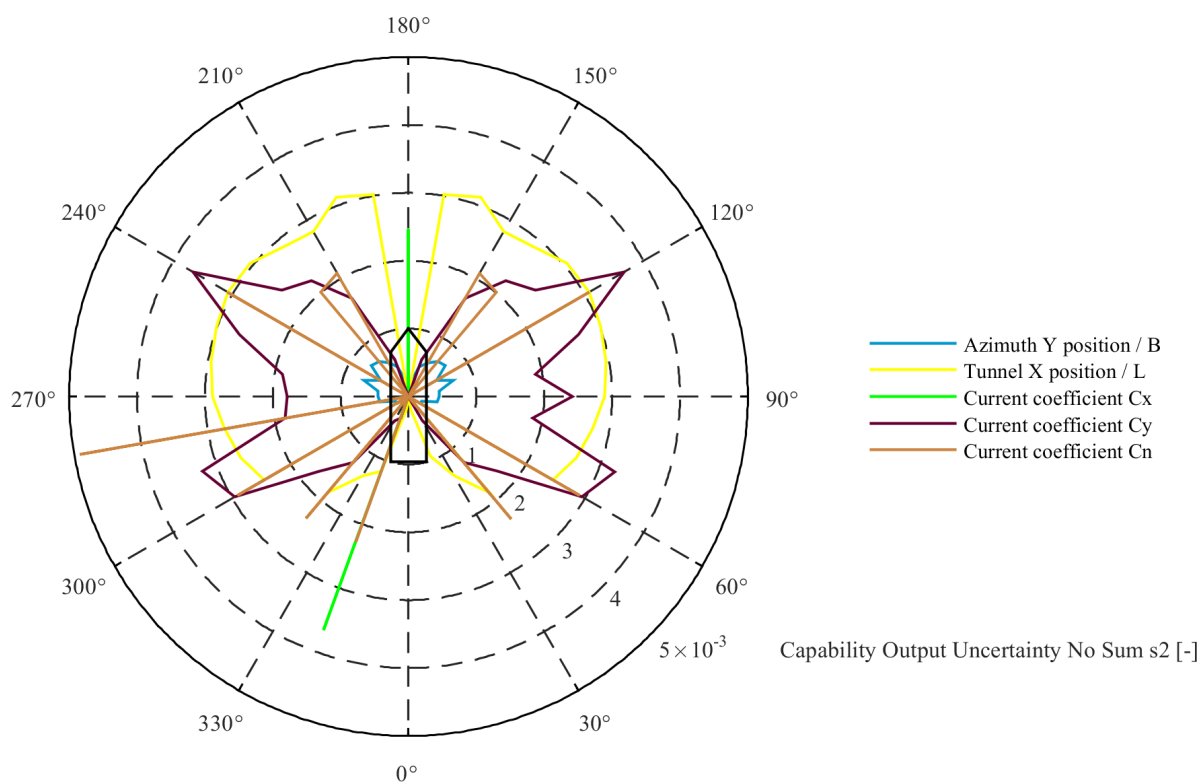


Figure 4.37: Capability output uncertainty axis 0.005

### 4.3.3. As built design stage

When considering the as built design stage output uncertainty, it is seen that all the basic parameters of the vessel have no contribution to the output uncertainty anymore. This is to be expected since these parameters have no input uncertainty in this stage. The five parameters that contribute the most to the output uncertainty are *Wind Coefficient C<sub>x</sub>* and *C<sub>y</sub>*, *Wave Coefficients C<sub>x</sub>* and *C<sub>y</sub>* and *Density Water / Density Air*. What stands out is that the wave coefficients seem to have a significant contribution to the output uncertainty. However since the sensitivity of these wave coefficients is not extremely high it suggests that mainly the input uncertainty of the wave coefficients contribute to this behaviour. Recalling that the input uncertainty was estimated one could argue if the magnitude was chosen a bit too high. However since only one data set is available for the wave coefficients which is not specifically calculated for the vessel the uncertainty can potentially quite large. Recalling that the same trends and magnitudes for the wave coefficients are chosen as for the other environmental coefficients it is therefore decided to remain the input uncertainty as chosen.

Another thing to note is that contribution to the output uncertainty due to the thrust of the thrusters is smaller than the contribution due to the ratio of water and air density. This shows that it can really pay off to investigate further in what conditions the vessel will operate instead of changing something on the thruster side of the vessel.

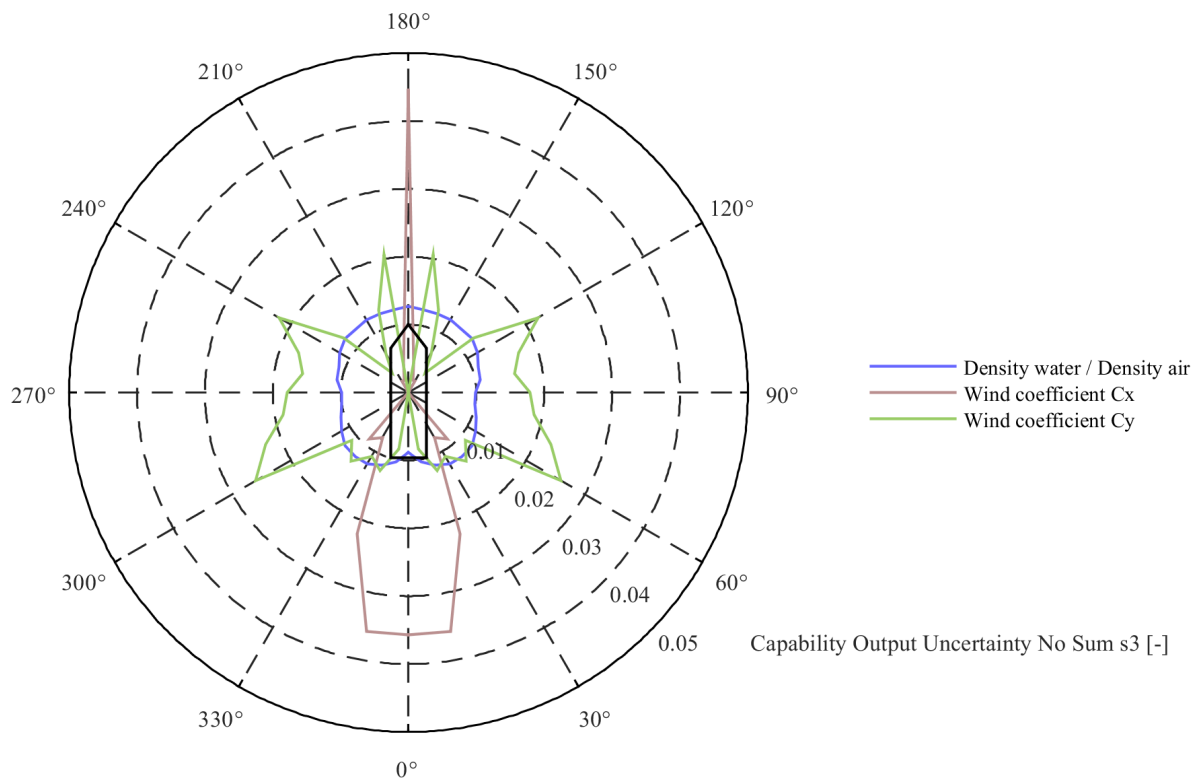


Figure 4.38: Capability output uncertainty axis 0.05

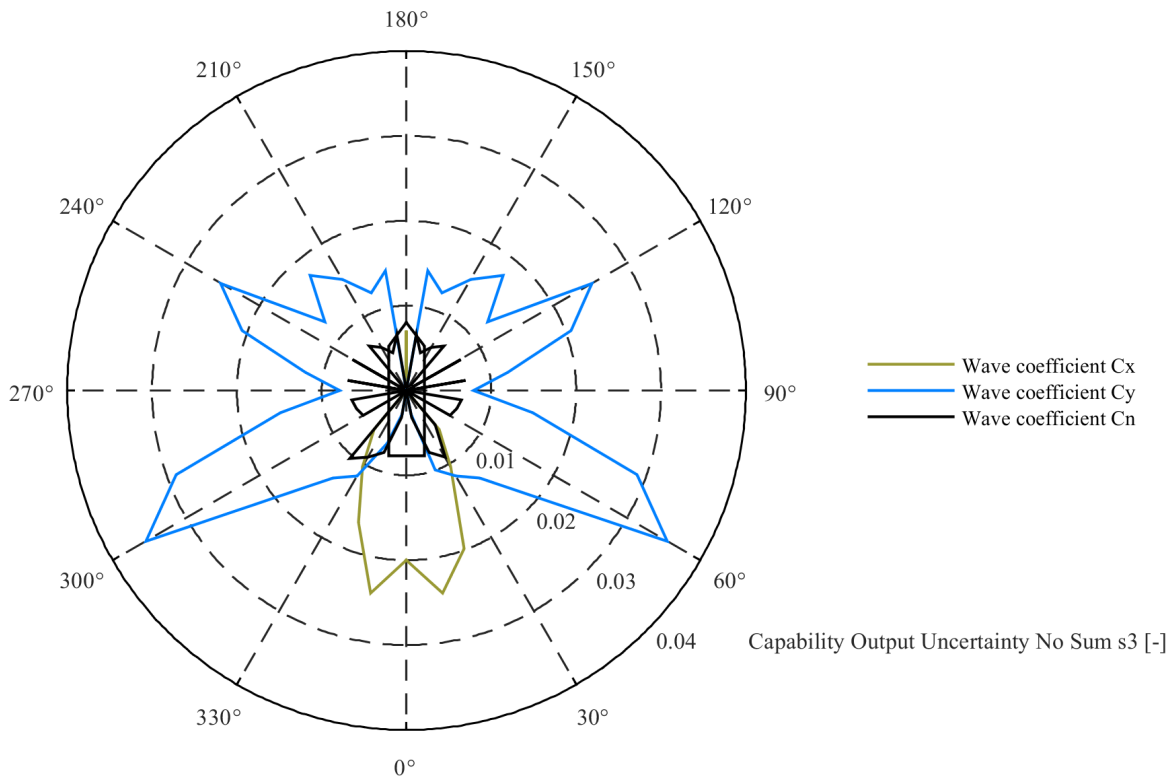


Figure 4.39: Capability output uncertainty axis 0.04

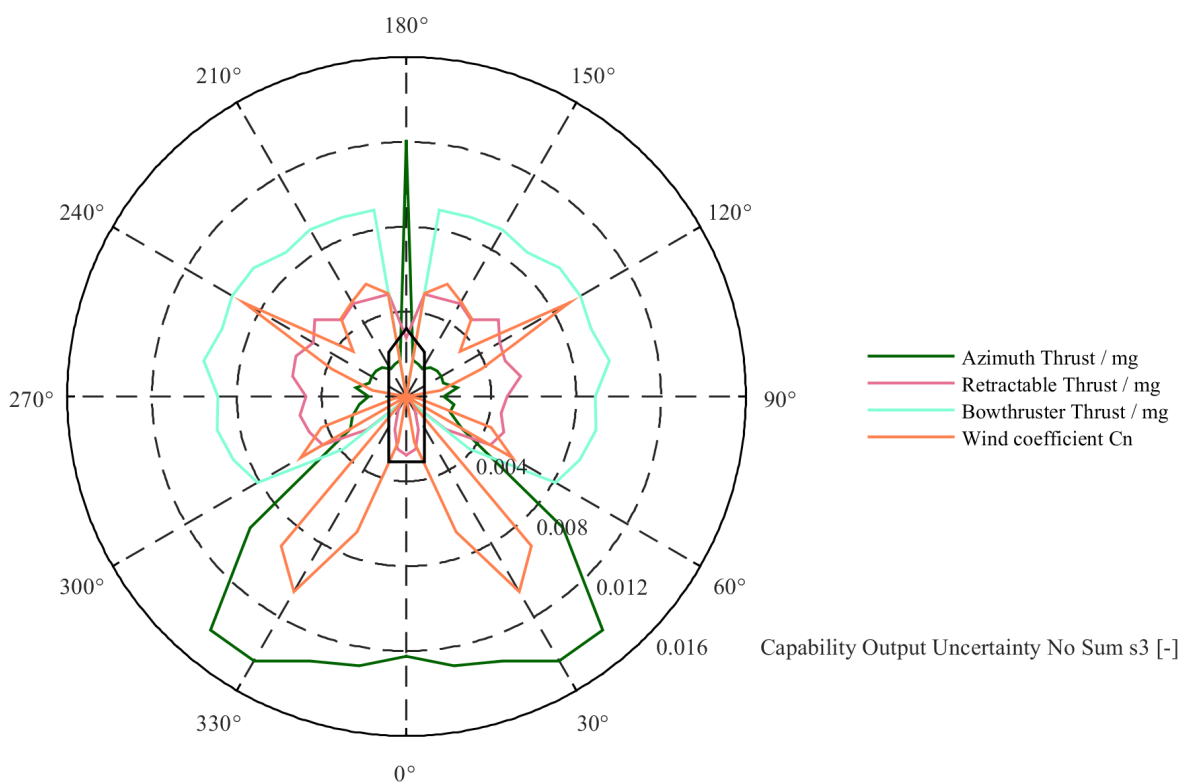


Figure 4.40: Capability output uncertainty axis 0.016

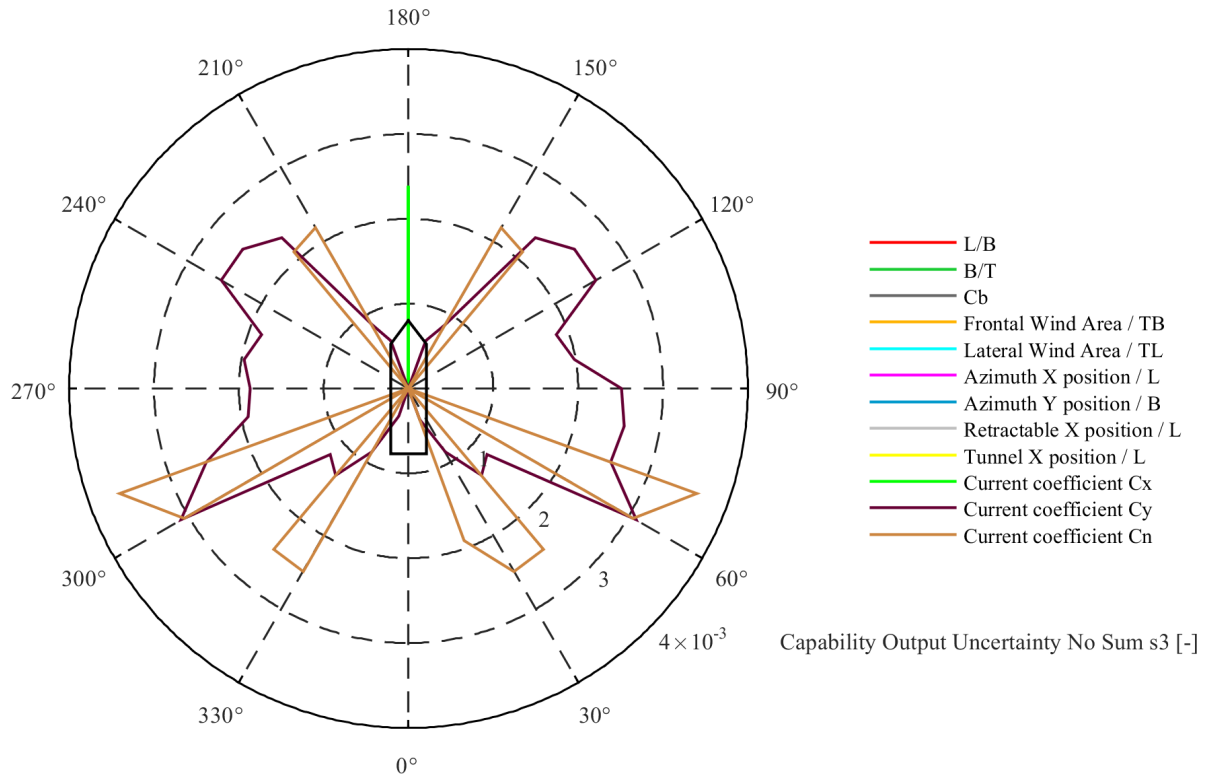


Figure 4.41: Capability output uncertainty axis 0.004

#### 4.3.4. Total capability output uncertainty

After evaluating the individual contribution of the parameters to the output uncertainty the total output uncertainty can be calculated and is illustrated in figure 4.42. As expected the total output uncertainty reduces when going through the design stages. Interesting to see is that for each angle the total uncertainty difference between the design stages is almost constant except for the conceptual design stage around 0 degrees. This is likely due to the fact that the azimuth thruster uncertainty is relatively small for the conceptual design stage and increases when moving to the preliminary design stage. This results in a relatively smaller decrease in total output uncertainty for angles which are around 0 degrees.

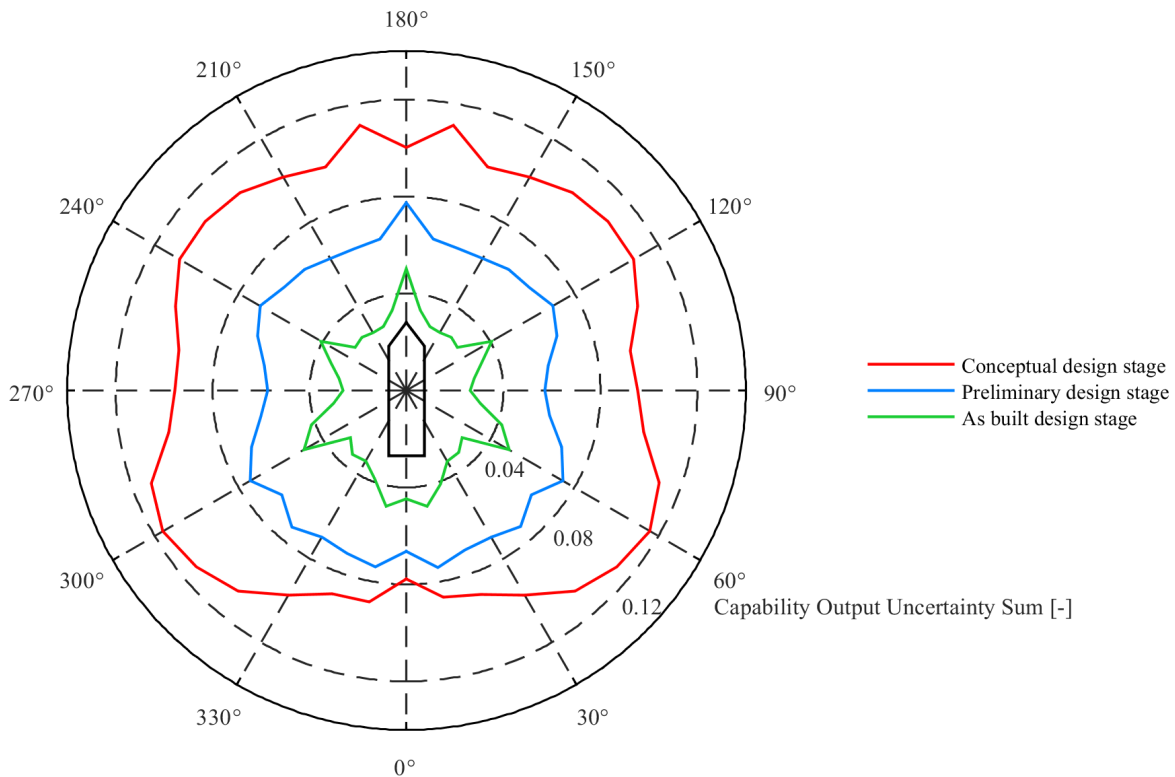


Figure 4.42: Total capability output uncertainty

#### 4.4. DPlab capability confidence interval

In section 4.3.4 the total capability output uncertainty is calculated and can be used to calculate the confidence intervals for the capability of the vessel. First the base case capability is plotted after which the upper and lower bound of the confidence interval can be determined. The total output uncertainty, as calculated in section 4.3.4, multiplied with the base case capability represents one times the standard deviation of the output capability. Now the 95% and the 99.7% confidence intervals, which are two and three times the standard deviation from the base case, can be plotted for each of the design stages.

#### 4.4.1. Conceptual design stage

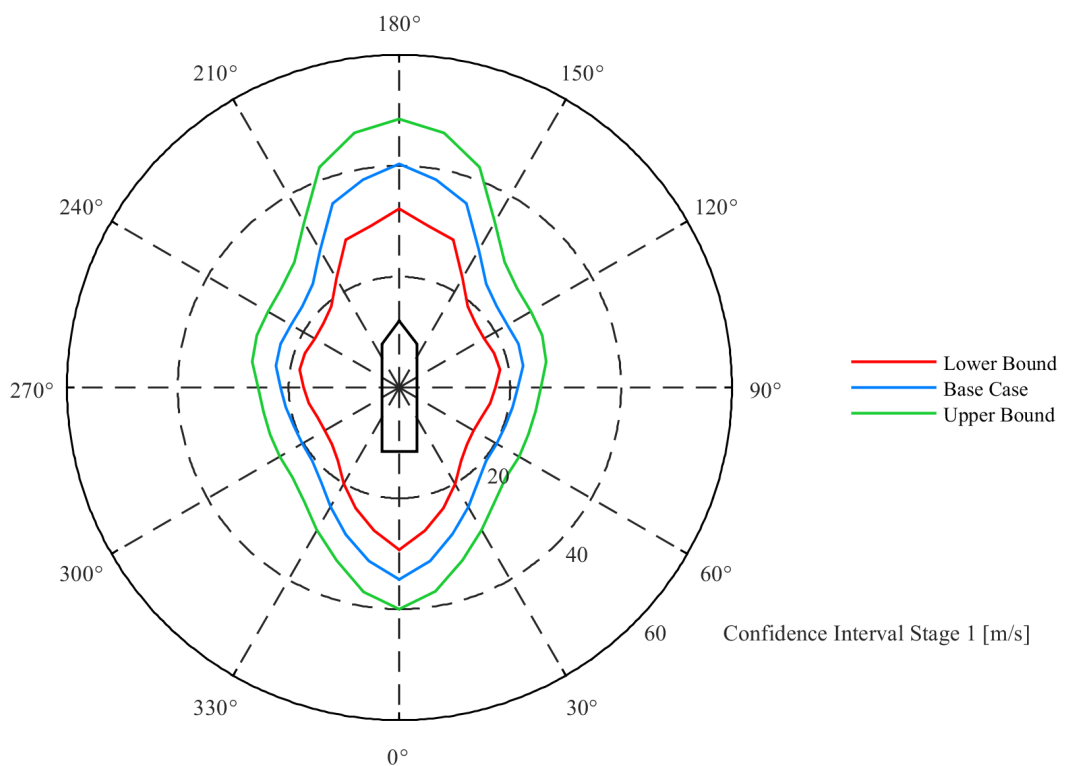


Figure 4.43: Capability 95% confidence interval conceptual design stage

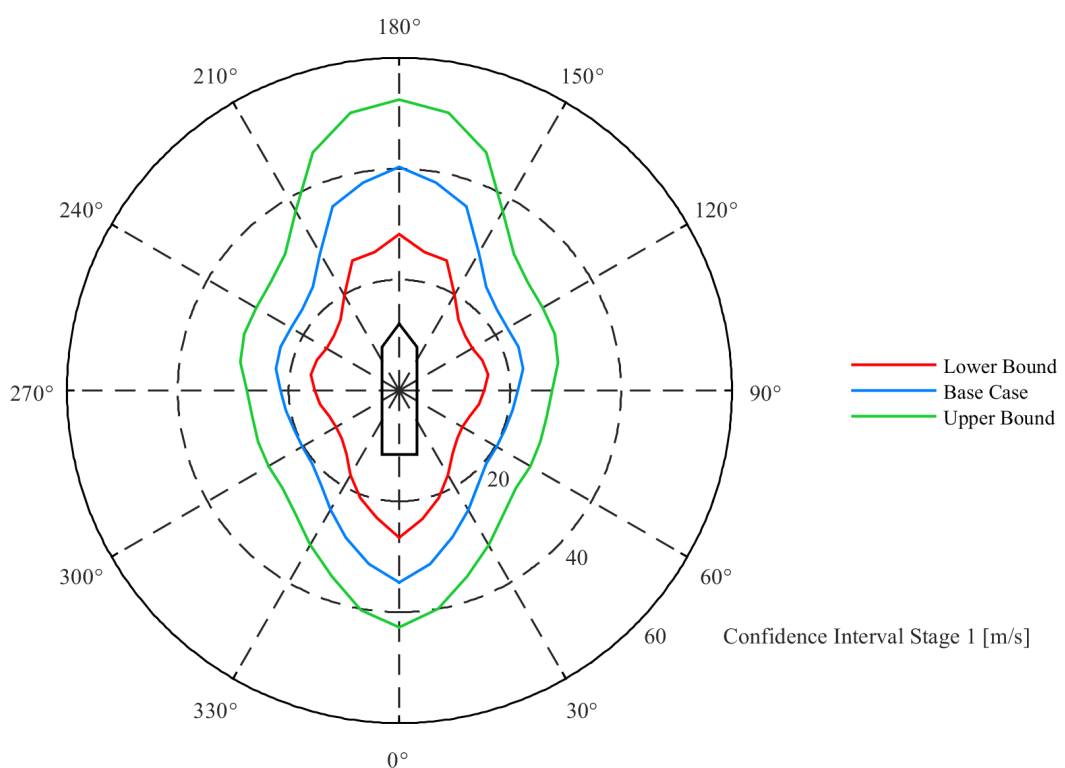


Figure 4.44: Capability 99% confidence interval conceptual design stage

#### 4.4.2. Preliminary design stage

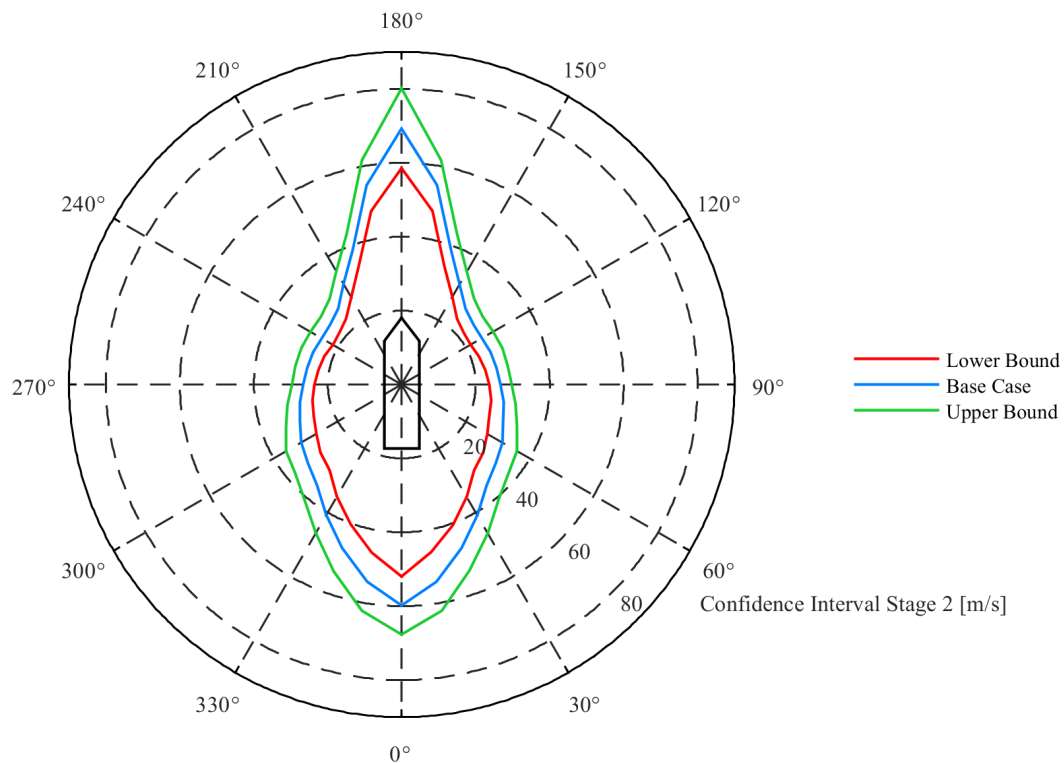


Figure 4.45: Capability 95% confidence interval preliminary design stage

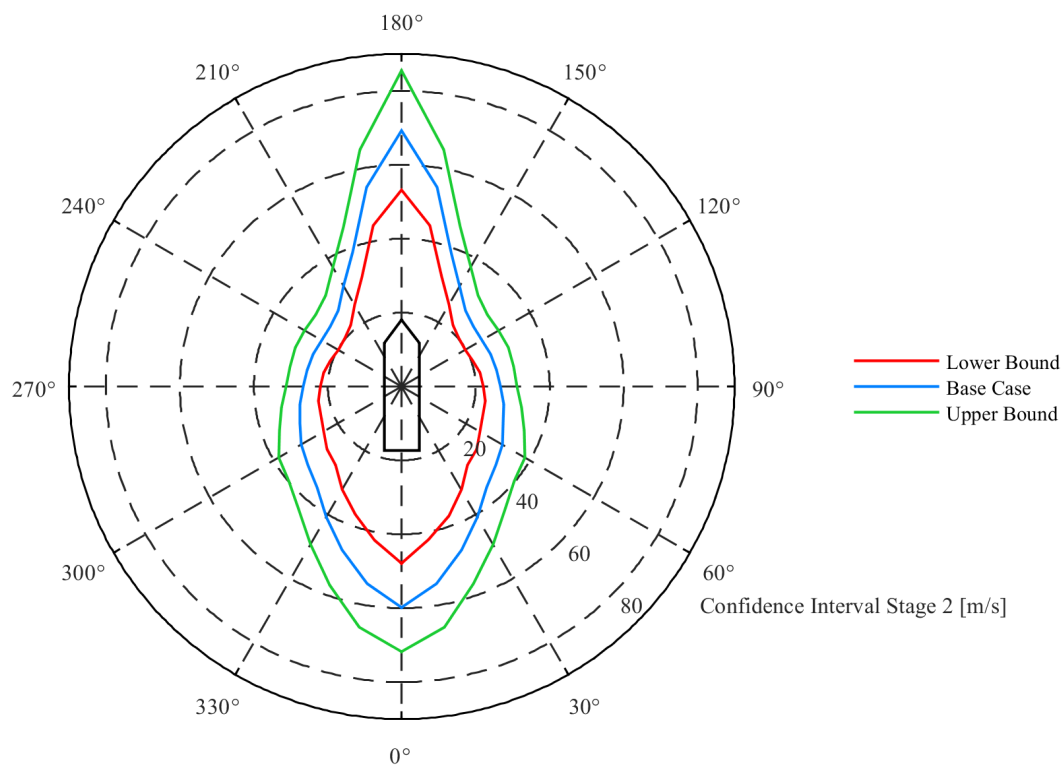


Figure 4.46: Capability 99% confidence interval preliminary design stage

#### 4.4.3. As built design stage

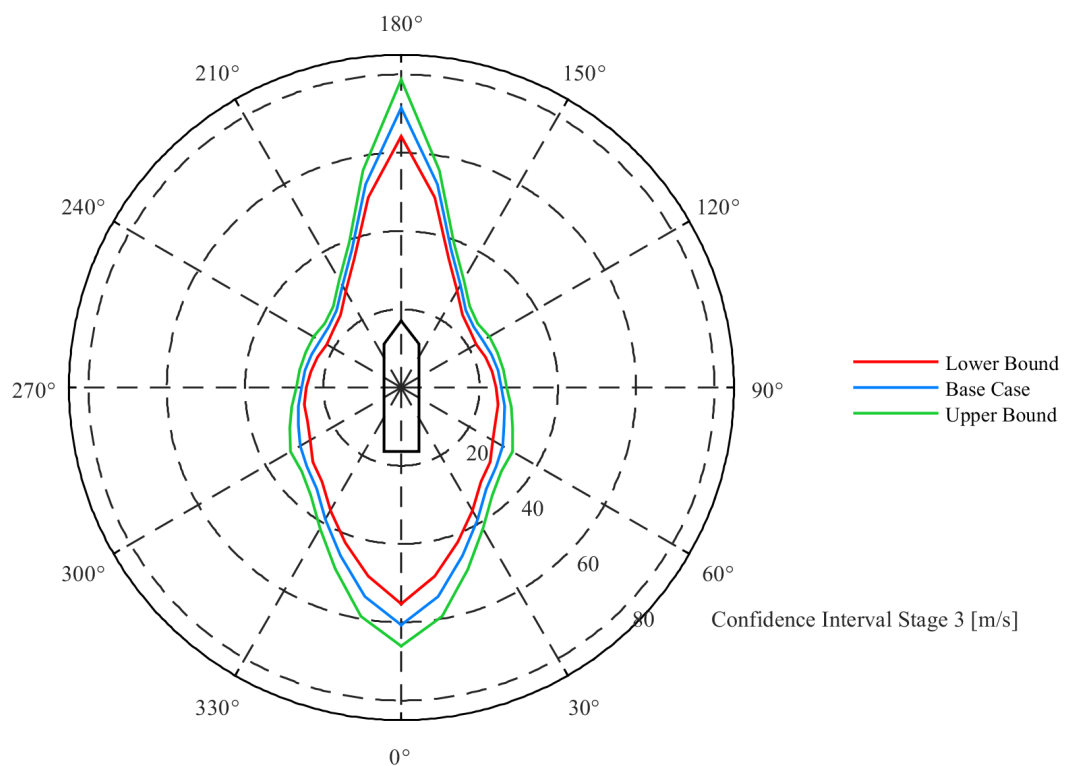


Figure 4.47: Capability 95% confidence interval as build design stage

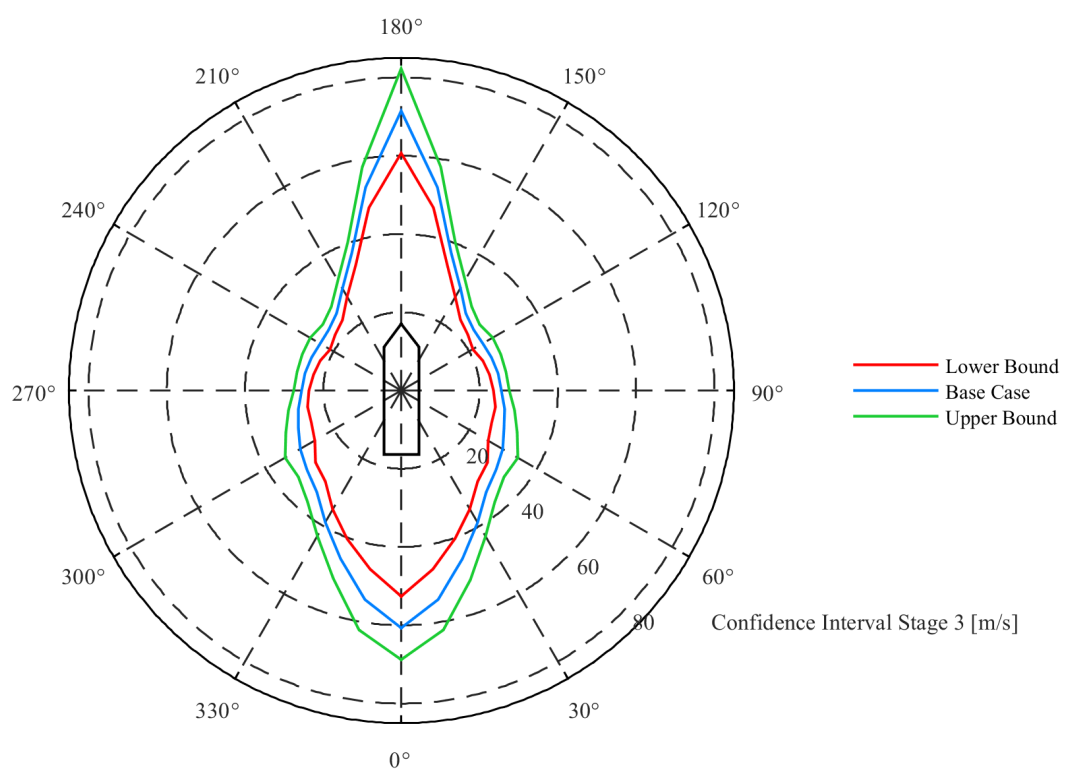


Figure 4.48: Capability 99% confidence interval as build design stage

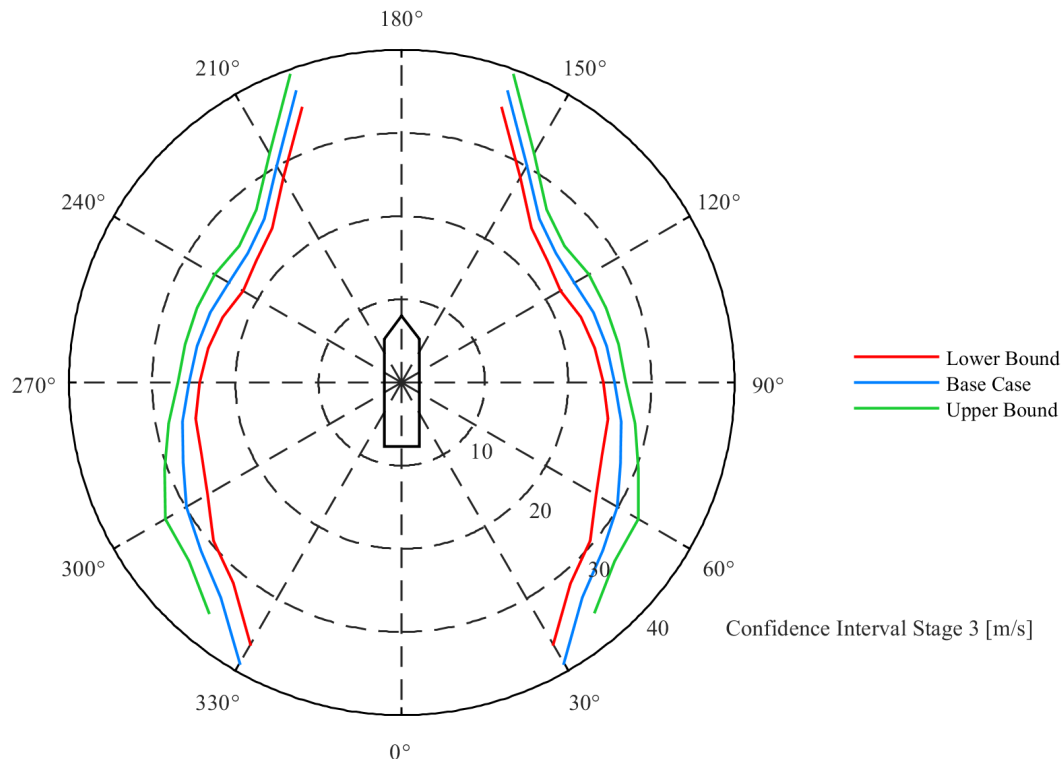


Figure 4.49: Capability 95% confidence interval as build design stage close up

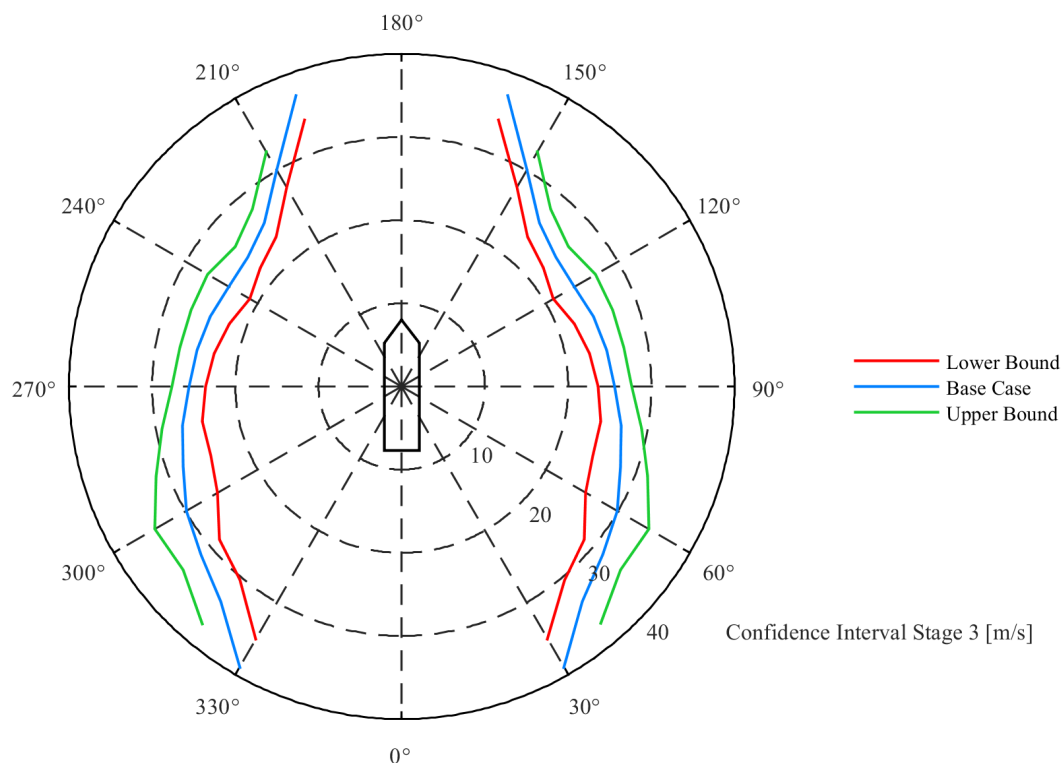


Figure 4.50: Capability 99% confidence interval as build design stage close up

## 4.5. aNySIM goodness of model fit

Before any of the results can be used it is necessary to check whether they are reliable. As explained in section 3.3.8 several parameters are checked to see if the model fitted is accurate enough for the purpose of uncertainty calculation. In this section a couple of examples are elaborated and the complete analysis can be found in appendix F.2. The requirements are defined as  $R\ Squared > 0.98$  and  $MAE < 0.005$ , this is considered really accurate to make sure the model can be used for the purpose of uncertainty calculation

First a series of calculations is done with 136 data points for all angles between 0 – 90 degrees with a step size of 5 degrees. On these data sets a 2nd order polynomial is fitted. After evaluating the parameters mentioned in section 3.3.8 a second run of simulations is done with 270 data points for the angles 0, 30 and 45 degrees and again a 2nd order fit is performed. The final run used for the purpose of uncertainty calculation is executed with 600 data points for the angles 5, 10, 15, 20, 35, 40, 45, 50, 55, 60, 65, 70 and 90 degrees.

In the tables following below several abbreviations are used which are already known to the reader but for the purpose of convenience are again briefly explained below. Also colours are visible in the figures, in the yellow part of the figure the order of fit is displayed. The blue part shows how many data points are used to make the fit and the red part shows for which environmental angle the fit is performed. Furthermore the green boxes indicate whether  $R\ Squared > 0.98$  and  $MAE < 0.005$ .

Table 4.1: Explanation terms used in goodness of fit tables

Name in table	Explanation
RSquare	R Squared
MAE	Mean Absolute Error
MAESTD	Mean Absolute Error Standard Deviation
CVRSquare	Leave One Out Cross Validation (LOOCV) R Squared
CVMAE	Leave One Out Cross Validation Mean Absolute Error
CVMAESD	Leave One Out Cross Validation Mean Absolute Error Standard Deviation
head <sub>max</sub>	Maximum obtained heading
head <sub>int</sub>	95% of the time within this heading
head <sub>avg time</sub>	When outside head <sub>int</sub> the average time before returning to head <sub>int</sub>
head <sub>max time</sub>	When outside head <sub>int</sub> the maximum time before returning to head <sub>int</sub>
head <sub>count</sub>	Amount of times outside of head <sub>int</sub>
offset <sub>max</sub>	Maximum obtained offset
offset <sub>int</sub>	95% of the time within this offset
offset <sub>avg time</sub>	When outside offset <sub>int</sub> the average time before returning to offset <sub>int</sub>
offset <sub>max time</sub>	When outside offset <sub>int</sub> the maximum time before returning to offset <sub>int</sub>
offset <sub>count</sub>	Amount of times outside of offset <sub>int</sub>

### 4.5.1. R squared and LOOCV R squared

The first thing to check is whether the model can explain the variation present in the data points, as explained in section 3.3.8 this is done by using the R squared. In figures 4.2 and 4.3 the results of the 2nd order fit on 0 degrees environmental angle for 136 and 270 data points can be compared. It is immediately visible that for heading the model does not fulfil the  $R^2 > 0.98$  not even when the amount of data points is enlarged since the performance of the R squared drops significantly. Not surprisingly this also means that the LOOCV R squared does not meet the requirements. For offset however the model performs really well. When the number of data points is increased the R squared slightly decreases which could indicate that 136 points is not enough to make a good fit. This is also visible when looking at the LOOCV R squared since their performance increases when increasing the amount of data points meaning that the model changes less when new data is used for fitting.

For 15 degrees of environmental angle the R squared performs already very well for both heading and offset as can be seen in figures 4.4 and 4.5. Again their performance drops slightly when using

more points which indicates that the amount of points used in the fit with 136 points was slightly too low. This is again seen in the LOOCV R squared since their performance increases with the increase of the amount of data points.

The last example shown is for 45 degrees of environmental angles in figures 4.6, 4.7 and 4.8. With 136 data points the R squared of the head<sub>max</sub> is the only one that does not meet the requirements. Even when increasing the amount of data points it does not comply although the shortcoming is minimal. Similar trends are observed where the R squared slightly decreases with the increase of data points and the LOOCV R squared increases with the increase of data points.

2nd order fit						
angle 0 degrees	136 data points					
	RSquare	MAE	MAESTD	CVRSquare	CVMAE	CVMAESD
head_max	0.78884	0.56313	1.50904	0.18394	1.11787	2.59470
head_int	0.75343	1.28755	6.92251	-0.22001	2.64722	12.93940
head_avg_time	0.88641	0.32821	0.42394	0.53377	0.68739	0.85653
head_max_time	0.88393	0.32193	0.45568	0.51999	0.66183	0.86039
head_count	0.83778	0.47579	0.48344	0.27098	0.10476	0.97991
offset_max	0.99945	0.00100	0.00076	0.99760	0.00209	0.00156
offset_int	0.99855	0.00182	0.00137	0.99290	0.00395	0.00306
offset_avg_time	0.90384	0.01292	0.00933	0.55760	0.02743	0.02049
offset_max_time	0.99616	0.00129	0.00101	0.98136	0.00280	0.00229
offset_count	0.90859	0.01280	0.00940	0.57906	0.02719	0.02053

Table 4.2: 0 degrees 2nd order fit on 136 points

2nd order fit						
angle 0 degrees	270 data points					
	RSquare	MAE	MAESTD	CVRSquare	CVMAE	CVMAESD
head_max	0.59213	1.17908	4.33485	0.22322	1.73811	6.66556
head_int	0.65024	1.22878	4.84759	0.32044	1.73675	6.83751
head_avg_time	0.76583	0.44616	0.49858	0.56443	0.61363	0.68864
head_max_time	0.78183	0.41025	0.53814	0.58220	0.57061	0.74910
head_count	0.78424	0.61791	0.68845	0.57787	0.85111	0.94851
offset_max	0.99899	0.00129	0.00106	0.99797	0.00180	0.00155
offset_int	0.99741	0.00236	0.00182	0.99493	0.00329	0.00255
offset_avg_time	0.82961	0.01870	0.01326	0.68286	0.02558	0.01803
offset_max_time	0.74062	0.00923	0.02823	0.48052	0.01299	0.03967
offset_count	0.84408	0.01829	0.01323	0.70913	0.02501	0.01800

Table 4.3: 0 degrees 2nd order fit on 270 points

2nd order fit						
angle 15 degrees	136 data points					
	RSquare	MAE	MAESTD	CVRSquare	CVMAE	CVMAESD
head_max	0.99975	0.00162	0.00131	0.99886	0.00340	0.00276
head_int	0.99855	0.00266	0.00215	0.99309	0.00575	0.00470
head_avg_time	0.94430	0.01820	0.01357	0.73210	0.03945	0.03007
head_max_time	0.99817	0.00092	0.00080	0.99195	0.00194	0.00166
head_count	0.94197	0.01850	0.01447	0.71713	0.04042	0.03307
offset_max	0.99900	0.00109	0.00085	0.99562	0.00230	0.00173
offset_int	0.99826	0.00179	0.00140	0.99142	0.00389	0.00317
offset_avg_time	0.87011	0.01697	0.01342	0.42365	0.03610	0.02766
offset_max_time	0.99319	0.00129	0.00095	0.96894	0.00274	0.00204
offset_count	0.86383	0.01725	0.01306	0.39430	0.03680	0.02719

Table 4.4: 15 degrees 2nd order fit on 136 points

2nd order fit						
angle 15 degrees	600 data points					
	RSquare	MAE	MAESTD	CVRSquare	CVMAE	CVMAESD
head_max	0.99921	0.00275	0.00254	0.99894	0.00314	0.00298
head_int	0.99732	0.00370	0.00308	0.99650	0.00422	0.00354
head_avg_time	0.90141	0.02467	0.01924	0.87404	0.02793	0.02166
head_max_time	0.99535	0.00154	0.00116	0.99389	0.00176	0.00133
head_count	0.89500	0.02488	0.01911	0.86580	0.02818	0.02156
offset_max	0.99794	0.00153	0.00124	0.99731	0.00174	0.00143
offset_int	0.99586	0.00273	0.00209	0.99456	0.00311	0.00242
offset_avg_time	0.80134	0.02007	0.01580	0.74160	0.02287	0.01807
offset_max_time	0.98605	0.00181	0.00146	0.98157	0.00207	0.00170
offset_count	0.80204	0.01984	0.01542	0.74239	0.02260	0.01762

Table 4.5: 15 degrees 2nd order fit on 600 points

2nd order fit						
angle 45 degrees	136 data points					
	RSquare	MAE	MAESTD	CVRSquare	CVMAE	CVMAESD
head_max	0.97577	0.00385	0.00295	0.88135	0.00830	0.00681
head_int	0.99827	0.00185	0.00148	0.99227	0.00395	0.00304
head_avg_time	0.76496	0.02550	0.01912	-0.18712	0.05462	0.04601
head_max_time	0.98065	0.00252	0.00199	0.90945	0.00538	0.00439
head_count	0.76148	0.02526	0.01896	-0.18799	0.05393	0.04581
offset_max	0.99793	0.00126	0.00097	0.98837	0.00278	0.00254
offset_int	0.99705	0.00233	0.00170	0.98452	0.00516	0.00406
offset_avg_time	0.86821	0.01709	0.01206	0.37828	0.03688	0.02679
offset_max_time	0.88093	0.05575	0.03951	0.44349	0.12057	0.08835
offset_count	0.87437	0.01668	0.01244	0.40881	0.03588	0.02712

Table 4.6: 45 degrees 2nd order fit on 136 points

2nd order fit						
angle 45 degrees	270 data points					
	RSquare	MAE	MAESTD	CVRSquare	CVMAE	CVMAESD
head_max	0.95573	0.00460	0.00412	0.90554	0.00651	0.00622
head_int	0.99752	0.00227	0.00167	0.99512	0.00315	0.00240
head_avg_time	0.66078	0.02769	0.02199	0.36949	0.03792	0.02967
head_max_time	0.97326	0.00293	0.00249	0.94752	0.00404	0.00358
head_count	0.65485	0.02724	0.02117	0.35778	0.03736	0.02868
offset_max	0.99555	0.00170	0.00153	0.99021	0.00240	0.00242
offset_int	0.99600	0.00246	0.00206	0.99180	0.00344	0.00309
offset_avg_time	0.78149	0.02178	0.01616	0.57283	0.03014	0.02296
offset_max_time	0.83431	0.06417	0.04591	0.69786	0.08725	0.06246
offset_count	0.78658	0.02102	0.01617	0.58506	0.02910	0.02289

Table 4.7: 45 degrees 2nd order fit on 270 points

2nd order fit						
angle 45 degrees	600 data points					
	RSquare	MAE	MAESTD	CVRSquare	CVMAE	CVMAESD
head_max	0.95331	0.00468	0.00419	0.93734	0.00537	0.00491
head_int	0.99706	0.00240	0.00186	0.99616	0.00273	0.00213
head_avg_time	0.63802	0.03117	0.02470	0.52894	0.03548	0.02822
head_max_time	0.96453	0.00340	0.00297	0.95275	0.00389	0.00349
head_count	0.63222	0.03082	0.02372	0.52210	0.03507	0.02714
offset_max	0.99481	0.00181	0.00169	0.99304	0.00207	0.00199
offset_int	0.99520	0.00272	0.00229	0.99359	0.00311	0.00268
offset_avg_time	0.74753	0.02271	0.01832	0.67009	0.02587	0.02102
offset_max_time	0.80583	0.07056	0.04706	0.74954	0.08012	0.05357
offset_count	0.74933	0.02243	0.01805	0.67326	0.02555	0.02073

Table 4.8: 45 degrees 2nd order fit on 600 points

### 4.5.2. Mean absolute error and LOOCV mean absolute error

For 0 degrees of environmental angle as seen in figures 4.2 and 4.3 both MAE and LOOCV MAE for heading have very low performance. This is to be expected since also the R squared is very low. When increasing the amount of data points the MAE and LOOCV MAE are not always performing worse as is seen with the R squared. This can be explained by the fact that the model is still predicting very poor but becomes less sensitive to new data points resulting in a lower LOOCV MAE when more data points are used.

When considering 15 degrees of environmental angle which displayed in figures 4.4 and 4.5 the MAE and LOOCV MAE are already performing really well with 136 data points. Only the  $\text{head}_{int}$  does not meet the requirements yet but with 600 data points it does. Also when comparing the 136 and 600 data points the MAE increases when increasing the amount of data points and the LOOCV MAE is decreasing when increasing the data points. This seems logical since the R squared performance decreases slightly when the amount of points are increased and therefore the MAE increases. The LOOCV MAE is expected to decrease with increasing amount of points since the model will be less sensitive to new data.

In the case of 45 degrees environmental angle the trends are similar to the two cases described above, MAE increases with an increase of the data points and LOOCV decreases with an increase of data points. One thing that stands out is that the LOOCV MAE does not comply just as seen with the R squared and LOOCV R squared. However the shortcoming is only 0.037%.

### 4.5.3. Mean absolute error standard deviation and LOOCV mean absolute error standard deviation

For all angles the same trends are visible, when the amount of points increases the MAESTD increases and the LOOCVSTD decreases. The increase of the MAESTD can be explained by the fact that for less points not all extreme situations are already present and therefore the spread is less. The decrease of the LOOCVSTD can be explained by the fact that the model become less sensitive to new data when more data points are used for fitting.

### 4.5.4. Residual

After the performance of the fit is within the specifications required, the residuals have to be checked to see if the model does not systematically under or over predicts the outputs. Four examples are illustrated below which are: maximum offset, offset interval, maximum heading and heading interval. All of these examples are taken at 15 degrees environmental angle. The complete residual analysis can be found in appendix F.1.

As seen in figures 4.51 - 4.54 the residuals show very nice random behaviour meaning that the model does not systematically under or over predicts the behaviour of the vessel. What is seen in some of the residual graphs is that on the boundaries of the model it seems like the model is sometimes under or over predicting just slightly but since the amount of points sampled in that region is relatively low it is more likely that there are just not enough points to statistically say that this is actually true. If it would be the case that in these regions the model would slightly under or over predict it would not be a big problem since it is looked at confidence intervals meaning that the most extreme values are not taken into account. Also the magnitude of the residual is relatively small and only occurs in a very small region making a potential over fitting of less importance.

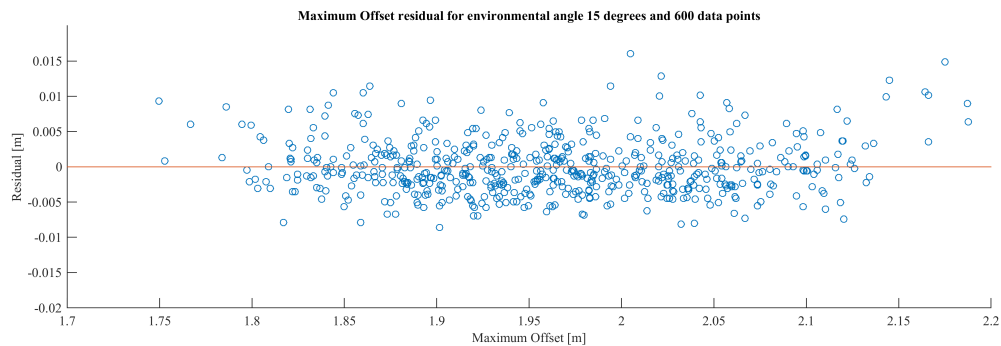


Figure 4.51: Maximum Offset Residual for 15 degrees of environmental angle with 600 data points

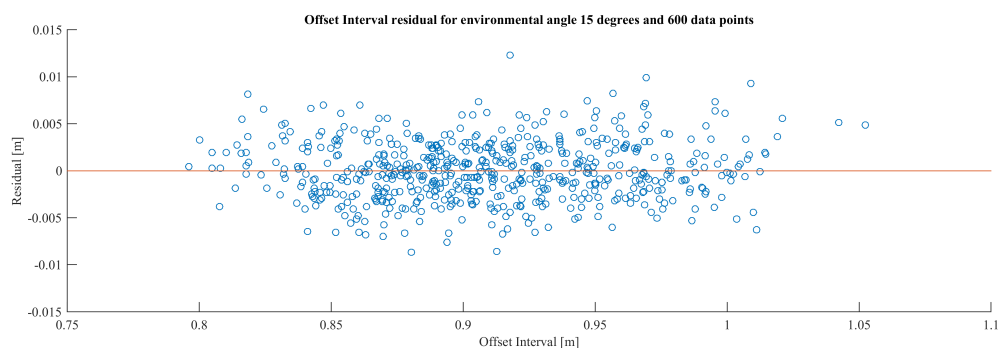


Figure 4.52: Offset Interval Residual for 15 degrees of environmental angle with 600 data points

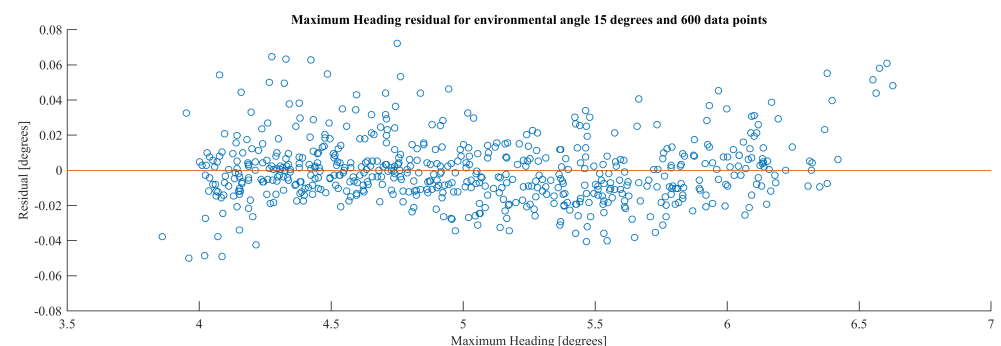


Figure 4.53: Maximum Heading Residual for 15 degrees of environmental angle with 600 data points

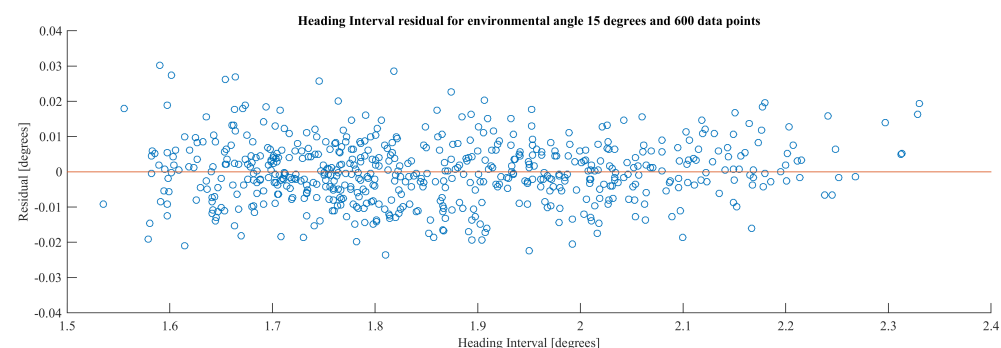


Figure 4.54: Heading Interval Residual for 15 degrees of environmental angle with 600 data points

## 4.6. aNySIM offset analysis

In section 4.5 it is concluded that the model is accurate enough for the purpose of uncertainty calculation. Therefore a Monte Carlo simulation with  $N = 10.000$  is executed for each environmental angle and output. The first outputs up for consideration are the maximum offset and the 95% offset interval as defined in section 3.3.3. For both these outputs the 99.7% confidence interval is evaluated below. As stated before the uncertainty in the wave coefficients is not taken into account in the dynamic DP calculation.

### 4.6.1. Maximum offset analysis

The maximum offset that the vessel will obtain is now not described as one fixed value but as a confidence interval where in between the maximum offset can be found. The confidence interval of 99.7% is illustrated in figure 4.55 where the upper and lower bound are the result of the input uncertainty. The angles represent the direction where the environment is coming from with the direction of wind waves and current collinear.

The tables throughout this section all have the same format where first the environmental angles are listed and then the upper and lower bound of the Monte Carlo simulation is shown. Thereafter the absolute difference between the upper and lower bound is calculated and finally the relative difference between the mean, of the upper and lower bound, and half of the absolute difference is shown. The mathematical formula for this is shown in equation 4.3.

$$\text{Diff. from mean} = \frac{\text{Diff./2}}{(\text{Lower Bound} + \text{Upper Bound}) / 2} \cdot 100 \quad (4.3)$$

In figure 4.55 and table 4.9 it is seen that the maximum offset is the smallest at 0 degrees of environmental angle and increases when moving towards 90 degrees. Also the difference between the lower and upper boundary increases when the angles increase. This is explained by the fact that surface on which the environment acts is getting bigger when the angle increases resulting in a higher average and peak forces. Another thing that stands out is a sharp edge with a straight line when looking between angles 70 and 90 degrees. This is not the real behaviour of the vessel but is due to the fact that only the angles 70 and 90 degrees are simulated resulting in a linear interpolation between these points.

If uncertainties should be taken into account depends in large extend on the type of operation performed with a DP vessel. In the specific case of the Bibby Wavemaster 1, DP is used to transfer people from the vessel to a wind turbine by means of a "Walk To Work" bridge. This bridge has a telescoping length of 8m meaning that when in operation, the telescope will be extended 4m such that it can extend or retract 4m. When now considering table 4.9 it is seen that the maximum difference between the upper and lower bound of the offset is 0.47m which is 11.75% of the 4m that the bridge can correct for. This could result into two things namely: the bridge is not able to extend any further, causing the operational window to be smaller than expected. Or the bridge is not able to retract more than the 4m, causing it to crash into the wind turbine resulting in serious safety and financial consequences. It is therefore fair to say that uncertainties are important to take into account, when a operation of people transferring by means of a "Walk To Work" bridge is performed, so that the risks involved with these uncertainties are known and can be mitigated.

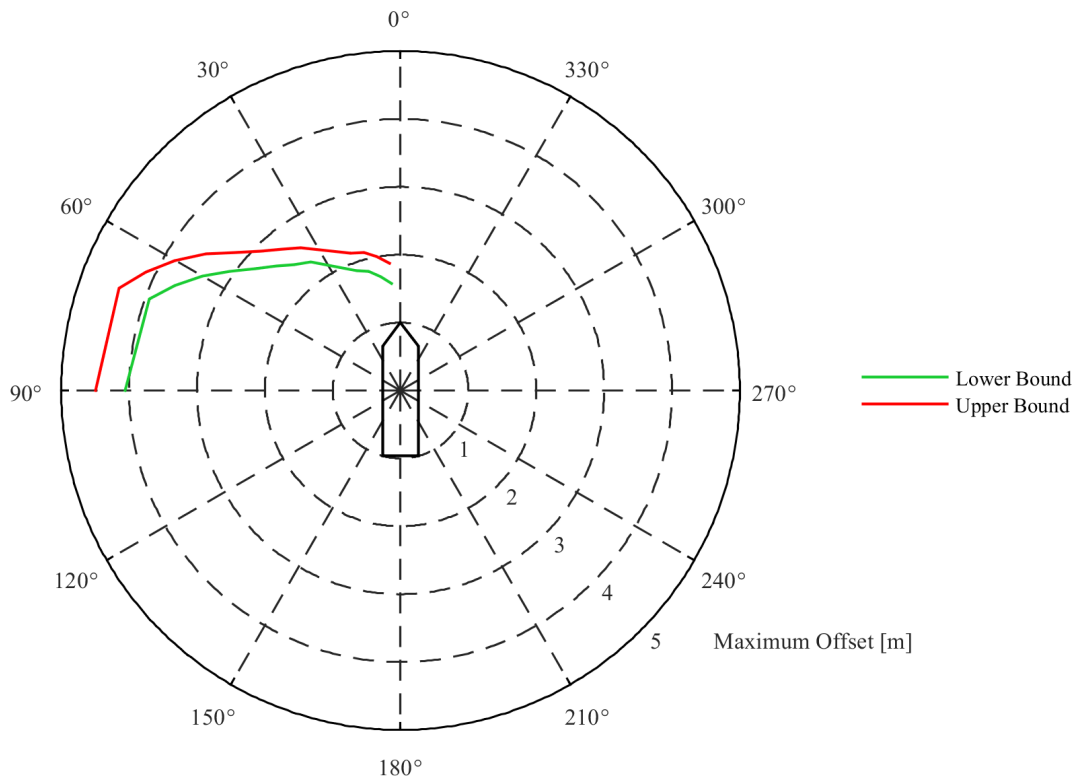


Figure 4.55: Maximum offset boundaries - 99.7% confidence interval

Table 4.9: Maximum Offset lower bound, upper bound and differences

Angles [°]	Maximum Offset			
	Lower Bound [m]	Upper Bound [m]	Diff. [m]	Diff. from mean [%]
5	1.58	1.88	0.30	8.70
10	1.70	2.00	0.30	8.15
15	1.82	2.10	0.29	7.29
20	1.88	2.15	0.27	6.70
35	2.31	2.57	0.26	5.27
40	2.42	2.71	0.29	5.61
45	2.59	2.90	0.31	5.72
50	2.79	3.17	0.38	6.43
55	3.07	3.50	0.44	6.63
60	3.36	3.84	0.47	6.55
65	3.67	4.14	0.46	5.95
70	3.94	4.41	0.47	5.62
90	4.06	4.50	0.44	5.09

### Sensitivity

To check if the Spearman's Correlation Analysis (SCA), as described in section 2.13.4, can be used for the purpose of ranking the importance of the input parameters the output should be monotonic. In figures 4.56 and 4.57 two examples are presented from which it can be seen that this is not the case for the maximum offset. When considering all the different inputs it was seen that for every angle at least one input does not result in a monotonic behaviour of the maximum offset output making it impossible to use the SCA method for the purpose of sensitivity analysis.

Another way to see which inputs are more important than others is by performing two separate

MC simulations. In the first MC simulation only the environmental parameters, the densities of air and water and the mass of the vessel are sampled meaning that the gains of the PID controller are kept constant. The lower and upper bound of the maximum offset resulting from this analysis are illustrated in figure 4.58 and table 4.10. In the second MC simulation only the PID gains are sampled and the result of this can be seen in figure 4.59 and table 4.11. It can now be concluded that the influence of the gains on the maximum offset is by far the biggest when compared to the environmental influences. It is seen that both the lower and upper bound are shifted to lower and higher values respectively resulting in a bigger difference in the maximum offset output.

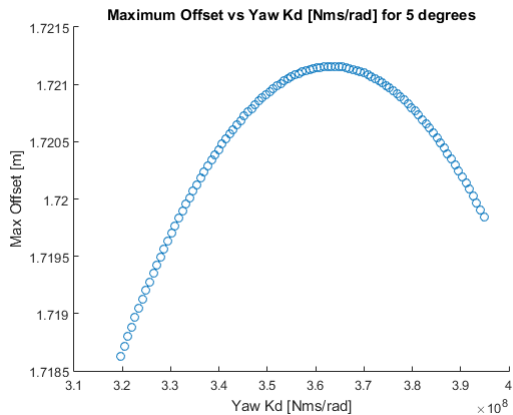


Figure 4.56: Maximum offset vs Yaw Kd for 5 degrees

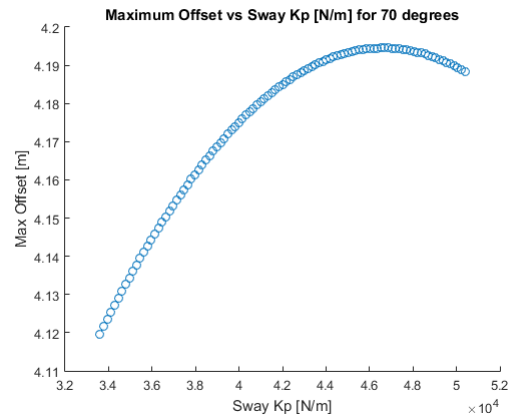


Figure 4.57: Maximum offset vs Sway Kp for 70 degrees

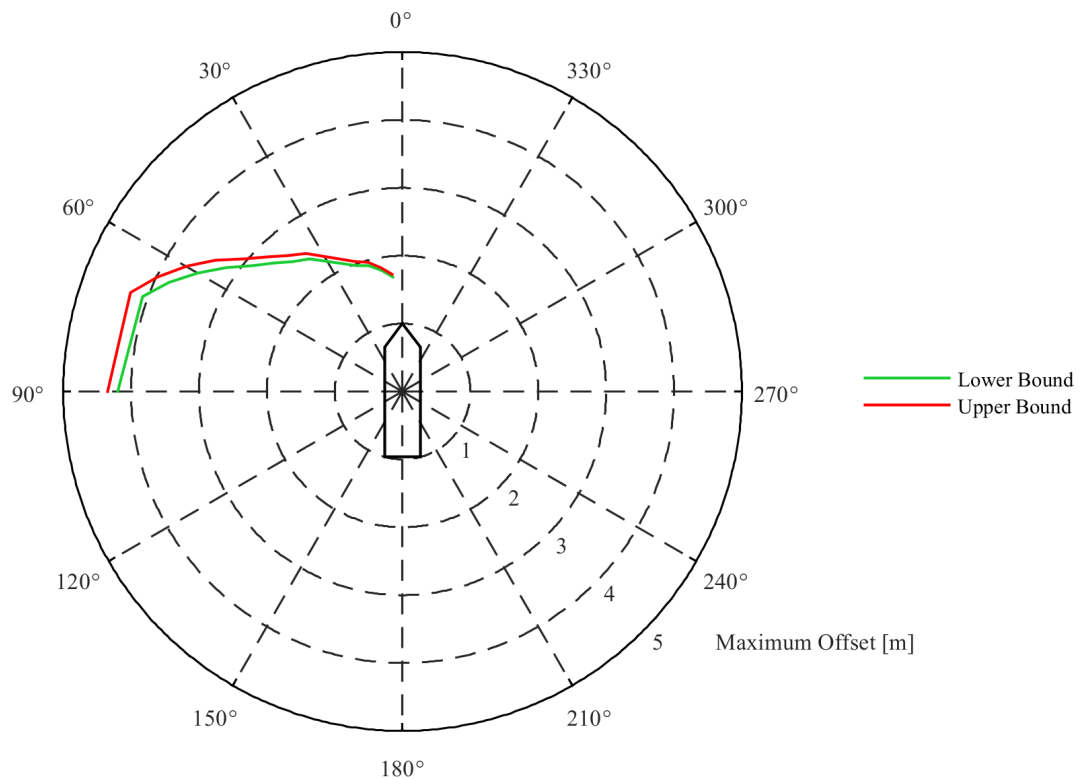


Figure 4.58: Maximum offset boundaries environmental influence - 99.7% confidence interval

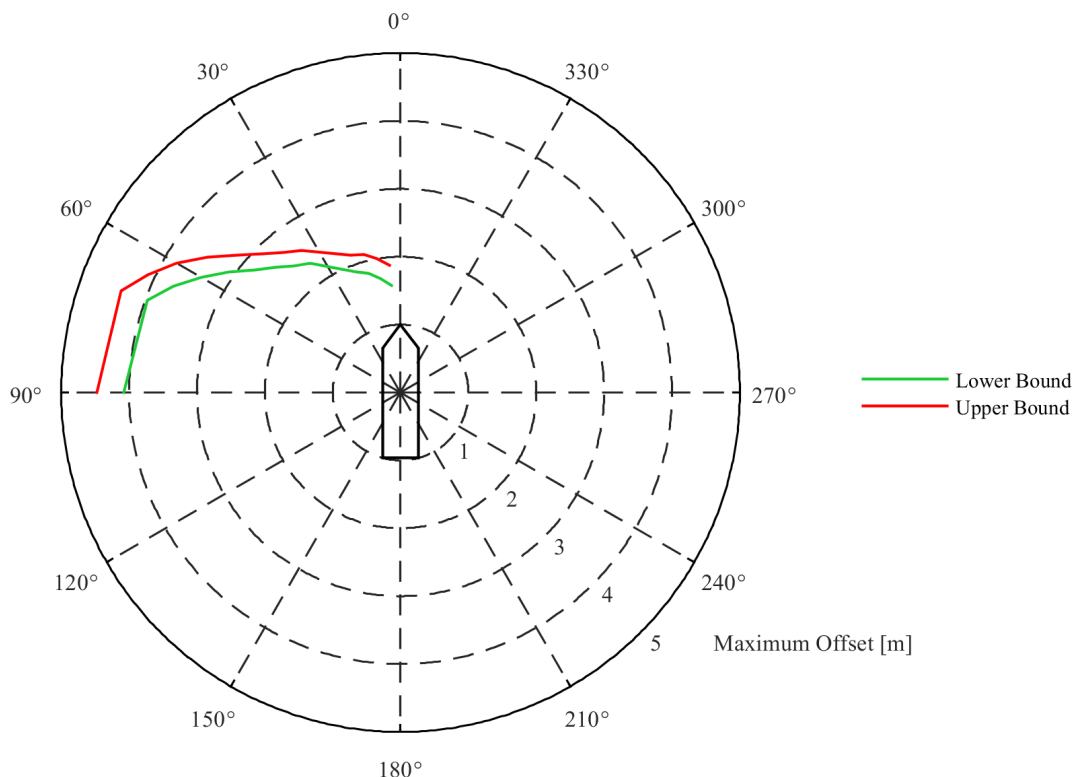


Figure 4.59: Maximum offset boundaries gain influence - 99.7% confidence interval

Table 4.10: Maximum Offset environmental influence

Angles [°]	Maximum Offset Environmental Influence			
	Lower Bound [m]	Upper Bound [m]	Diff. [m]	Diff. from mean [%]
5	1.70	1.73	0.04	1.17
10	1.81	1.86	0.04	1.09
15	1.92	1.97	0.05	1.29
20	1.98	2.03	0.06	1.50
35	2.39	2.48	0.09	1.85
40	2.50	2.61	0.11	2.15
45	2.67	2.81	0.13	2.37
50	2.88	3.04	0.16	2.70
55	3.18	3.36	0.19	2.91
60	3.48	3.68	0.20	2.79
65	3.80	3.98	0.19	2.44
70	4.08	4.26	0.19	2.28
90	4.20	4.34	0.14	1.64

Table 4.11: Maximum Offset Gain influence

Angles [°]	Maximum Offset Gain Influence			
	Lower Bound [m]	Upper Bound [m]	Diff. [m]	Diff. from mean [%]
5	1.58	1.88	0.30	8.67
10	1.70	2.00	0.30	8.11
15	1.82	2.10	0.28	7.14
20	1.89	2.15	0.26	6.44
35	2.32	2.55	0.24	4.93
40	2.44	2.69	0.25	4.87
45	2.61	2.89	0.28	5.09
50	2.81	3.15	0.34	5.70
55	3.09	3.47	0.38	5.79
60	3.40	3.82	0.42	5.82
65	3.70	4.11	0.42	5.38
70	3.97	4.38	0.41	4.91
90	4.08	4.48	0.40	4.67

#### 4.6.2. Offset interval analysis

The offset interval illustrated in figure 4.60 and table 4.12 shows similar trends as the maximum offset analysis. The offset interval is the smallest at 0 degrees of environmental angle and increases when moving towards 90 degrees. Also the difference between the lower and upper boundary increases when the angles increases. This is explained by the fact that surface on which the environment acts is getting bigger when the angle increases resulting in a higher average and peak forces. Another thing that stands out is a sharp edge with a straight line when looking between angles 70 and 90 degrees. This is not the real behaviour of the vessel but is due to the fact that only the angles 70 and 90 degrees are simulated resulting in a linear interpolation between these points.

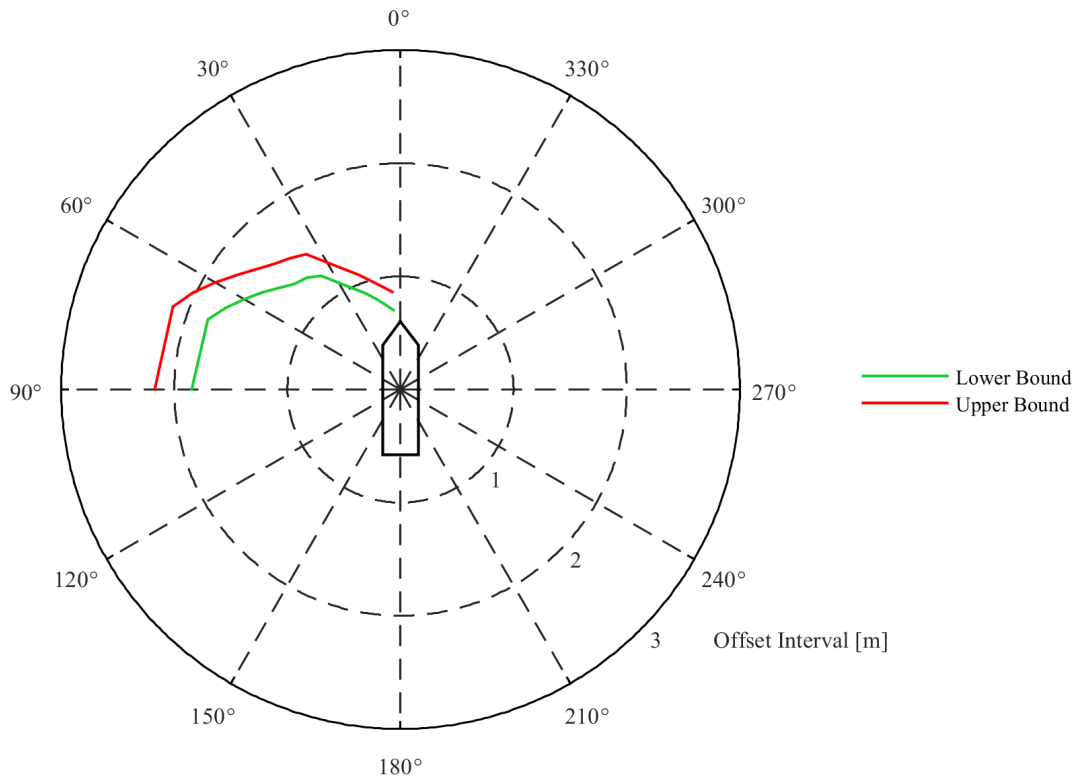


Figure 4.60: Offset interval boundaries - 99.7% confidence interval

Table 4.12: Offset Interval lower bound, upper bound and differences

Angles [°]	Offset Interval			
	Lower Bound [m]	Upper Bound [m]	Diff. [m]	Diff. from mean [%]
5	0.71	0.86	0.16	10.06
10	0.76	0.93	0.16	9.67
15	0.82	0.99	0.16	9.07
20	0.91	1.08	0.17	8.58
35	1.23	1.46	0.23	8.68
40	1.29	1.52	0.23	8.28
45	1.32	1.57	0.25	8.59
50	1.40	1.66	0.26	8.46
55	1.50	1.77	0.27	8.32
60	1.60	1.89	0.30	8.45
65	1.71	2.03	0.32	8.49
70	1.81	2.14	0.33	8.42
90	1.84	2.17	0.33	8.13

### Sensitivity

For the offset interval it is also checked if the Spearman's Correlation Analysis (SCA) can be used for the purpose of ranking the importance of the input parameters. In figures 4.61 and 4.62 two examples are presented from which it can be seen that this is not the case for the offset interval. When considering all the different inputs it was seen that for every angle at least one input does not result in a monotonic behaviour of the offset interval output making it impossible to use the SCA method for the purpose of sensitivity analysis.

Just as with the maximum offset two separate MC simulations are performed to see which parameters have more influence on the offset interval. In the first MC simulation only the environmental parameters, the densities of air and water and the mass of the vessel are sampled meaning that the gains of the PID controller are kept constant. The lower and upper bound of the offset interval resulting from this analysis is illustrated in figure 4.63 and table 4.13. In the second MC simulation only the PID gains are sampled and the result of this can be seen in 4.64 and table 4.14. Similar as with the maximum offset the PID gains prove to have the biggest influence on the offset interval. For the PID gains MC simulation the lower and upper bound are again shifted to lower and higher values respectively resulting in a bigger difference in the offset interval output.

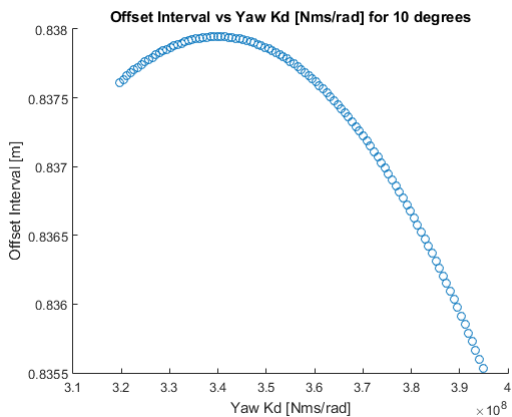


Figure 4.61: Offset Interval vs Yaw Kd for 10 degrees

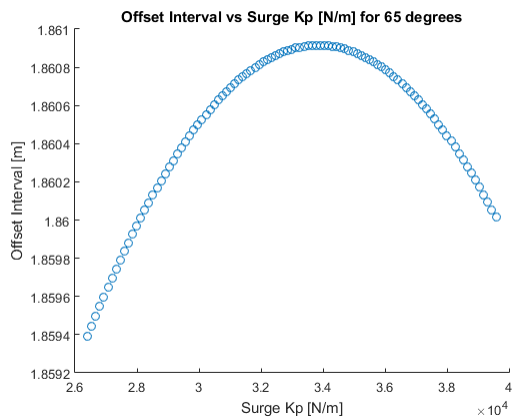


Figure 4.62: Offset Interval vs Surge Kp for 65 degrees

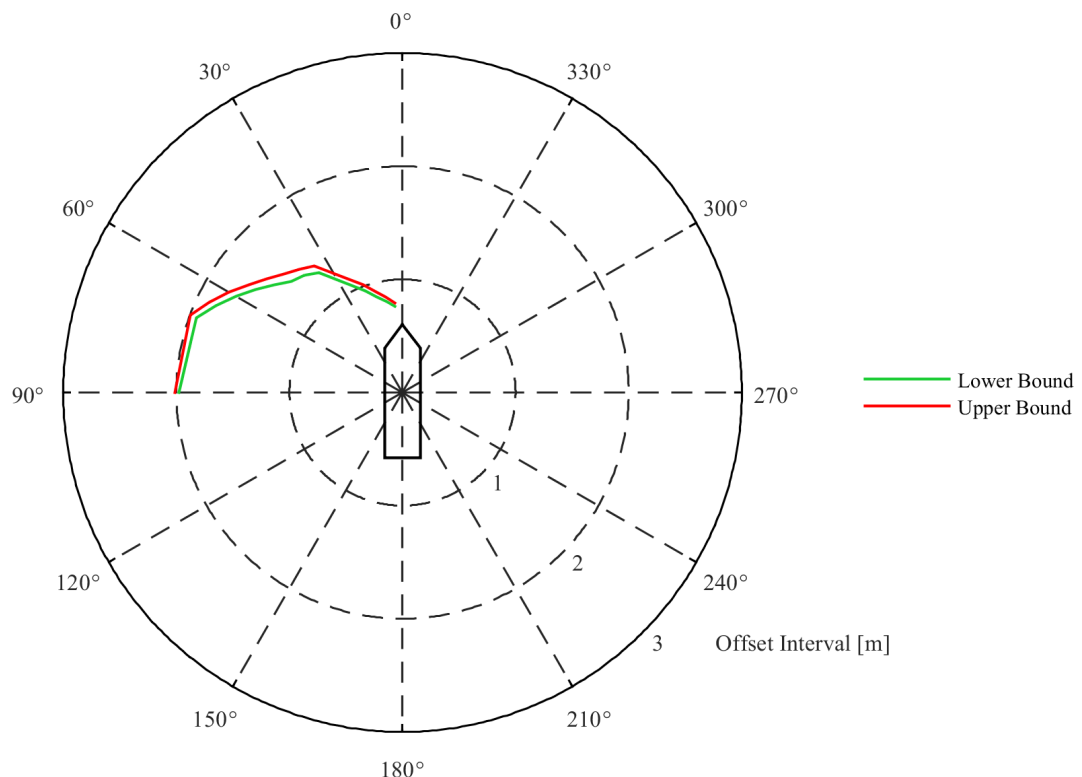


Figure 4.63: Offset interval boundaries environmental influence - 99.7% confidence interval

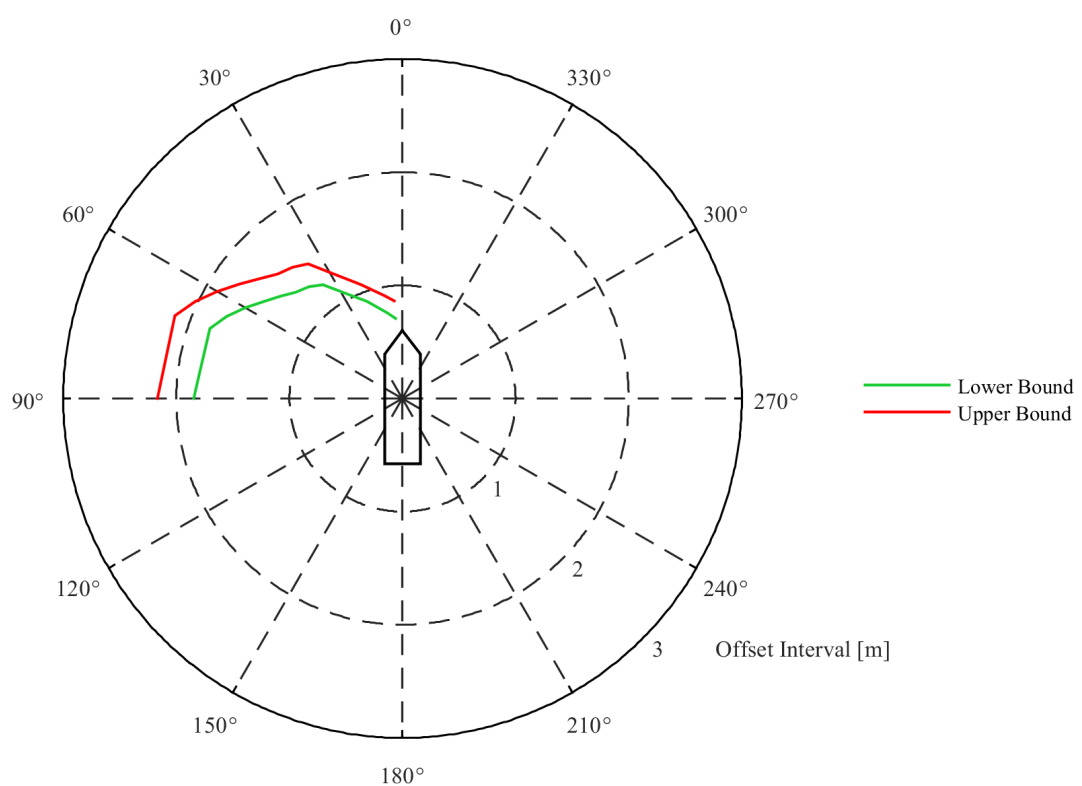


Figure 4.64: Offset interval boundaries gain influence - 99.7% confidence interval

Table 4.13: Offset Interval environmental influence

Angles [°]	Offset Interval Environmental Influence			
	Lower Bound [m]	Upper Bound [m]	Diff. [m]	Diff. from mean [%]
5	0.76	0.79	0.03	1.94
10	0.82	0.86	0.04	2.38
15	0.88	0.92	0.05	2.78
20	0.96	1.01	0.06	3.05
35	1.29	1.37	0.07	2.63
40	1.35	1.42	0.07	2.53
45	1.39	1.48	0.09	3.14
50	1.48	1.56	0.09	2.96
55	1.58	1.66	0.08	2.47
60	1.70	1.77	0.07	2.02
65	1.82	1.89	0.06	1.62
70	1.94	1.99	0.06	1.53
90	1.98	2.01	0.04	1.00

Table 4.14: Offset Interval Gain influence

Angles [°]	Offset Interval Gain Influence			
	Lower Bound [m]	Upper Bound [m]	Diff. [m]	Diff. from mean [%]
5	0.71	0.86	0.15	9.55
10	0.77	0.92	0.16	9.47
15	0.83	0.99	0.15	8.24
20	0.91	1.07	0.16	8.08
35	1.23	1.45	0.22	8.21
40	1.29	1.51	0.22	7.86
45	1.33	1.56	0.23	7.96
50	1.41	1.65	0.24	7.84
55	1.50	1.76	0.26	7.98
60	1.60	1.89	0.29	8.31
65	1.71	2.02	0.31	8.31
70	1.81	2.14	0.33	8.35
90	1.84	2.17	0.32	7.98

## 4.7. aNySIM heading analysis

For heading it was shown in section 4.5 that the model was also found to be accurate enough for the purpose of uncertainty calculation. Again a Monte Carlo simulation with  $N = 10.000$  is done for each environmental angle and output.

The tables throughout this section all have the same format where first the environmental angles are listed and then the upper and lower bound of the Monte Carlo simulation is shown. Thereafter the absolute difference between the upper and lower bound is calculated and finally the relative difference between the mean, of the upper and lower bound, and half of the absolute difference is shown. The mathematical formula for this is shown in equation 4.4.

$$\text{Diff. from mean} = \frac{\text{Diff./2}}{(\text{Lower Bound} + \text{Upper Bound})/2} \cdot 100 \quad (4.4)$$

### 4.7.1. Maximum heading

The maximum heading that the vessel will obtain is now not described as one fixed value but as a confidence interval where in between the maximum heading can be found. The confidence interval

of 99.7% is illustrated in figure 4.65 where the upper and lower bound are the result of the input uncertainty. The angles represent the direction where the environment is coming from with the direction of wind waves and current collinear.

In figure 4.65 and table 4.15 it is seen that the maximum obtained headings are the smallest for 0 and 90 degrees environmental angle. This can be explained due to the symmetry of the vessel because it is or almost is symmetric over lateral and longitudinal plane. This symmetry results in a low moment of force meaning that less thrust is required to keep the desired heading of the vessel. The highest maximum headings are obtained between 15 and 45 degrees environmental angle. Interesting to see is that these angles partly coincide with the angles of 30 to 60 degrees where the capability of the vessel is limited for the static calculations. The biggest difference between the lower and upper bound is found to be at 20 degrees.

Just as with the offset part of the analysis, if uncertainties should be taken into account depends in large extend on the type of operation performed with a DP vessel. In the specific case of the Bibby Wavemaster 1, DP is used to transfer people from the vessel to a wind turbine by means of a "Walk To Work" bridge. This bridge can compensate a maximum of 40 degrees yaw to each side. When now considering table 4.15 it is seen that the maximum difference between the upper and lower bound of the maximum heading is 2.54 degrees which is 6.35% of the 40 degrees that the bridge can correct for. It is seen that this percentage is lower than for the maximum offset. When the bridge is not able to correct for heading only the operational window will decrease but no collision is expected making the incorporation of uncertainties of slightly less importance than for maximum offset, although penalties can be involved when the operational window is not met.

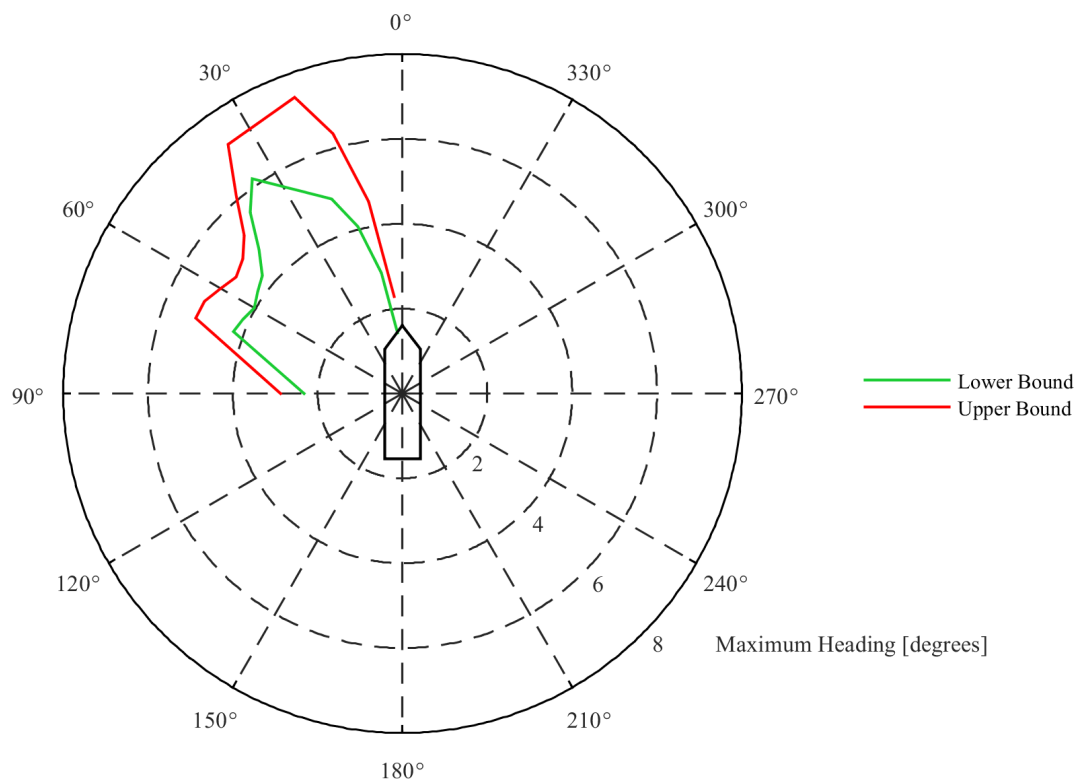


Figure 4.65: Maximum heading boundaries - 99.7% confidence interval

Table 4.15: Maximum Heading lower bound, upper bound and differences

Angles [°]	Maximum Heading			
	Lower Bound [°]	Upper Bound [°]	Diff. [°]	Diff. from mean [%]
5	1.44	2.30	0.86	23.10
10	2.88	4.60	1.72	22.98
15	4.07	6.33	2.26	21.71
20	4.88	7.42	2.54	20.64
35	6.18	7.16	0.98	7.33
40	5.58	6.11	0.53	4.54
45	4.80	5.28	0.48	4.78
50	4.32	4.93	0.60	6.51
55	4.16	4.79	0.63	7.03
60	4.04	4.96	0.92	10.22
65	4.15	5.15	1.01	10.84
70	4.25	5.18	0.93	9.90
90	2.32	2.88	0.56	10.82

### Sensitivity

To check if the Spearman's Correlation Analysis (SCA), as described in section 2.13.4, can be used for the purpose of ranking the importance of the input parameters the output should be monotonic. In figures 4.66 and 4.67 two examples are presented from which it can be seen that this is not the case for the maximum heading. When considering all the different inputs it was seen that for every angle at least one input does not result in a monotonic behaviour of the maximum heading output making it impossible to use the SCA method for the purpose of sensitivity analysis.

Another way to see which inputs are more important than other is by performing two separate MC simulations. In the first MC simulation only the environmental parameters, the densities of air and water and the mass of the vessel are sampled meaning that the gains of the PID controller are kept constant. The lower and upper bound of the maximum heading resulting from this analysis is illustrated in figure 4.68 and table 4.16. In the second MC simulation only the PID gains are sampled and the result of this can be seen in 4.69 and table 4.17. It can now be concluded that the influence of the gains on the maximum heading is by far the biggest when compared to the environmental influences. It is seen that both the lower and upper bound are shifted to lower and higher values respectively resulting in a bigger difference in the maximum heading output.

The only angle for which the above statements do not apply is 90 degrees, here it is seen that the lower bound due to the influence of the environmental angles is smaller than the lower bound due to the gain influence and also the upper bound due to the influence of the environmental angles is higher than the upper bound due to the gain influence.

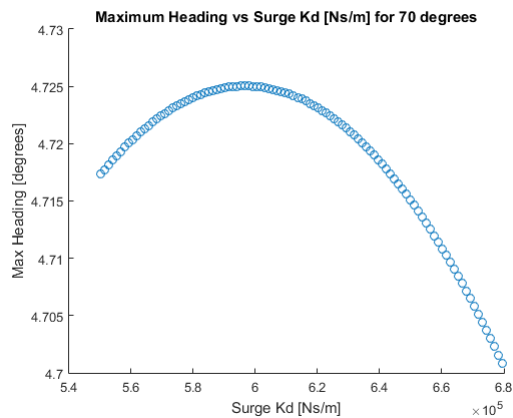


Figure 4.66: Maximum Heading vs Surge Kd for 70 degrees

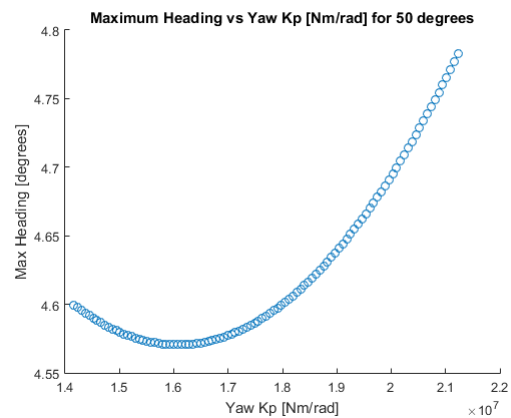


Figure 4.67: Maximum Heading vs Yaw Kp for 50 degrees

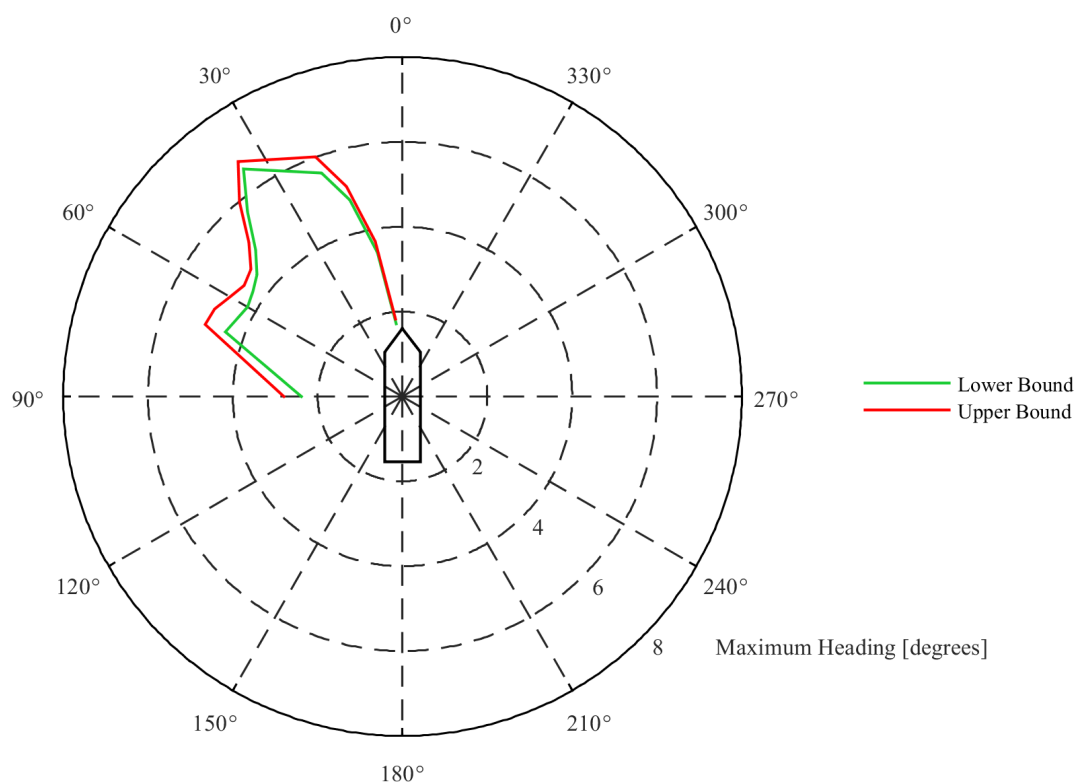


Figure 4.68: Maximum heading boundaries environmental influence - 99.7% confidence interval

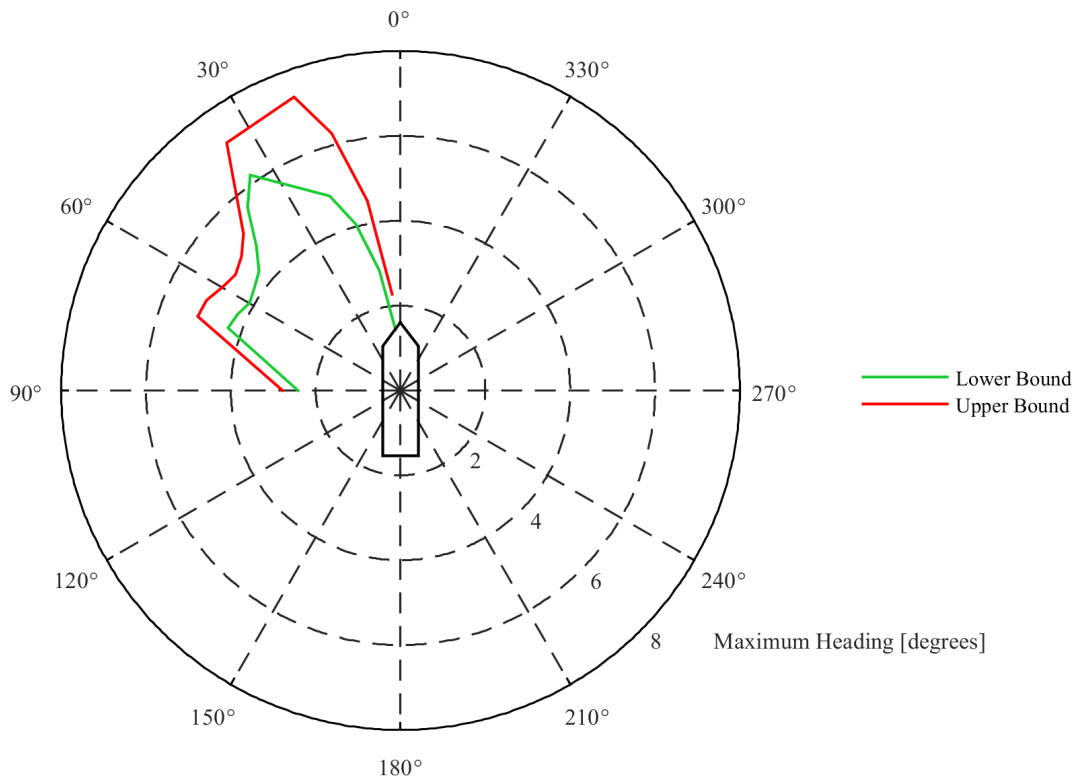


Figure 4.69: Maximum heading boundaries gain influence - 99.7% confidence interval

Table 4.16: Maximum Heading Environmental Influence

Angles [°]	Maximum Heading Environmental Influence			
	Lower Bound [°]	Upper Bound [°]	Diff. [°]	Diff. from mean [%]
5	1.73	1.84	0.11	3.08
10	3.45	3.70	0.25	3.50
15	4.80	5.13	0.33	3.32
20	5.60	6.01	0.41	3.53
35	6.54	6.75	0.21	1.58
40	5.68	5.99	0.31	2.66
45	4.90	5.13	0.24	2.39
50	4.48	4.66	0.18	1.97
55	4.31	4.57	0.25	2.82
60	4.21	4.70	0.49	5.50
65	4.32	4.88	0.56	6.09
70	4.45	4.95	0.50	5.32
90	2.38	2.80	0.41	7.92

Table 4.17: Maximum Heading Gain Influence

Angles [°]	Maximum Heading Gain Influence			
	Lower Bound [°]	Upper Bound [°]	Diff. [°]	Diff. from mean [%]
5	1.44	2.28	0.85	22.85
10	2.87	4.55	1.68	22.64
15	4.06	6.27	2.21	21.39
20	4.88	7.35	2.47	20.20
35	6.19	7.14	0.95	7.13
40	5.62	6.04	0.42	3.60
45	4.82	5.23	0.41	4.08
50	4.36	4.90	0.54	5.83
55	4.20	4.75	0.55	6.15
60	4.12	4.87	0.75	8.34
65	4.24	5.04	0.80	8.62
70	4.34	5.09	0.75	7.95
90	2.42	2.79	0.36	6.91

#### 4.7.2. Heading interval

The heading interval illustrated in figure 4.70 and table 4.18 shows a somewhat different trend than the maximum heading analysis. Again the minimum heading is obtained with 0 and 90 degrees of environmental angle. However the maximum heading interval is obtained between 35 and 55 degrees which is slightly different from the maximum heading. Also this coincides more with the angles of 30 to 60 degrees where the capability of the vessel is limited for the static calculations.

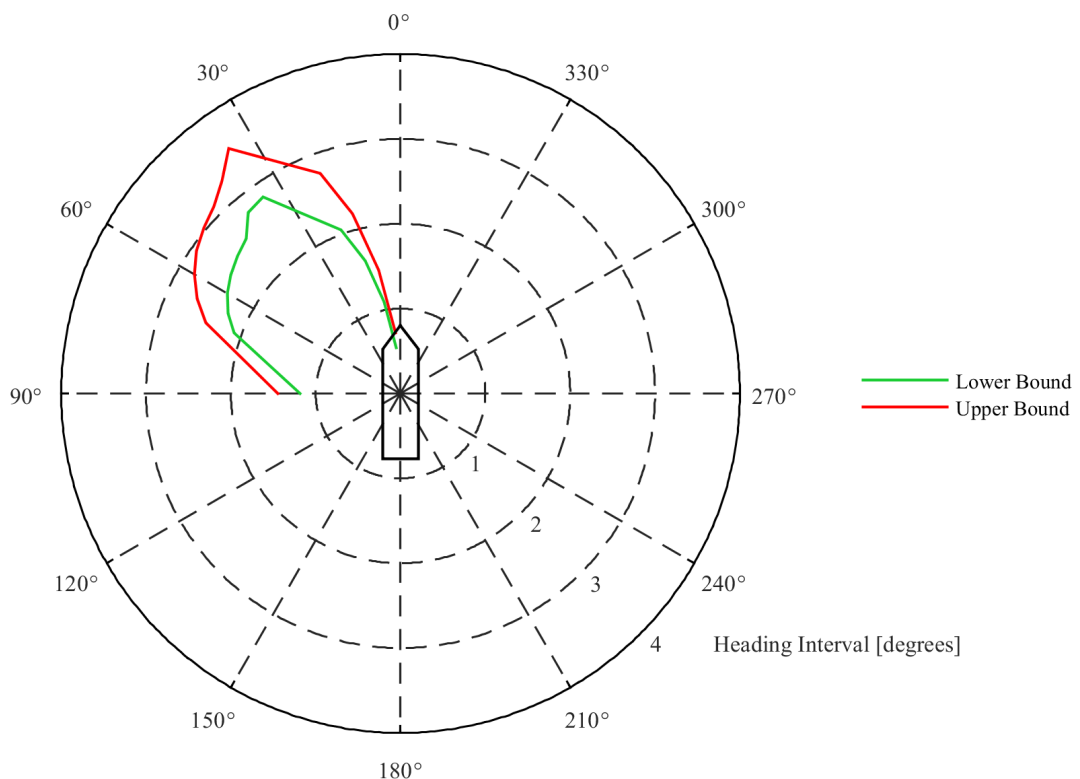


Figure 4.70: Heading interval boundaries - 99.7% confidence interval

Table 4.18: Heading Interval lower bound, upper bound and differences

Angles [°]	Heading Interval			
	Lower Bound [°]	Upper Bound [°]	Diff. [°]	Diff. from mean [%]
5	0.54	0.72	0.18	13.98
10	1.10	1.48	0.38	14.72
15	1.62	2.20	0.58	15.07
20	2.05	2.76	0.71	14.76
35	2.83	3.53	0.70	11.05
40	2.79	3.27	0.48	7.96
45	2.58	3.11	0.54	9.42
50	2.51	3.03	0.52	9.35
55	2.44	2.93	0.49	9.19
60	2.36	2.81	0.45	8.77
65	2.24	2.64	0.40	8.21
70	2.09	2.45	0.35	7.81
90	1.18	1.45	0.26	9.90

### Sensitivity

For the heading interval it is also checked if the Spearman's Correlation Analysis (SCA) can be used for the purpose of ranking the importance of the input parameters. In figures 4.71 and 4.72 two examples are presented from which it can be seen that this is not the case for the heading interval. When considering all the different inputs it was seen that for every angle at least one input does not result in a monotonic behaviour of the heading interval output making it impossible to use the SCA method for the purpose of sensitivity analysis.

Just as with the maximum heading two separate MC simulations are performed to see which parameters have more influence on the heading interval. In the first MC simulation only the environmental parameters, the densities of air and water and the mass of the vessel are sampled meaning that the gains of the PID controller are kept constant. The lower and upper bound of the heading interval resulting from this analysis are illustrated in figure 4.73 and table 4.19. In the second MC simulation only the PID gains are sampled and the result of this can be seen in 4.74 and table 4.20. Similar as with the maximum heading the PID gains prove to have the biggest influence on the heading interval. For the PID gains MC simulation the lower and upper bound are again shifted to lower and higher values respectively resulting in a bigger difference in the heading interval output.

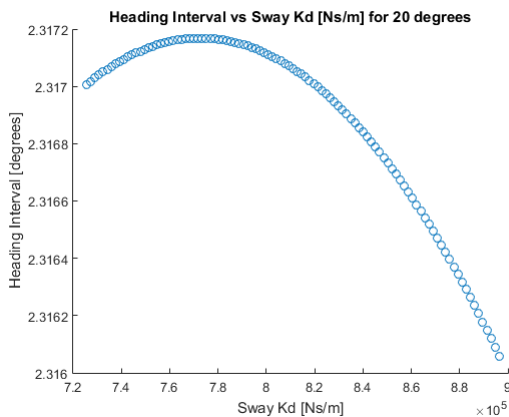


Figure 4.71: Heading Interval vs Sway Kd for 20 degrees

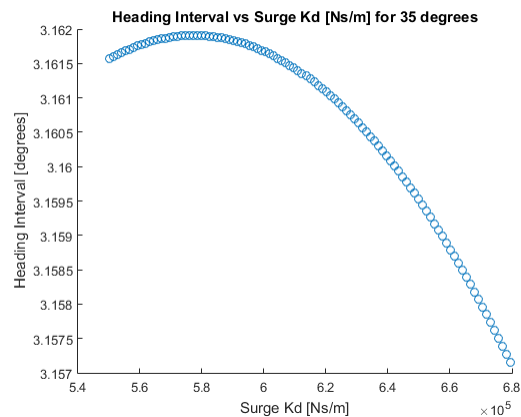


Figure 4.72: Heading Interval vs Surge Kd for 35 degrees

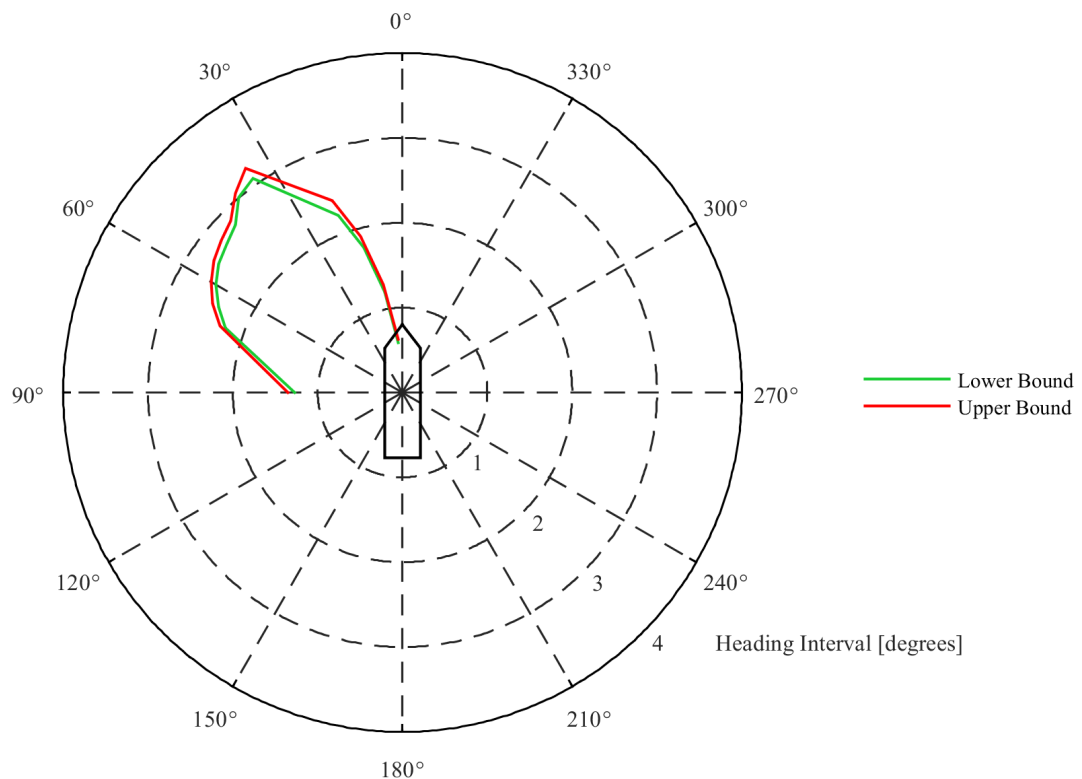


Figure 4.73: Heading interval boundaries environmental influence - 99.7% confidence interval

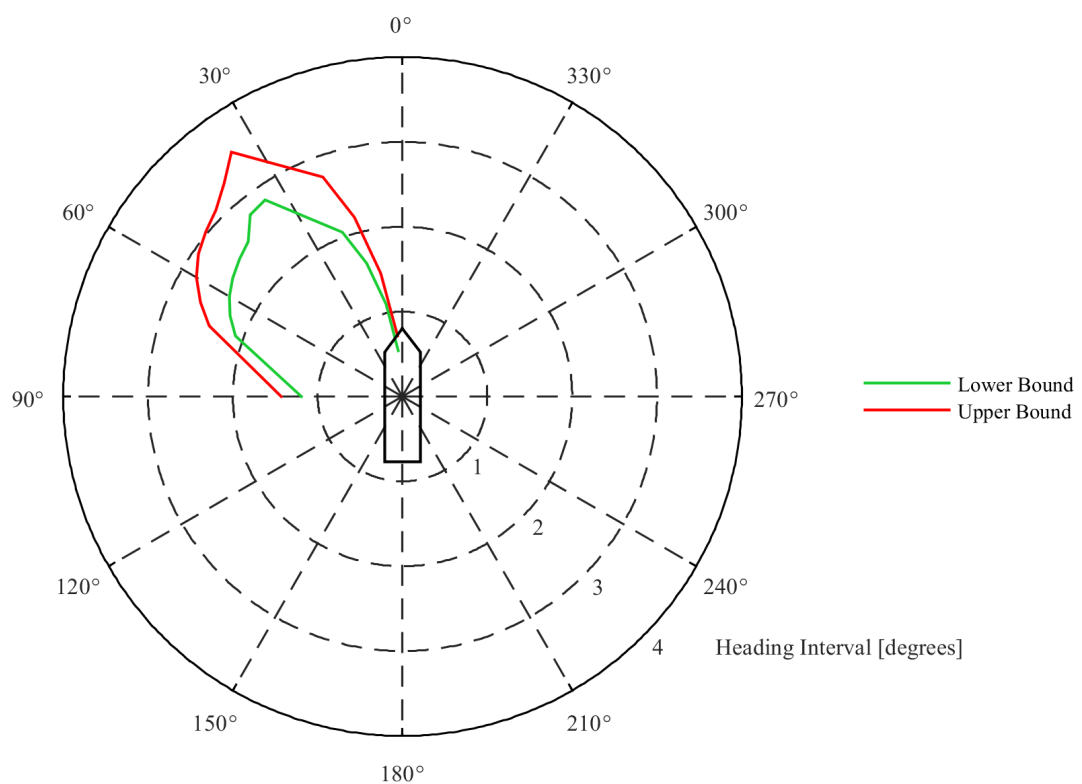


Figure 4.74: Heading interval boundaries gain influence - 99.7% confidence interval

Table 4.19: Heading Interval Environmental Influence

Angles [°]	Heading Interval Environmental Influence			
	Lower Bound [°]	Upper Bound [°]	Diff. [°]	Diff. from mean [%]
5	0.59	0.63	0.04	3.28
10	1.20	1.29	0.09	3.61
15	1.76	1.91	0.14	3.81
20	2.22	2.41	0.19	4.10
35	3.08	3.23	0.15	2.38
40	3.01	3.07	0.06	0.99
45	2.79	2.87	0.08	1.41
50	2.71	2.79	0.08	1.45
55	2.64	2.71	0.07	1.31
60	2.54	2.60	0.06	1.17
65	2.39	2.48	0.09	1.85
70	2.22	2.29	0.07	1.55
90	1.27	1.35	0.08	3.05

Table 4.20: Heading Interval Gain Influence

Angles [°]	Heading Interval Gain Influence			
	Lower Bound [°]	Upper Bound [°]	Diff. [°]	Diff. from mean [%]
5	0.54	0.71	0.17	13.60
10	1.10	1.47	0.37	14.40
15	1.62	2.18	0.56	14.74
20	2.06	2.75	0.69	14.35
35	2.82	3.52	0.69	10.88
40	2.80	3.27	0.48	7.91
45	2.57	3.11	0.53	9.33
50	2.51	3.03	0.51	9.21
55	2.44	2.93	0.49	9.12
60	2.36	2.80	0.45	8.72
65	2.24	2.63	0.38	7.80
70	2.09	2.43	0.33	7.30
90	1.19	1.43	0.24	9.16

# 5

## Conclusions and recommendations

### 5.1. Conclusions

In this research a clear distinction is made between the static and the dynamic part of calculating DP capability. In both static and dynamic DP calculations three different design stages are distinguished namely: conceptual design, preliminary design and as built design. Recalling the research question and its sub questions as formulated in section 1.3.1, these questions are answered according to the calculation method and design stage.

#### 5.1.1. Static

In general it can be stated that for the static DP calculation method the total output uncertainty, which is the capability of the vessel expressed in  $m/s$  wind speed, reduces when going through the design stages. Despite this reduction, still a standard deviation of approximately 4% of the output is present for the as built design stage. This results in the fact that, when considering the 99.7% confidence interval, the capability of the vessel can either be calculated to be 12% higher or lower. It is therefore concluded that input uncertainties should be taken into account, especially when the capability of the vessel is calculated to be very close to the required specification. This is due to the fact that when the capability calculated is exactly the capability that is required, there is almost a 50% chance that the vessel is not able to maintain position and will drift off. Furthermore is it is concluded that the results obtained in this thesis can be used for similar shaped vessels with a comparable thruster layout.

#### Sensitivity

Overall the sensitivity does not change significantly throughout the design stages, although the point around which the sensitivity is calculated changes quite significantly for some parameters. Examples of these parameters are for instance the length, azimuth thrust and draught. These big changes in the input parameters are however only seen when changing from the conceptual to the preliminary design stage. The output is the most sensitive to the main dimensions of the vessel, the thruster thrust and the density ratio of water and air for all design stages. The current coefficients have shown to be the least sensitive parameters for all of the design stages. The sensitivity of the bow thruster thrust is the only parameter that reduces quite a bit when moving from the conceptual to the preliminary design stage.

Summarising the above it is concluded that rules of thumb can be used, for similar shaped vessels with a comparable thruster layout, when considering sensitivity since the sensitivity of the dimensionless parameters as derived in section 3.2.1 do not change when the vessels parameters are adjusted.

#### Input uncertainty

In the static calculation analysis, all the parameters that are considered to have uncertainties are determined depending on the design stage that is evaluated. It is seen that regardless of the design stage the current coefficients in x and n direction, the wind coefficient in x direction and the wave coefficients in x, y and n direction always have the biggest input uncertainty.

When looking at the conceptual design stage the main dimensions of the vessel have the biggest input uncertainty, after the most uncertain parameters as stated above. The density ratio between air and water has the single lowest input uncertainty in this design stage.

In the preliminary design stage it is seen that after the most uncertain parameters, as mentioned earlier, the thrust has the biggest input uncertainty and the ratio between air and water density becomes relatively bigger compared to other parameters.

Finally in the as built design stage it can be concluded that after the most uncertain parameters, as stated above, the wind coefficients in y and n direction and the current coefficient in y direction have the biggest input uncertainty. Furthermore the density ratio between air and water has the lowest input uncertainty in this design stage.

#### **Output uncertainty**

The output uncertainty is calculated for each parameter separately to study their contribution to the total output uncertainty. For the conceptual design stage the main dimensions of the vessel have the biggest contribution to the output uncertainty, of which the block coefficient is the most dominant. Interestingly the wind coefficient in x direction also has a big part in the output uncertainty in this design stage already, although it only concerns environmental angles around 0 and 180 degrees.

When considering the preliminary design stage the contribution to the output uncertainty by the main dimensions of the vessel is clearly reduced, although some of them still have a big contribution to the output uncertainty.

In the as built design stage the output uncertainty is mainly explained by the contribution of the wind and wave coefficients in x and y direction and the density ratio of water and air. What stands out is that, for all the design stages, the current coefficients do not contribute to the output uncertainty although they were found to have a big input uncertainty.

Summarising the above it can be concluded that no effort should be taken to reduce the uncertainty of the current coefficients since they do not contribute to the output uncertainty. A uncertainty reduction in wind and wave coefficients is however recommend since in the as built stage they still contribute to the output uncertainty.

#### **5.1.2. Dynamic**

In the dynamic DP calculation analysis only the as built stage is considered. It is concluded that machine learning methods are able to describe the dynamic behaviour of the vessel, reducing the calculating time from 17 minutes to a fraction of a second and making it possible to construct more general DP calculation models. Practically this means that when some parameters of a vessel are changed, there is no need to redo the dynamic simulations but instead the machine learning model can be used to calculate the vessels new dynamic behaviour. It is shown that for the environmental angles of 5 to 20, 35 to 70 and 90 degrees a second order polynomial regression model, with 600 data points for each heading, is able to represent the dynamic simulations accurate enough for the purpose of uncertainty calculation.

Using the machine learning model, a Monte Carlo simulation is executed to determine the as built output uncertainty of the vessel. Depending on the output and the environmental angle, and taking the 97.7% confidence interval, it is seen that the offset can be calculated to be up to 8.7% too high or too low and the heading up to 23.1% too high or too low when compared to the mean. This could result in the "Walk To Work" bridge to crash into the wind turbine, causing serious safety risks, or in a reduction of the operational window which could lead to contractual penalties. It is therefore concluded that when DP is used, for the purpose of people transferring by means of a "Walk To Work" bridge, uncertainties should be taken into account to reduce both safety and contractual risks.

#### **Sensitivity**

Due to the non monotonic response of the input on the output in some of the dynamic calculations, it is impossible to use Spearman's Correlation Analysis to rank the input variables based on order of

importance. To be able to say something about the importance of the parameters two different Monte Carlo simulations are executed. One simulation in which only the uncertainty in the environmental coefficients, the density of air and water and the mass of the vessel is sampled. In the second Monte Carlo simulation only the gains of the PID controller are sampled. From this it is seen that the influence of the PID gains is significantly bigger than the influence of the environmental parameters for all of the outputs.

### Input uncertainty

Due to the dynamic nature of the calculations a couple of new parameters are introduced which are the PID controller gains which are also assumed to be uncertain. Furthermore the uncertainty of the environmental coefficients, the density of air and water and the mass of the vessel is taken to be the same as with the static calculation.

### Output uncertainty

The output uncertainty due to the uncertain parameters shows to be quite significant. A maximum offset difference of  $0.47m$  is seen with a lower bound of  $3.36m$  and an upper bound of  $3.84m$ . The biggest relative maximum offset is calculated to be 8.70% too low or too high when compared to the mean, with a lower bound and upper bound of  $1.58m$  and  $1.88m$  respectively.

For heading the differences are even bigger, a maximum heading difference of 2.54 degrees is seen with a lower bound of 4.88 degrees and an upper bound of 7.42 degrees. The biggest relative maximum heading is calculated to be 23.10% too low or too high when compared to the mean, with a lower bound and upper bound of 1.44 degrees and 2.30 degrees respectively.

## 5.2. Recommendations

During this thesis it was seen that there are some points of interest that are worth looking into further in future research projects. As throughout this whole thesis the recommendations made are split up in a static and a dynamic part.

### 5.2.1. Static

Damen can use the outcome of this thesis to systematically identify vessel parameters that have a big influence on the static DP capability. At this point in time, when a vessel is statically not able to fulfil a certain capability, the only option left is to increase the thruster power which is expensive. Not only a more powerful thruster should be bought but also the power of the generators might increase to deliver the required power for the new thruster. When using the output uncertainty plots as illustrated in section 4.3 other parameters can be used to achieve the desired capability. An example of this could be to decide to run a CFD to obtain more certain wind coefficients, which could increase the capability of the vessel with up to 6% in the as build stage as shown in figure 4.38.

For the static calculation analysis only saturated conditions are looked into, meaning that always the maximum capability of the vessel is determined and therefore at least one of the thrusters always operate in full thrust. Instead of considering the maximum capability of the vessel in m/s wind speed, also the total amount of delivered thrust could be considered. Using this as an output and selecting a fixed, non limiting environmental condition, the non saturating cases can also be evaluated. An attempt to evaluate this method was made but it is concluded, that at this moment in time, DPlab is unable to perform this analysis. This has to do with the solver of DPlab which is not always able to find all possible solutions but starts at a specific point and tries to find the nearest solutions. When choosing a non limiting case multiple solutions are possible for the vessel to stay in position and when a parameter is varied the starting point of the solver will be different. This results in the fact that the most optimum solution is not always found in terms of total used thrust which relates to the total used power.

During this research only the intact condition of the thrusters was considered. Since the intact condition is never the limiting one when looking at the capability of the vessel it could be interesting to evaluate failure cases as well, especially the most critical failure case. It could be that here the sensitivities and therefore also the output uncertainty changes significantly.

### 5.2.2. Dynamic

In the Dynamic part of the DP calculation analysis, only the as built design stage was evaluated. From a design perspective it would however be interesting to also evaluate the preliminary design stage. By doing so the main dimensions of the vessel and the thrust of the thrusters can be adjusted, if the dynamic behaviour of the vessel is correctly captured by the machine learning model. If this proves to be working, it is recommended to Damen to create this general DP model for different series of vessels in their preliminary design stage. These models can be used to calculate position and heading offsets without running the time expensive time domain simulations for each separate configuration, making it possible to say something about the capability of the vessel in a very early design phase.

It is seen that the gains of the PID controller have a big influence on the capability of the vessel. These gains are calculated with rules of thumb and afterwards tuned manually which takes a lot of time. It is therefore recommended to use the machine learning model to find the optimal settings which can be done in only a couple of seconds. This will drastically decrease the uncertainty in the PID controller gains, reducing both safety and contractual risks.

The model created during this thesis is successfully able to capture the outputs defined for the dynamic simulations for a certain range of environmental angles. Since the model is not able to generate output for all possible directions, it is recommended to investigate other supervised machine learning methods to see whether different models are able to cover the full range of environmental angles.

The environmental forces considered in this thesis are always assumed to act collinear, meaning that they all approach the vessel from the same direction. In reality this is almost never the case as wind, waves and current are more likely to approach from different directions. It would therefore be interesting to see if a model can be created that also incorporates the different angles of approach for each environmental force. Furthermore only one specific environmental condition was chosen to execute the simulations, it would however be desirable to include at least a range of different environmental scenarios in the machine learning model if possible. This would require the model to have inputs for current speed, wave height, wave period and wind speed.

A limiting factor of aNySIM at this moment is the fact that it is only possible to use one PID controller for the purpose of DP calculations, which is the in-house designed PID controller of MARIN. They did however mention that in the future the possibility of incorporating other controllers in aNySIM should be possible. This way the controller that will be used on the actual vessel can also already be applied in the simulations, making it very easy to compare different suppliers op DP control units.

At this point in time, aNySIM is not capable of taking power restrictions of the switchboards and generators into account. Some post processing of the time series of aNySIM is already done by Damen and it is seen that, at some moments in time, the amount of power used by the thrusters exceeded the amount of power that was available from the generators. The influence on the DP capability of the vessel by this phenomenon is not known and is therefore worthwhile to investigate. Damen already initiated a conversation with MARIN to see if a coupling between Simulink and aNySIM is possible to incorporate the power and inertia restrictions of the system.

# List of Figures

1.1 Dynamic Positioning - Vessel Motions, Environmental Forces and Thruster Forces [3] . . . . .	2
1.2 Kongsberg DP capability plot [6] . . . . .	3
1.3 Input-output flowchart . . . . .	5
2.1 DP system block diagram [11] . . . . .	9
2.2 Azimuth Thrusters [15] . . . . .	10
2.3 Tunnel Thrusters [16] . . . . .	10
2.4 DP classes overview [20] . . . . .	12
2.5 Superposition of Waves [22] . . . . .	15
2.6 Second order motion spectrum comparison [9] . . . . .	20
2.7 Time variable second order wave drift and wind forces [8] . . . . .	21
2.8 Dynamic margin for different offsets [32] . . . . .	22
2.9 Hull vicinity influence layout [33] . . . . .	23
2.10 Hull vicinity drift loads influence for head and beam seas [33] . . . . .	23
2.11 DP capability hull vicinity influence [33] . . . . .	23
2.12 Shallow water influence on drift loads [33] . . . . .	24
2.13 Shallow water influence on DP capability [33] . . . . .	24
2.14 DP capability pipe-laying influence [33] . . . . .	25
2.15 Heading window comparison results [34] . . . . .	26
2.16 Thruster utilisation comparison [35] . . . . .	27
2.17 Coordinate System DPLab . . . . .	28
2.18 Coordinate System aNySIM . . . . .	28
2.19 Schematic thruster layout Bibby Wavemaster 1 . . . . .	28
2.20 Relation between two sub-models [39] . . . . .	31
3.1 Response Surface Map . . . . .	40
3.2 Machine Learning Styles [47] . . . . .	41
3.3 Random DOE . . . . .	43
3.4 Full Factorial DOE . . . . .	43
3.5 Sobol DOE . . . . .	43
3.6 Low R Squared [51] . . . . .	44
3.7 High R Squared [51] . . . . .	44
3.8 Regression with R squared = 98.5% [52] . . . . .	45
3.9 Biased Residuals [52] . . . . .	45
3.10 Time step offset 90 degrees . . . . .	47
3.11 Time step heading 90 degrees . . . . .	47
4.1 Capability Output Sensitivity +1% axis 0.8 . . . . .	50
4.2 Capability Output Sensitivity +1% axis 0.6 . . . . .	51
4.3 Capability Output Sensitivity +1% axis 0.5 . . . . .	51
4.4 Capability Output Sensitivity +1% axis 0.2 . . . . .	52
4.5 Capability Output Sensitivity +1% axis 0.14 . . . . .	52
4.6 Capability Output Sensitivity +1% axis 0.6 . . . . .	53
4.7 Capability Output Sensitivity +1% axis 0.6 . . . . .	54
4.8 Capability Output Sensitivity +1% axis 0.5 . . . . .	54
4.9 Capability Output Sensitivity +1% axis 0.2 . . . . .	55
4.10 Capability Output Sensitivity +1% axis 0.1 . . . . .	55
4.11 Capability Output Sensitivity +1% axis 0.6 . . . . .	56
4.12 Capability Output Sensitivity +1% axis 0.6 . . . . .	57

4.13 Capability Output Sensitivity +1% axis 0.5 . . . . .	57
4.14 Capability Output Sensitivity +1% axis 0.21 . . . . .	58
4.15 Capability Output Sensitivity +1% axis 0.1 . . . . .	58
4.16 Capability input uncertainty axis 2.0 . . . . .	59
4.17 Capability input uncertainty axis 0.5 . . . . .	60
4.18 Capability input uncertainty axis 0.12 . . . . .	60
4.19 Capability input uncertainty axis 0.12 . . . . .	61
4.20 Capability input uncertainty axis 2.0 . . . . .	62
4.21 Capability input uncertainty axis 0.5 . . . . .	62
4.22 Capability input uncertainty axis 0.12 . . . . .	63
4.23 Capability input uncertainty axis 0.08 . . . . .	63
4.24 Capability input uncertainty axis 2.0 . . . . .	64
4.25 Capability input uncertainty axis 0.2 . . . . .	65
4.26 Capability input uncertainty axis 0.12 . . . . .	65
4.27 Capability input uncertainty axis 0.04 . . . . .	66
4.28 Capability input uncertainty axis 0.04 . . . . .	66
4.29 Capability output uncertainty axis 0.08 . . . . .	68
4.30 Capability output uncertainty axis 0.04 . . . . .	68
4.31 Capability output uncertainty axis 0.03 . . . . .	69
4.32 Capability output uncertainty axis 0.012 . . . . .	69
4.33 Capability output uncertainty axis 0.05 . . . . .	70
4.34 Capability output uncertainty axis 0.03 . . . . .	71
4.35 Capability output uncertainty axis 0.014 . . . . .	71
4.36 Capability output uncertainty axis 0.01 . . . . .	72
4.37 Capability output uncertainty axis 0.005 . . . . .	72
4.38 Capability output uncertainty axis 0.05 . . . . .	73
4.39 Capability output uncertainty axis 0.04 . . . . .	74
4.40 Capability output uncertainty axis 0.016 . . . . .	74
4.41 Capability output uncertainty axis 0.004 . . . . .	75
4.42 Total capability output uncertainty . . . . .	76
4.43 Capability 95% confidence interval conceptual design stage . . . . .	77
4.44 Capability 99% confidence interval conceptual design stage . . . . .	77
4.45 Capability 95% confidence interval preliminary design stage . . . . .	78
4.46 Capability 99% confidence interval preliminary design stage . . . . .	78
4.47 Capability 95% confidence interval as build design stage . . . . .	79
4.48 Capability 99% confidence interval as build design stage . . . . .	79
4.49 Capability 95% confidence interval as build design stage close up . . . . .	80
4.50 Capability 99% confidence interval as build design stage close up . . . . .	80
4.51 Maximum Offset Residual for 15 degrees of environmental angle with 600 data points . . . . .	84
4.52 Offset Interval Residual for 15 degrees of environmental angle with 600 data points . . . . .	84
4.53 Maximum Heading Residual for 15 degrees of environmental angle with 600 data points . . . . .	84
4.54 Heading Interval Residual for 15 degrees of environmental angle with 600 data points . . . . .	84
4.55 Maximum offset boundaries - 99.7% confidence interval . . . . .	86
4.56 Maximum offset vs Yaw Kd for 5 degrees . . . . .	87
4.57 Maximum offset vs Sway Kp for 70 degrees . . . . .	87
4.58 Maximum offset boundaries environmental influence - 99.7% confidence interval . . . . .	87
4.59 Maximum offset boundaries gain influence - 99.7% confidence interval . . . . .	88
4.60 Offset interval boundaries - 99.7% confidence interval . . . . .	89
4.61 Offset Interval vs Yaw Kd for 10 degrees . . . . .	90
4.62 Offset Interval vs Surge Kp for 65 degrees . . . . .	90
4.63 Offset interval boundaries environmental influence - 99.7% confidence interval . . . . .	91
4.64 Offset interval boundaries gain influence - 99.7% confidence interval . . . . .	91
4.65 Maximum heading boundaries - 99.7% confidence interval . . . . .	93
4.66 Maximum Heading vs Surge Kd for 70 degrees . . . . .	95
4.67 Maximum Heading vs Yaw Kp for 50 degrees . . . . .	95
4.68 Maximum heading boundaries environmental influence - 99.7% confidence interval . . . . .	95

4.69 Maximum heading boundaries gain influence - 99.7% confidence interval . . . . .	96
4.70 Heading interval boundaries - 99.7% confidence interval . . . . .	97
4.71 Heading Interval vs Sway Kd for 20 degrees . . . . .	98
4.72 Heading Interval vs Surge Kd for 35 degrees . . . . .	98
4.73 Heading interval boundaries environmental influence - 99.7% confidence interval . . . . .	99
4.74 Heading interval boundaries gain influence - 99.7% confidence interval . . . . .	99
A.1 schematic overview . . . . .	111
B.1 Monotonic and Non Monotonic relationships . . . . .	114
D.1 Input Output overview DPlab . . . . .	123
D.2 Input for environmental forces calculation DPlab . . . . .	124
E.1 Output overview aNySIM . . . . .	131
E.2 Input overview aNySIM . . . . .	132
F.1 Maximum Offset Residual for 5 degrees of environmental angle with 600 data points . . . . .	139
F.2 Maximum Offset Residual for 10 degrees of environmental angle with 600 data points . . . . .	139
F.3 Maximum Offset Residual for 15 degrees of environmental angle with 600 data points . . . . .	140
F.4 Maximum Offset Residual for 20 degrees of environmental angle with 600 data points . . . . .	140
F.5 Maximum Offset Residual for 35 degrees of environmental angle with 600 data points . . . . .	140
F.6 Maximum Offset Residual for 40 degrees of environmental angle with 600 data points . . . . .	140
F.7 Maximum Offset Residual for 45 degrees of environmental angle with 600 data points . . . . .	141
F.8 Maximum Offset Residual for 50 degrees of environmental angle with 600 data points . . . . .	141
F.9 Maximum Offset Residual for 55 degrees of environmental angle with 600 data points . . . . .	141
F.10 Maximum Offset Residual for 60 degrees of environmental angle with 600 data points . . . . .	141
F.11 Maximum Offset Residual for 65 degrees of environmental angle with 600 data points . . . . .	142
F.12 Maximum Offset Residual for 70 degrees of environmental angle with 600 data points . . . . .	142
F.13 Maximum Offset Residual for 90 degrees of environmental angle with 600 data points . . . . .	142
F.14 Offset Interval Residual for 5 degrees of environmental angle with 600 data points . . . . .	142
F.15 Offset Interval Residual for 10 degrees of environmental angle with 600 data points . . . . .	143
F.16 Offset Interval Residual for 15 degrees of environmental angle with 600 data points . . . . .	143
F.17 Offset Interval Residual for 20 degrees of environmental angle with 600 data points . . . . .	143
F.18 Offset Interval Residual for 35 degrees of environmental angle with 600 data points . . . . .	143
F.19 Offset Interval Residual for 40 degrees of environmental angle with 600 data points . . . . .	144
F.20 Offset Interval Residual for 45 degrees of environmental angle with 600 data points . . . . .	144
F.21 Offset Interval Residual for 50 degrees of environmental angle with 600 data points . . . . .	144
F.22 Offset Interval Residual for 55 degrees of environmental angle with 600 data points . . . . .	144
F.23 Offset Interval Residual for 60 degrees of environmental angle with 600 data points . . . . .	145
F.24 Offset Interval Residual for 65 degrees of environmental angle with 600 data points . . . . .	145
F.25 Offset Interval Residual for 70 degrees of environmental angle with 600 data points . . . . .	145
F.26 Offset Interval Residual for 90 degrees of environmental angle with 600 data points . . . . .	145
F.27 Maximum Heading Residual for 5 degrees of environmental angle with 600 data points . . . . .	146
F.28 Maximum Heading Residual for 10 degrees of environmental angle with 600 data points . . . . .	146
F.29 Maximum Heading Residual for 15 degrees of environmental angle with 600 data points . . . . .	146
F.30 Maximum Heading Residual for 20 degrees of environmental angle with 600 data points . . . . .	146
F.31 Maximum Heading Residual for 35 degrees of environmental angle with 600 data points . . . . .	147
F.32 Maximum Heading Residual for 40 degrees of environmental angle with 600 data points . . . . .	147
F.33 Maximum Heading Residual for 45 degrees of environmental angle with 600 data points . . . . .	147
F.34 Maximum Heading Residual for 50 degrees of environmental angle with 600 data points . . . . .	147
F.35 Maximum Heading Residual for 55 degrees of environmental angle with 600 data points . . . . .	148
F.36 Maximum Heading Residual for 60 degrees of environmental angle with 600 data points . . . . .	148
F.37 Maximum Heading Residual for 65 degrees of environmental angle with 600 data points . . . . .	148
F.38 Maximum Heading Residual for 70 degrees of environmental angle with 600 data points . . . . .	148
F.39 Maximum Heading Residual for 90 degrees of environmental angle with 600 data points . . . . .	149
F.40 Heading Interval Residual for 5 degrees of environmental angle with 600 data points . . . . .	149

F.41 Heading Interval Residual for 10 degrees of environmental angle with 600 data points .	149
F.42 Heading Interval Residual for 15 degrees of environmental angle with 600 data points .	149
F.43 Heading Interval Residual for 20 degrees of environmental angle with 600 data points .	150
F.44 Heading Interval Residual for 35 degrees of environmental angle with 600 data points .	150
F.45 Heading Interval Residual for 40 degrees of environmental angle with 600 data points .	150
F.46 Heading Interval Residual for 45 degrees of environmental angle with 600 data points .	150
F.47 Heading Interval Residual for 50 degrees of environmental angle with 600 data points .	151
F.48 Heading Interval Residual for 55 degrees of environmental angle with 600 data points .	151
F.49 Heading Interval Residual for 60 degrees of environmental angle with 600 data points .	151
F.50 Heading Interval Residual for 65 degrees of environmental angle with 600 data points .	151
F.51 Heading Interval Residual for 70 degrees of environmental angle with 600 data points .	152
F.52 Heading Interval Residual for 90 degrees of environmental angle with 600 data points .	152

# List of Tables

1.1 Various design stages DP system with accuracy [4] . . . . .	2
1.2 Design stages . . . . .	5
3.1 Design stages . . . . .	36
3.2 Environmental Variables . . . . .	38
3.3 Comparison of simulation time between Response Surface Method and Monte Carlo Simulation . . . . .	39
4.1 Explanation terms used in goodness of fit tables . . . . .	81
4.2 0 degrees 2nd order fit on 136 points . . . . .	82
4.3 0 degrees 2nd order fit on 270 points . . . . .	82
4.4 15 degrees 2nd order fit on 136 points . . . . .	82
4.5 15 degrees 2nd order fit on 600 points . . . . .	82
4.6 45 degrees 2nd order fit on 136 points . . . . .	82
4.7 45 degrees 2nd order fit on 270 points . . . . .	82
4.8 45 degrees 2nd order fit on 600 points . . . . .	82
4.9 Maximum Offset lower bound, upper bound and differences . . . . .	86
4.10 Maximum Offset environmental influence . . . . .	88
4.11 Maximum Offset Gain influence . . . . .	89
4.12 Offset Interval lower bound, upper bound and differences . . . . .	90
4.13 Offset Interval environmental influence . . . . .	92
4.14 Offset Interval Gain influence . . . . .	92
4.15 Maximum Heading lower bound, upper bound and differences . . . . .	94
4.16 Maximum Heading Environmental Influence . . . . .	96
4.17 Maximum Heading Gain Influence . . . . .	97
4.18 Heading Interval lower bound, upper bound and differences . . . . .	98
4.19 Heading Interval Environmental Influence . . . . .	100
4.20 Heading Interval Gain Influence . . . . .	100
C.1 Quantities and their basic dimensions . . . . .	115
C.2 Parameters static DP and their basic dimensions . . . . .	116
D.1 Effected forces by parameters . . . . .	125
D.2 Mean and standard deviations for static DP . . . . .	126
D.3 Mean and standard deviations for wind coefficients . . . . .	127
D.4 Mean and standard deviations for current coefficients . . . . .	128
D.5 Density of water . . . . .	129
D.6 Density of water . . . . .	129
D.7 Wind wave relation . . . . .	129
E.1 Varied parameters and their boundary values for sobol space . . . . .	133
E.2 Effect on parameters when tuning P gain . . . . .	134
E.3 Effect on parameters when tuning I gain . . . . .	134
E.4 Effect on parameters when tuning D gain . . . . .	134
E.5 Converting angles . . . . .	135
F.1 0 degrees 2nd order fit on 136 points . . . . .	152
F.2 0 degrees 2nd order fit on 270 points . . . . .	152
F.3 5 degrees 2nd order fit on 136 points . . . . .	152

F.4	5 degrees 2nd order fit on 600 points . . . . .	152
F.5	10 degrees 2nd order fit on 136 points . . . . .	153
F.6	10 degrees 2nd order fit on 600 points . . . . .	153
F.7	15 degrees 2nd order fit on 136 points . . . . .	153
F.8	15 degrees 2nd order fit on 600 points . . . . .	153
F.9	20 degrees 2nd order fit on 136 points . . . . .	153
F.10	20 degrees 2nd order fit on 600 points . . . . .	153
F.11	25 degrees 2nd order fit on 136 points . . . . .	153
F.12	30 degrees 2nd order fit on 136 points . . . . .	154
F.13	30 degrees 2nd order fit on 270 points . . . . .	154
F.14	35 degrees 2nd order fit on 136 points . . . . .	154
F.15	35 degrees 2nd order fit on 600 points . . . . .	154
F.16	40 degrees 2nd order fit on 136 points . . . . .	154
F.17	40 degrees 2nd order fit on 600 points . . . . .	154
F.18	45 degrees 2nd order fit on 136 points . . . . .	154
F.19	45 degrees 2nd order fit on 270 points . . . . .	154
F.20	45 degrees 2nd order fit on 600 points . . . . .	155
F.21	50 degrees 2nd order fit on 136 points . . . . .	155
F.22	50 degrees 2nd order fit on 600 points . . . . .	155
F.23	55 degrees 2nd order fit on 136 points . . . . .	155
F.24	55 degrees 2nd order fit on 600 points . . . . .	155
F.25	60 degrees 2nd order fit on 136 points . . . . .	155
F.26	60 degrees 2nd order fit on 600 points . . . . .	155
F.27	65 degrees 2nd order fit on 136 points . . . . .	156
F.28	65 degrees 2nd order fit on 600 points . . . . .	156
F.29	70 degrees 2nd order fit on 136 points . . . . .	156
F.30	70 degrees 2nd order fit on 600 points . . . . .	156
F.31	75 degrees 2nd order fit on 136 points . . . . .	156
F.32	80 degrees 2nd order fit on 136 points . . . . .	156
F.33	85 degrees 2nd order fit on 136 points . . . . .	156
F.34	90 degrees 2nd order fit on 136 points . . . . .	157
F.35	90 degrees 2nd order fit on 600 points . . . . .	157

# A

## Project overview

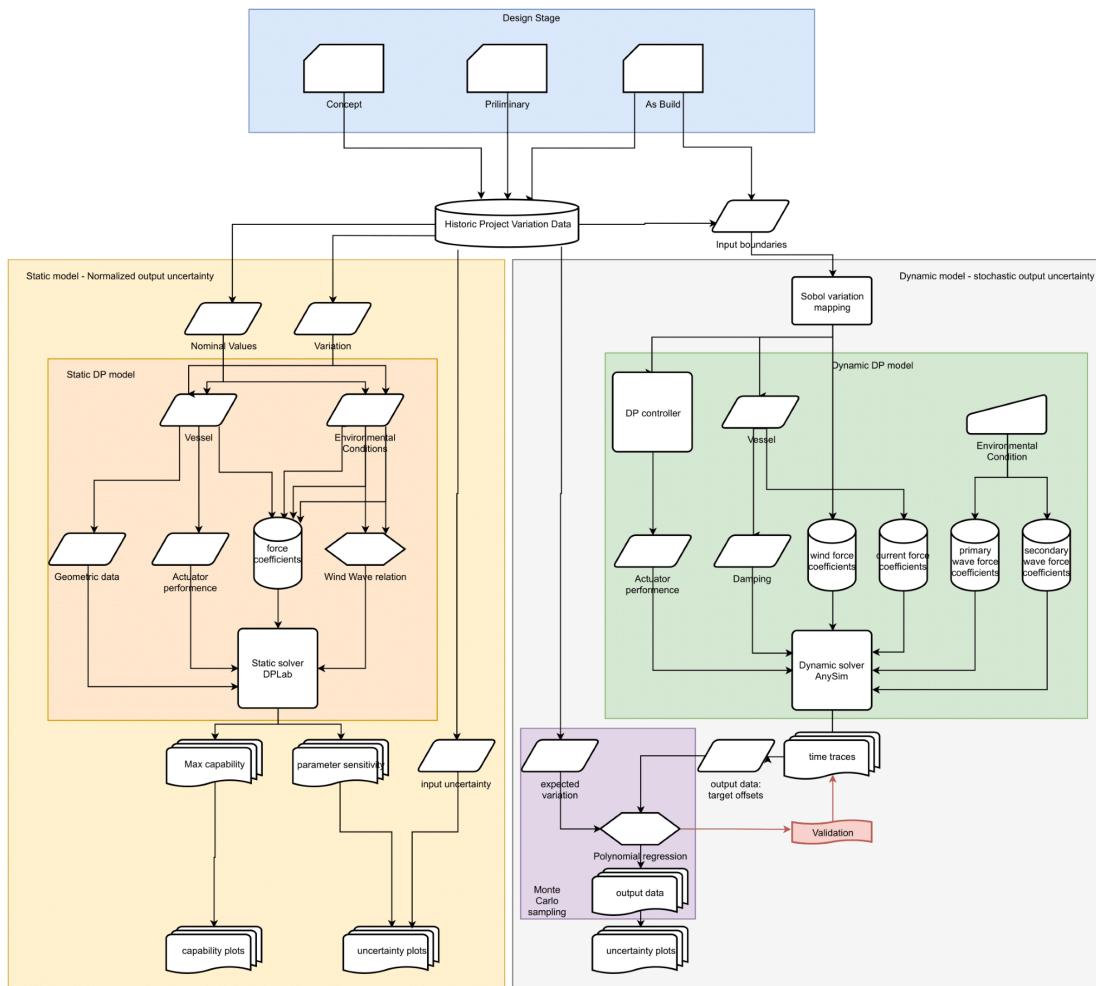


Figure A.1: schematic overview



# B

## Data types

The type of data that is available, put in or generated by a model determines which sensitivity analysis can be used to uncover relationships between the input and output. Here a couple of often used data types is elaborated on.

### B.1. Nominal

Nominal variables are defined as variables that have two or more categories, which can not be ordered or ranked meaning that they don't have an intrinsic order [55]. For example, a car garage could classify their types of vehicles into distinct categories such as sedan, station wagon, convertible and sport. Now it can be stated that the "type of car" is a nominal value with 4 different categories which are called sedan, station wagon, convertible and sport.

### B.2. Dichotomous

Dichotomous variables are defined as variables that have only two categories [55]. An example could be when it was asked to someone if he or she owns a boat, here we can categorise boat ownership as either "yes" or "no". Another example could be when looking at gender, again two categories could be defined namely "male" and "female".

### B.3. Ordinal

Ordinal variables are variables that have two or more categories just like nominal values have, the difference is however that ordinal values can also be ordered or ranked. When you would ask someone if they are cold they could answer with "not at all", "a little" or "Yes extremely". These are called ordinal variables since it is now possible to rank them from most positive ("not at all") to a middle response ("a little") to the least positive ("Yes extremely").

### B.4. Interval

Interval variables are variables that can be measured on a continuous and numeric scale. An example is temperature in degrees Celsius. Here the difference between 10°C and 20°C is the same as the difference between 20°C and 30°C.

### B.5. Ratio

Ratio variables are the same as interval variables but with the addition that when 0 is measured it indicates that there is none of that variable. When looking at the example of temperature measured in degrees Celsius, 0°C does not mean there is no temperature and therefore does not qualify as a ratio variable. Examples of ratio variables are mass, distance, volume and many more.

## B.6. Monotonic relationship

A relationship can be referred to as monotonic when one of the following conditions are met:

- If one value of a variable increases then the other variable should also increase
- If one value of a variable increases then the other variable should decrease

Examples of monotonic and non monotonic relationships are illustrated in figure B.1.

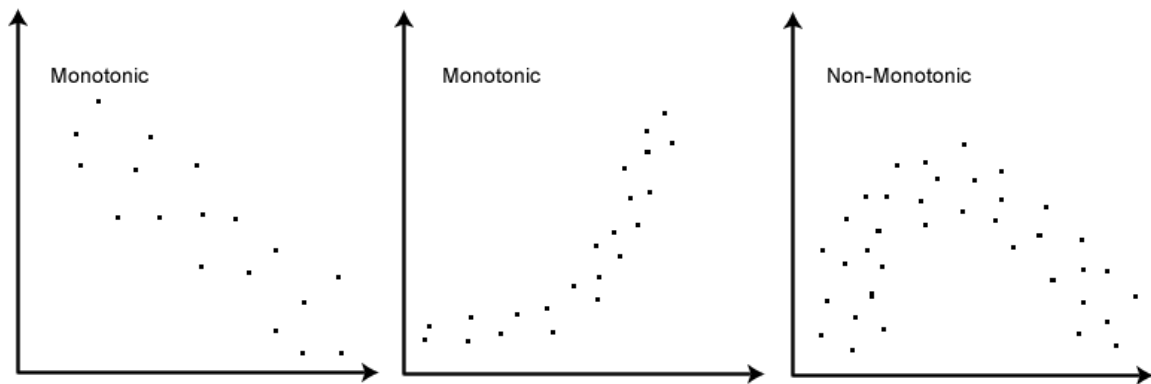


Figure B.1: Monotonic and Non Monotonic relationships

# C

## Dimensional analysis

Dimensional analysis is a method often used for reducing the complexity and the number of variables which influence a physical phenomenon [56]. When a certain physical phenomenon depends upon  $n$  dimensional variables the dimensional analysis method is able to reduce the problem to only  $(n - k)$  dimensionless variable groups. Here  $k$  is the number of basic dimensions that play a role. The four basic dimensions are usually taken to be mass  $M$ , length  $L$ , time  $T$  and temperature  $\Theta$ . For example regardless of whether a volume is expressed in units of cubic foot, cubic inches or in cubic meter, its physical (basic) dimension remains the same. An overview of the quantities expressed in their basic dimensions is given in table C.1.

Table C.1: Quantities and their basic dimensions

Quantity	Physical dimensions	SI
Mass	$M$	$kg$
Length	$L$	$m$
Time	$T$	$s$
Temperature	$\Theta$	$K$
Area	$L^2$	$m^2$
Volume	$L^3$	$m^3$
Angular velocity	$T^{-1}$	$rad/s$
Angular acceleration	$T^{-2}$	$rad/s^2$
Velocity	$LT^{-1}$	$m/s$
Acceleration	$LT^{-2}$	$m/s^2$
Mass flow	$MT^{-1}$	$kg/s$
Momentum	$MLT^{-1}$	$kgm/s$
Force, Weight	$MLT^{-2}$	$kgm/s^2 (N)$
Moment, Energy or Work	$ML^2T^{-2}$	$Nm (J)$
Power	$ML^2T^{-3}$	$Nm/s (W)$
Density	$ML^{-3}$	$kg/m^3$
Pressure	$ML^{-1}T^{-2}$	$N/m^2 (P_a)$
Viscosity	$ML^{-1}T^{-1}$	$Ns/m^2$
Heat value	$L^2T^{-2}$	$J/kg$
Gas constant	$L^2T^{-2}\Theta^{-1}$	$J/kgK$
Angle	$M^0L^0T^0$	radian
Adiabatic index	$M^0L^0T^0$	—
Relative humidity	$M^0L^0T^0$	—

For the purpose of static dynamic positioning calculation the dimensional parameters influencing the capability of the vessel were determined and listed in table C.2.

Table C.2: Parameters static DP and their basic dimensions

Nr	Parameter	Short name	SI unit	Basic dimensions
1	Length Waterline	$L_{wl}$	[m]	$L$
2	Breadth	$B$	[m]	$L$
3	Draught	$T$	[m]	$L$
4	Volume	$\nabla$	[ $m^3$ ]	$L^3$
5	Frontal wind area	$Af_w$	[ $m^2$ ]	$L^2$
6	Lateral wind area	$Al_w$	[ $m^2$ ]	$L^2$
7	Density water	$\rho_w$	[ $kg/m^3$ ]	$M/L^3$
8	Density air	$\rho_a$	[ $kg/m^3$ ]	$M/L^3$
9	Azimuth x position port side	$Azi_p \ pos_x$	[m]	$L$
10	Azimuth x position starboard	$Azi_s \ pos_x$	[m]	$L$
11	Azimuth y position port side	$Azi_p \ pos_y$	[m]	$L$
12	Azimuth y position starboard	$Azi_s \ pos_y$	[m]	$L$
13	Retractable x position	$Retr \ pos_x$	[m]	$L$
14	Retractable y position	$Retr \ pos_y$	[m]	$L$
15	Bow thruster x position fore	$Bow_f \ pos_x$	[m]	$L$
16	Bow thruster x position aft	$Bow_a \ pos_x$	[m]	$L$
17	Bow thruster y position fore	$Bow_f \ pos_y$	[m]	$L$
18	Bow thruster y position aft	$Bow_a \ pos_y$	[m]	$L$
19	Azimuth thrust	$Azi_T$	[N]	$ML/T^2$
20	Retractable thrust	$Retr_T$	[N]	$ML/T^2$
21	Bow thruster thrust	$Bow_T$	[N]	$ML/T^2$
22	Mass of the vessel	$m$	[kg]	$M$
23	Gravitational acceleration	$g$	[ $m/s^2$ ]	$L/T^2$

Now that all parameters are found it can be seen that there are  $n = 23$  parameters and  $k = 3$  basic dimensions, namely  $M$ ,  $L$  and  $T$ . Then according to the Buckingham  $\Pi$  theorem [56] there are  $j = n - k = 23 - 3 = 20$  independent dimensionless variables to be found. To find these independent dimensionless variables first a choice of fundamental variables should be made. These fundamental variables are used to make other variables dimensionless by using their product. The choice of these variables can be made arbitrarily however the variables should be chosen such that all the basic dimensions are present [57]. Here the length on the waterline  $Lwl$ , mass  $m$  and gravitational acceleration  $g$  are chosen as fundamental variables. Now the following is obtained:

$$\begin{aligned}\Pi_1 &= (L_{wl})^{a_1} \cdot (m)^{b_1} \cdot (g)^{c_1} \cdot B \\ \Pi_2 &= (L_{wl})^{a_2} \cdot (m)^{b_2} \cdot (g)^{c_2} \cdot T \\ \Pi_3 &= (L_{wl})^{a_3} \cdot (m)^{b_3} \cdot (g)^{c_3} \cdot \nabla \\ \Pi_4 &= (L_{wl})^{a_4} \cdot (m)^{b_4} \cdot (g)^{c_4} \cdot Af_w \\ \Pi_5 &= (L_{wl})^{a_5} \cdot (m)^{b_5} \cdot (g)^{c_5} \cdot Al_w \\ \Pi_6 &= (L_{wl})^{a_6} \cdot (m)^{b_6} \cdot (g)^{c_6} \cdot \rho_w \\ \Pi_7 &= (L_{wl})^{a_7} \cdot (m)^{b_7} \cdot (g)^{c_7} \cdot \rho_a \\ \Pi_8 &= (L_{wl})^{a_8} \cdot (m)^{b_8} \cdot (g)^{c_8} \cdot Azi_p \ pos_x \\ \Pi_9 &= (L_{wl})^{a_9} \cdot (m)^{b_9} \cdot (g)^{c_9} \cdot Azi_s \ pos_x \\ \Pi_{10} &= (L_{wl})^{a_{10}} \cdot (m)^{b_{10}} \cdot (g)^{c_{10}} \cdot Azi_p \ pos_y \\ \Pi_{11} &= (L_{wl})^{a_{11}} \cdot (m)^{b_{11}} \cdot (g)^{c_{11}} \cdot Azi_s \ pos_y \\ \Pi_{12} &= (L_{wl})^{a_{12}} \cdot (m)^{b_{12}} \cdot (g)^{c_{12}} \cdot Retr \ pos_x\end{aligned}$$

$$\begin{aligned}
\Pi_{13} &= (L_{wl})^{a_{13}} \cdot (m)^{b_{13}} \cdot (g)^{c_{13}} \cdot \text{Retr pos}_y \\
\Pi_{14} &= (L_{wl})^{a_{14}} \cdot (m)^{b_{14}} \cdot (g)^{c_{14}} \cdot \text{Bow}_f \text{ pos}_x \\
\Pi_{15} &= (L_{wl})^{a_{15}} \cdot (m)^{b_{15}} \cdot (g)^{c_{15}} \cdot \text{Bow}_a \text{ pos}_x \\
\Pi_{16} &= (L_{wl})^{a_{16}} \cdot (m)^{b_{16}} \cdot (g)^{c_{16}} \cdot \text{Bow}_f \text{ pos}_y \\
\Pi_{17} &= (L_{wl})^{a_{17}} \cdot (m)^{b_{17}} \cdot (g)^{c_{17}} \cdot \text{Bow}_a \text{ pos}_y \\
\Pi_{18} &= (L_{wl})^{a_{18}} \cdot (m)^{b_{18}} \cdot (g)^{c_{18}} \cdot \text{Azi}_T \\
\Pi_{19} &= (L_{wl})^{a_{19}} \cdot (m)^{b_{19}} \cdot (g)^{c_{19}} \cdot \text{Retr}_T \\
\Pi_{20} &= (L_{wl})^{a_{20}} \cdot (m)^{b_{20}} \cdot (g)^{c_{20}} \cdot \text{Bow}_T
\end{aligned}$$

The next step to find the specific form of the dimensionless  $\Pi$  groups is to replace all parameters with their known  $k$  basic dimensions equivalent. In this case the basic dimensions present are  $M$ ,  $L$  and  $T$ . After the substitution the following is obtained.

$$\begin{aligned}
\Pi_1 &= (L)^{a_1} \cdot (M)^{b_1} \cdot (LT^{-2})^{c_1} \cdot (L) \\
\Pi_2 &= (L)^{a_2} \cdot (M)^{b_2} \cdot (LT^{-2})^{c_2} \cdot (L) \\
\Pi_3 &= (L)^{a_3} \cdot (M)^{b_3} \cdot (LT^{-2})^{c_3} \cdot (L^3) \\
\Pi_4 &= (L)^{a_4} \cdot (M)^{b_4} \cdot (LT^{-2})^{c_4} \cdot (L^2) \\
\Pi_5 &= (L)^{a_5} \cdot (M)^{b_5} \cdot (LT^{-2})^{c_5} \cdot (L^2) \\
\Pi_6 &= (L)^{a_6} \cdot (M)^{b_6} \cdot (LT^{-2})^{c_6} \cdot (ML^{-3}) \\
\Pi_7 &= (L)^{a_7} \cdot (M)^{b_7} \cdot (LT^{-2})^{c_7} \cdot (ML^{-3}) \\
\Pi_8 &= (L)^{a_8} \cdot (M)^{b_8} \cdot (LT^{-2})^{c_8} \cdot (L) \\
\Pi_9 &= (L)^{a_9} \cdot (M)^{b_9} \cdot (LT^{-2})^{c_9} \cdot (L) \\
\Pi_{10} &= (L)^{a_{10}} \cdot (M)^{b_{10}} \cdot (LT^{-2})^{c_{10}} \cdot (L) \\
\Pi_{11} &= (L)^{a_{11}} \cdot (M)^{b_{11}} \cdot (LT^{-2})^{c_{11}} \cdot (L) \\
\Pi_{12} &= (L)^{a_{12}} \cdot (M)^{b_{12}} \cdot (LT^{-2})^{c_{12}} \cdot (L) \\
\Pi_{13} &= (L)^{a_{13}} \cdot (M)^{b_{13}} \cdot (LT^{-2})^{c_{13}} \cdot (L) \\
\Pi_{14} &= (L)^{a_{14}} \cdot (M)^{b_{14}} \cdot (LT^{-2})^{c_{14}} \cdot (L) \\
\Pi_{15} &= (L)^{a_{15}} \cdot (M)^{b_{15}} \cdot (LT^{-2})^{c_{15}} \cdot (L) \\
\Pi_{16} &= (L)^{a_{16}} \cdot (M)^{b_{16}} \cdot (LT^{-2})^{c_{16}} \cdot (L) \\
\Pi_{17} &= (L)^{a_{17}} \cdot (M)^{b_{17}} \cdot (LT^{-2})^{c_{17}} \cdot (L) \\
\Pi_{18} &= (L)^{a_{18}} \cdot (M)^{b_{18}} \cdot (LT^{-2})^{c_{18}} \cdot (MLT^{-2}) \\
\Pi_{19} &= (L)^{a_{19}} \cdot (M)^{b_{19}} \cdot (LT^{-2})^{c_{19}} \cdot (MLT^{-2}) \\
\Pi_{20} &= (L)^{a_{20}} \cdot (M)^{b_{20}} \cdot (LT^{-2})^{c_{20}} \cdot (MLT^{-2})
\end{aligned}$$

In order to make the  $\Pi$  groups dimensionless it is necessary that the summation of the powers of  $L$ ,  $M$  and  $T$  are equal to zero.

So for  $\Pi_1$ :

$$\left. \begin{array}{l} a_1 + c_1 + 1 = 0 \\ b_1 = 0 \\ -2c_1 = 0 \end{array} \right\} \quad \text{gives} \quad \begin{array}{l} a_1 = -1 \\ b_1 = 0 \\ c_1 = 0 \end{array}$$

$$\Pi_1 = (L_{wl})^{-1} \cdot (m)^0 \cdot (g)^0 \cdot B = \frac{B}{L_{wl}}$$

So for  $\Pi_2$ :

$$\left. \begin{array}{l} a_2 + c_2 + 1 = 0 \\ b_2 = 0 \\ -2c_2 = 0 \end{array} \right\} \quad \text{gives} \quad \begin{array}{l} a_2 = -1 \\ b_2 = 0 \\ c_2 = 0 \end{array}$$

$$\Pi_2 = (L_{wl})^{-1} \cdot (m)^0 \cdot (g)^0 \cdot T = \frac{T}{L_{wl}}$$

So for  $\Pi_3$ :

$$\left. \begin{array}{l} a_3 + c_3 + 3 = 0 \\ b_3 = 0 \\ -2c_3 = 0 \end{array} \right\} \quad \text{gives} \quad \begin{array}{l} a_3 = -3 \\ b_3 = 0 \\ c_3 = 0 \end{array}$$

$$\Pi_3 = (L_{wl})^{-3} \cdot (m)^0 \cdot (g)^0 \cdot \nabla = \frac{\nabla}{L_{wl}^3}$$

So for  $\Pi_4$ :

$$\left. \begin{array}{l} a_4 + c_4 + 2 = 0 \\ b_4 = 0 \\ -2c_4 = 0 \end{array} \right\} \quad \text{gives} \quad \begin{array}{l} a_4 = -2 \\ b_4 = 0 \\ c_4 = 0 \end{array}$$

$$\Pi_4 = (L_{wl})^{-2} \cdot (m)^0 \cdot (g)^0 \cdot Af_w = \frac{Af_w}{L_{wl}^2}$$

So for  $\Pi_5$ :

$$\left. \begin{array}{l} a_5 + c_5 + 2 = 0 \\ b_5 = 0 \\ -2c_5 = 0 \end{array} \right\} \quad \text{gives} \quad \begin{array}{l} a_5 = -2 \\ b_5 = 0 \\ c_5 = 0 \end{array}$$

$$\Pi_5 = (L_{wl})^{-2} \cdot (m)^0 \cdot (g)^0 \cdot Al_w = \frac{Al_w}{L_{wl}^2}$$

So for  $\Pi_6$ :

$$\left. \begin{array}{l} a_6 + c_6 - 3 = 0 \\ b_6 + 1 = 0 \\ -2c_6 = 0 \end{array} \right\} \quad \text{gives} \quad \begin{array}{l} a_6 = 3 \\ b_6 = -1 \\ c_6 = 0 \end{array}$$

$$\Pi_6 = (L_{wl})^3 \cdot (m)^{-1} \cdot (g)^0 \cdot rho_w = \frac{rho_w \cdot L_{wl}^3}{m}$$

So for  $\Pi_7$ :

$$\left. \begin{array}{l} a_7 + c_7 - 3 = 0 \\ b_7 + 1 = 0 \\ -2c_7 = 0 \end{array} \right\} \quad \text{gives} \quad \begin{array}{l} a_7 = 3 \\ b_7 = -1 \\ c_7 = 0 \end{array}$$

$$\Pi_7 = (L_{wl})^3 \cdot (m)^{-1} \cdot (g)^0 \cdot rho_a = \frac{rho_a \cdot L_{wl}^3}{m}$$

So for  $\Pi_8$ :

$$\left. \begin{array}{l} a_8 + c_8 + 1 = 0 \\ b_8 = 0 \\ -2c_8 = 0 \end{array} \right\} \quad \text{gives} \quad \begin{array}{l} a_8 = -1 \\ b_8 = 0 \\ c_8 = 0 \end{array}$$

$$\Pi_8 = (L_{wl})^{-1} \cdot (m)^0 \cdot (g)^0 \cdot Azi_p pos_x = \frac{Azi_p pos_x}{L_{wl}}$$

So for  $\Pi_9$ :

$$\left. \begin{array}{l} a_9 + c_9 + 1 = 0 \\ b_9 = 0 \\ -2c_9 = 0 \end{array} \right\} \quad \text{gives} \quad \begin{array}{l} a_9 = -1 \\ b_9 = 0 \\ c_9 = 0 \end{array}$$

$$\Pi_9 = (L_{wl})^{-1} \cdot (m)^0 \cdot (g)^0 \cdot Azi_s pos_x = \frac{Azi_s pos_x}{L_{wl}}$$

So for  $\Pi_{10}$ :

$$\left. \begin{array}{l} a_{10} + c_{10} + 1 = 0 \\ b_{10} = 0 \\ -2c_{10} = 0 \end{array} \right\} \quad \text{gives} \quad \begin{array}{l} a_{10} = -1 \\ b_{10} = 0 \\ c_{10} = 0 \end{array}$$

$$\Pi_{10} = (L_{wl})^{-1} \cdot (m)^0 \cdot (g)^0 \cdot Azi_p pos_y = \frac{Azi_p pos_y}{L_{wl}}$$

So for  $\Pi_{11}$ :

$$\left. \begin{array}{l} a_{11} + c_{11} + 1 = 0 \\ b_{11} = 0 \\ -2c_{11} = 0 \end{array} \right\} \quad \text{gives} \quad \begin{array}{l} a_{11} = -1 \\ b_{11} = 0 \\ c_{11} = 0 \end{array}$$

$$\Pi_{11} = (L_{wl})^{-1} \cdot (m)^0 \cdot (g)^0 \cdot Azi_s pos_y = \frac{Azi_s pos_y}{L_{wl}}$$

So for  $\Pi_{12}$ :

$$\left. \begin{array}{l} a_{12} + c_{12} + 1 = 0 \\ b_{12} = 0 \\ -2c_{12} = 0 \end{array} \right\} \quad \text{gives} \quad \begin{array}{l} a_{12} = -1 \\ b_{12} = 0 \\ c_{12} = 0 \end{array}$$

$$\Pi_{12} = (L_{wl})^{-1} \cdot (m)^0 \cdot (g)^0 \cdot Retr pos_x = \frac{Retr pos_x}{L_{wl}}$$

So for  $\Pi_{13}$ :

$$\left. \begin{array}{l} a_{13} + c_{13} + 1 = 0 \\ b_{13} = 0 \\ -2c_{13} = 0 \end{array} \right\} \quad \text{gives} \quad \begin{array}{l} a_{13} = -1 \\ b_{13} = 0 \\ c_{13} = 0 \end{array}$$

$$\Pi_{13} = (L_{wl})^{-1} \cdot (m)^0 \cdot (g)^0 \cdot Retr pos_y = \frac{Retr pos_y}{L_{wl}}$$

So for  $\Pi_{14}$ :

$$\left. \begin{array}{l} a_{14} + c_{14} + 1 = 0 \\ b_{14} = 0 \\ -2c_{14} = 0 \end{array} \right\} \quad \text{gives} \quad \begin{array}{l} a_{14} = -1 \\ b_{14} = 0 \\ c_{14} = 0 \end{array}$$

$$\Pi_{14} = (L_{wl})^{-1} \cdot (m)^0 \cdot (g)^0 \cdot Bow_f pos_x = \frac{Bow_f pos_x}{L_{wl}}$$

So for  $\Pi_{15}$ :

$$\left. \begin{array}{l} a_{15} + c_{15} + 1 = 0 \\ b_{15} = 0 \\ -2c_{15} = 0 \end{array} \right\} \quad \text{gives} \quad \begin{array}{l} a_{15} = -1 \\ b_{15} = 0 \\ c_{15} = 0 \end{array}$$

$$\Pi_{15} = (L_{wl})^{-1} \cdot (m)^0 \cdot (g)^0 \cdot Bow_a pos_x = \frac{Bow_a pos_x}{L_{wl}}$$

So for  $\Pi_{16}$ :

$$\left. \begin{array}{l} a_{16} + c_{16} + 1 = 0 \\ b_{16} = 0 \\ -2c_{16} = 0 \end{array} \right\} \quad \text{gives} \quad \begin{array}{l} a_{16} = -1 \\ b_{16} = 0 \\ c_{16} = 0 \end{array}$$

$$\Pi_{16} = (L_{wl})^{-1} \cdot (m)^0 \cdot (g)^0 \cdot Bow_f pos_y = \frac{Bow_f pos_y}{L_{wl}}$$

So for  $\Pi_{17}$ :

$$\left. \begin{array}{l} a_{17} + c_{17} + 1 = 0 \\ b_{17} = 0 \\ -2c_{17} = 0 \end{array} \right\} \quad \text{gives} \quad \begin{array}{l} a_{17} = -1 \\ b_{17} = 0 \\ c_{17} = 0 \end{array}$$

$$\Pi_{17} = (L_{wl})^{-1} \cdot (m)^0 \cdot (g)^0 \cdot Bow_a pos_y = \frac{Bow_a pos_y}{L_{wl}}$$

So for  $\Pi_{18}$ :

$$\left. \begin{array}{l} a_{18} + c_{18} + 1 = 0 \\ b_{18} + 1 = 0 \\ -2c_{18} - 2 = 0 \end{array} \right\} \quad \text{gives} \quad \begin{array}{l} a_{18} = 0 \\ b_{18} = -1 \\ c_{18} = -1 \end{array}$$

$$\Pi_{18} = (L_{wl})^0 \cdot (m)^{-1} \cdot (g)^{-1} \cdot Azi_T = \frac{Azi_T}{m \cdot g}$$

So for  $\Pi_{19}$ :

$$\left. \begin{array}{l} a_{19} + c_{19} + 1 = 0 \\ b_{19} + 1 = 0 \\ -2c_{19} - 2 = 0 \end{array} \right\} \quad \text{gives} \quad \begin{array}{l} a_{19} = 0 \\ b_{19} = -1 \\ c_{19} = -1 \end{array}$$

$$\Pi_{19} = (L_{wl})^0 \cdot (m)^{-1} \cdot (g)^{-1} \cdot Retr_T = \frac{Retr_T}{m \cdot g}$$

So for  $\Pi_{20}$ :

$$\left. \begin{array}{l} a_{20} + c_{20} + 1 = 0 \\ b_{20} + 1 = 0 \\ -2c_{20} - 2 = 0 \end{array} \right\} \quad \text{gives} \quad \begin{array}{l} a_{20} = 0 \\ b_{20} = -1 \\ c_{20} = -1 \end{array}$$

$$\Pi_{20} = (L_{wl})^0 \cdot (m)^{-1} \cdot (g)^{-1} \cdot Bow_T = \frac{Bow_T}{m \cdot g}$$

To obtain physically sensible dimensionless groups the  $\Pi$  groups can be multiplied with each other [57]. The following multiplications are executed where the groups used for multiplication will disappear in the final set of equations and is replaced by their multiplication:

$$1 \cdot \Pi_1^{-1} = \frac{L_{wl}}{B} = \lambda$$

$$\Pi_1 \cdot \Pi_2^{-1} = \frac{B}{L_{wl}} \cdot \frac{L_{wl}}{T} = \frac{B}{T} = \beta$$

$$\begin{aligned}
\Pi_3 \cdot \Pi_1^{-1} \cdot \Pi_2^{-1} &= \frac{\nabla}{L_{wl}^3} \cdot \frac{L_{wl}}{B} \cdot \frac{L_{wl}}{T} = \frac{\nabla}{L_{wl}BT} = C_b \\
\Pi_4 \cdot \Pi_1^{-1} \cdot \Pi_2^{-1} &= \frac{Af_w}{L_{wl}^2} \cdot \frac{L_{wl}}{B} \cdot \frac{L_{wl}}{T} = \frac{Af_w}{TB} \\
\Pi_5 \cdot \Pi_2^{-1} &= \frac{Al_w}{L_{wl}^2} \cdot \frac{L_{wl}}{T} = \frac{Al_w}{TL} \\
\Pi_6 \cdot \Pi_7^{-1} &= \frac{\rho_w \cdot L_{wl}^3}{m} \cdot \frac{m}{\rho_a \cdot L_{wl}^3} = \frac{\rho_w}{\rho_a} \\
\Pi_{10} \cdot \Pi_1^{-1} &= \frac{Azi_p pos_y}{L_{wl}} \cdot \frac{L_{wl}}{B} = \frac{Azi_p pos_y}{B} \\
\Pi_{11} \cdot \Pi_1^{-1} &= \frac{Azi_s pos_y}{L_{wl}} \cdot \frac{L_{wl}}{B} = \frac{Azi_s pos_y}{B} \\
\Pi_{13} \cdot \Pi_1^{-1} &= \frac{Retr pos_y}{L_{wl}} \cdot \frac{L_{wl}}{B} = \frac{Retr pos_y}{B} \\
\Pi_{16} \cdot \Pi_1^{-1} &= \frac{Bow_f pos_y}{L_{wl}} \cdot \frac{L_{wl}}{B} = \frac{Bow_f pos_y}{B} \\
\Pi_{17} \cdot \Pi_1^{-1} &= \frac{Bow_a pos_y}{L_{wl}} \cdot \frac{L_{wl}}{B} = \frac{Bow_a pos_y}{B}
\end{aligned}$$

Finally the resulting dimensionless  $\Pi$  groups can be formulated as follow:

$$\begin{aligned}
\Pi_{1^*} &= \frac{L_{wl}}{B} = \lambda \\
\Pi_{2^*} &= \frac{B}{T} = \beta \\
\Pi_{3^*} &= \frac{\nabla}{L_{wl}BT} = \frac{m}{\rho_w \cdot L_{wl}BT} = C_b \\
\Pi_{4^*} &= \frac{Af_w}{TB} \\
\Pi_{5^*} &= \frac{Al_w}{TL} \\
\Pi_{6^*} &= \frac{\rho_w}{\rho_a} \\
\Pi_{7^*} &= \frac{Azi_p Pos_x}{L_{wl}} \\
\Pi_{8^*} &= \frac{Azi_s Pos_x}{L_{wl}} \\
\Pi_{9^*} &= \frac{Azi_p Pos_y}{B} \\
\Pi_{10^*} &= \frac{Azi_s Pos_y}{B} \\
\Pi_{11^*} &= \frac{Retr Pos_x}{L_{wl}} \\
\Pi_{12^*} &= \frac{Retr Pos_y}{B} \\
\Pi_{13^*} &= \frac{Bow_f Pos_x}{L_{wl}}
\end{aligned}$$

$$\Pi_{14^*} = \frac{Bow_a \ Pos_x}{L_{wl}}$$

$$\Pi_{15^*} = \frac{Bow_f \ Pos_y}{B}$$

$$\Pi_{16^*} = \frac{Bow_a \ Pos_y}{B}$$

$$\Pi_{17^*} = \frac{Azi_T}{m \cdot g}$$

$$\Pi_{18^*} = \frac{Retr_T}{m \cdot g}$$

$$\Pi_{19^*} = \frac{Bow_T}{m \cdot g}$$

# D

## DPlab



Figure D.1: Input Output overview DPlab

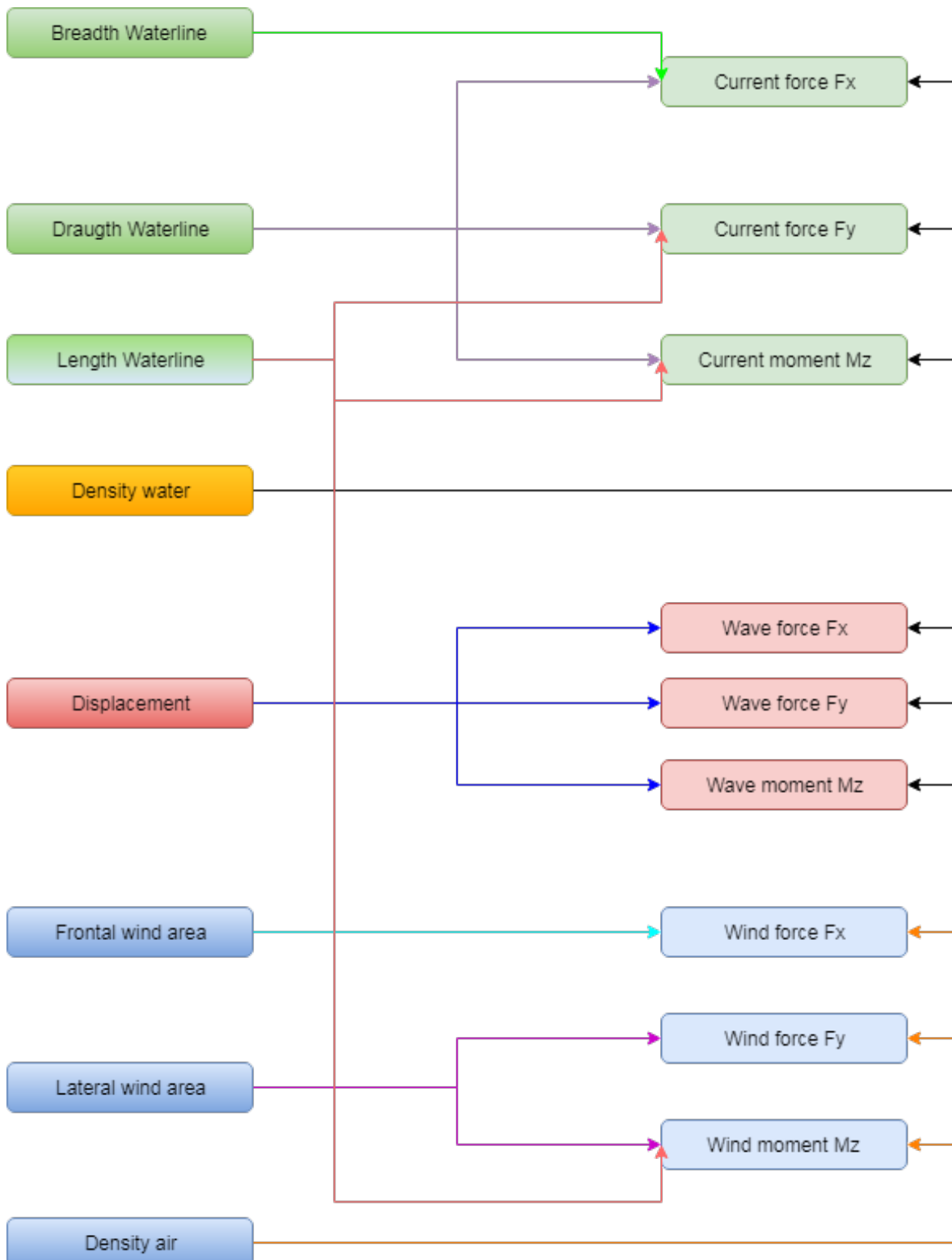


Figure D.2: Input for environmental forces calculation DPlab

## D.1. Sensitivity

Table D.1: Effected forces by parameters

Parameter	Effect on $F_x$	Effect on $F_y$	Effect on $M_z$
Waterline Length		x	x
Waterline Breadth	x		
Draught	x	x	x
Frontal wind area	x		
Longitudinal wind area		x	x
Water density	x	x	x
Air density	x	x	x
X position Azimuthing thrusters			x
Y position Azimuthing thrusters			x
X position Retractable thruster			x
X position Tunnel thrusters			x
Power Azimuthing thruster	x	x	x
Thrust Azimuthing thruster	x	x	x
Power Retractable thruster	x	x	x
Thrust Retractable thruster	x	x	x
Power Tunnel thrusters		x	x
Thrust Tunnel thrusters		x	x
Wind coefficients Cx	x		x
Wind coefficients Cy		x	
Wind coefficients Cn			x
Current coefficients Cx	x		
Current coefficients Cy		x	
Current coefficients Cn			x
Wave coefficients Cx	x		
Wave coefficients Cy		x	
Wave coefficients Cn			x

## D.2. Input uncertainty

In this appendix the input uncertainty for the different parameters used in DPlab are listed.

### D.2.1. Main particulars

Table D.2: Mean and standard deviations for static DP

Parameters	Stage 1		Stage 2		Stage 3	
	Mean	Std	Mean	Std	Mean	Std
Length Waterline	74.65	5.18	91.05	1.18	87.70	0
Breadth Waterline	19.00	0.33	19.50	0.17	20.00	0
Draught	5.25	0.42	4.40	0.20	4.80	0
Displacement	5320	212	5453	275	5956	0
L/B ( $\lambda$ )	3.93	0.28	4.67	0.07	4.39	0
B/T ( $\beta$ )	3.62	0.29	4.43	0.20	4.17	0
Block coefficient ( $C_b$ )	0.71	0.08	0.70	0.05	0.71	0
Frontal wind area	360.00	13.33	407.50	7.50	392.00	0
Lateral wind area	978.00	47.33	1178.65	66.22	1366.00	0
Density water	1024.72	1.99	1024.72	1.99	1024.72	1.985
Density air	1.257	0.037	1.257	0.037	1.257	0.037
Azimuth x position port side	-32.95	1.98	-40.50	0.03	-40.45	0
Azimuth x position starboard side	-32.95	1.98	-40.50	0.03	-40.45	0
Azimuth y position port side	5.00	0.10	5.66	0.05	5.52	0
Azimuth y position starboard side	-5.00	0.10	-5.66	0.05	-5.52	0
Retractable x position			33.90	1.17	30.40	0
Retractable y position			0	0	0	0
Fore tunnel x position	30.60	1.83	35.25	0.62	37.10	0
Fore tunnel y position	0	0	0	0	0	0
Aft tunnel x position	28.10	1.70	32.05	0.55	33.70	0
Aft tunnel y position	0	0	0	0	0	0
Azimuth power	723.00	32.00	1625.00	175.00	1600.00	0
Azimuth thrust	106.18	1.56	286.20	19.07	293.70	7.34
Azimuth specific thrust	16.50	0.00	18.41	0.94	18.71	0
Retractable power			755.00	35.00	860.00	0
Retractable thrust			123.40	5.20	136.10	3.40
Retractable specific thrust			16.23	0.51	16.13	0
Bowthruster power	1086.00	55.67	900.00	66.67	860.00	0
Bowthruster thrust	131.04	6.72	113.20	5.63	116.00	2.90
Bowthruster specific thrust	12.30	0.00	13.12	0.35	13.75	0

### D.2.2. Wind coefficients

Table D.3: Mean and standard deviations for wind coefficients

Wind coefficients	Cx		Cy		Cn	
	Mean	Std	Mean	Std	Mean	Std
0 degrees	0.476	0.057	0.002	0.001	0.002	0.001
10 degrees	0.556	0.085	0.150	0.017	-0.034	0.002
20 degrees	0.545	0.110	0.345	0.021	-0.065	0.005
30 degrees	0.436	0.129	0.558	0.021	-0.091	0.008
40 degrees	0.204	0.122	0.779	0.031	-0.114	0.010
50 degrees	-0.055	0.071	0.885	0.023	-0.119	0.008
60 degrees	-0.094	0.102	0.882	0.049	-0.092	0.006
70 degrees	-0.131	0.111	0.869	0.047	-0.061	0.005
80 degrees	-0.086	0.059	0.829	0.041	-0.032	0.001
90 degrees	-0.012	0.013	0.813	0.043	0.000	0.001
100 degrees	0.025	0.035	0.833	0.041	0.031	0.003
110 degrees	0.035	0.067	0.866	0.045	0.060	0.006
120 degrees	0.048	0.084	0.903	0.059	0.098	0.010
130 degrees	0.002	0.039	0.906	0.036	0.114	0.005
140 degrees	-0.164	0.048	0.813	0.009	0.113	0.006
150 degrees	-0.364	0.042	0.581	0.012	0.088	0.005
160 degrees	-0.497	0.068	0.364	0.017	0.063	0.003
170 degrees	-0.532	0.082	0.163	0.013	0.035	0.002
180 degrees	-0.496	0.052	0.002	0.003	-0.001	0.000
190 degrees	-0.532	0.082	-0.163	0.013	-0.035	0.002
200 degrees	-0.497	0.068	-0.364	0.017	-0.063	0.003
210 degrees	-0.364	0.042	-0.581	0.012	-0.088	0.005
220 degrees	-0.164	0.048	-0.813	0.009	-0.113	0.006
230 degrees	0.002	0.039	-0.906	0.036	-0.114	0.005
240 degrees	0.048	0.084	-0.903	0.059	-0.098	0.010
250 degrees	0.035	0.067	-0.866	0.045	-0.060	0.006
260 degrees	0.025	0.035	-0.833	0.041	-0.031	0.003
270 degrees	-0.012	0.013	-0.813	0.043	0.000	0.001
280 degrees	-0.086	0.059	-0.829	0.041	0.032	0.001
290 degrees	-0.131	0.111	-0.869	0.047	0.061	0.005
300 degrees	-0.094	0.102	-0.882	0.049	0.092	0.006
310 degrees	-0.055	0.071	-0.885	0.023	0.119	0.008
320 degrees	0.204	0.122	-0.779	0.031	0.114	0.010
330 degrees	0.436	0.129	-0.558	0.021	0.091	0.008
340 degrees	0.545	0.110	-0.345	0.021	0.065	0.005
350 degrees	0.556	0.085	-0.150	0.017	0.034	0.002
360 degrees	0.476	0.057	-0.002	0.001	-0.002	0.001

### D.2.3. Current coefficients

Table D.4: Mean and standard deviations for current coefficients

Current coefficients	Cx		Cy		Cn	
	Mean	Std	Mean	Std	Mean	Std
0 degrees	0.143	0.047	-0.001	0.002	-0.003	0.002
10 degrees	0.135	0.045	0.111	0.005	-0.021	0.003
20 degrees	0.126	0.043	0.224	0.008	-0.040	0.007
30 degrees	0.117	0.041	0.338	0.011	-0.058	0.011
40 degrees	0.048	0.039	0.441	0.020	-0.071	0.012
50 degrees	-0.027	0.041	0.559	0.021	-0.082	0.014
60 degrees	-0.083	0.052	0.642	0.039	-0.091	0.016
70 degrees	-0.042	0.029	0.674	0.032	-0.069	0.014
80 degrees	-0.044	0.028	0.706	0.024	-0.045	0.012
90 degrees	-0.029	0.050	0.725	0.023	-0.021	0.011
100 degrees	-0.041	0.051	0.673	0.022	0.001	0.005
110 degrees	-0.056	0.052	0.608	0.027	0.022	0.003
120 degrees	-0.073	0.054	0.542	0.033	0.046	0.007
130 degrees	-0.077	0.064	0.457	0.028	0.055	0.006
140 degrees	-0.096	0.067	0.366	0.022	0.054	0.006
150 degrees	-0.129	0.062	0.269	0.014	0.044	0.006
160 degrees	-0.143	0.050	0.175	0.008	0.031	0.004
170 degrees	-0.138	0.048	0.085	0.003	0.016	0.002
180 degrees	-0.133	0.045	0.001	0.002	0.004	0.002
190 degrees	-0.138	0.048	-0.085	0.003	-0.016	0.002
200 degrees	-0.143	0.050	-0.175	0.008	-0.031	0.004
210 degrees	-0.129	0.062	-0.269	0.014	-0.044	0.006
220 degrees	-0.096	0.067	-0.366	0.022	-0.054	0.006
230 degrees	-0.077	0.064	-0.457	0.028	-0.055	0.006
240 degrees	-0.073	0.054	-0.542	0.033	-0.046	0.007
250 degrees	-0.056	0.052	-0.608	0.027	-0.022	0.003
260 degrees	-0.041	0.051	-0.672	0.022	-0.001	0.005
270 degrees	-0.029	0.050	-0.724	0.023	0.021	0.011
280 degrees	-0.044	0.028	-0.706	0.024	0.045	0.012
290 degrees	-0.042	0.029	-0.674	0.032	0.069	0.014
300 degrees	-0.083	0.052	-0.642	0.039	0.091	0.016
310 degrees	-0.027	0.041	-0.559	0.021	0.082	0.014
320 degrees	0.048	0.039	-0.441	0.020	0.071	0.012
330 degrees	0.117	0.041	-0.338	0.011	0.058	0.011
340 degrees	0.126	0.043	-0.226	0.007	0.037	0.008
350 degrees	0.135	0.045	-0.114	0.003	0.017	0.005
360 degrees	0.143	0.047	-0.001	0.002	-0.003	0.002

### D.2.4. Water density

The density of water is mainly dependent on three things which are pressure, temperature and the salinity of the water. Since only atmospheric pressures are present at sea level this factor is neglected. From <http://www.ospo.noaa.gov/Products/ocean/sst/contour/> it is seen that the temperature of the sea surface varies approximately from -2°C to 30°C. According to <https://en.wikipedia.org/wiki/Seawater> the salinity varies between 31 [ $\frac{g}{kg}$ ] and 38 [ $\frac{g}{kg}$ ].

It is now possible to calculate the density of the seawater for the four different extremes using the method of <http://web.mit.edu/seawater/>. The result of these are listed in table D.5. The lowest and highest values are taken to be the boundaries of the certainty intervals

Table D.5: Density of water

<b>Temperature / Salinity</b>	$31 \frac{\text{g}}{\text{kg}}$	$38 \frac{\text{g}}{\text{kg}}$
-2°C	1024.96 [kg/m <sup>3</sup> ]	1030.67 [kg/m <sup>3</sup> ]
30°C	1018.76 [kg/m <sup>3</sup> ]	1024.00 [kg/m <sup>3</sup> ]

**D.2.5. Air density**

The density of air is mainly dependent on the temperature.

Table D.6: Density of water

<b>Air temperature</b>	<b>Air density</b>
-15°C	1.367 [kg/m <sup>3</sup> ]
35°C	1.146 [kg/m <sup>3</sup> ]

**D.3. Wind wave relation**

Table D.7: Wind wave relation

<b>Wind speed [m/s]</b>	<b>Wave height [m]</b>	<b>Zero crossing period [s]</b>
0	0	3
1.40	0.66	3
2.19	0.79	3
3.30	1.00	3
4.95	1.35	4.1
6.21	1.70	5.1
7.48	1.90	5.7
8.74	2.30	6.9
10.01	2.60	7.8
11.39	3.00	9
13.11	3.50	9
15.53	4.20	9
17.60	4.90	9
19.32	5.30	9
19.90	5.60	9
20.59	5.80	9
21.51	6.10	9
51.44	15.86	9
102.87	31.72	9



# E

## aNySIM

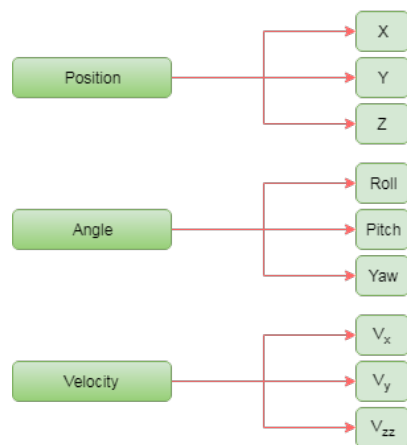
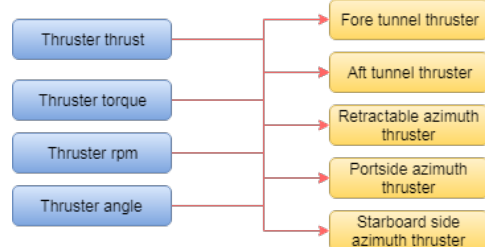
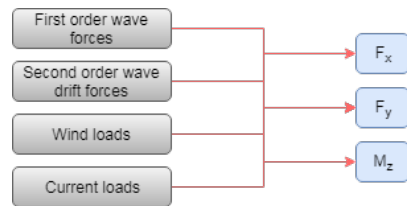


Figure E.1: Output overview aNySIM

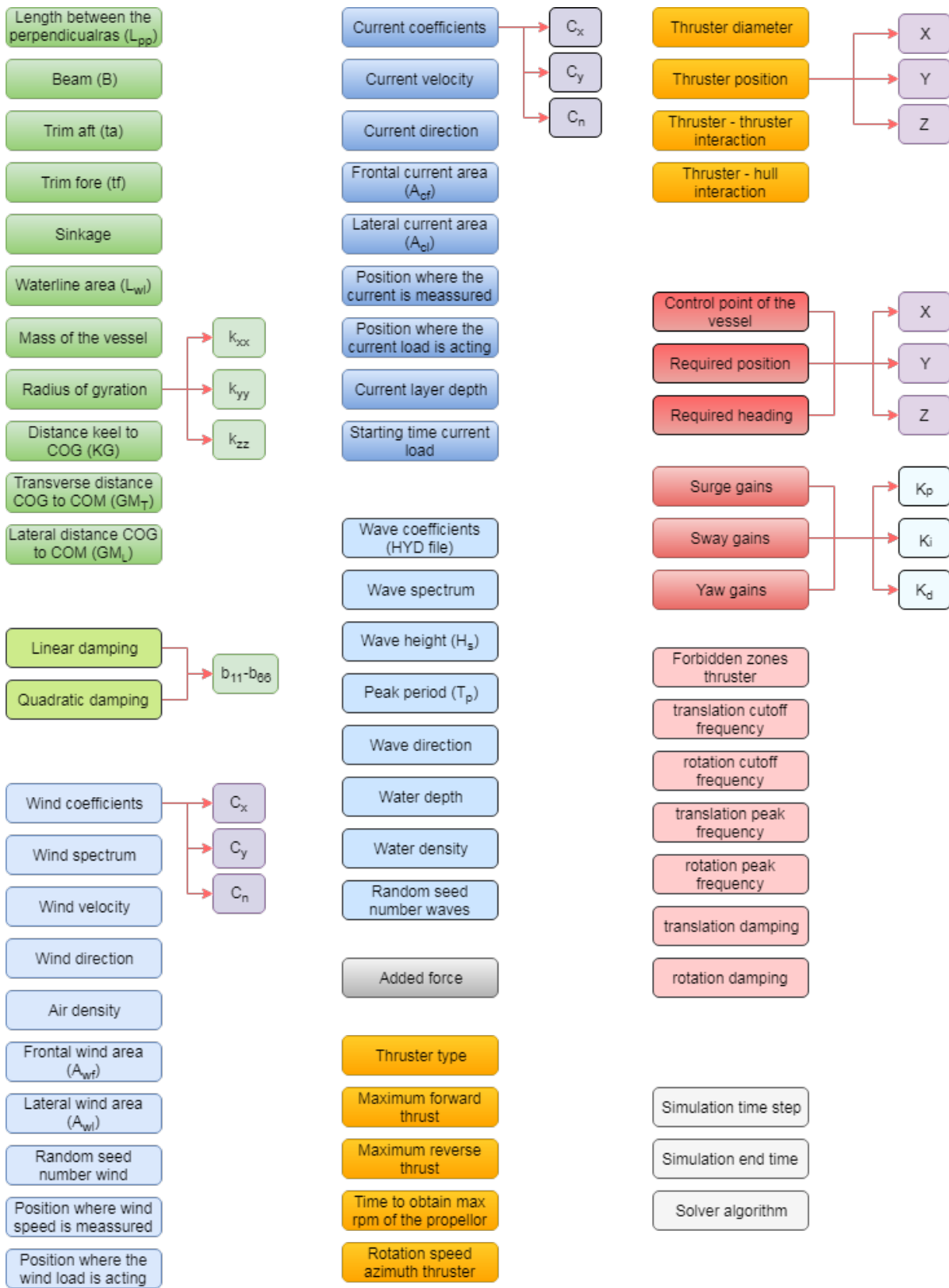


Figure E.2: Input overview aNySIM

## E.1. Parameter variation

During the dynamic simulations the parameters are varied within a certain range and are listed in table E.1. The wind and current coefficients are also varied and are varied with plus and minus three times the standard deviation from their mean as seen in tables D.3 and D.4.

Table E.1: Varied parameters and their boundary values for sobol space

Parameter	Lower boundary	Upper Boundary	Unit
Water density	1018.76	1030.67	[kg/m <sup>3</sup> ]
Air density	1.146	1.1367	[kg/m <sup>3</sup> ]
Surge gain Kp	26400	39600	[N/m]
Surge gain Kd	550020	679800	[Ns/m]
Sway gain Kp	33600	50400	[N/m]
Sway gain Kd	725350	896500	[Ns/m]
Yaw gain Kp	14160000	21240000	[Nm/rad]
Yaw gain Kd	319510000	394900000	[Nms/rad]

## E.2. PID gains

The Proportional Integral Derivative (PID) controller is used in the DP system to make sure the vessel stays in its desired position. It can be considered as a control loop feedback system which is used throughout multiple industries. The control loop is normally expressed using a transfer function which is shown in equation E.1.

$$G(s) = K_P + K_I \cdot \frac{1}{s} + K_D \cdot s \quad (\text{E.1})$$

When using a PID controller for the purpose of Dynamic Positioning the position and heading are the variables of interest and depend on time. The transfer function can therefore be rewritten [58] to form shown in equation E.2.

$$u(t) = K_P \cdot e(t) + K_I \int_0^t e(\tau) d\tau + K_D \cdot \frac{d}{dt} y(t) \quad (\text{E.2})$$

where:

- $K_p$  = P gain of the controller [N/m] or [Nm/rad]
- $K_I$  = I gain of the controller [N/ms] or [Nm/rads]
- $K_D$  = D gain of the controller [Ns/m] or [Nms/rad]
- $e$  = Error as function of time [m] or [rad]
- $t$  = discrete time signal [s]
- $\tau$  = continuous time signal [s]

The gains have to be set according to the vessels properties. The following equations provide a good first estimate for calculating the PID gains after which they can be tuned further.

$$P = \frac{\sum_1^N T_{max}}{(50 - 70\%) \cdot R_{max}} \quad (\text{E.3})$$

where:

- $P$  = P gain of the controller [N/m] or [Nm/rad]
- $N$  = Amount of thrusters [-]
- $T_{max}$  = Maximum thrust [kN] or [kNm]
- $R_{max}$  = Maximum desired offset [m]

$$D = (50 - 70\%) \cdot 2 \cdot \sqrt{(M + a) \cdot P} \quad (\text{E.4})$$

where:

- $D$  = D gain of the controller [ $Ns/m$ ] or [ $Nms/rad$ ]
- $M$  = Mass or mass moment of inertia [ $t$ ] or [ $tm^2$ ]
- $a$  = Added mass or added mass moment of inertia [ $t$ ] or [ $tm^2$ ]
- $P$  = P gain of the controller [ $N/m$ ] or [ $Nm/rad$ ]

The I gain rule of thumb calculation method is as follow:

$$\frac{P}{I} \approx \text{between 30 and 60} \quad (\text{E.5})$$

The individual contributions of each gain to the system as a whole are listed below [58].

Table E.2: Effect on parameters when tuning P gain

Parameter	Reaction to P-gain increase
rise time	decrease
overshoot	increase
settling time	small increase
steady state error	decrease
stability	degrade

Table E.3: Effect on parameters when tuning I gain

Parameter	Reaction to I-gain increase
rise time	small decrease
overshoot	increase
settling time	increase
steady state error	large decrease
stability	degrade

Table E.4: Effect on parameters when tuning D gain

Parameter	Reaction to D-gain increase
rise time	small decrease
overshoot	decrease
settling time	decrease
steady state error	minor change
stability	improve

## E.3. Environmental angle converter

Table E.5: Converting angles

Environmental angles [°]		
aNySIM axis "going to"	aNySIM axis "coming from"	DPlab axis "coming from"
0	180	0
10	190	10
20	200	20
30	210	30
40	220	40
50	230	50
60	240	60
70	250	70
80	260	80
90	270	90
100	280	100
110	290	110
120	300	120
130	310	130
140	320	140
150	330	150
160	340	160
170	350	170
180	360	180
190	10	190
200	20	200
210	30	210
220	40	220
230	50	230
240	60	240
250	70	250
260	80	260
270	90	270
280	100	280
290	110	290
300	120	300
310	130	310
320	140	320
330	150	330
340	160	340
350	170	350
360	180	360

## E.4. aNySIM info sheet

More info on the time domain simulation program aNySIM developed by MARIN can be found on the following pages.

### Time Domain Analysis of Multi Body Dynamics for Offshore Operations

## aNySIM

#### Multi-body time domain simulation tool

MARIN has been developing, using and selling hydrodynamic simulation software for many years. Specialised tools were developed for specific areas: coupled mooring analysis, Dynamic Positioning, multiple-body lifting operations, riser dynamics, offloading operations, etc. Developments in the offshore industry in recent years showed the need for a more integrated and flexible tool. Therefore, MARIN decided to develop the new modular 'aNySIM' code. It brings together the capabilities of the different software packages and has become MARIN's main in-house hydrodynamic toolbox. Various modules can be coupled to the central N-body time domain simulation module. As an example, this makes possible studying a DP heading controlled moored FPSO with a shuttle tanker behind it, including all the hydrodynamic and mechanical interactions.

In 2006 MARIN started with the development of the new time domain program aNySIM. aNySIM can simulate the coupled motion behaviour of multiple floating bodies including effects such as mooring systems and hydrodynamic interactions. The program integrates the equation of motion taking into account the own inertia, added inertia, wave loads, damping loads and hydrostatic restoring forces:

$$\sum_{j=1}^{6N} (M_{kj} + m_{kj}) \ddot{x}_j + \int_{-\infty}^t R_{kj}(t-\tau) \dot{x}(\tau) d\tau + C_{kj}x_j = F_k(t)$$

where:

- $x_j$  = motion in j-th mode
- $F_k(t)$  = arbitrarily in time varying external force in the k-th mode of motion
- $M$  = inertia matrix
- $m$  = added inertia matrix (frequency independent)
- $R$  = matrix of retardation functions
- $C$  = matrix of hydrostatic restoring forces



The inertia matrix consists of the mass of the ship and the distribution of the masses with respect to the centre of gravity (radii of inertia).

The right-hand side forcing function  $F$  includes the following forces:

- Wind forces.
- Current forces.
- Wave forces (first order).
- Mean wave drift forces.
- Slowly varying wave drift forces.
- Viscous damping forces.
- Restoring forces of mooring system.
- Restoring forces of lifting arrangement.
- Thruster forces.
- Rudder forces.

#### Computational approach

The mathematical model is based on a time-step solution of the system of coupled differential equations of motion in which the fluid reaction forces are described with convolution integrals according to the Cummins' formulation. The program uses linear diffraction data, wave forces, added mass and damping. In this way arbitrary hull forms can be accounted for.

Frequency dependent added mass and damping coefficients are transformed into inertia coefficients, retardation functions and response functions, such as described in the formula on the left. The instantaneous first and second order wave forces can be taken into account. These are the wave forces for the actual position of the vessel.



## Modular approach

aNySIM was developed by implementing the functionalities step by step making sure that every step is validated and benchmarked against model tests and previous time domain software. At present the following modules are available in aNySIM:

- Time domain integration of equation of motion.
- Wave forces (1<sup>st</sup> and 2<sup>nd</sup> order).
- Current forces.
- Wind forces.
- Fenders.
- Lines.
- Anchor lines (quasi static and dynamic).
- Thrusters and rudders.
- Kalman filter.
- DP controllers.

## User defined module

aNySIM offers an interface through which external subroutines can be called. In this way the user can extend the functionality of aNySIM by developing additional modules in FORTRAN90. The interface is such that data from the other modules is available for the user to compute additional signals. For example the current loads on the truss of a spar can be computed by requesting the current velocities at various water depths along the truss and then multiplying them by the Cd values.

## Input

Typical input parameters that are needed to run a simulation are:

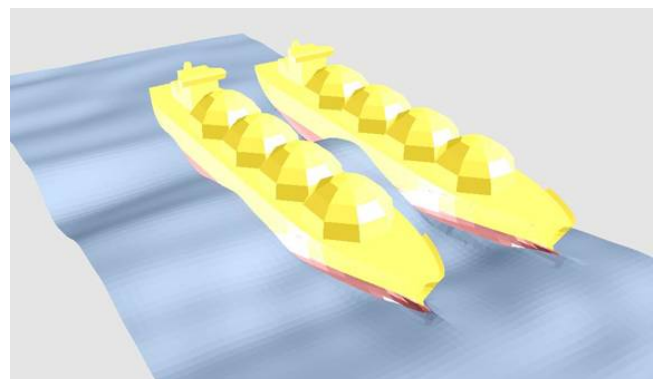
- Geometry, inertia and stability of floating bodies.
- Loading conditions and draughts.
- Water depth and diffraction data.
- Wind, wave and current conditions.
- Mooring arrangement.
- Propulsion arrangement.

## Output

The standard output option consists of time traces of the motions in the centers of gravity, crane tip motions, mooring loads, fender forces,

relative motions etc. Additional output records may be defined by the user as functions of all available state variables in the user interface algorithm. This is a module where user defined forces can be programmed.

aNySIM concludes with a concise statistical analysis yielding extreme and mean values and standard deviations of all selected output signals. aNySIM output (including the diffracted wave field) can be visualized using the in-house visualisation tool Neptune as shown below.



## Batch runs

The aNySIM program is equipped with a batch functionality that allows running large batches on MARIN's computer network. With this approach it becomes feasible to perform workability analyses for long term environmental data in limited simulation time. (Up to 10.000 runs is feasible in a few days)

## Project based version for clients: aNySIM-pro

A project based version of aNySIM is now also available for clients. Further information about this software can be found on the aNySIM-pro leaflet. A demo version of the program can be obtained through the contact details below.

For more information please contact the Maritime Simulation & Software Group;

T +31 317 493 237

E msg@marin.nl



# F

## Model validation

### F.1. Residuals

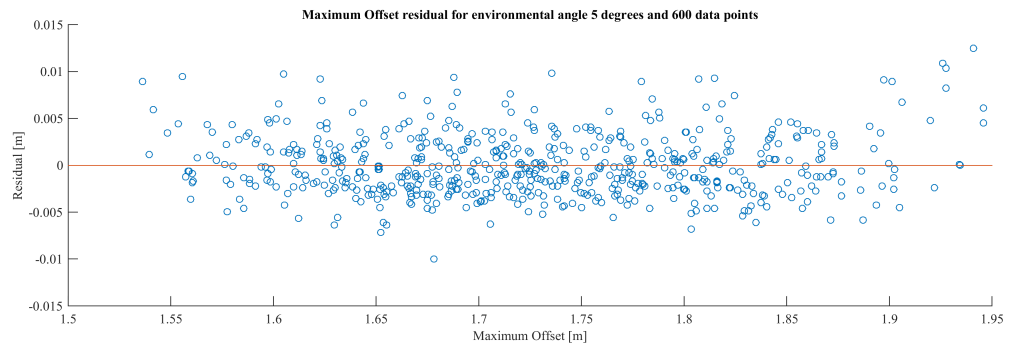


Figure F.1: Maximum Offset Residual for 5 degrees of environmental angle with 600 data points

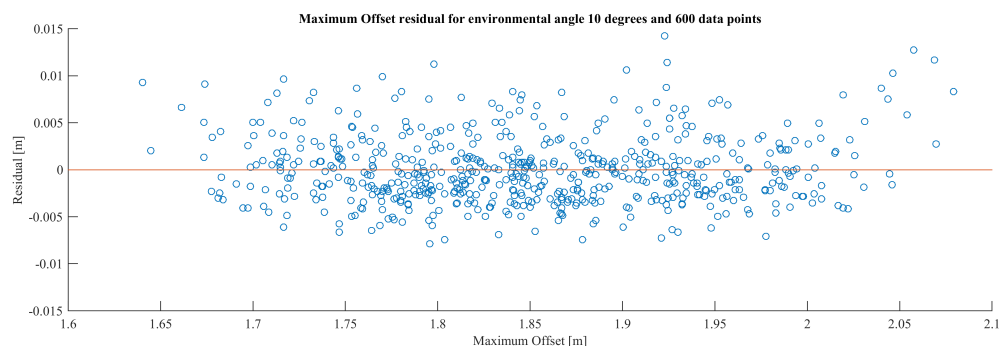


Figure F.2: Maximum Offset Residual for 10 degrees of environmental angle with 600 data points

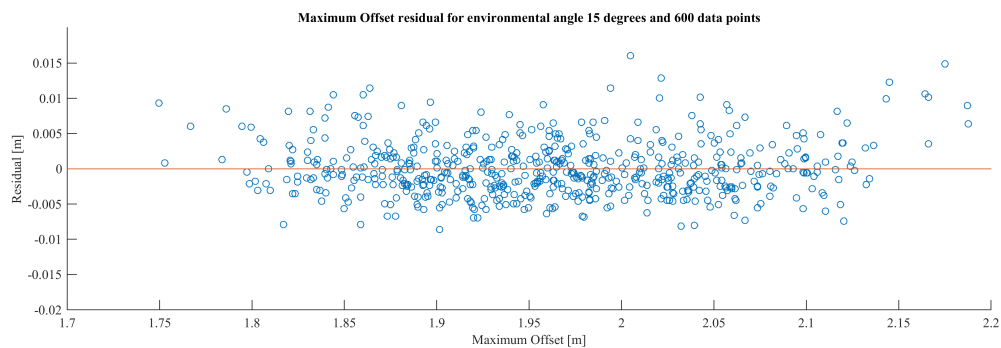


Figure F.3: Maximum Offset Residual for 15 degrees of environmental angle with 600 data points

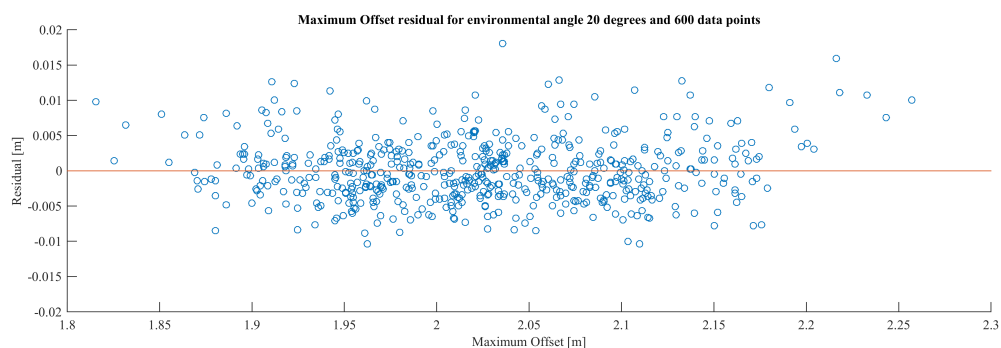


Figure F.4: Maximum Offset Residual for 20 degrees of environmental angle with 600 data points

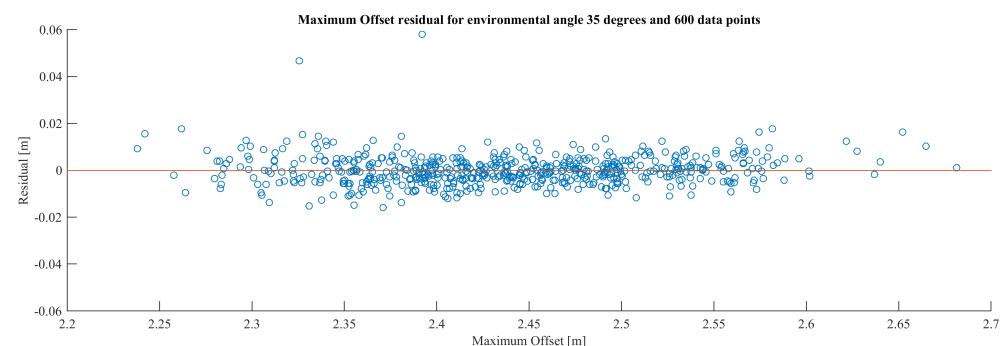


Figure F.5: Maximum Offset Residual for 35 degrees of environmental angle with 600 data points

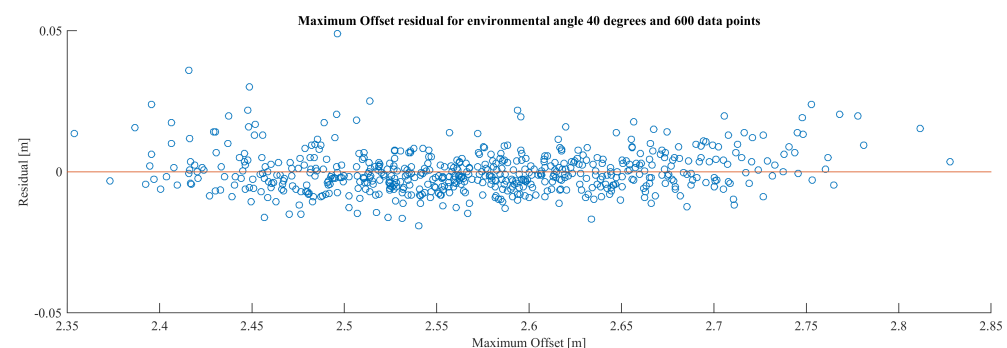


Figure F.6: Maximum Offset Residual for 40 degrees of environmental angle with 600 data points

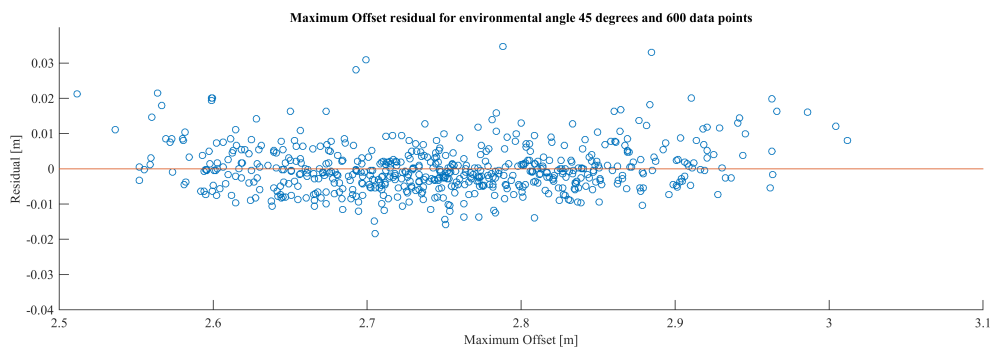


Figure F.7: Maximum Offset Residual for 45 degrees of environmental angle with 600 data points

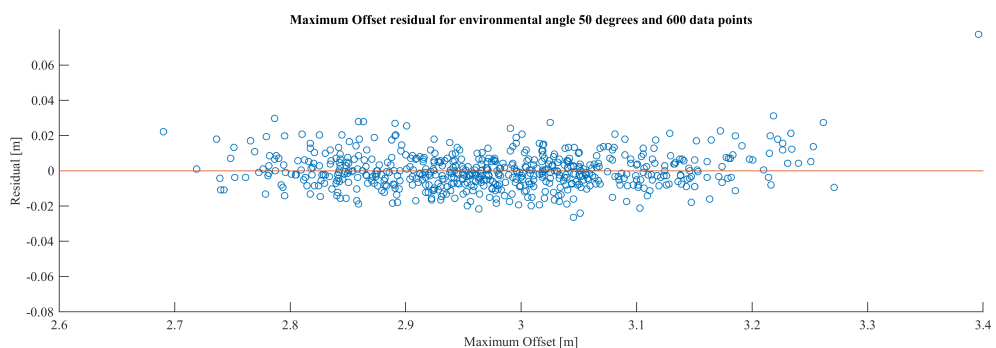


Figure F.8: Maximum Offset Residual for 50 degrees of environmental angle with 600 data points

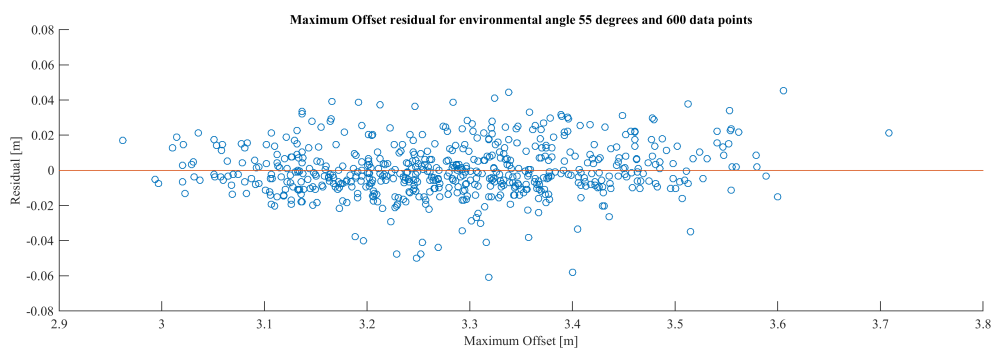


Figure F.9: Maximum Offset Residual for 55 degrees of environmental angle with 600 data points

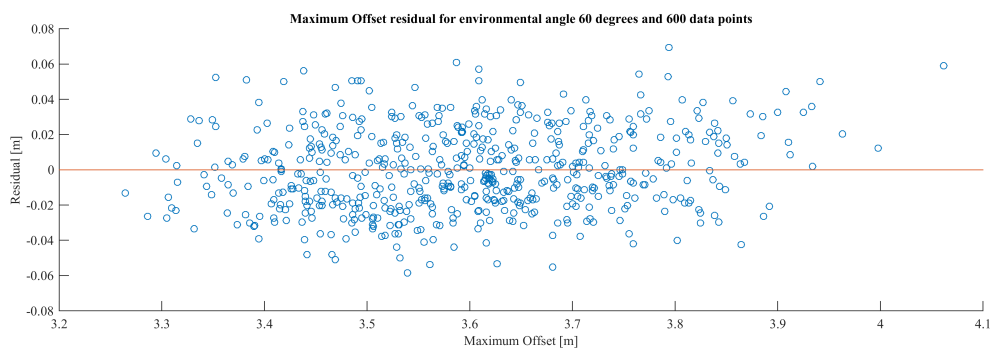


Figure F.10: Maximum Offset Residual for 60 degrees of environmental angle with 600 data points

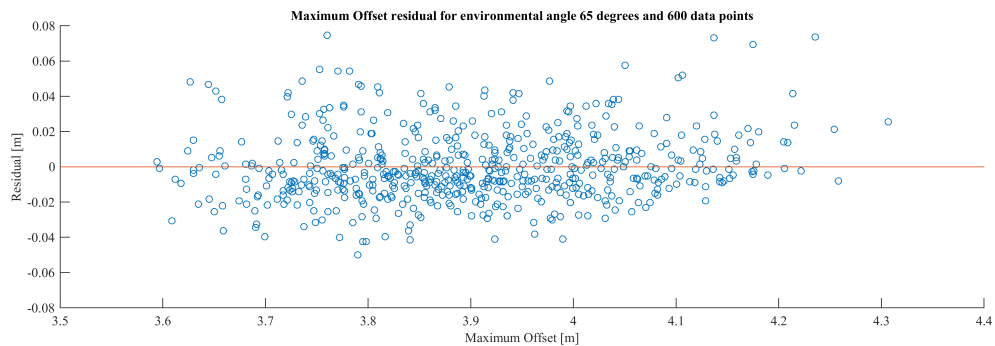


Figure F.11: Maximum Offset Residual for 65 degrees of environmental angle with 600 data points

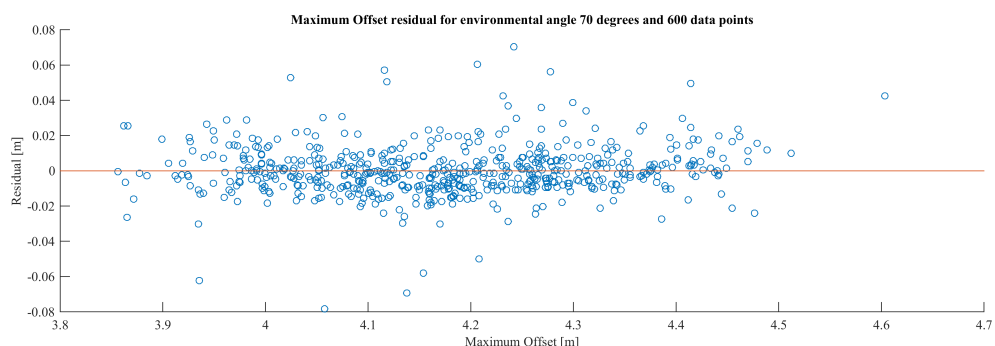


Figure F.12: Maximum Offset Residual for 70 degrees of environmental angle with 600 data points

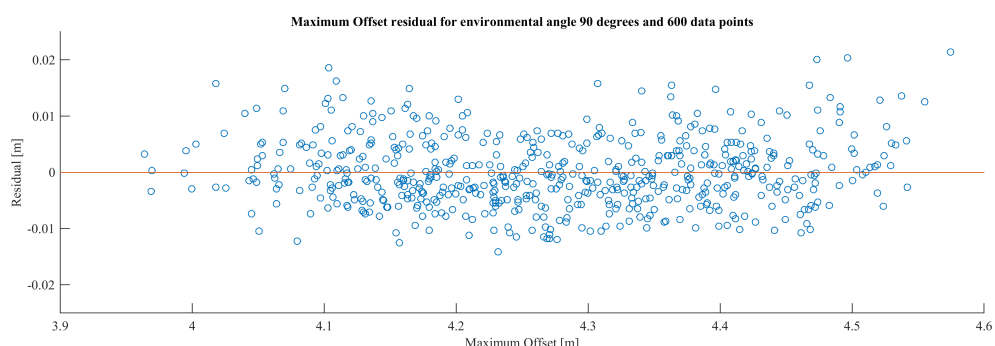


Figure F.13: Maximum Offset Residual for 90 degrees of environmental angle with 600 data points

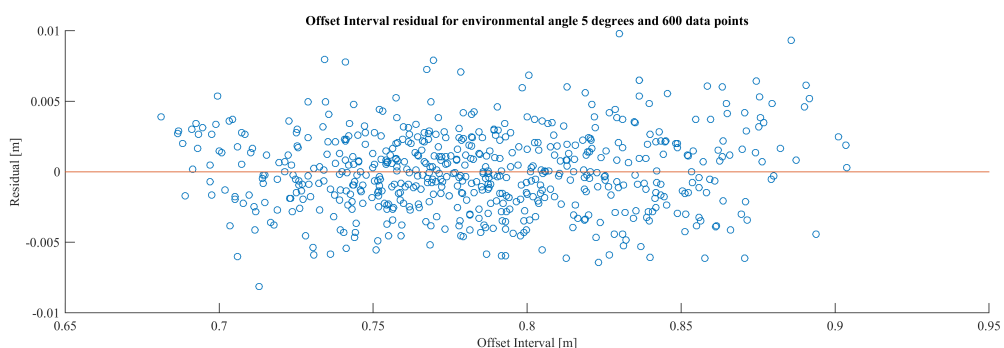


Figure F.14: Offset Interval Residual for 5 degrees of environmental angle with 600 data points

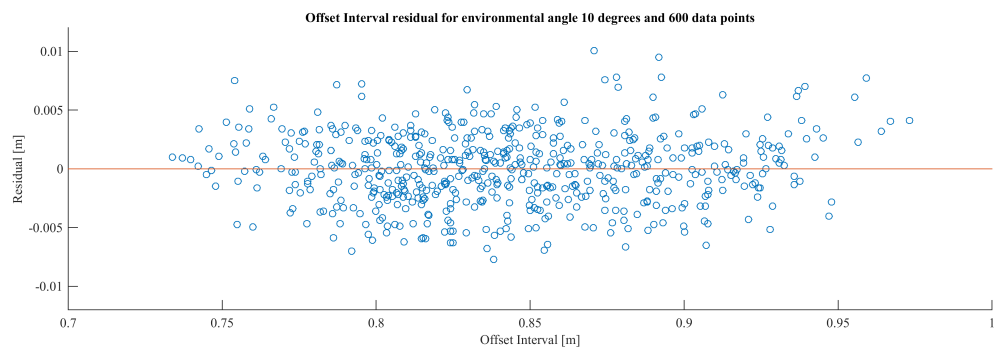


Figure F.15: Offset Interval Residual for 10 degrees of environmental angle with 600 data points

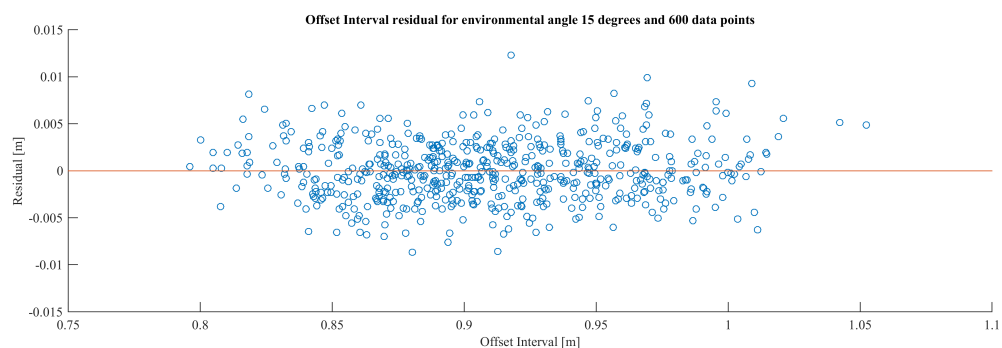


Figure F.16: Offset Interval Residual for 15 degrees of environmental angle with 600 data points

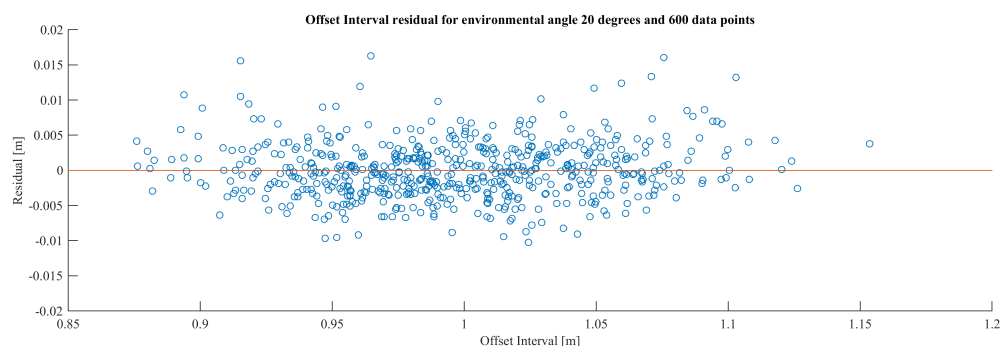


Figure F.17: Offset Interval Residual for 20 degrees of environmental angle with 600 data points

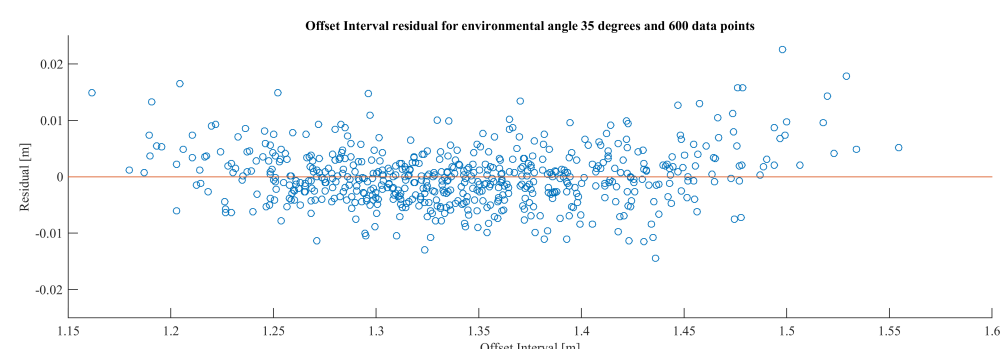


Figure F.18: Offset Interval Residual for 35 degrees of environmental angle with 600 data points

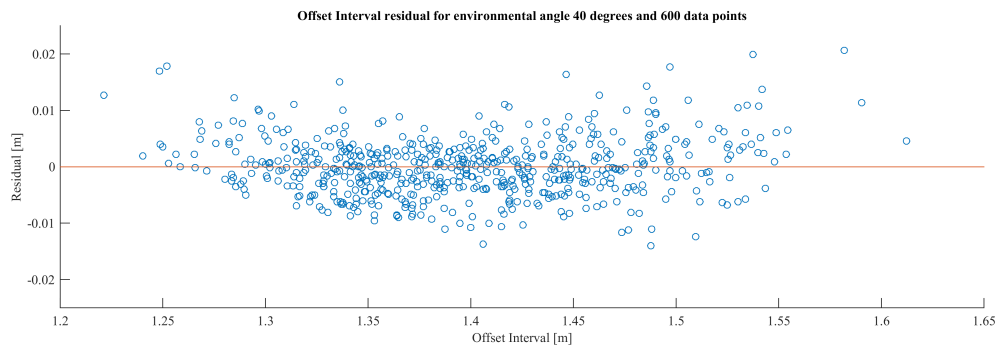


Figure F.19: Offset Interval Residual for 40 degrees of environmental angle with 600 data points

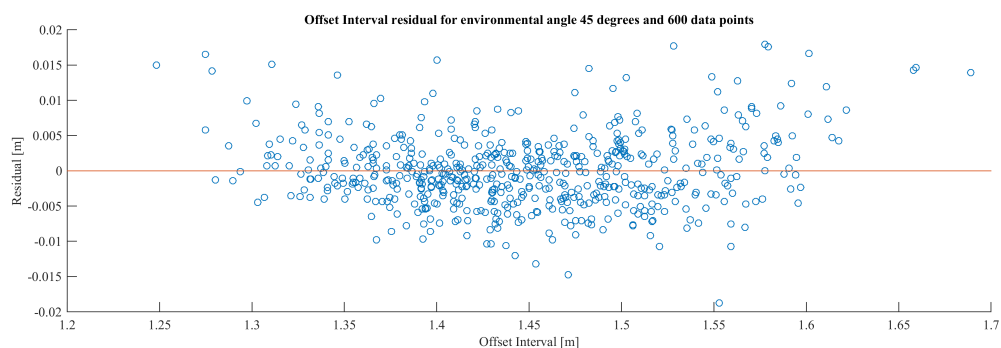


Figure F.20: Offset Interval Residual for 45 degrees of environmental angle with 600 data points

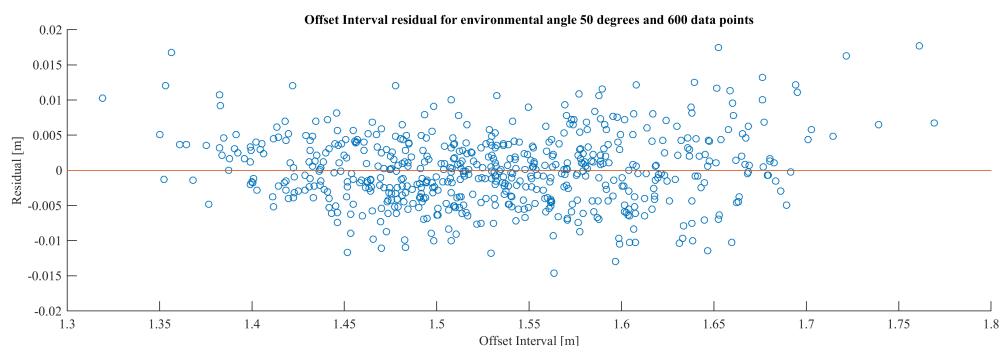


Figure F.21: Offset Interval Residual for 50 degrees of environmental angle with 600 data points

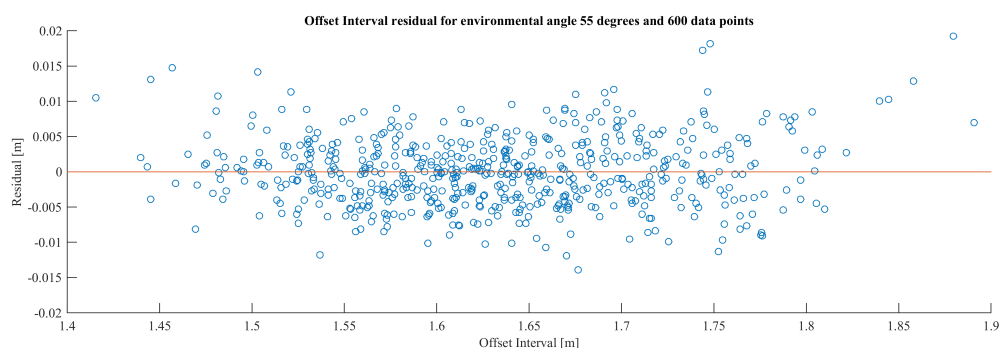


Figure F.22: Offset Interval Residual for 55 degrees of environmental angle with 600 data points

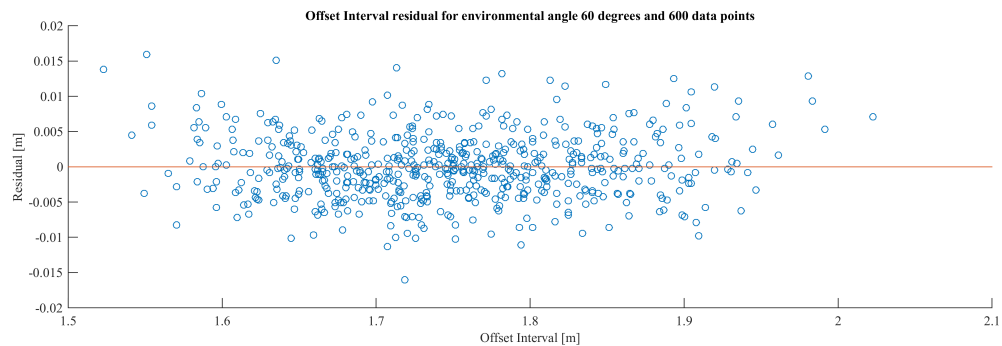


Figure F.23: Offset Interval Residual for 60 degrees of environmental angle with 600 data points

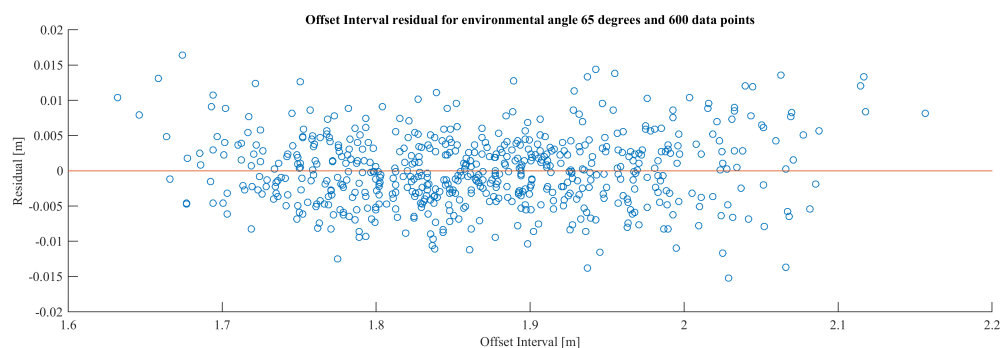


Figure F.24: Offset Interval Residual for 65 degrees of environmental angle with 600 data points

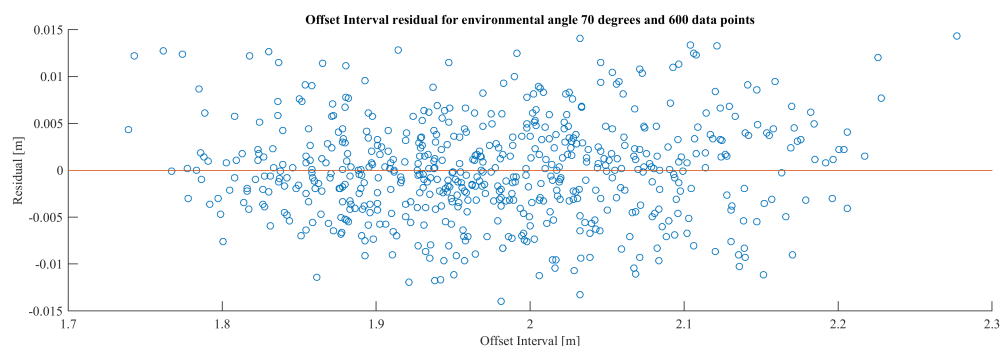


Figure F.25: Offset Interval Residual for 70 degrees of environmental angle with 600 data points

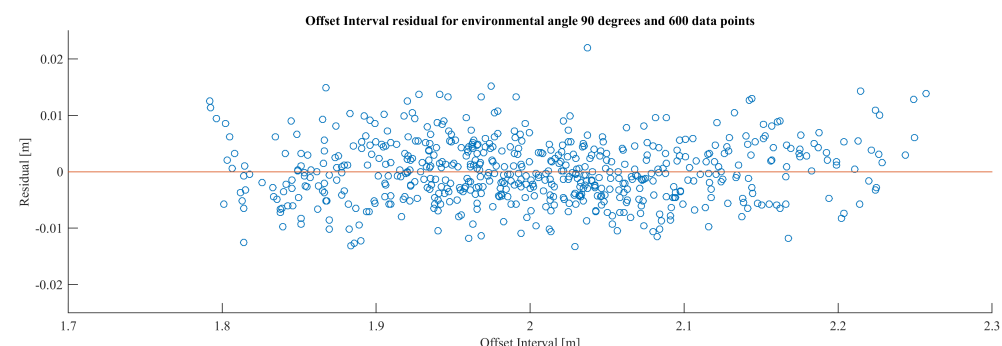


Figure F.26: Offset Interval Residual for 90 degrees of environmental angle with 600 data points

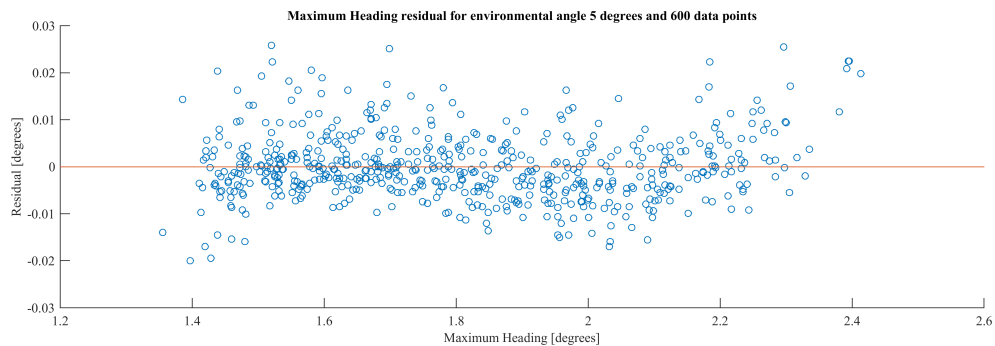


Figure F.27: Maximum Heading Residual for 5 degrees of environmental angle with 600 data points

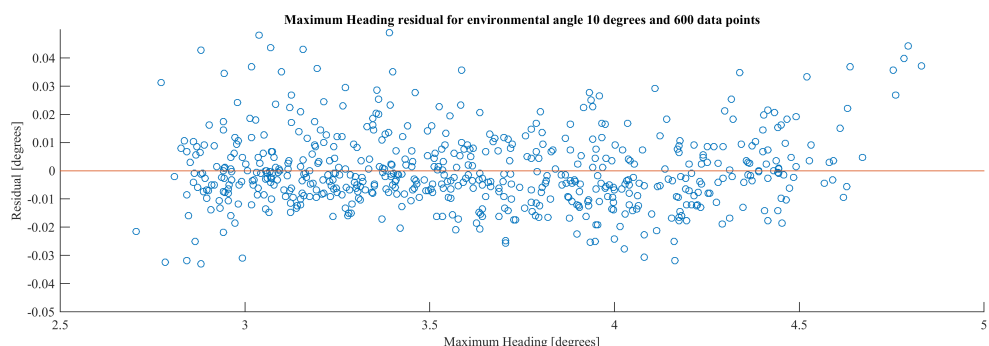


Figure F.28: Maximum Heading Residual for 10 degrees of environmental angle with 600 data points

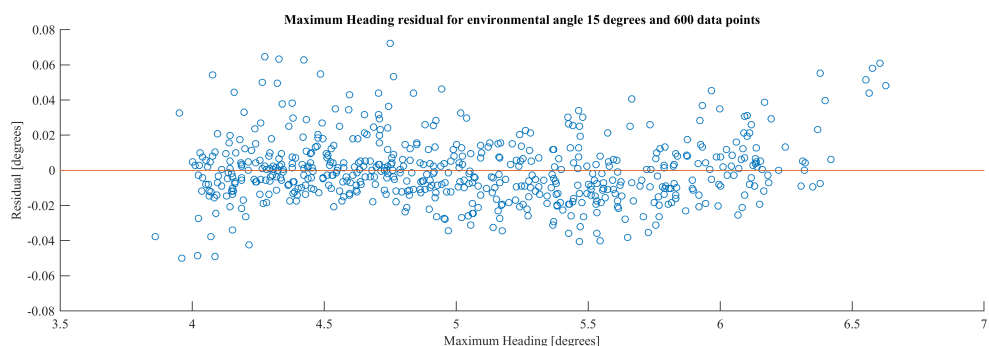


Figure F.29: Maximum Heading Residual for 15 degrees of environmental angle with 600 data points

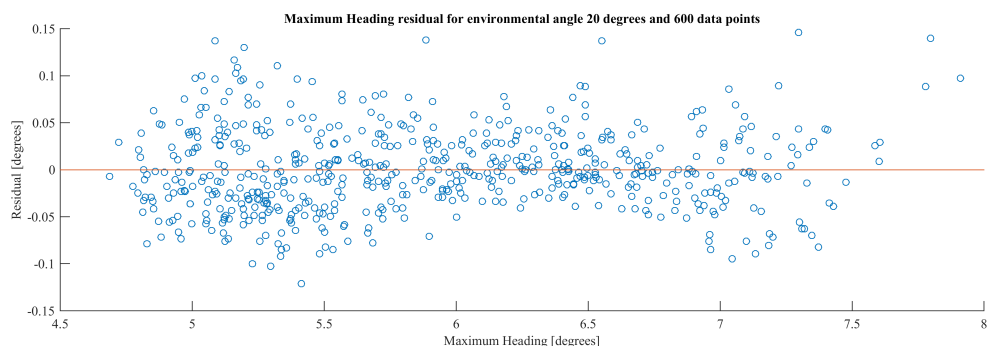


Figure F.30: Maximum Heading Residual for 20 degrees of environmental angle with 600 data points

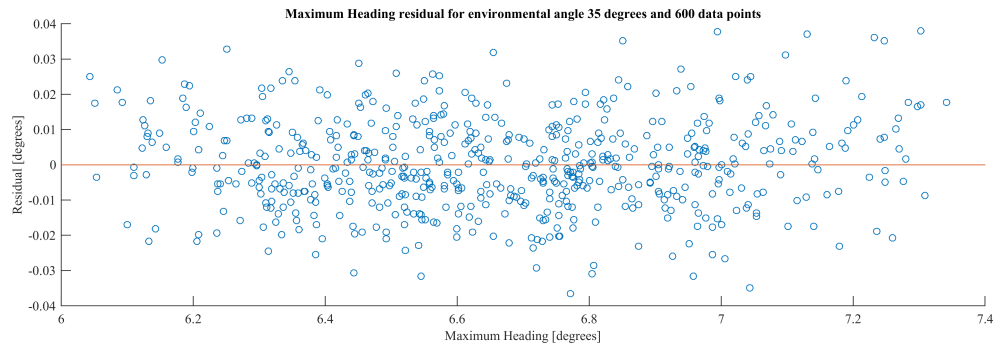


Figure F.31: Maximum Heading Residual for 35 degrees of environmental angle with 600 data points

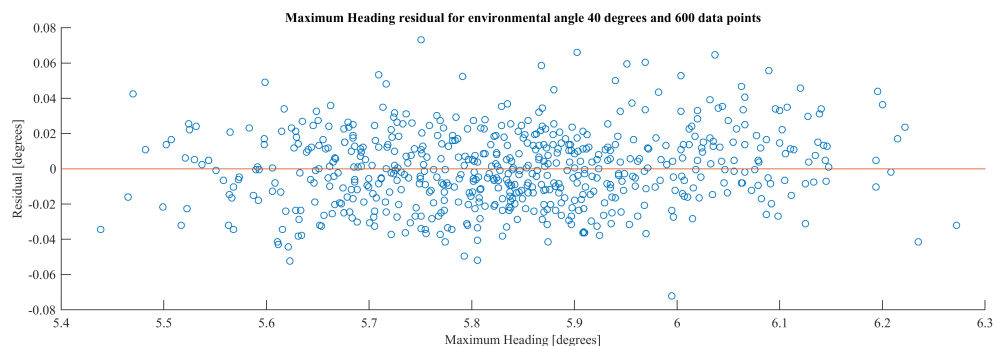


Figure F.32: Maximum Heading Residual for 40 degrees of environmental angle with 600 data points

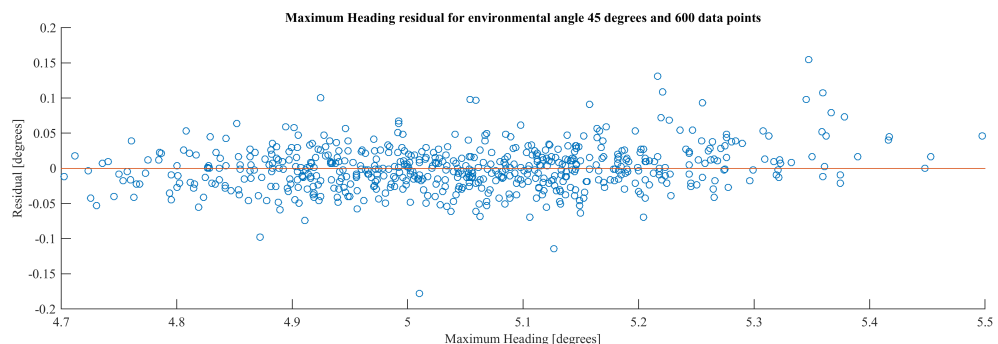


Figure F.33: Maximum Heading Residual for 45 degrees of environmental angle with 600 data points

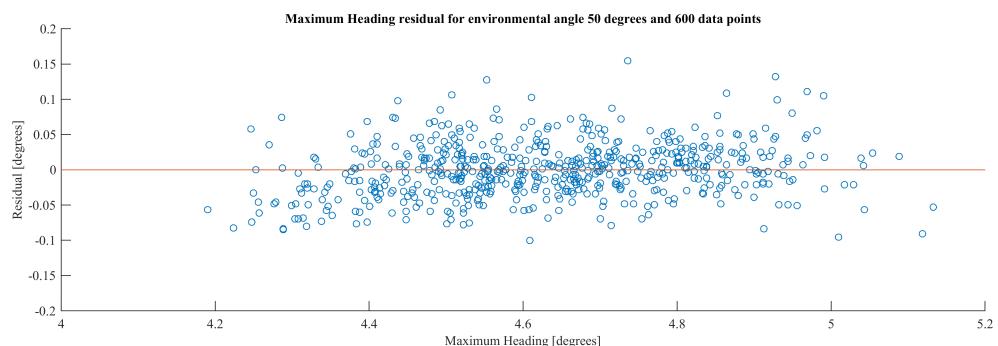


Figure F.34: Maximum Heading Residual for 50 degrees of environmental angle with 600 data points

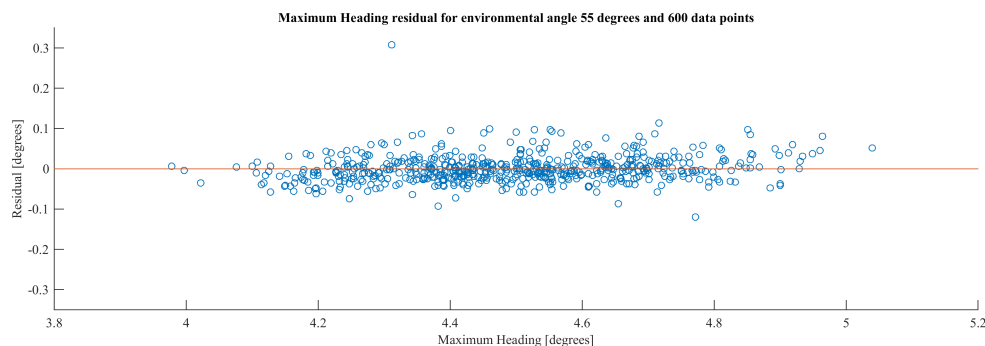


Figure F.35: Maximum Heading Residual for 55 degrees of environmental angle with 600 data points

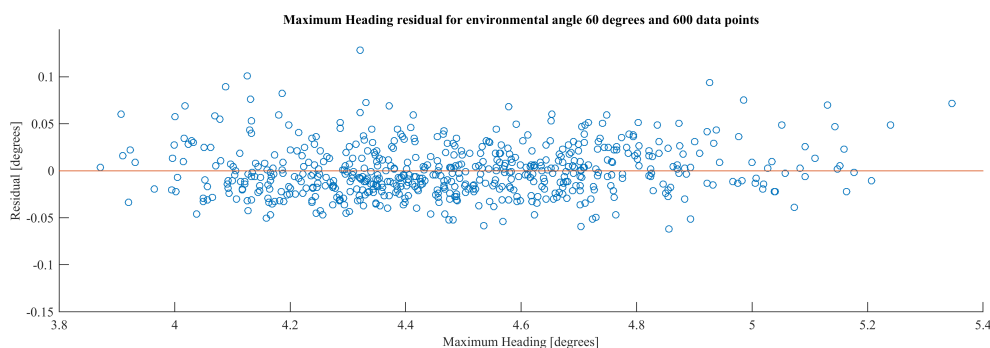


Figure F.36: Maximum Heading Residual for 60 degrees of environmental angle with 600 data points

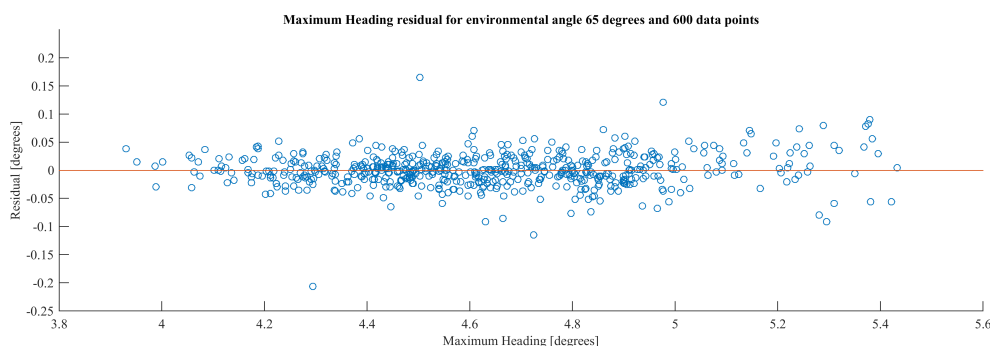


Figure F.37: Maximum Heading Residual for 65 degrees of environmental angle with 600 data points

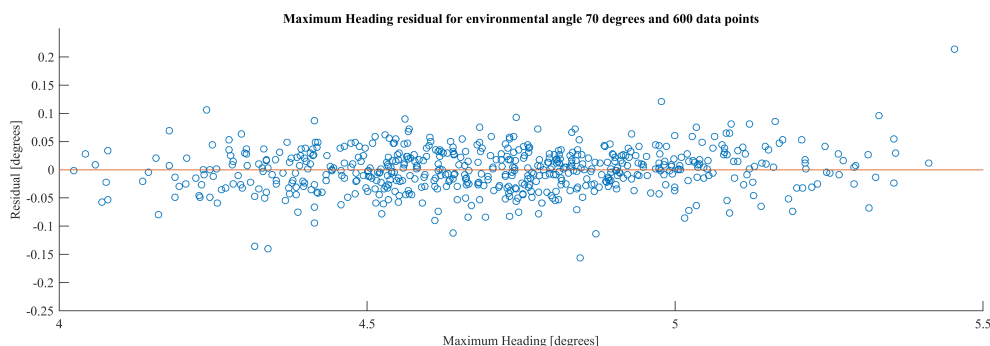


Figure F.38: Maximum Heading Residual for 70 degrees of environmental angle with 600 data points

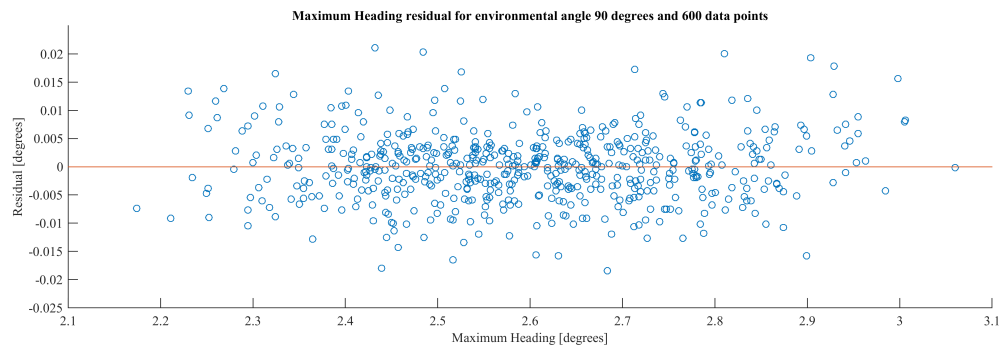


Figure F.39: Maximum Heading Residual for 90 degrees of environmental angle with 600 data points

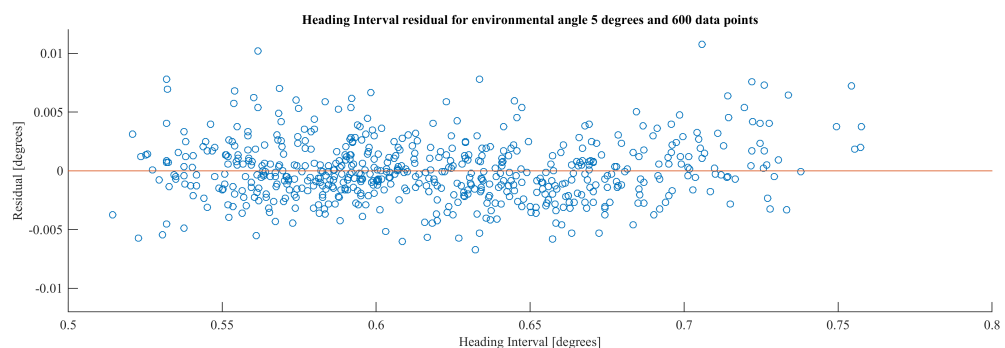


Figure F.40: Heading Interval Residual for 5 degrees of environmental angle with 600 data points

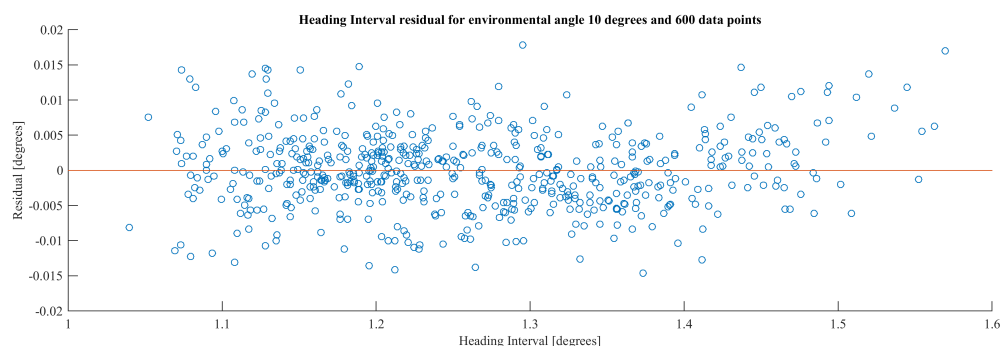


Figure F.41: Heading Interval Residual for 10 degrees of environmental angle with 600 data points

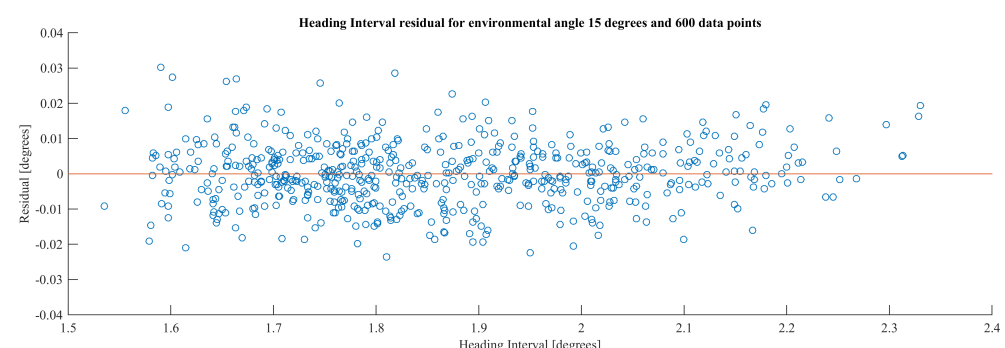


Figure F.42: Heading Interval Residual for 15 degrees of environmental angle with 600 data points

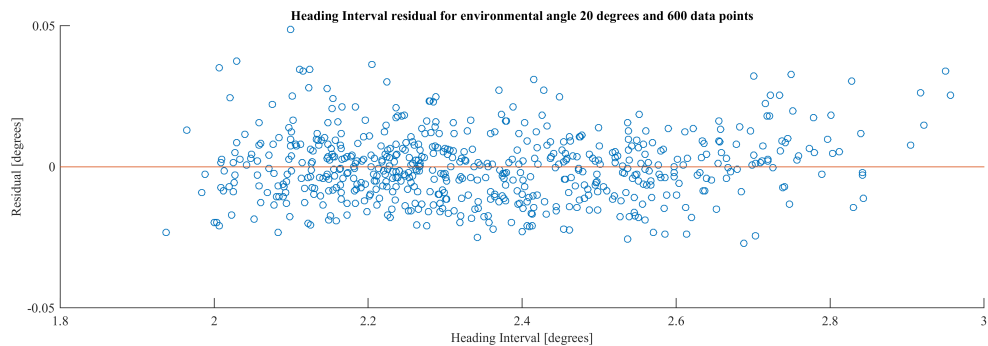


Figure F.43: Heading Interval Residual for 20 degrees of environmental angle with 600 data points

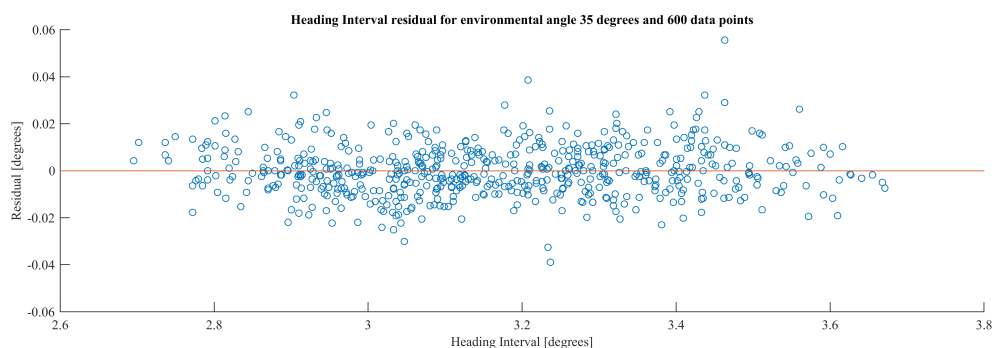


Figure F.44: Heading Interval Residual for 35 degrees of environmental angle with 600 data points

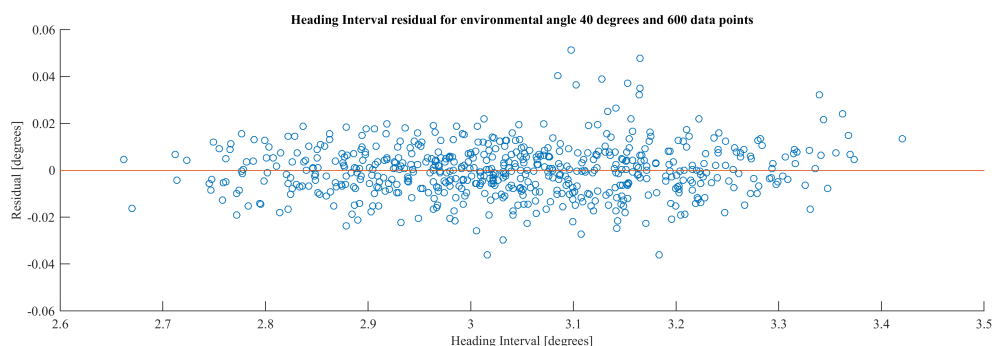


Figure F.45: Heading Interval Residual for 40 degrees of environmental angle with 600 data points

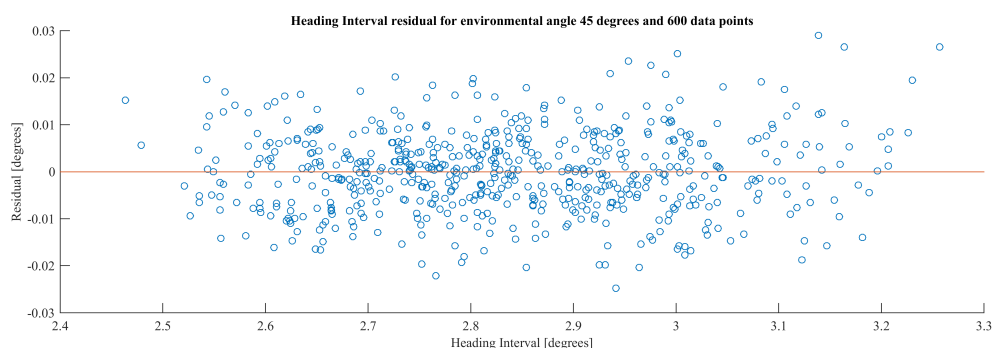


Figure F.46: Heading Interval Residual for 45 degrees of environmental angle with 600 data points

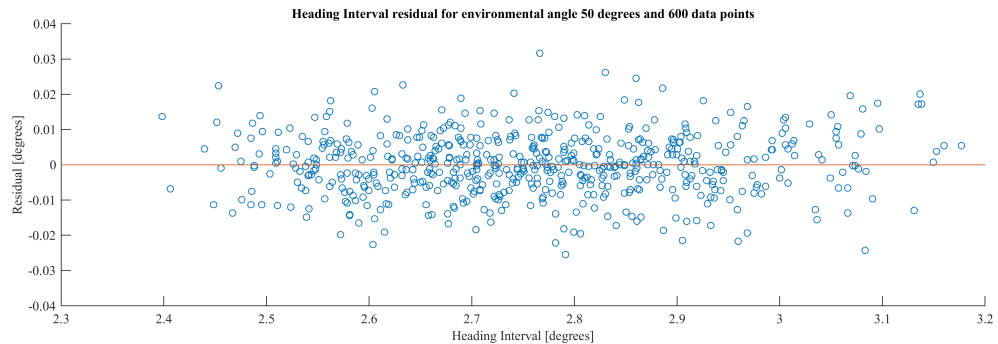


Figure F.47: Heading Interval Residual for 50 degrees of environmental angle with 600 data points

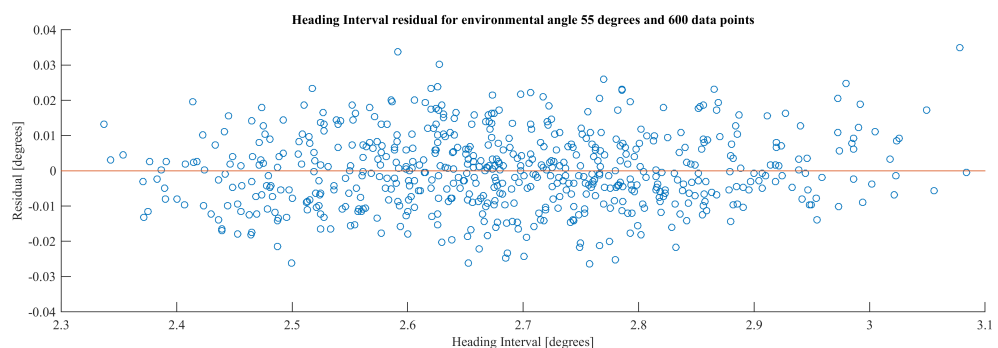


Figure F.48: Heading Interval Residual for 55 degrees of environmental angle with 600 data points

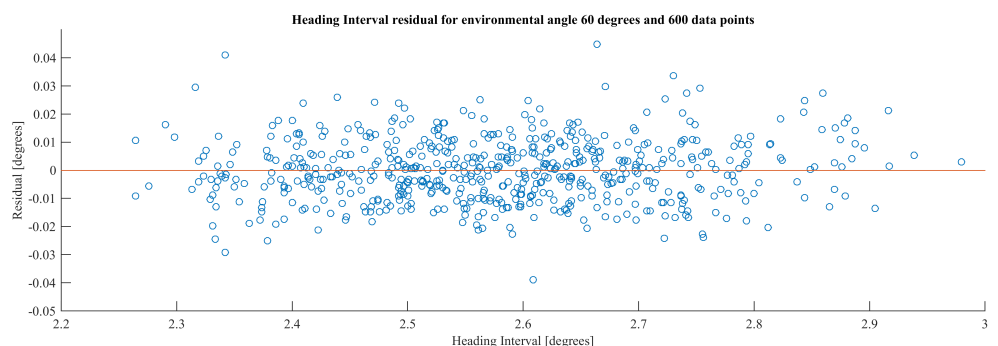


Figure F.49: Heading Interval Residual for 60 degrees of environmental angle with 600 data points

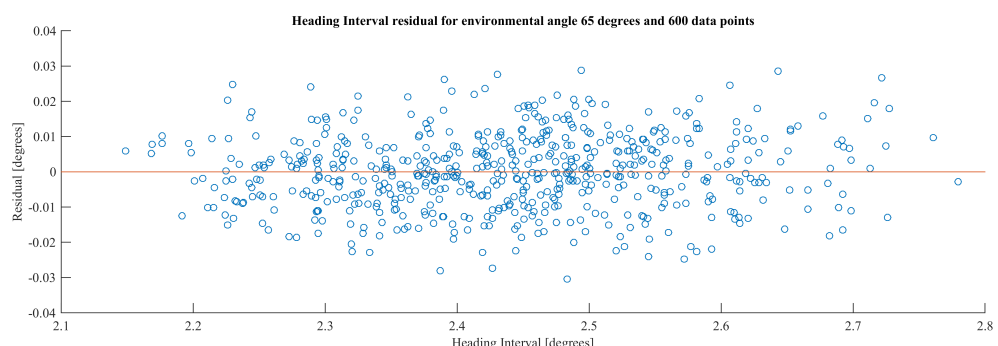


Figure F.50: Heading Interval Residual for 65 degrees of environmental angle with 600 data points

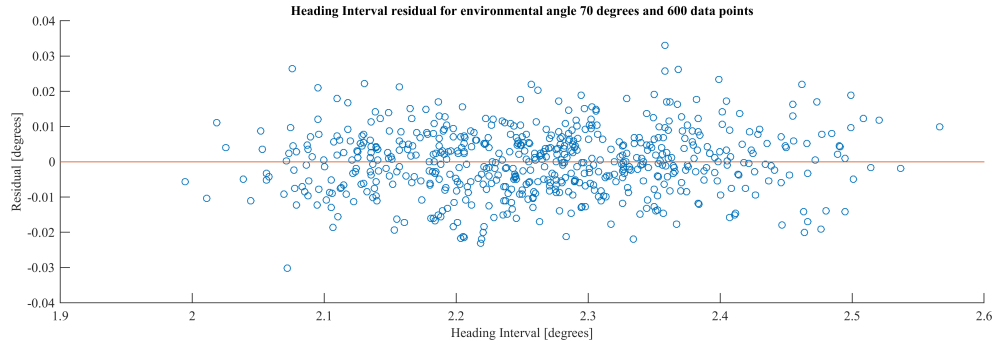


Figure F.51: Heading Interval Residual for 70 degrees of environmental angle with 600 data points

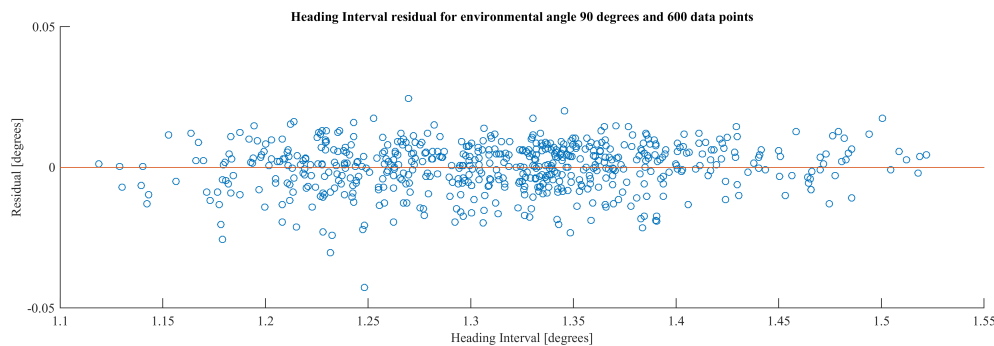


Figure F.52: Heading Interval Residual for 90 degrees of environmental angle with 600 data points

## F.2. (LOOCV) R squared, MAE and standard deviation

2nd order fit		136 data points					
angle 0 degrees		RSquare	MAE	MAESTD	CVRSquare	CVMAE	CVMAESD
head_max	0.78884	0.56313	1.50904	0.18394	1.11787	2.59470	
head_int	0.75343	1.28755	6.92251	-0.22001	2.64722	12.93940	
head_avg_time	0.88641	0.32821	0.42394	0.53377	0.68739	0.85653	
head_max_time	0.88393	0.32193	0.45568	0.51999	0.66183	0.86039	
head_count	0.83778	0.47579	0.48344	0.27098	1.01476	0.97991	
offset_max	0.99945	0.00100	0.00076	0.99760	0.00209	0.00156	
offset_int	0.99855	0.00182	0.00137	0.99290	0.00395	0.00306	
offset_avg_time	0.90384	0.01292	0.00933	0.55760	0.02743	0.02049	
offset_max_time	0.99615	0.00129	0.00101	0.98136	0.00280	0.00229	
offset_count	0.90859	0.01280	0.00940	0.57906	0.02719	0.02053	

Table F.1: 0 degrees 2nd order fit on 136 points

2nd order fit		270 data points					
angle 0 degrees		RSquare	MAE	MAESTD	CVRSquare	CVMAE	CVMAESD
head_max	0.59213	1.17908	4.33485	0.22322	1.73811	6.66556	
head_int	0.65024	1.22878	4.84759	0.32044	1.73675	6.83751	
head_avg_time	0.76583	0.44616	0.49858	0.56443	0.61363	0.68864	
head_max_time	0.78183	0.41025	0.53814	0.58220	0.57061	0.74910	
head_count	0.78424	0.61791	0.68845	0.57787	0.85111	0.94851	
offset_max	0.99899	0.00129	0.00106	0.99797	0.00180	0.00155	
offset_int	0.99741	0.00236	0.00182	0.99493	0.00329	0.00255	
offset_avg_time	0.82961	0.01870	0.01326	0.68286	0.02558	0.01803	
offset_max_time	0.74062	0.00923	0.02823	0.48052	0.01299	0.03967	
offset_count	0.84408	0.01829	0.01323	0.70913	0.02501	0.01800	

Table F.2: 0 degrees 2nd order fit on 270 points

2nd order fit		136 data points					
angle 5 degrees		RSquare	MAE	MAESTD	CVRSquare	CVMAE	CVMAESD
head_max	0.99977	0.00170	0.00129	0.99898	0.00353	0.00261	
head_int	0.99912	0.00201	0.00149	0.99601	0.00426	0.00314	
head_avg_time	0.95135	0.01563	0.01291	0.76528	0.03340	0.02858	
head_max_time	0.99838	0.00095	0.00074	0.99309	0.00198	0.00148	
head_count	0.94833	0.01462	0.01173	0.75412	0.03152	0.02690	
offset_max	0.99935	0.00106	0.00078	0.99706	0.00226	0.00165	
offset_int	0.99799	0.00207	0.00166	0.99018	0.00452	0.00378	
offset_avg_time	0.84908	0.01585	0.01055	0.20251	0.03482	0.02653	
offset_max_time	0.99510	0.00130	0.00103	0.97639	0.00282	0.00231	
offset_count	0.85141	0.01584	0.01046	0.21043	0.03477	0.02656	

Table F.3: 5 degrees 2nd order fit on 136 points

2nd order fit		600 data points					
angle 5 degrees		RSquare	MAE	MAESTD	CVRSquare	CVMAE	CVMAESD
head_max	0.99919	0.00299	0.00275	0.99891	0.00342	0.00322	
head_int	0.99759	0.00319	0.00271	0.99680	0.00365	0.00315	
head_avg_time	0.91202	0.02147	0.01639	0.88655	0.02439	0.01858	
head_max_time	0.99716	0.00125	0.00099	0.99624	0.00143	0.00115	
head_count	0.91169	0.02038	0.01528	0.88638	0.02316	0.01732	
offset_max	0.99866	0.00149	0.00116	0.99826	0.00169	0.00133	
offset_int	0.99642	0.00283	0.00215	0.99534	0.00322	0.00247	
offset_avg_time	0.74766	0.01950	0.01347	0.67294	0.02216	0.01539	
offset_max_time	0.99200	0.00171	0.00130	0.98948	0.00195	0.00150	
offset_count	0.75281	0.01931	0.01315	0.67955	0.02194	0.01503	

Table F.4: 5 degrees 2nd order fit on 600 points

2nd order fit		136 data points					
angle 10 degrees		RSquare	MAE	MAESTD	CVRSquare	CVMAE	CVMAESD
head_max		0.99977	0.00167	0.00124	0.99900	0.00349	0.00254
head_int		0.99908	0.00210	0.00173	0.99617	0.00437	0.00335
head_avg_time		0.96673	0.01409	0.01074	0.83885	0.03040	0.02384
head_max_time		0.99880	0.00083	0.00062	0.99418	0.00178	0.00139
head_count		0.96494	0.01416	0.01177	0.82924	0.03108	0.02678
offset_max		0.99926	0.00107	0.00078	0.99690	0.00223	0.00153
offset_int		0.99771	0.00228	0.00158	0.98941	0.00485	0.00348
offset_avg_time		0.89511	0.01213	0.00955	0.53017	0.02574	0.02021
offset_max_time		0.99581	0.00101	0.00077	0.97900	0.00221	0.00178
offset_count		0.89342	0.01194	0.00942	0.52408	0.02528	0.01979

Table F.5: 10 degrees 2nd order fit on 136 points

2nd order fit		600 data points					
angle 10 degrees		RSquare	MAE	MAESTD	CVRSquare	CVMAE	CVMAESD
head_max		0.99929	0.00279	0.00251	0.99906	0.00319	0.00295
head_int		0.99765	0.00338	0.00277	0.99692	0.00385	0.00319
head_avg_time		0.93731	0.02016	0.01509	0.91882	0.02289	0.01719
head_max_time		0.99727	0.00127	0.00088	0.99643	0.00145	0.00102
head_count		0.93338	0.02026	0.01525	0.91364	0.02302	0.01746
offset_max		0.99836	0.00153	0.00123	0.99785	0.00174	0.00142
offset_int		0.99613	0.00286	0.00215	0.99494	0.00325	0.00248
offset_avg_time		0.75860	0.01999	0.01483	0.68681	0.02276	0.01691
offset_max_time		0.98952	0.00166	0.00119	0.98651	0.00188	0.00135
offset_count		0.75295	0.01968	0.01435	0.67899	0.02242	0.01638

Table F.6: 10 degrees 2nd order fit on 600 points

2nd order fit		136 data points					
angle 15 degrees		RSquare	MAE	MAESTD	CVRSquare	CVMAE	CVMAESD
head_max		0.99975	0.00162	0.00131	0.99886	0.00340	0.00276
head_int		0.99855	0.00266	0.00215	0.99309	0.00575	0.00470
head_avg_time		0.94430	0.01820	0.01357	0.73210	0.03945	0.03007
head_max_time		0.99817	0.00092	0.00080	0.99195	0.00194	0.00166
head_count		0.94197	0.01850	0.01447	0.71713	0.04042	0.03307
offset_max		0.99900	0.00109	0.00085	0.99562	0.00230	0.00173
offset_int		0.99826	0.00179	0.00140	0.99142	0.00389	0.00317
offset_avg_time		0.87011	0.01697	0.01342	0.42365	0.03610	0.02766
offset_max_time		0.99319	0.00129	0.00095	0.96894	0.00274	0.00204
offset_count		0.86383	0.01725	0.01306	0.39430	0.03680	0.02719

Table F.7: 15 degrees 2nd order fit on 136 points

2nd order fit		600 data points					
angle 15 degrees		RSquare	MAE	MAESTD	CVRSquare	CVMAE	CVMAESD
head_max		0.99921	0.00275	0.00254	0.99894	0.00314	0.00298
head_int		0.99732	0.00370	0.00308	0.99650	0.00422	0.00354
head_avg_time		0.90141	0.02467	0.01924	0.87404	0.02793	0.02166
head_max_time		0.99535	0.00154	0.00116	0.99389	0.00176	0.00133
head_count		0.89500	0.02488	0.01911	0.86580	0.02818	0.02156
offset_max		0.99794	0.00153	0.00124	0.99731	0.00174	0.00143
offset_int		0.99586	0.00273	0.00209	0.99456	0.00311	0.00242
offset_avg_time		0.80134	0.02007	0.01580	0.74160	0.02287	0.01807
offset_max_time		0.98605	0.00181	0.00146	0.98157	0.00207	0.00170
offset_count		0.80204	0.01984	0.01542	0.74239	0.02260	0.01762

Table F.8: 15 degrees 2nd order fit on 600 points

2nd order fit		136 data points					
angle 20 degrees		RSquare	MAE	MAESTD	CVRSquare	CVMAE	CVMAESD
head_max		0.99800	0.00447	0.00347	0.99045	0.00959	0.00766
head_int		0.99852	0.00263	0.00211	0.99328	0.00556	0.00444
head_avg_time		0.94559	0.01449	0.01170	0.74529	0.03135	0.02536
head_max_time		0.99797	0.00113	0.00088	0.99104	0.00238	0.00182
head_count		0.94774	0.01409	0.01105	0.75304	0.03044	0.02419
offset_max		0.99846	0.00118	0.00099	0.99318	0.00252	0.00204
offset_int		0.99745	0.00210	0.00160	0.98794	0.00451	0.00357
offset_avg_time		0.66532	0.01909	0.01460	0.58393	0.04097	0.03291
offset_max_time		0.98385	0.00219	0.00170	0.92887	0.00465	0.00351
offset_count		0.67622	0.01916	0.01446	-0.54736	0.04101	0.03240

Table F.9: 20 degrees 2nd order fit on 136 points

2nd order fit		600 data points					
angle 20 degrees		RSquare	MAE	MAESTD	CVRSquare	CVMAE	CVMAESD
head_max		0.99650	0.00589	0.00485	0.99533	0.00676	0.00567
head_int		0.99672	0.00401	0.00329	0.99570	0.00457	0.00380
head_avg_time		0.89258	0.02108	0.01625	0.86007	0.02401	0.01866
head_max_time		0.99317	0.00206	0.00161	0.99107	0.00235	0.00184
head_count		0.89300	0.02057	0.01531	0.86042	0.02340	0.01755
offset_max		0.99696	0.00169	0.00134	0.99603	0.00192	0.00154
offset_int		0.99380	0.00307	0.00256	0.99168	0.00351	0.00301
offset_avg_time		0.51874	0.02408	0.01810	0.37304	0.02740	0.02081
offset_max_time		0.97293	0.00275	0.00231	0.96363	0.00315	0.00272
offset_count		0.52817	0.02379	0.01799	0.38403	0.02706	0.02066

Table F.10: 20 degrees 2nd order fit on 600 points

2nd order fit		136 data points					
angle 25 degrees		RSquare	MAE	MAESTD	CVRSquare	CVMAE	CVMAESD
head_max		0.99536	0.00558	0.00462	0.98256	0.01133	0.00833
head_int		0.99750	0.00374	0.00341	0.99013	0.00783	0.00623
head_avg_time		0.85297	0.01786	0.01489	0.28824	0.03889	0.03339
head_max_time		0.98147	0.00291	0.00275	0.92767	0.00603	0.00512
head_count		0.85953	0.01706	0.01429	0.32030	0.03700	0.03187
offset_max		0.97710	0.00392	0.00283	0.88783	0.00844	0.00651
offset_int		0.99511	0.00305	0.00248	0.97543	0.00667	0.00557
offset_avg_time		0.77481	0.02163	0.01689	-0.15559	0.04747	0.03988
offset_max_time		0.91688	0.01030	0.00839	0.63537	0.02174	0.01731
offset_count		0.76917	0.02085	0.01650	-0.20380	0.04588	0.04004

Table F.11: 25 degrees 2nd order fit on 136 points

2nd order fit		136 data points					
angle 30 degrees		Rsquare	MAE	MAESTD	CVRsquare	CVMAE	CVMAESD
head_max		0.99164	0.00456	0.00375	0.96279	0.00975	0.00780
head_int		0.99843	0.00291	0.00201	0.99188	0.00635	0.00488
head_avg_time		0.76786	0.02234	0.01778	-0.13777	0.04854	0.04062
head_max_time		0.98550	0.00218	0.00154	0.93435	0.00463	0.00326
head_count		0.76684	0.02223	0.01795	-0.13581	0.04825	0.04050
offset_max		0.97152	0.00583	0.00456	0.88008	0.01215	0.00898
offset_int		0.99602	0.00302	0.00249	0.97934	0.00667	0.00595
offset_avg_time		0.84704	0.02167	0.01699	0.22553	0.04715	0.04024
offset_max_time		0.94577	0.00335	0.00272	0.74111	0.00724	0.00606
offset_count		0.85420	0.02143	0.01690	0.26446	0.04663	0.03979

Table F.12: 30 degrees 2nd order fit on 136 points

2nd order fit		270 data points					
angle 30 degrees		Rsquare	MAE	MAESTD	CVRsquare	CVMAE	CVMAESD
head_max		0.98820	0.00561	0.00418	0.97688	0.00779	0.00595
head_int		0.99680	0.00373	0.00315	0.99350	0.00525	0.00458
head_avg_time		0.74428	0.02309	0.01763	0.51555	0.03160	0.02416
head_max_time		0.96601	0.00336	0.00238	0.93196	0.00467	0.00347
head_count		0.73404	0.02299	0.01750	0.50297	0.03151	0.02415
offset_max		0.94503	0.00838	0.00649	0.89228	0.01159	0.00932
offset_int		0.99066	0.00440	0.00353	0.98021	0.00623	0.00545
offset_avg_time		0.77083	0.02987	0.02246	0.56674	0.04112	0.03059
offset_max_time		0.90366	0.00484	0.00386	0.80717	0.00675	0.00560
offset_count		0.76479	0.02973	0.02145	0.55482	0.04099	0.02960

Table F.13: 30 degrees 2nd order fit on 270 points

2nd order fit		136 data points					
angle 35 degrees		Rsquare	MAE	MAESTD	CVRsquare	CVMAE	CVMAESD
head_max		0.99904	0.00107	0.00082	0.99583	0.00226	0.00168
head_int		0.99855	0.00204	0.00159	0.99233	0.00452	0.00383
head_avg_time		0.85707	0.01636	0.01279	0.26411	0.03623	0.03006
head_max_time		0.99188	0.00138	0.00118	0.96009	0.00304	0.00262
head_count		0.85523	0.01622	0.01305	0.25375	0.03600	0.03083
offset_max		0.99688	0.00146	0.00112	0.98369	0.00317	0.00277
offset_int		0.99742	0.00217	0.00167	0.98644	0.00479	0.00406
offset_avg_time		0.87361	0.01396	0.01156	0.39547	0.03029	0.02556
offset_max_time		0.77119	0.01816	0.01905	-0.16719	0.03984	0.04519
offset_count		0.86873	0.01366	0.01118	0.36740	0.02965	0.02502

Table F.14: 35 degrees 2nd order fit on 136 points

2nd order fit		600 data points					
angle 35 degrees		Rsquare	MAE	MAESTD	CVRsquare	CVMAE	CVMAESD
head_max		0.99802	0.00153	0.00117	0.99742	0.00174	0.00135
head_int		0.99741	0.00266	0.00216	0.99658	0.00303	0.00250
head_avg_time		0.70961	0.02415	0.01865	0.62280	0.02743	0.02134
head_max_time		0.98449	0.00195	0.00166	0.97925	0.00223	0.00195
head_count		0.69274	0.02399	0.01815	0.60197	0.02726	0.02074
offset_max		0.99351	0.00188	0.00187	0.99120	0.00216	0.00221
offset_int		0.99517	0.00279	0.00239	0.99347	0.00320	0.00282
offset_avg_time		0.69788	0.02175	0.01780	0.60848	0.02475	0.02026
offset_max_time		0.54949	0.02033	0.03240	0.40552	0.02330	0.03719
offset_count		0.69384	0.02140	0.01750	0.60363	0.02434	0.01992

Table F.15: 35 degrees 2nd order fit on 600 points

2nd order fit		136 data points					
angle 40 degrees		Rsquare	MAE	MAESTD	CVRsquare	CVMAE	CVMAESD
head_max		0.99352	0.00175	0.00142	0.96846	0.00380	0.00319
head_int		0.99749	0.00181	0.00152	0.98779	0.00390	0.00345
head_avg_time		0.77732	0.01994	0.01468	-0.05245	0.04291	0.03219
head_max_time		0.98939	0.00161	0.00134	0.95428	0.00340	0.00271
head_count		0.76535	0.01990	0.01410	-0.10526	0.04311	0.03117
offset_max		0.99776	0.00132	0.00096	0.98796	0.00287	0.00249
offset_int		0.99718	0.00216	0.00170	0.98543	0.00475	0.00408
offset_avg_time		0.83823	0.01853	0.01418	0.21902	0.03998	0.03196
offset_max_time		0.90250	0.03573	0.02789	0.54160	0.07680	0.06302
offset_count		0.84197	0.01812	0.01391	0.24611	0.03894	0.03134

Table F.16: 40 degrees 2nd order fit on 136 points

2nd order fit		600 data points					
angle 40 degrees		Rsquare	MAE	MAESTD	CVRsquare	CVMAE	CVMAESD
head_max		0.98127	0.00292	0.00219	0.97539	0.00333	0.00254
head_int		0.99422	0.00275	0.00233	0.99224	0.00315	0.00274
head_avg_time		0.48253	0.02796	0.02051	0.32912	0.03180	0.02334
head_max_time		0.97944	0.00240	0.00181	0.97310	0.00273	0.00208
head_count		0.49028	0.02768	0.02073	0.34056	0.03149	0.02364
offset_max		0.99249	0.00216	0.00201	0.98984	0.00247	0.00238
offset_int		0.99459	0.00281	0.00234	0.99272	0.00322	0.00277
offset_avg_time		0.78343	0.02140	0.01599	0.71771	0.02436	0.01837
offset_max_time		0.81038	0.04884	0.04070	0.75644	0.05545	0.04605
offset_count		0.78460	0.02120	0.01563	0.71909	0.02412	0.01794

Table F.17: 40 degrees 2nd order fit on 600 points

2nd order fit		136 data points					
angle 45 degrees		Rsquare	MAE	MAESTD	CVRsquare	CVMAE	CVMAESD
head_max		0.97577	0.00385	0.00295	0.88135	0.00830	0.00681
head_int		0.99827	0.00185	0.00148	0.99227	0.00395	0.00304
head_avg_time		0.76496	0.02550	0.01912	-0.18712	0.05462	0.04601
head_max_time		0.98065	0.00252	0.00199	0.90945	0.00538	0.00439
head_count		0.76148	0.02526	0.01896	-0.18799	0.05393	0.04581
offset_max		0.99793	0.00126	0.00097	0.98837	0.00278	0.00254
offset_int		0.99705	0.00233	0.00170	0.98452	0.00516	0.00406
offset_avg_time		0.86821	0.01709	0.01206	0.37828	0.03688	0.02679
offset_max_time		0.88093	0.05575	0.03951	0.44349	0.12057	0.08835
offset_count		0.87437	0.01668	0.01244	0.40881	0.03588	0.02712

Table F.18: 45 degrees 2nd order fit on 136 points

2nd order fit		270 data points					
angle 45 degrees		Rsquare	MAE	MAESTD	CVRsquare	CVMAE	CVMAESD
head_max		0.95573	0.00460	0.00412	0.90554	0.00651	0.00622
head_int		0.99752	0.00227	0.00167	0.99512	0.00315	0.00240
head_avg_time		0.66078	0.02769	0.02199	0.36949	0.03792	0.02967
head_max_time		0.97326	0.00293	0.00249	0.94752	0.00404	0.00358
head_count		0.65485	0.02724	0.02117	0.35778	0.03736	0.02868
offset_max		0.99555	0.00170	0.00153	0.99021	0.00240	0.00242
offset_int		0.99600	0.00246	0.00206	0.99180	0.00344	0.00309
offset_avg_time		0.78149	0.02178	0.01616	0.57283	0.03014	0.02296
offset_max_time		0.83431	0.06417	0.04591	0.69786	0.08725	0.06246
offset_count		0.78658	0.02102	0.01617	0.5		

2nd order fit		600 data points					
angle 45 degrees		RSquare	MAE	MAESTD	CVRSquare	CVMAE	CVMAESD
head_max		0.95331	0.00468	0.00419	0.93734	0.00537	0.00491
head_int		0.99706	0.00240	0.00186	0.99616	0.00273	0.00213
head_avg_time		0.63802	0.03117	0.02470	0.52894	0.03548	0.02822
head_max_time		0.96453	0.00340	0.00297	0.95275	0.00389	0.00349
head_count		0.63222	0.03082	0.02372	0.52210	0.03507	0.02714
offset_max		0.99481	0.00181	0.00169	0.99304	0.00207	0.00199
offset_int		0.99520	0.00272	0.00229	0.99359	0.00311	0.00268
offset_avg_time		0.74753	0.02271	0.01832	0.67009	0.02587	0.02102
offset_max_time		0.80583	0.07056	0.04706	0.74954	0.08012	0.05357
offset_count		0.74933	0.02243	0.01805	0.67326	0.02555	0.02073

Table F.20: 45 degrees 2nd order fit on 600 points

2nd order fit		136 data points					
angle 50 degrees		RSquare	MAE	MAESTD	CVRSquare	CVMAE	CVMAESD
head_max		0.97484	0.00458	0.00402	0.88768	0.00972	0.00850
head_int		0.99918	0.00126	0.00099	0.99632	0.00270	0.00208
head_avg_time		0.81710	0.01878	0.01431	0.25562	0.03881	0.02765
head_max_time		0.93426	0.01094	0.00854	0.71719	0.02291	0.01720
head_count		0.81651	0.01908	0.01437	0.24324	0.03948	0.02813
offset_max		0.99648	0.00184	0.00142	0.98183	0.00402	0.00340
offset_int		0.99699	0.00228	0.00173	0.98449	0.00505	0.00404
offset_avg_time		0.89706	0.01495	0.01180	0.55220	0.03147	0.02416
offset_max_time		0.87794	0.06784	0.05147	0.46475	0.14374	0.11557
offset_count		0.90472	0.01434	0.01129	0.58215	0.03018	0.02355

Table F.21: 50 degrees 2nd order fit on 136 points

2nd order fit		600 data points					
angle 50 degrees		RSquare	MAE	MAESTD	CVRSquare	CVMAE	CVMAESD
head_max		0.95617	0.00642	0.00521	0.94294	0.00731	0.00595
head_int		0.99695	0.00243	0.00196	0.99602	0.00277	0.00224
head_avg_time		0.48710	0.02876	0.02268	0.32902	0.03279	0.02596
head_max_time		0.89645	0.01391	0.01300	0.86529	0.01583	0.01491
head_count		0.48540	0.02847	0.02202	0.32889	0.03248	0.02528
offset_max		0.99218	0.00253	0.00218	0.98964	0.00289	0.00253
offset_int		0.99594	0.00255	0.00200	0.99465	0.00291	0.00231
offset_avg_time		0.77706	0.02426	0.01959	0.70714	0.02773	0.02258
offset_max_time		0.79984	0.08707	0.06324	0.74222	0.09894	0.07201
offset_count		0.78849	0.02353	0.01931	0.72215	0.02687	0.02221

Table F.22: 50 degrees 2nd order fit on 600 points

2nd order fit		136 data points					
angle 55 degrees		RSquare	MAE	MAESTD	CVRSquare	CVMAE	CVMAESD
head_max		0.98890	0.00365	0.00287	0.95575	0.00751	0.00542
head_int		0.99785	0.00207	0.00157	0.99043	0.00438	0.00325
head_avg_time		0.89611	0.01649	0.01287	0.52760	0.03501	0.02738
head_max_time		0.95659	0.01841	0.01576	0.80276	0.03925	0.03409
head_count		0.90495	0.01588	0.01231	0.58431	0.03366	0.02552
offset_max		0.99092	0.00284	0.00232	0.95462	0.00624	0.00534
offset_int		0.99813	0.00180	0.00141	0.99040	0.00395	0.00329
offset_avg_time		0.86318	0.02132	0.01605	0.39762	0.04498	0.03379
offset_max_time		0.84241	0.08570	0.06668	0.32040	0.18250	0.14295
offset_count		0.85713	0.02071	0.01560	0.37189	0.04337	0.03236

Table F.23: 55 degrees 2nd order fit on 136 points

2nd order fit		600 data points					
angle 55 degrees		RSquare	MAE	MAESTD	CVRSquare	CVMAE	CVMAESD
head_max		0.96935	0.00538	0.00530	0.95965	0.00613	0.00611
head_int		0.99502	0.00317	0.00237	0.99349	0.00361	0.00272
head_avg_time		0.72761	0.02831	0.02133	0.64438	0.03226	0.02449
head_max_time		0.93722	0.02257	0.02380	0.91867	0.02570	0.02699
head_count		0.74577	0.02794	0.02096	0.66758	0.03184	0.02412
offset_max		0.98659	0.00342	0.00296	0.98238	0.00390	0.00341
offset_int		0.99658	0.00234	0.00183	0.99550	0.00267	0.00213
offset_avg_time		0.82395	0.02264	0.01714	0.77151	0.02577	0.01954
offset_max_time		0.79484	0.09745	0.06711	0.73723	0.11052	0.07620
offset_count		0.82545	0.02192	0.01672	0.77389	0.02493	0.01906

Table F.24: 55 degrees 2nd order fit on 600 points

2nd order fit		136 data points					
angle 60 degrees		RSquare	MAE	MAESTD	CVRSquare	CVMAE	CVMAESD
head_max		0.99536	0.00318	0.00257	0.97897	0.00685	0.00546
head_int		0.99688	0.00239	0.00181	0.98593	0.00506	0.00387
head_avg_time		0.73209	0.02592	0.02329	-0.15394	0.05521	0.04455
head_max_time		0.92412	0.04831	0.04422	0.68437	0.09927	0.08738
head_count		0.72071	0.02561	0.02172	-0.16880	0.05485	0.04347
offset_max		0.98353	0.00399	0.00298	0.92893	0.00842	0.00593
offset_int		0.99845	0.00169	0.00115	0.99255	0.00365	0.00262
offset_avg_time		0.88416	0.01745	0.01339	0.44073	0.03766	0.03114
offset_max_time		0.86837	0.07371	0.05594	0.40448	0.15944	0.12194
offset_count		0.88077	0.01698	0.01284	0.41670	0.03641	0.02907

Table F.25: 60 degrees 2nd order fit on 136 points

2nd order fit		600 data points					
angle 60 degrees		RSquare	MAE	MAESTD	CVRSquare	CVMAE	CVMAESD
head_max		0.98992	0.00471	0.00385	0.98681	0.00535	0.00444
head_int		0.99353	0.00342	0.00263	0.99158	0.00389	0.00301
head_avg_time		0.64291	0.03314	0.02556	0.53505	0.03773	0.02929
head_max_time		0.85430	0.06561	0.06451	0.80700	0.07510	0.07489
head_count		0.65302	0.03278	0.02472	0.54721	0.03735	0.02834
offset_max		0.97278	0.00536	0.00363	0.96464	0.00609	0.00415
offset_int		0.99739	0.00205	0.00169	0.99657	0.00234	0.00195
offset_avg_time		0.80157	0.02161	0.01681	0.74375	0.02459	0.01906
offset_max_time		0.79137	0.09315	0.06431	0.73281	0.10558	0.07252
offset_count		0.80665	0.02104	0.01628	0.75037	0.02393	0.01847

Table F.26: 60 degrees 2nd order fit on 600 points

2nd order fit		136 data points					
angle 65 degrees		RSquare	MAE	MAESTD	CVRSquare	CVMAE	CVMAESD
head_max		0.99492	0.00351	0.00271	0.97639	0.00749	0.00600
head_int		0.99516	0.00286	0.00200	0.97779	0.00614	0.00428
head_avg_time		0.80254	0.03010	0.02183	0.16910	0.06266	0.04243
head_max_time		0.83370	0.09209	0.07877	0.31673	0.19062	0.14658
head_count		0.78854	0.03000	0.02073	0.11648	0.06286	0.04122
offset_max		0.99150	0.00275	0.00210	0.95620	0.00608	0.00495
offset_int		0.99818	0.00174	0.00139	0.99124	0.00373	0.00313
offset_avg_time		0.89469	0.01530	0.01101	0.51890	0.03231	0.02395
offset_max_time		0.87938	0.07275	0.05047	0.43991	0.15506	0.11036
offset_count		0.89621	0.01496	0.01096	0.52983	0.03157	0.02376

Table F.27: 65 degrees 2nd order fit on 136 points

2nd order fit		600 data points					
angle 65 degrees		RSquare	MAE	MAESTD	CVRSquare	CVMAE	CVMAESD
head_max		0.99006	0.00451	0.00435	0.98682	0.00515	0.00507
head_int		0.99258	0.00344	0.00257	0.99032	0.00392	0.00295
head_avg_time		0.64416	0.03908	0.02882	0.54447	0.04422	0.03234
head_max_time		0.75612	0.11104	0.08080	0.68653	0.12575	0.09105
head_count		0.62358	0.03855	0.02820	0.52058	0.04367	0.03185
offset_max		0.98001	0.00385	0.00326	0.97400	0.00437	0.00374
offset_int		0.99726	0.00214	0.00163	0.99644	0.00244	0.00186
offset_avg_time		0.79458	0.02032	0.01587	0.73661	0.02302	0.01793
offset_max_time		0.78659	0.08950	0.06783	0.72431	0.10164	0.07671
offset_count		0.79880	0.02001	0.01580	0.74244	0.02267	0.01787

Table F.28: 65 degrees 2nd order fit on 600 points

2nd order fit		136 data points					
angle 70 degrees		RSquare	MAE	MAESTD	CVRSquare	CVMAE	CVMAESD
head_max		0.99141	0.00451	0.00338	0.95972	0.00979	0.00724
head_int		0.99672	0.00205	0.00179	0.98546	0.00436	0.00371
head_avg_time		0.86125	0.02206	0.01644	0.39293	0.04637	0.03355
head_max_time		0.88079	0.06693	0.05481	0.46127	0.14154	0.11947
head_count		0.85271	0.02223	0.01642	0.35476	0.04702	0.03431
offset_max		0.99397	0.00202	0.00173	0.96639	0.00448	0.00435
offset_int		0.99851	0.00161	0.00117	0.99257	0.00351	0.00269
offset_avg_time		0.92435	0.01307	0.01122	0.68393	0.02730	0.02227
offset_max_time		0.88446	0.07888	0.05724	0.46176	0.16778	0.12557
offset_count		0.92214	0.01258	0.01037	0.67283	0.02633	0.02061

Table F.29: 70 degrees 2nd order fit on 136 points

2nd order fit		600 data points					
angle 70 degrees		RSquare	MAE	MAESTD	CVRSquare	CVMAE	CVMAESD
head_max		0.98125	0.00615	0.00515	0.97522	0.00701	0.00596
head_int		0.99274	0.00320	0.00247	0.99042	0.00366	0.00286
head_avg_time		0.74935	0.03021	0.02370	0.67426	0.03440	0.02707
head_max_time		0.67856	0.09463	0.08419	0.58953	0.10748	0.09526
head_count		0.74108	0.02973	0.02310	0.66353	0.03385	0.02637
offset_max		0.98967	0.00240	0.00248	0.98651	0.00273	0.00285
offset_int		0.99728	0.00207	0.00164	0.99649	0.00235	0.00186
offset_avg_time		0.83085	0.02040	0.01468	0.78179	0.02316	0.01667
offset_max_time		0.78436	0.09565	0.07672	0.72407	0.10847	0.08651
offset_count		0.82273	0.01979	0.01419	0.77187	0.02246	0.01609

Table F.30: 70 degrees 2nd order fit on 600 points

2nd order fit		136 data points					
angle 75 degrees		RSquare	MAE	MAESTD	CVRSquare	CVMAE	CVMAESD
head_max		0.78740	0.03299	0.02749	0.07790	0.06896	0.05523
head_int		0.99343	0.00307	0.00231	0.97015	0.00656	0.00491
head_avg_time		0.77502	0.02499	0.01826	-0.10097	0.05357	0.04205
head_max_time		0.75203	0.05673	0.04970	-0.32015	0.12330	0.11167
head_count		0.78460	0.02422	0.01737	-0.03943	0.05202	0.04042
offset_max		0.96158	0.00556	0.00411	0.82627	0.01174	0.00875
offset_int		0.99817	0.00182	0.00128	0.99029	0.00402	0.00312
offset_avg_time		0.93235	0.01423	0.01150	0.68020	0.03106	0.02460
offset_max_time		0.88937	0.07413	0.06447	0.53545	0.15267	0.12849
offset_count		0.92790	0.01406	0.01091	0.65770	0.03075	0.02395

Table F.31: 75 degrees 2nd order fit on 136 points

2nd order fit		136 data points					
angle 80 degrees		RSquare	MAE	MAESTD	CVRSquare	CVMAE	CVMAESD
head_max		0.85510	0.02672	0.01828	0.32287	0.05770	0.03914
head_int		0.98732	0.00481	0.00404	0.93928	0.01046	0.00899
head_avg_time		0.57212	0.02985	0.02565	-1.16718	0.06540	0.05804
head_max_time		0.61634	0.05038	0.04339	-1.25234	0.11451	0.11128
head_count		0.56749	0.02970	0.02474	-1.16802	0.06559	0.05816
offset_max		0.94996	0.00665	0.00492	0.77169	0.01407	0.01073
offset_int		0.99858	0.00149	0.00124	0.99311	0.00321	0.00278
offset_avg_time		0.89125	0.01809	0.01351	0.53255	0.03785	0.02726
offset_max_time		0.89346	0.07776	0.06034	0.55731	0.16011	0.12157
offset_count		0.89472	0.01763	0.01321	0.55016	0.03690	0.02705

Table F.32: 80 degrees 2nd order fit on 136 points

2nd order fit		136 data points					
angle 85 degrees		RSquare	MAE	MAESTD	CVRSquare	CVMAE	CVMAESD
head_max		0.94232	0.01531	0.01117	0.69207	0.03413	0.02728
head_int		0.97624	0.00923	0.00688	0.89169	0.01971	0.01461
head_avg_time		0.84039	0.03406	0.02480	0.27677	0.07191	0.05087
head_max_time		0.86405	0.07622	0.06569	0.39951	0.16093	0.13484
head_count		0.85181	0.03275	0.02411	0.35395	0.06955	0.05116
offset_max		0.99172	0.00215	0.00185	0.95070	0.00481	0.00490
offset_int		0.99814	0.00172	0.00134	0.99061	0.00369	0.00316
offset_avg_time		0.86692	0.01449	0.01093	0.42173	0.03057	0.02217
offset_max_time		0.82981	0.02139	0.01912	-0.25675	0.04825	0.04962
offset_count		0.86518	0.01416	0.01067	0.41522	0.02985	0.02182

Table F.33: 85 degrees 2nd order fit on 136 points

2nd order fit		136 data points					
angle 90 degrees	RSquare	MAE	MAESTD	CVRSquare	CVMAE	CVMAESD	
head_max	0.99933	0.00126	0.00110	0.99725	0.00262	0.00211	
head_int	0.99478	0.00334	0.00276	0.97678	0.00706	0.00583	
head_avg_time	0.87473	0.01819	0.01441	0.47409	0.03757	0.02882	
head_max_time	0.85969	0.03497	0.02658	0.24936	0.07711	0.06381	
head_count	0.87478	0.01741	0.01380	0.48186	0.03604	0.02768	
offset_max	0.99874	0.00087	0.00067	0.99425	0.00184	0.00144	
offset_int	0.99871	0.00137	0.00118	0.99455	0.00284	0.00243	
offset_avg_time	0.81042	0.01638	0.01208	0.05445	0.03563	0.02811	
offset_max_time	0.94790	0.00831	0.00613	0.75981	0.01771	0.01318	
offset_count	0.80612	0.01613	0.01179	0.03525	0.03510	0.02762	

Table F.34: 90 degrees 2nd order fit on 136 points

2nd order fit		600 data points					
angle 90 degrees	RSquare	MAE	MAESTD	CVRSquare	CVMAE	CVMAESD	
head_max	0.99864	0.00181	0.00153	0.99824	0.00207	0.00174	
head_int	0.98833	0.00511	0.00410	0.98469	0.00581	0.00476	
head_avg_time	0.69096	0.02766	0.02199	0.60050	0.03147	0.02492	
head_max_time	0.70041	0.04232	0.04248	0.60313	0.04862	0.04930	
head_count	0.69534	0.02729	0.02176	0.60698	0.03105	0.02470	
offset_max	0.99783	0.00113	0.00087	0.99718	0.00129	0.00100	
offset_int	0.99703	0.00218	0.00165	0.99610	0.00249	0.00191	
offset_avg_time	0.68324	0.01940	0.01485	0.59355	0.02201	0.01681	
offset_max_time	0.74675	0.01288	0.01559	0.65398	0.01472	0.01826	
offset_count	0.67995	0.01911	0.01470	0.58914	0.02167	0.01661	

Table F.35: 90 degrees 2nd order fit on 600 points



# Bibliography

- [1] Crude Oil Prices - 70 Year Historical Chart, Available at <http://www.macrotrends.net/1369/crude-oil-price-history-chart>, date accessed [2017-10-31].
- [2] Global Cumulative Installed Wind Capacity 2001-2016, Available at <http://www.gwec.net/wp-content/uploads/2012/06/Global-Cumulative-Installed-Wind-Capacity-2001-2016.jpg>, date accessed [2017-10-31].
- [3] J. W. Choi and J. J. Park, "A Study on the Effects of Wind Load on the DP Capability," pp. 564–571, 2014.
- [4] C. Willemse, H. Grimmelius, and A. Tjallema, *Dynamic positioning OE5663*. Delft University of Technology, 2008.
- [5] IMCA, "Specification for DP Capability Plots," Tech. Rep. June, IMCA, 2000.
- [6] Kongsberg DP Cabability Plot, Available at [http://www.motorship.com/\\_\\_data/assets/image/0023/420377/varieties/carousel2.jpg](http://www.motorship.com/__data/assets/image/0023/420377/varieties/carousel2.jpg), date accessed [2017-05-15].
- [7] API, "Design and Analysis of Stationkeeping Systems for Floating Structures," tech. rep., American Petroleum Institute RP2SK, 1997.
- [8] Gachet, M., v. t. Veer, and R., "Dynamic Positioning: Early Design, Capability and Offsets — A Novel Approach," *Proceedings of the ASME 2011 30th International Conference on Ocean, Offshore and Arctic Engineering*, no. January 2011, 2011.
- [9] W. Antheunisse, D. Chalkias, and R. Huijsmans, "Offset requirements in quasi static DP capability calculations," *Proceedings of the International Offshore and Polar Engineering Conference*, vol. 2016-Janua, pp. 1602–1608, 2016.
- [10] I. M. V. D. Vossen, "Masters Thesis: Improving the combined operation of Dynamic Positioning and motion compensation from a control engineering perspective," tech. rep., Delft University of Technology, Delft, 2017.
- [11] MARIN, "DP-JIP Summary Of Model Scale And Full Scale Tests," tech. rep., MARIN, 2009.
- [12] DNV, "Rules for Classification Ships Part 6 Additional class notations Chapter 2 Propulsion , power generation and auxiliary systems," Tech. Rep. July, DNV, 2016.
- [13] IMO, "Guidelines for vessels with Dynamic Positioning systems 1," Tech. Rep. July, IMO, 1994.
- [14] G. L. Ag, "Rules for Classification and Construction Naval Ship Technology," *Lloydia (Cincinnati)*, no. January, pp. 1–12, 2004.
- [15] Azimuth Thrusters, Available at [http://rmpropulsion.com/wp-content/uploads/2015/09/Union\\_Sapphire\\_p4\\_in\\_the\\_drydocks\\_at\\_Antwerp\\_Belgium\\_11-Jan-2005-Medium.jpg](http://rmpropulsion.com/wp-content/uploads/2015/09/Union_Sapphire_p4_in_the_drydocks_at_Antwerp_Belgium_11-Jan-2005-Medium.jpg), date accessed [2017-05-17].
- [16] Tunnel Thrusters, Available at <http://www.brunvoll.no/product/the-complete-thruster-system/tunnel-thrusters>, date accessed [2017-05-17].
- [17] American Bureau of Shipping, "Guide for Dynamic Positioning Systems," Tech. Rep. July, American Bureau of Shipping, 2014.

- [18] F. van Diggelen and P. Enge, "The World's first GPS MOOC and Worldwide Laboratory using Smartphones," *Proceedings of the 28th International Technical Meeting of The Satellite Division of the Institute of Navigation (ION GNSS)*, 2015.
- [19] O. Cadet, "Introduction to Kalman Filter and its use in Dynamic Positioning Systems," *Proceedings of Dynamic Positioning ...*, pp. 1–33, 2003.
- [20] I. C. Giddings, "IMO Guidelines for vessels with dynamic positioning systems," *MTS Dynamic Positioning Conference, 2013, October 15-16, Houston, Texas, USA*, 2013.
- [21] R. For and C. Of, "Ships Special Equipment And Systems – Additional Class Miscellaneous Notifications," *DNV Det Norske Veritas*, no. July, 2014.
- [22] J. Journée and W. W. Massie, *Offshore Hydromechanics*. No. January, Delft University of Technology, 2001.
- [23] M. Zaaijer, "Introduction to Wind energy." Delft University of Technology, 2015.
- [24] H. Lie, K. Mo, and K. E. Kaasen, *MIMOSA - User's Documentation Program Version 5.7*. MARINTEK, 2003.
- [25] L. H. Holthuijsen, *Waves in Oceanic and Coastal Waters*. Cambridge university press, 2009.
- [26] R. S. Langley, "A statistical analysis of low frequency second-order forces and motions," *Applied Ocean Research*, vol. 9, no. 3, pp. 163–170, 1987.
- [27] J. a. Pinkster, *Low frequency second order wave exciting forces on floating structures*. PhD thesis, Delft University of Technology, 1980.
- [28] B. Jensen, H. F. Hansen, and J. Kirkegaard, "Estimating Quadratic Transfer Functions for Floating Structures using Model Test Data from Irregular Sea States," (Kona, Big Island, Hawaii), ISOPE, 2015.
- [29] G. M. Hertzberger, *The influence of wave field descriptions on real time deep water drift forces*. PhD thesis, Delft University of Technology, 2013.
- [30] W. E. Cummins, "The impulse response function and ship motions," 1962.
- [31] J. Serraris, "Time Domain Analysis for DP Simulations," in *Proceedings of the ASME 2009 28th International*, (Honolulu, Hawai), ASME, 2009.
- [32] J. van der Weiden, "A study into the relationship between the static and dynamic calculations methods for Dynamic Positioning of Offshore Support Vessels," tech. rep., Delft University of Technology, 2013.
- [33] C. Brun, D. Coache, Y. Giorgiutti, and F. Rezende, "Influences on Dynamic Positioning System Capability," *International Ocean and Polar Engineering Conference*, pp. 627–634, 2015.
- [34] H.-j. Kim, S.-y. Hong, W.-j. Yoo, and S.-k. Hong, "Analysis on DP Performance of a Shuttle Tanker with Various Analysis Methods," *ISOPE Pacific/Asia Offshore Mechanics Symposium*, 2002.
- [35] L. Sun, X. Zhu, B. Li, and W. Ma, "Comparison of Time Domain Simulation and Steady State Capability Analysis of Dynamic Positioning," *International Ocean and Polar Engineering Conference*, 2015.
- [36] J. C. Refsgaard, J. P. van der Sluijs, A. L. Højberg, and P. A. Vanrolleghem, "Uncertainty in the environmental modelling process - A framework and guidance," *Environmental Modelling and Software*, vol. 22, no. 11, pp. 1543–1556, 2007.
- [37] S. Funtowicz and J. Ravetz, *Uncertainty and Quality in Science for Policy*. Dordrecht: Kluwer Academic Publishers, 1990.
- [38] W. Walker, J. Rotmans, P. Sluijs, and M. P. K. Krauss, "A Conceptual Basis for Uncertainty Management," *Integrated Assessment*, vol. 4, no. 1, pp. 5–17, 2003.

- [39] P. Schulten and P. D. Stapersma, "A study of the validity of a complex simulation model," *Journal of Marine Engineering and Technology*, vol. A10, pp. 67 – 77, 2007.
- [40] D. B. Pengra, L. T. Dillman, and O. Wesleyan, "Notes on Data Analysis and Experimental Uncertainty," tech. rep., Wesleyan University, Ohio, 2009.
- [41] D. M. Hamby, "A review of techniques for parameter sensitivity analysis of environmental models," *Environmental Monitoring and Assessment*, vol. 32, no. 2, pp. 135–154, 1994.
- [42] R. Iman and J. Helton, "An Investigation of Uncertainty and Sensitivity Analysis Techniques for Computer Models," *Risk Analysis*, vol. 8, no. 1, pp. 71–90, 1988.
- [43] T. Krieger, C. Durston, and D. Albright, "Statistical Determination of Effective Variables in Sensitivity Analysis," *Trans. Am. Nuc. Soc.*, vol. 28, pp. 515–516, 1977.
- [44] A. Mokhtari and H. C. Frey, "Review and Recommendation of Methods for Sensitivity and Uncertainty Analysis for the Stochastic Human Exposure and Dose Simulation (SHEDS) Models - Volume 1," *Review of Available Methods for Conducting Sensitivity and Uncertainty Analysis in Probabilistic Models*, vol. Volume 1, p. 99, 2005.
- [45] Pearson Product-Moment Correlation, Available at <https://statistics.laerd.com/statistical-guides/pearson-correlation-coefficient-statistical-guide.php>, date accessed [2018-02-07].
- [46] Machine Learning Styles, Available at <https://machinelearningmastery.com/supervised-and-unsupervised-machine-learning-algorithms>, date accessed [2018-05-01].
- [47] Machine Learning Styles Picture, Available at <https://blogs.sas.com/content/subconsciousmusings/files/2017/09/styles-of-learning.jpg>, date accessed [2018-05-01].
- [48] Machine Learning methods and algorithms, Available at <https://www.kdnuggets.com/2017/06/which-machine-learning-algorithm.html>, date accessed [2018-05-01].
- [49] I. G. Macdonald, *Symmetric Functions and Hall Polynomials*. Oxford University Press, 2nd ed., 1998.
- [50] M. Cavazzuti, *Optimization methods: From theory to design scientific and technological aspects in mechanics*. Springer-Verlag Berlin Heidelberg, 2013.
- [51] R squared visual representation, Available at <http://statisticsbyjim.com/regression/interpret-r-squared-regression>, date accessed [2018-05-02].
- [52] Residual Example, Available at [https://blog.minitab.com/hubfs/Imported\\_Blog\\_Media/fpllinear-1.gif?t=1529098214777](https://blog.minitab.com/hubfs/Imported_Blog_Media/fpllinear-1.gif?t=1529098214777), date accessed [2018-05-02].
- [53] Mean Absolute Error, Available at <https://medium.com/human-in-a-machine-world/mae-and-rmse-which-metric-is-better-e60ac3bde13d>, date accessed [2018-05-02].
- [54] R. J. Meijer and J. J. Goeman, "Efficient approximate k-fold and leave-one-out cross-validation for ridge regression," *Biometrical Journal*, vol. 55, no. 2, pp. 141–155, 2013.
- [55] Types of Variables, Available at <https://statistics.laerd.com/statistical-guides/types-of-variable.php>, date accessed [2018-02-07].
- [56] F. M. White, *Fluid Mechanics*. McGraw-Hill, 4th ed., 1999.
- [57] A. Hoencamp, *Helicopter-Ship Qualification Testing*. Ipskamp drukkers, 2015.
- [58] K. H. Ang, G. Chong, and Y. Li, "PID control system analysis, design, and technology," *IEEE Transactions on Control Systems Technology*, vol. 13, no. 4, pp. 559–576, 2005.